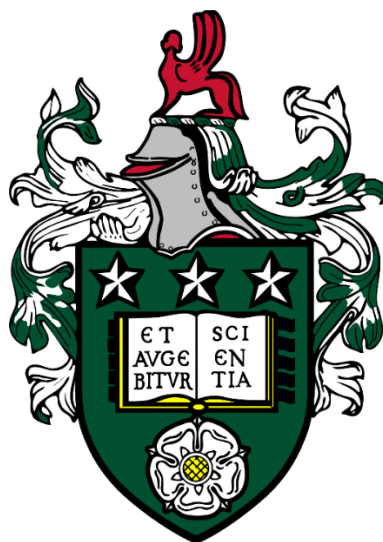# PhD Thesis
Augmentation of biochar in anaerobic digestion

Jessica Quintana Najera

Submitted in accordance with the requirements for the degree of Doctor of Philosophy

School of Chemical and Process Engineering

University of Leeds

January 2022

To my mother,

For her unconditional love, support, and her dedicated partnership
for success in my life.

Declaration

The candidate confirms that the work submitted is her own and that appropriate credit has been given where reference has been made to the work of others.

Publications

J Quintana-Najera, AJ Blacker, LA Fletcher, AB Ross (2021) The effect of augmentation of biochar and hydrochar in anaerobic digestion of a model substrate. Bioresource Technology 321, 124494.

J Quintana-Najera, AJ Blacker, LA Fletcher, AB Ross (2022) Influence of augmentation of biochar during anaerobic co-digestion of *Chlorella vulgaris* and cellulose. Bioresource Technology 343, 126086.

J Quintana-Najera, AJ Blacker, LA Fletcher, DG Bray, AB Ross (2022) The influence of biochar augmentation and digestion conditions on the anaerobic digestion of water hyacinth. Energies 15,2524.

Acknowledgements

I would like to thank the University of Leeds for the opportunity given to me for becoming a researcher and a Doctor of Philosophy. A most grateful acknowledgement to my supervisors Dr Andrew Ross, Prof John Blacker and Dr Louise Fletcher for their continuous guidance and support. I would like to thank the Energy research group Iram Razaq, Oliver Grasham, James Hammerton, Poppy Cooney, Douglas Bray, Yahaya Umar and Jeanine Williams for their friendship and support. I would like to express my greatest appreciation to Aaron Brown for his friendship and for always being there to provide me with support and guidance. Special thanks to my dear friends Ramon Quiñonez Arce, Daisy Thomas, and Katy Honour whose gracious self, filled the days with joy. I would like to thank the friends of the Energy Building Richard Birley, Nicola Wood, Flora Brocza, Scott Prichard, Andy Price and Charlotte Weaver.

Special thanks to the laboratory leaders, technicians, and staff at the School of Chemical and Process Engineering who always helped me carry out my work, Ed Woodhouse, Karine Alves Thorne, Ben Douglas, Simon Lloyd, and Andrew Britton. Also, by the technicians at the School of Civil Engineering Emma Tidswell, David Elliot, and Morgan McGowan. I would also like to thank Sean Scully and Eva Ingvadottir for graciously receiving me during my placement at the University of Akureyri.

I am most grateful to my country, Mexico, for allowing me to become a PhD researcher. I am very appreciative of the funding provided by the Mexican Council for Science and Technology and the Secretary of Energy (CONACYT-SENER). Also, the funding provided by my alma mater, the Autonomous University of Sinaloa. I would like to thank the Biotechnology and Biological Sciences Research Council (BBSRC) for the BEFWAM project.

I would like to thank my family, the people I love the most. To my mom Luz Elvia Najera Chavez for her endless love, and encouragement to move abroad and follow a career as a researcher, I hope that she is proud of me. To my sister Ana Lucía Quintana Najera and brother Manuel Iván Quintana Najera, for their love, support and for always being there for me. I would also like to thank my mother-in-law, Soila Gaxiola, for always supporting our endeavours.

To my husband, Jaime Eleazar Borbolla Gaxiola, who has been by my side since we were nineteen years old. For his support, encouragement, love and for moving to the other side of the world with me to pursue our dreams. We became adults and now researchers together, and hopefully will continue to become so much more.

Abstract

The augmentation of carbonaceous adsorbent materials, such as biochar and hydrochar, in anaerobic digestion (AD), provides several advantages. The benefits of these materials are attributed to specific material properties, such as porosity, surface area, alkalinity, and the presence of surface functional groups. Biochar can thus adsorb metabolites, provide a buffering effect, act as a support for the immobilisation of cells, and work as an intermediary for direct interspecies electron transfer (DIET) mechanisms. A primary advantage of AD technology is the possibility to use a large variety of biomass substrates, however, the complexity of the biomass often compromises the effectiveness of the microbial community, and in consequence biomethane production. Biochar augmentation is a prospective option for overcoming some of the inherent limitations observed in AD while improving the efficiency and stability of the digester.

This area of research is gaining significant interest since the implementation of a low cost sustainable material for stabilising and improving AD is considered to have huge economic benefits. The efforts in the scientific community have focussed on using biochars generated from different feedstocks, produced under a range of conditions, and augmentation with AD of different substrates operating under different conditions, thereby exhibiting diverse outcomes. Even though the general trend is for biochar to improve AD performance, there are contradictory results that create a certain ambiguity. Therefore, it is crucial to determine the most important variables and mechanisms involved in biochar augmentation.

In this work, biochar and hydrochar materials were produced and thoroughly characterised to correlate their final properties with feedstock composition, and the pyrolysis and hydrothermal carbonisation (HTC) conditions employed for their production. This research sets out to investigate the effect of biochar and hydrochar during the AD of both model and complex substrate, and to develop correlations between their performance and properties. Oak wood and water hyacinth biochars produced at intermediate temperatures improved biomethane production from cellulose, resulting in a doubling of methane production rate, while higher-temperature biochars have no significant effect on AD. The presence of oxygenated functional groups (OFGs) proved to be the most important feature for biochar amendment in AD. Conversely, seaweed biochars

and hydrochars from all feedstocks exhibited an unfavourable effect on methane production, attributed to the presence of toxic or inhibitory by-products.

Design of experiment (DOE) and optimisation was employed for investigating complex feedstocks during the digestion of water hyacinth and co-digestion of *Chlorella vulgaris* and cellulose. The variables of the study included biochar load, inoculum to substrate ratio (ISR), and C/N ratio. The findings indicate that biochar amendment is more beneficial under stressful conditions, such as low ISR, and unfavourable C/N ratios. Small amounts of biochar (up to 0.6 % of a volume basis) are sufficient for providing the mentioned benefits, whereas higher doses are shown to be detrimental to the process.

Furthermore, the effect of biochar augmentation in AD resulting from this work in combination with a vast compilation of literature reports was evaluated by principal component analysis (PCA). The PCA agreed with the experimental results generated in this work and established that the biochar must possess a large availability of OFGs, and low ash content. This could be achieved by selecting low ash feedstock, most likely derived from woody biomass, and treated by slow pyrolysis at intermediate temperatures (450-550 °C). The PCA indicated that BC augmentation was more favourable for complex substrates and stressful conditions, such as low ISR. The results also suggest that all the mentioned benefits were subject to an appropriate biochar dosage ranging from 0.4 to 0.6 % (w/v). The integration of biochar and AD is shown to be an important approach for improving the biotransformation efficiency of biomass into biomethane. To help bridge the gap between these heterogeneous and complex technologies, the outcome of this work is to provide an understanding of the most important factors influencing biochar augmentation. This is of great relevance since such knowledge could guide the application and further development of biochar augmentation in AD in the future.

Table of contents

List of tables

List of figures

List of abbreviations

Å	Angstrom unit
AC	Activated carbon
AcoD	Anaerobic co-digestion
AD	Anaerobic digestion
AFBR	Anaerobic fluidised bed reactor
AFOLU	Agriculture, forestry and other land use
AMPTS	Automatic Methane Potential Test System
ANOVA	Analysis of variance
APBR	Anaerobic packed bed reactor
AS	Anaerobic sludge
ATR	Attenuated total reflectance
BC	Biochar
BD	Biodegradability
BET	Brunauer-Emmett-Teller
BMP	Biochemical methane potential
CAB	Control-alginate beads
CEC	Cation exchange capacity
CHP	Combined heat and power
CM	Conductive material
CMISR	Continuous mixed immobilised sludge reactor
CNTs	Carbon nanotubes
CoA	Coenzyme A
CSTR	Continuous-stirred tank reactor
DFT	Density functional theory
DIET	Direct interspecies electron transfer
FA	Factor analysis
FC	Fixed carbon
FDH	Formate dehydrogenase
FHL	Formate hydrogen lyase
FID	Flame ionisation detector
FS	Fucus serratus
FTIR	Fourier transform infrared spectroscopy
GAC	Granular activated carbon

GC	Gas chromatography
GHG	Greenhouse gases
GtCO$_2$eq	Giga-tons carbon dioxide equivalent
HC	Hydrochar
HMF	Hydroxyl-methyl-furfural
HHT	Highest heating temperature
HRT	Hydraulic retention time
HTC	Hydrothermal carbonisation
IBI	International Biochar Initiative
ID	Internal diameter
IET	Interspecies electron transfer
ISR	Inoculum to substrate ration
k	Reaction rate coefficient
LCB	Lignocellulosic biomass
MSW	Municipal solid wastes
Mtoe	Million tonnes of oil equivalent
N-5	Pyrrolic nitrogen
N-6	Pyridinic nitrogen
N-Q	Quaternary nitrogen
N-X	Oxide nitrogen
NADH	Nicotinamide adenine dinucleotide
NAP	Near ambient pressure
NFGs	Nitrogen functional groups
NLDFT	Nonlocal density functional theory
OFMSW	Organic fraction of municipal solid waste
OFGs	Oxygen functional groups
OLR	Organic loading rate
OW	Oak wood
PAC	Powdered activated carbon
PCA	Principal component analysis
pH	Potential of hydrogen
PID	Proportional integral derivative
PSD	Pore size distribution
PV	Pore volume
PW	Process water

SA	Surface area
SCFA	Short chain fatty acid
SD	Sustainable development
SEM	Scanning electron microscopy
SS	Solvent soluble
SW	Saw wrack
TAN	Total ammonium nitrogen
TCD	Thermal conductivity detector
TGA	Thermogravimetric analyser
TOC	Total organic carbon
TS	Total solids
UASB	Up flow anaerobic sludge blanket
UHV	Ultra-high vacuum
VFA	Volatile fatty acid
VM	Volatile matter
VS	Volatile solids
WDXRF	Wavelength dispersive X-ray fluorescence
WH	Water hyacinth
WS	Water soluble
WSIS	Water solvent insoluble
WSS	Water solvent soluble
WV	Working volume
WWT	Wastewater treatment
XPS	X-ray photoelectron spectroscopy
XRF	X-ray fluorescence

Chapter I

Introduction

1.1   Background and justification

1.1.1 Climate change and sustainability

The productive systems for goods and energy require fundamental transformations to mitigate climate change and decelerate global warming. Human activity is responsible for the unprecedented increase in greenhouse gas (GHG) emissions, principally due to the burning of fossil fuels for electricity, heat, and transport. GHG allows the trapping of heat in the atmosphere, contributing to global warming. The composition of GHG are carbon dioxide 80 %, methane 10 %, nitrous oxide 7 % and fluorinated gases 3 % [1]. Since 1750, the concentration of CO_2, CH_4 and N_2O have increased by 47, 156 and 23 %, respectively. Global GHG emissions are continually increasing since 1970 due to globalisation. In 2019, GHG emissions reached an annual average of 410 parts per million (ppm) of CO_2, 1866 parts per billion (ppb) of CH_4 and 332 ppb of N_2O. The global surface temperature increased by 0.99 °C during 2001-2020, in comparison to the temperature maintained during 1850-1900. This value exceeded by 0.19 °C the estimated in 2014 due to further global warming. Energy production is the greatest contributor to emissions, principally in the electricity generation sector. If no actions are undertaken to mitigate climate change, it is predicted for the global mean surface temperature to increase by 3.7-4.8 °C compared to pre-industrial levels. Climate change within this drastic scenario could change rainfall patterns and increase sea levels, resulting in a greater risk of heatwaves, floods, droughts and fires [2].

Fossil fuel combustion was accountable for 78 % of the total GHG emission by 2010 with a tendency to increase by 1-2 % annually. Five countries account for half of the global emissions, including China, the USA, India, Japan, and Russia in order of consumption. These upper-middle-income countries exhibit an increasing trend toward GHG emissions. A large fraction of the intensive global industrialisation is directed to the creation of goods for fulfilling the needs of the

world, mainly the high middle-income countries [3]. The above contributed to the global 'material footprint' increasing by 70 % between 2000 and 2017 [4].

In 2020 more than 119 million people were pushed back into extreme poverty due to the pandemic crisis. The global economic slowdown was not reflected in reducing GHG emissions, thereby the imminent climate and financial crisis challenge the world, especially in lower-income countries. The share of total final renewable energy increased from 16.4 % in 2010 to 17.1 % in 2019. Although 2.6 billion people still use dangerous and inefficient cooking systems and 759 million people lack access to electricity. From the total final energy consumption by 2019, the share of renewable energy for the electricity, heat and transport sectors only accounted for 25.4, 9.2 and 3.4 %, respectively. There is an urgency to accelerate the development of renewable energy, especially in the heating and transport sectors [4].

The United Nations Framework Convention on Climate Change (UNFCCC) is the main international forum for climate negotiations. At the UNFCCC, the international community has committed under the Kyoto Protocol targets to reduce emissions. In addition, the Copenhagen and Cancún agreements established mitigation actions to limit the global temperature to an increase of 2 °C above the pre-industrial levels. The UNFCCC pursuits global efforts to limit the temperature increase up to 1.5 °C [2]. Mitigating climate change is non-excludable, meaning that every nation, institution and individual must cooperate in its pursuit [5].

Nonetheless, the world is off-track to meeting the targets and reaching the goals for sustainable development (SD) [4]. SD is defined as 'development that meets the needs of the present without compromising the ability of future generations to meet their own needs' [3]. Economies must shift towards carbon neutrality, thereby further structural transformations to strengthen social security, increasing investment in research and technology, improving the economic development of lower-income countries, and investing in sustainable industry and clean energy are key for the SD. A multilateral system for the implementation of a coherent global response requires the participation of all sectors of society, including Governments, academia, private sectors and the civil population [4].

Drastic changes in energy production and utilisation are necessary to counteract climate change. Sustainable energy services must have a low environmental impact while ensuring the essential goods and services for all societies. Equity is one of the greatest challenges of humanity since it emphasizes the just distribution of goods across all countries and within generations. Equity

between powerful and deprived countries, equity between current and future generations to reach similar levels of well-being, equality before law, interests, income, and wealth. Therefore, sustainable social and economic approaches for assuring affordable and sustainable energy services are necessary for achieving prosperity and preventing climate change [6].

The transition towards renewable energy (RE) and reduction of fossil fuel dependency is one necessary approach for mitigating climate change. RE consist of any form of energy obtained from biological, solar, or geophysical sources. For RE to be sustainable, they must be affordable over the long-term, not increase GHG emissions, affect food security, and require excessive amounts of water or chemical that could threaten biodiversity [6]. RE accounted for 6.3 % of the total energy supply by 2019 (**Figure 1.1**) [7]. However, renewable power needs to grow by 7 % annually to meet the SD mitigation scenario established for 2030 (**Figure 1.2**) [8]. It is worth mentioning that since the start of the Covid-19 pandemic in 2020, the equity performance of RE has remained resilient due to supportive strategic policies. The decline in energy demand due to movement restrictions, lockdown and economic slowdown had a minor impact on RE while affecting other fossil-dependent sectors [9].
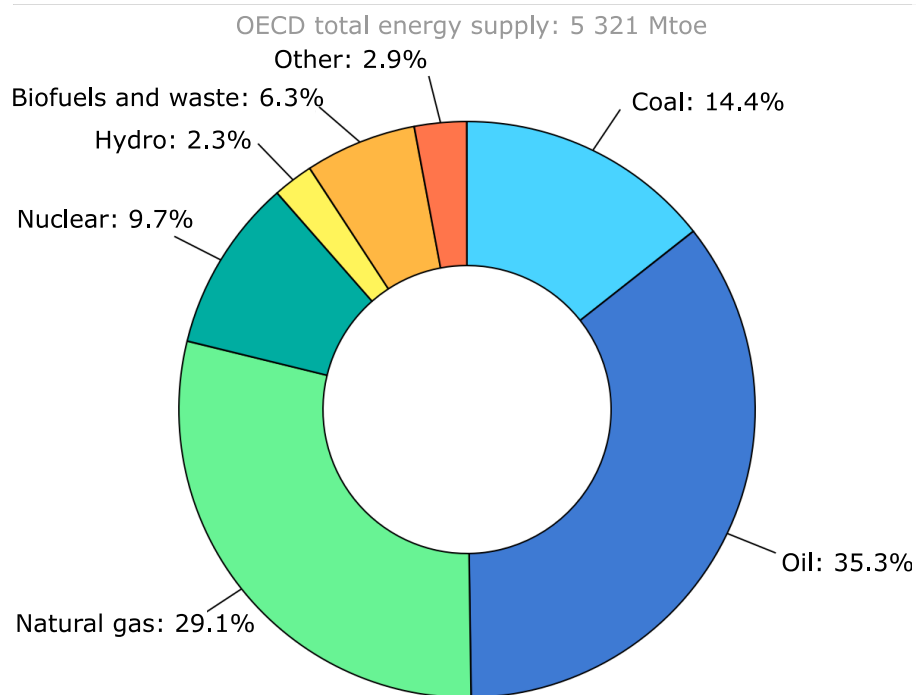
Figure 1.1. OECD total energy supply by source according to IEA [7].
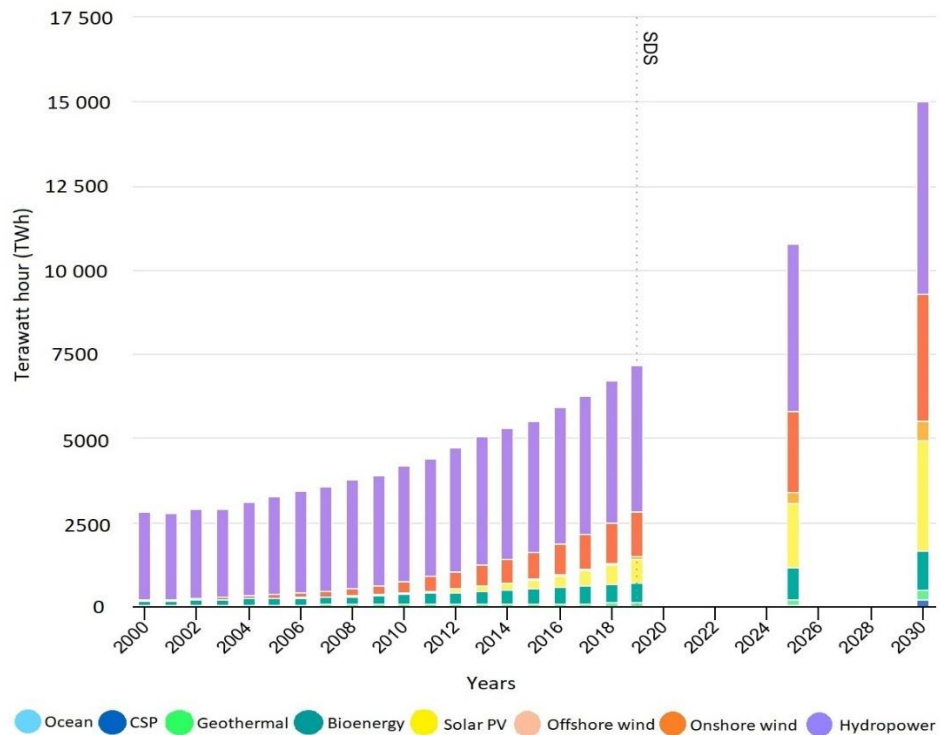
Figure 1.2. Renewable power generation by technology for 2030 sustainable development scenario (SDS) according to IEA [8].

Several strategies have been proposed to reduce GHG emissions. To start, fossil fuels will continue to be the main source of energy in the near future. Thus, it is necessary to improve the efficiency of fossil fuel plants. At the same time, the development of power capacity from sustainable options must be supported by all countries, according to their necessities and availability of resources. The increasing development of RE could help with the always increasing energy demand while consistently reducing fossil dependency. The more supported options are associated with increasing electricity generation from renewable sources, including wind, solar, hydro, geothermal and biofuels [1]. These sources are called 'renewable' because the energy from the sun, wind, rivers flow and growing plants are naturally replenished. **Figure 1.2** shows hydropower as the largest source of renewable electricity, followed by the continuous growth of onshore wind and solar PV. The bioenergy from biomass sources has a substantially smaller contribution, with modest but stable growth. The IEA main case scenario expects an increase in renewable electricity, with a forecast share of 33 % by 2025 [10]. From the RE sources, biomass has a large and continuous availability and can employ different technologies for energy generation, including combustion, gasification, pyrolysis, and anaerobic digestion. In the last two decades, the efforts for developing technologies for the efficient production

of biofuels from renewable biomass sources have grown greatly [11]. The most important fuels produced from the fermentation of renewable biomass are ethanol, butanol, methane and hydrogen [12]. However, the industrial production of these biofuels has still many challenges to overcome to be economically competitive. Nonetheless, the technological research and political actions for biofuels are boosting the continually growing global production.

1.1.2 Gaseous biofuels

The production and use of biogas from organic waste embody the concept of a circular economy by improving waste management, resource efficiency and reducing GHG emissions. The development of biogas into a sustainable energy future fluctuates among countries since it depends on a myriad of factors, including feedstock availability, prevailing market conditions and policy priorities. The current production of biogas and biomethane is led by Europe, the United States and China (**Figure 1.3**). European biogas industry capacity. There is a large availability of sustainable feedstocks for producing biogas, including municipal solid waste, wastewater, agricultural waste, and animal manure. Initially, energy crops were the feedstock employed for feeding biogas plants but the changes in policies are pointing towards outcrop residues, livestock waste and the direct capture of methane at landfill sites [13].
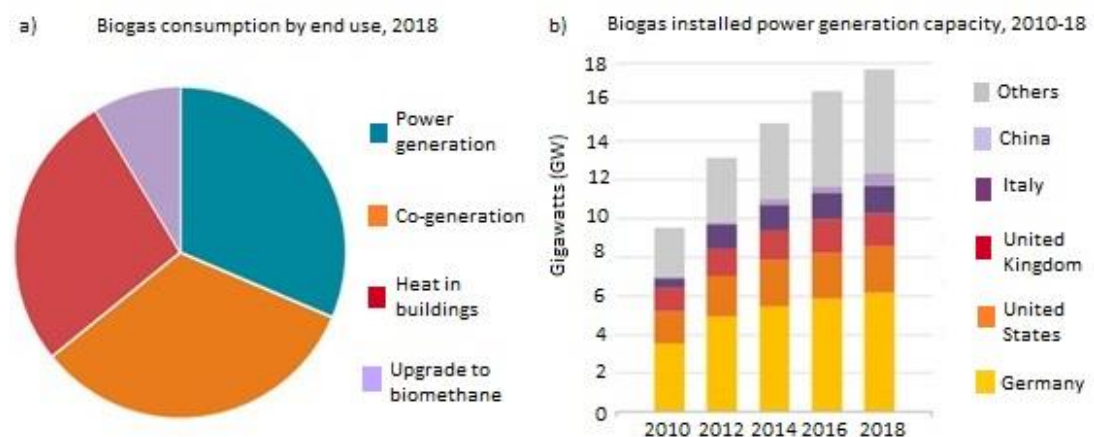
Figure 1.3. Worldwide biogas according to the IEA [13]: a) biogas consumption by use; b) biogas installed power generation capacity.

The policies of China are supporting the installation of household digesters in rural areas, which count for around 70 % of their entire biogas capacity. They have announced the push of policies for the construction of large-scale biogas

plants for producing both heat and power. In addition, the upgrading of biogas and the addition of biomethane into the transport sector [13]. The development of the biogas industry in China increased by 43 % between 2009 and 2015. This dramatic rise involved both large-scale biogas plants and a centralised biogas supply for households. Cities are benefited from the creation of thousands of small, medium, large, and industrial biogas digesters integrated into natural gas pipe networks. Rural biogas production in small biogas plants and household-based digesters represents a large fraction of the energy supply in rural areas [14]. For the United States, 90 % of the current biogas is produced at landfill sites and just as China, they are pushing for the implementation of biomethane into the transport sector. Biogas could contribute to the energy demand resulting from the rapid urbanisation, economic growth, and expansion of the energy demand. However, biogas production and efficiency continue to be challenged due to undeveloped technologies and industries. Thus, the expansion of biogas and biomethane production will require coordination in the policymaking between the energy, transport, agriculture, environment and waste management sectors [13].

Since 2010, the installed biogas power generation capacity has been growing by 4 % annually. However, biogas and biomethane still represent only 0.3 % of the total primary energy demand. The biogas and biomethane production in 2018 was 35 million tonnes of oil equivalent (Mtoe). Almost two-thirds were used for electricity and heat, the other 30 % was used for household heating and cooking and the remaining was upgraded to biomethane. Nevertheless, if the full potential of biogas and biomethane were achieved, it would be possible to fulfil 20 % of the worldwide gas demand [13]. Pure biomethane can be obtained by upgrading biogas from anaerobic digestion or gasification of biomass. The percentage of biogas upgraded into biomethane varies worldwide, with values of 15, 35, 10 and 2 % for North America, South America, Europe, and Asia, respectively. The upgrading and use of biomethane provide great benefits in the reduction of GHG emissions by giving use to the biomass that otherwise would decompose and release further GHG. Whereas carbon dioxide, the main co-product of biogas upgrading, can be further combined with hydrogen to yield additional methane, or it can be stored underground for achieving a CO_2-negative source of energy [13].

One of the main benefits of biomethane towards a path to a sustainable and low-emissions future is its compatibility with the current gas infrastructure. The biomethane can be transported in the existing pipelines and be further distributed. Currently, biomethane represents only 0.1% of natural gas demand,

however, recent policy changes towards decarbonising transport are supporting its injection into natural gas grids. Even though the production of biomethane is more costly than natural gas, the price gap is expected to narrow over time along with technological development and the rise of natural gas costs due to fossil fuel depletion. A growth in biomethane production during the 2020´s decade is expected with the following distribution: 60 % of the biomethane will be injected into the current gas distribution networks, 20 % as a vehicle fuel and the remaining will be destined for different local uses. A further raise in biomethane production is expected by 2030 and even more by 2040 (**Figure 1.4**) [13].
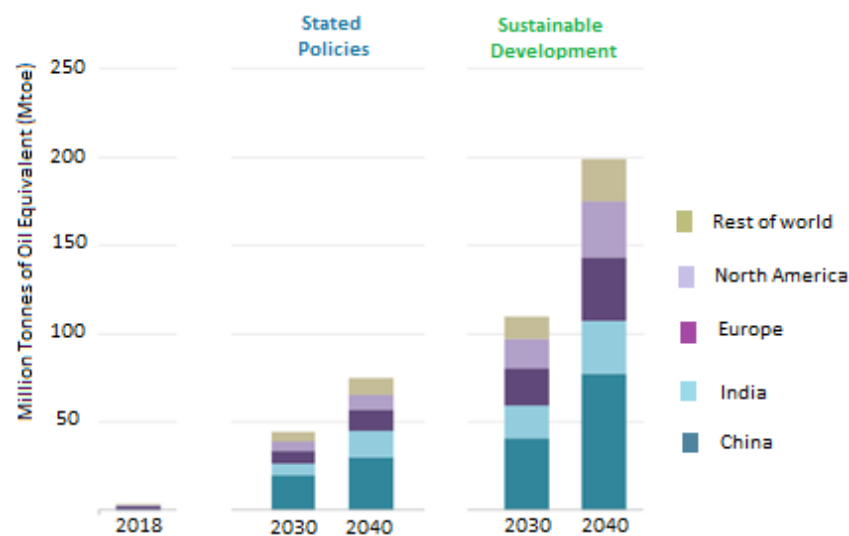
Figure 1.4. Outlook for global consumption of biomethane according to IEA [13].

1 Mtoe=11.63 TWh=1.21 bcm-equivalent of natural gas

1.1.3 Integration of different technologies

One approach for improving the biotransformation efficiency of the feedstocks into biofuels and other high-value chemicals is the integration of different technologies. Hybrid processes combining biochemical (AD) and thermochemical (pyrolysis and HTC) technologies for the management of wastes and production of goods are reported to enhance efficiency and conversion stability [14,15].

For biochemical technologies, AD is designed for the sustainable management of a wide variety of wastes and the production of biogas (methane and carbon dioxide) and digestate. The biogas is usually destined for heat, steam, and electricity, while the digestate is employed as fertiliser in agriculture. AD is a

robust and largely established technology, although, given its complexity, it continues to face challenges. The operational instability of the process represents a major problem for AD as inhibitory compounds present on the organic feedstocks or produced during their hydrolysis detriment the process yields [16,17]. Hence, AD still requires gradual technological changes for increasing the yields and economic feasibility. Several approaches proposed for improving AD performance, include genetic engineering for improving bacterial strains, product purification, integration with other technologies, and addition of adsorptive materials for amendment and/or immobilisation of cells. Further research is necessary for ensuring a breakthrough in material design for additives, process optimisation, separation membranes, process amendment, and reactor design. These improvements are necessary for the development of this biochemical technology while achieving economic feasibility [18].

For the thermochemical conversion technologies, pyrolysis consists of the decomposition of biomass in non-oxidative conditions and high temperatures. Pyrolysis is a mature and developed technology for the transformation of biomass into energy products (biochar, bio-oil, and bio-syngas). In contrast, HTC involves the processing of biomass in water at sub-critical conditions, usually between 180 and 250 °C. This results in the production of a carbonaceous solid called 'hydrochar', a gaseous phase, and a liquid phase also known as 'process water' [19].

These thermochemical technologies are considered promising options for the generation of energy, fuels, chemicals, and functional char materials. Two types of chars are outlined in this project, biochar (BC) and hydrochar (HC). For this work, the term 'char' is used to refer to both biochar and hydrochar. The chars offer a wide range of applications, including soil amendment, bioenergy, bioremediation of soils, use as a carbon sink, and use as adsorbents or catalyst supports. Recently, given their physicochemical and structural properties, chars are considered a promising adsorbent and amendment additive for AD [20]. These properties could donate the chars the capacity to act as support materials for the immobilisation of cells and enzymes. The latter is an underdeveloped but promising research area [21].

The integration of different products of thermochemical technologies with AD has been suggested to enhance efficiency, stability, and economic feasibility. Reports of different approaches for coupling thermochemical biomass conversion and AD for enhancing energy performance and digestate quality can be placed within four categories. Category 1, adding char in the AD reactor

stabilises the biological processes and enhances the retention capacity of the digestate. Category 2, employing the AD digestate as a feedstock for thermochemical treatment. Category 3, using the aqueous phase from the thermochemical processes as a feedstock for AD. Category 4, high recovery and reuse by thermochemical treatment of the digestate and application of the solid and liquid products as stabiliser and feedstock for AD [22]. Even though all these approaches have shown great potential, this work is focused on category 1. The addition of chars in the digesters with the principal objective to improve AD stability and performance.

Several additives and immobilisation supports can be applied for AD. Although the use of chars has a growing interest due to their low-cost, sustainable origin and physicochemical properties [23]. The advantageous properties of the chars include inertness, porosity, high surface area, and high content of functional groups [21,24–26]. It has been suggested that the oxygenated functional groups (OFGs) from the surface of the chars could promote electrostatic interactions that lead to greater interaction, adsorption and immobilisation performance [27]. The latter could benefit the syntrophic and fermentative performance during AD. In effect, several publications have emphasised the positive effects of char addition in AD. Among the most relevant observations are the mitigation of ammonia inhibition [17], promotion of archaea growth, and increase in methane yield and productivity [28]. Thus, the generation of knowledge regarding the pyrolysis and HTC parameters on the properties of the char products and their potential as additives in AD are promising areas of research [29].

1.2 Research gap

Given the nature of the thermochemical processes, the properties of BC and HC differ significantly, broadening the portfolio of potential applications. There is a direct relationship between the treatment temperature, feedstock composition and the final physical, chemical and physicochemical properties of the chars [25,30]. Hence, to optimise and exploit the desired properties of biochar it is necessary to understand, control and combine the factors affecting them [31]. Several studies have investigated the influence of the feedstock and processing conditions on the final properties of the chars [32]. However, the information available about the control of these conditions and the performance of the char is mostly related to their application in soil amendment and pollutant removal. Hence, the study of the relation between the processing conditions, the properties of the BC and HC, and their potential as a support material is an

important area of research for the integration of 'designed' materials in biotechnological processes.

In the last couple of years, numerous publications searching for the potential of biochar as an amendment additive in AD have emerged [33–39]. It is important to comment on this trend since at the time this research project was proposed, there were only a few initial reports. This intense attention that has been given to the subject supports the pertinence of integrating char products in fermentative technologies. Nonetheless, there is no established protocol for integrating chars in AD, and the extent of the effect of the chars in AD varies largely. There is a gap in knowledge between the influence of the char properties and their effect in AD. Hence, this work aims to contribute to linking the char properties and their potential application to AD.

1.3 Aims and objectives

The overall aim of this research is to determine the potential for augmentation of biochar, produced by pyrolysis, and hydrochar, produced by hydrothermal carbonisation, to be used as an amendment support material for improving the digestion of different substrates during anaerobic digestion. In particular, it aims to provide a better understanding of the property function relationships of different biochar and hydrochar when used as additives in AD. How the production route affects the properties of the chars and understanding how the properties of the different materials influence their behaviour when augmented with different substrates, under different fermentation conditions. Using a combination of experimental studies and statistical analysis, this research aims to gain the necessary insight to understand the potential of augmentation of carbonaceous chars into fermentative AD technology as outlined in **Figure 1.5**. This research also aims to create recommendations to realise the development of this novel and complex field. These aims have been facilitated by the following specific objectives:

1. Perform an extensive literature review of the behaviour of biochar and hydrochar during anaerobic digestion to cover Chapters 2 and 7. This will be done by carrying out a literature review of previous works and more published throughout this PhD project on biochar addition in anaerobic digestion.

2. Develop a quantitative understanding of the impact of processing conditions and feedstock choice on the final properties of biochar and hydrochar. This allows detailed property function relationships to be

investigated under different fermentation conditions and provides data for the correlation of their impact when applied in anaerobic digestion. This will be achieved through the production of biochars and hydrochars from different feedstocks and treatment temperatures, followed by the detailed characterisation of the chemical, physical and functional properties of the chars using a range of characterisation methods. This information is described in Chapter 4.

3. Perform an experimental assessment of the potential of the produced biochar and hydrochar for use as amendment additives and immobilisation supports for supporting the anaerobic digestion of the model substrate cellulose in batch digesters. The results from these experiments would allow the correlation of the properties of the chars with their impact on methane generation and digestion performance. This objective would cover Chapter 5.

4. Perform an experimental assessment of the potential of selected chars with optimum properties as amendment additives for the anaerobic mono and co-digestion of complex substrates. This will be achieved by using factorial design of experiments approaches to evaluate and optimise the effect of the selected biochar on anaerobic digestion behaviour, such as methane generation, lag time and production rate, and identify optimum digestion conditions via the design of experiments. The experiments and results from this objective would cover Chapter 6.

5. Establish the main factors influencing the behaviour and benefits of using biochar additives during anaerobic digestion by undertaking an extensive principal component analysis of both the experimental data produced in this work, in combination with data published in the literature. This will allow the identification of the most relevant biochar properties and fermentation conditions influencing the anaerobic digestion performance through the kinetic variables of final and maximum methane yield, methane production rate and lag phase. The findings of this objective would cover Chapter 7.
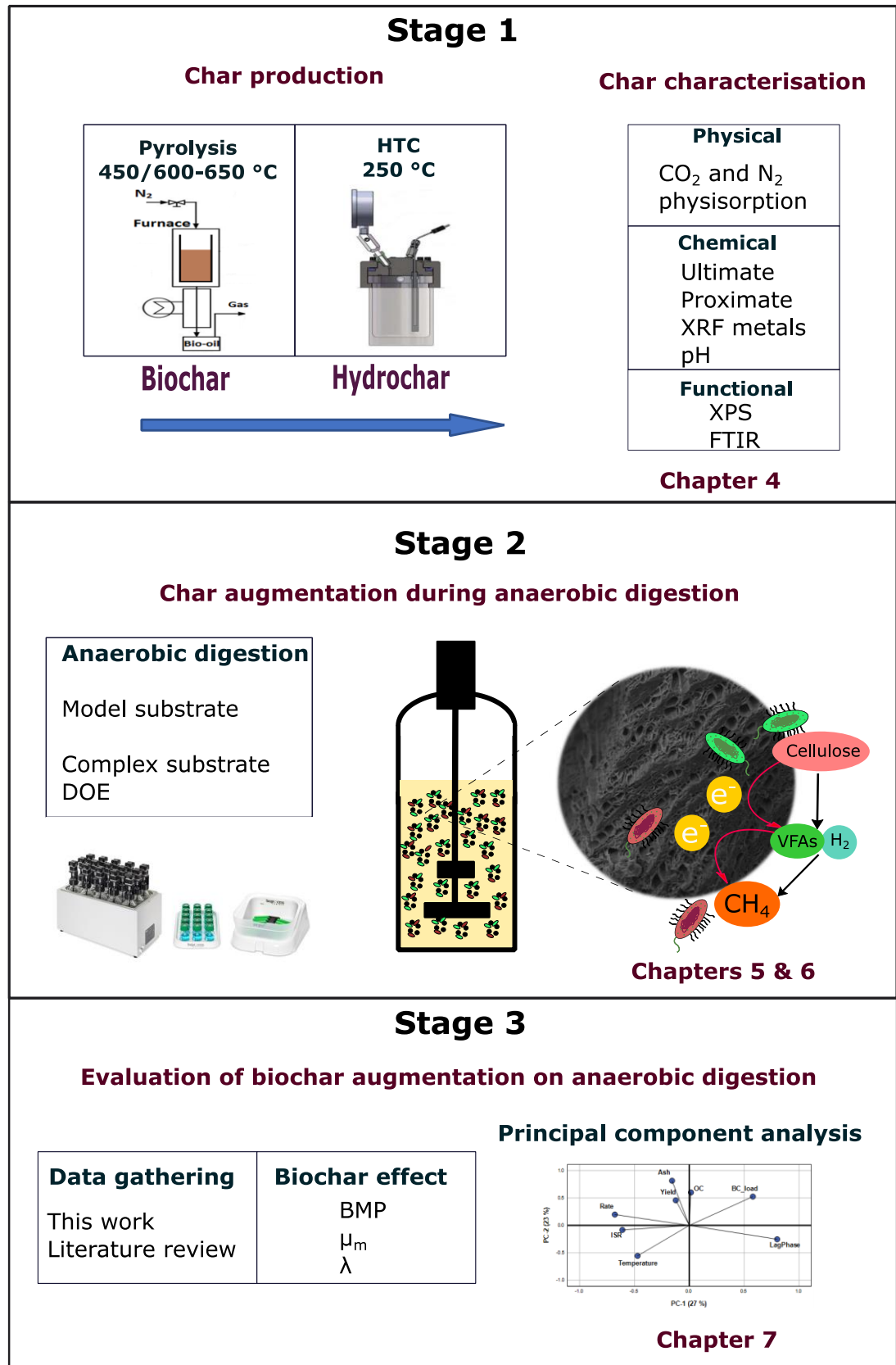
Figure 1.5. Outline of the experiments and analysis performed during this PhD research.

1.4 Thesis plan

A general description of each chapter is detailed for outlining the thesis content and facilitating the connection between them.

Chapter I. Introduction – establishes the background of climate change and energy security. It is within the mitigation of these problems that this project finds a niche, purpose, and importance. The aims, objectives and outline of the thesis structure are also here described.

Chapter II. Literature review – conceptualises the potential of the gaseous biofuel methane for mitigating climate change, while describing the principles of anaerobic digestion. The challenges of this technology are also established, with a focus on the potential of char amendment on anaerobic digestion. This chapter also details the technologies for thermochemical degradation of biomass, pyrolysis, and hydrothermal carbonisation. The influence of the thermochemical conditions over the reaction pathways and the properties of biochar and hydrochars are emphasized. This chapter covered Objective 1.

Chapter III. Materials and methods – the materials and methods used throughout the project are here described. This chapter is divided into three stages for facilitating the connection with further result chapters. (i) describes the materials and conditions used for thermochemical processing of biomass, and the methods used for characterising the chars. (ii) describes the materials, equipment and conditions used for anaerobic digestion. It states the conditions for char addition to anaerobic digestion and the design of experiments. (iii) outlines the statistical methods used for comparing the results originating from this work with literature reports regarding the role of biochar addition in anaerobic digestion.

Chapter IV. Characterisation of biochar and hydrochar – describes the chemical, physical and functional characteristics of the untreated biomass, and resulting biochar and hydrochar materials. Discusses these properties based on the differences in feedstock composition and processing conditions, principally thermochemical treatment - pyrolysis and hydrothermal carbonisation - and processing temperature, covering Objective 2.

Chapter V. Char and hydrochar augmentation on anaerobic digestion of model substrate – explores the effect of biochar, hydrochar and magnesium activated biochar addition on methane yields and kinetic parameters during the digestion of cellulose. Briefly describes the ability of the chars to act as

immobilisation supports via adsorption. This chapter focuses on Objective 3 of the thesis.

Chapter VI. Biochar augmentation on anaerobic digestion of complex substrate – biochar selected based on Chapter V findings is further used for the digestion of complex substrates: (i) anaerobic co-digestion of microalgae and cellulose, (ii) anaerobic digestion of water hyacinth. Design of experiments is used for evaluating the effect of biochar and establishing optimum digestion conditions, covering Objective 4.

Chapter VII. Principal component analysis of biochar augmentation on anaerobic digestion - compiles the publications of biochar addition in anaerobic digestion found in the literature in addition to the results obtained in previous chapters. This chapter evaluates the effect of biochar in anaerobic digestion and the main factors influencing methane generation via descriptive statistics and principal component analysis. This chapter covers Objectives 1, 2 and 5.

Chapter VIII. Conclusions – synthesises the results and key findings revisiting the established aims and objectives. Discusses the limitations of the project and outline recommendations for future work.

Chapter II

Literature review

2.1 Biofuels

The current energy demand is provided mainly by fossil fuels, whereas only 10 % is produced as bioenergy in the gaseous, liquid, and solid forms. Of all the bioenergy demand, biogas account for less than 3 %, liquid biofuels mainly bioethanol 7 %, and solid biomass for the remaining 90 %. There is a great interest in the development of clean technologies for the exploitation of biomass feedstocks for reducing the dependency on fossil fuels and achieving sustainable production of biofuels and valuable chemicals [40]. The industrial production of biofuels is an important sector for both developing and industrialised countries.

 The biofuels can be classified according to the biomass employed for their production as a first, second and third-generation biofuel (**Table 2.1**). First-generation biofuels are usually produced by conventional fermentation technologies using mainly grains like wheat for bioethanol and sunflower seeds for biodiesel. Bioethanol is produced mainly from starch and sugar food crops, although, lignocellulosic biomass is considered a potential long-term alternative [41]. Biobutanol is produced during the acetone-butanol-ethanol (ABE) fermentation mainly of corn, rice, and barley. Biobutanol is considered a superior liquid biofuel to bioethanol because it possesses better fuel properties and higher energy content [42]. The transesterification of vegetable oils and animal fats produced biodiesel, which is comprised of fatty acids formed by glycerol and three organic acids of varied length (4-30 C atoms). Biodiesel has a higher cetane number than diesel, representing an increased power output, and reduced exhaust smoke. The combustion of biodiesel also produces less sulphur, unsaturated fatty acids, emission of polycyclic aromatic hydrocarbons and other pollutants than conventional diesel. Second and third generation biofuels employ non-food substrates and are considered advanced biofuels. The use of non-edible oily crops (e.g., jatropha, tail oil, and silk cotton tree) and algae for producing biodiesel via transesterification have been extensively studied [41]. The main advantages of algae are the simplicity of its cultivation, its large oil fraction and conversion efficiency. The use of biofuels has been demonstrated to

reduce GHG emissions and have a positive impact on the environment, however, they still require the development of technologies and policies for their larger application [43].

Table 2.1. Classification of biofuels. Adapted from [41].

Classification	Feedstock	Biofuel
First Generation Biofuels	Starch, sugar, and vegetable oil from seeds and grains	Bioalcohol, biodiesel, biogas, syngas, vegetable oil
Second Generation Biofuels	Non-food crops, agricultural and municipal waste	Bioalcohol, biogas, biomethane, biohydrogen, bio-oil and biodiesel
Third Generation Biofuels	Algae	Biodiesel, vegetable oil

The production of biofuels should have the lowest possible environmental impact. Thus, instead of dedicating food crops for first-generation biofuels, it would be more appropriate to dedicate residual biomass for energy generation. The production of second-generation biofuels from organic residues is considered a promising option, with feedstock, such as agricultural wastes, municipal waste, and energy crops (e.g. miscanthus and switchgrass) [44]. Among the obstacles to the second-generation biofuel production, are the inability of microorganisms to naturally consume the mixture of sugars present on the lignocellulosic biomass (LCB), the low biofuel titres obtained, the complicated hydrolysis pre-treatment of complex feedstocks (e.g., LCB), and the inhibitory effect of the sugars and by-products produced from the pretreatment [45].

2.2 Anaerobic digestion

2.2.1 Fermentation process

Anaerobic digestion (AD) is a technology designed for the sustainable management of waste while producing energy. AD is a biological process taking place in the absence of oxygen where the electron acceptors are carbon dioxide and organic compounds. The digestate comprised of microorganisms degrades the waste or organic matter through a series of reactions to generate energy and valuable products. A great advantage of AD is the ability to use a wide variety of locally available residues as listed in **Table 2.2**. AD converts organic matter into

biogas, an energy-rich and alternative gaseous biofuel, and organic fertiliser (bio-digested slurry) [46]. Biogas is composed principally of methane and carbon dioxide and traces amounts of other compounds (**Table 2.3**). Biogas is usually destined to heat, steam and electricity, or be upgraded to biomethane. The current large-scale AD plants use the biogas principally to produce electricity via combined heat and power (CHP) engines or fuel cells. While the upgraded biomethane can be directly employed as a transportation fuel; or be purified to achieve the natural gas quality for diverse applications [47].

Table 2.2 Organic biowastes employed as feedstocks for anaerobic digestion. Adapted from [46].

Common Feedstocks	Emerging Feedstocks
Wood wastes	Microalgae
Grass, leaves	Seaweed
Agricultural residues	By-products of other bioenergy technologies:
Food industry resides	Syngas
Animal industry residues	Fermentation residues
Organic fraction of municipal solid waste (OFMSW)	Extraction residues
Anaerobic sludge	
Energy crops	

Table 2.3. Composition of biogas produced by anaerobic digestion. Adapted from [47].

Component	Concentration (v/v)
Methane (CH_4)	40-75 %
Carbon dioxide (CO_2)	15-60 %
Water (H_2O)	1-5 %
Nitrogen (N_2)	0-5 %
Hydrogen (H_2)	Traces
Hydrogen sulphide (H_2S)	0-5000 ppm
Oxygen (O_2)	< 2 %
Trace gases	< 2 %
Ammonia	0-500 ppm

The AD of organic matter takes place in anaerobic conditions involving four steps: hydrolysis, acidogenesis, acetogenesis/dehydrogenation, and methanogenesis (**Figure 2.1**). First, during hydrolysis, hydrolytic bacteria degrade the complex insoluble organic matter (e.g., carbohydrates, proteins, lipids, nucleic acids) into simpler soluble compounds [47,48]. Second, the acidogenesis step degrades the hydrolysed soluble compounds into a variety of products, including volatile fatty acids (VFAs), alcohols, H_2, CO_2, H_2S, and other trace molecules. Third, during acetogenesis, the VFAs and alcohols are converted into acetate by acetogenic bacteria. Fourth, during the methanogenesis step, the methane is produced while involving two groups of methanogenic bacteria and archaea: (i) the acetotrophics degrade acetate into CH_4 and CO_2, and (ii) the hydrogenotrophic methanogens consume H_2 to produce CH_4. It is worth noting that all methanogens are capable of consuming H_2 for CH_4 production, whereas there are just a few reports of acetotrophic bacteria, which usually belonged to the *Methanosarcina sp.* genus. [47,48]. Nonetheless, the metabolism of the microorganisms involved in each step is interrelated by balanced syntrophic interactions.
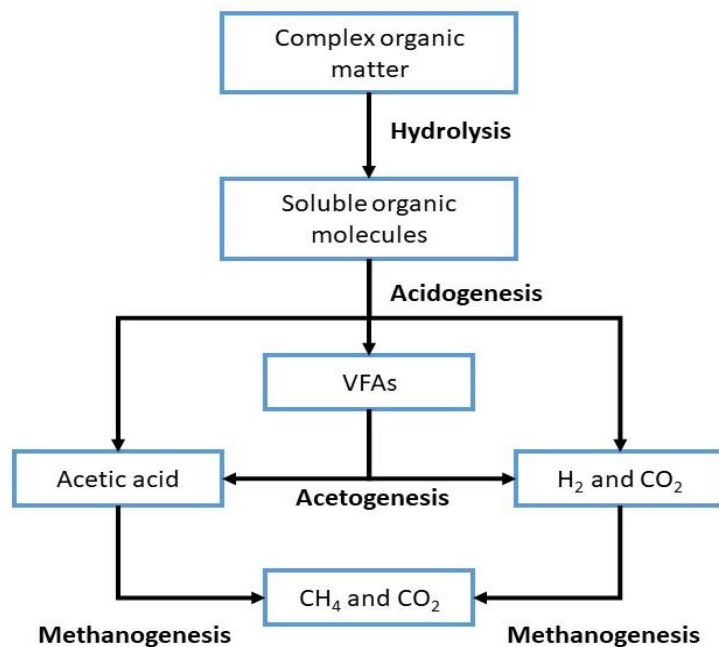
Figure 2.1. Process diagram for anaerobic digestion of organic biomass. Adapted from [47].

During hydrolysis, bacteria produce extracellular enzymes, such as cellulase, cellobiose, xylanase and lipase for transforming organic matter. The hydrolysis

rate is limited by the substrate as the activities of the extracellular enzymes are exposed to bulk factors [49]. A large number of bacteria genera are involved in hydrolysis, including strict anaerobes (e.g., *Clostridium sp.*), and facultative anaerobes (e.g., *Streptococci* and *Enterobacterium*) [47,48]. The hydrolytic bacteria are also involved in acidogenesis where the intermediary soluble compounds are further reduced to VFAs, alcohols, hydrogen, and carbon dioxide. VFAs have six or fewer atoms of carbon and are short-chain fatty acids. Pyruvate works as the pivotal control point from which a series of metabolic pathways can take place as outlined in **Figure 2.2**. The proportions of which metabolic pathway is taken are dependent on the microorganisms, substrate and environmental conditions [50].
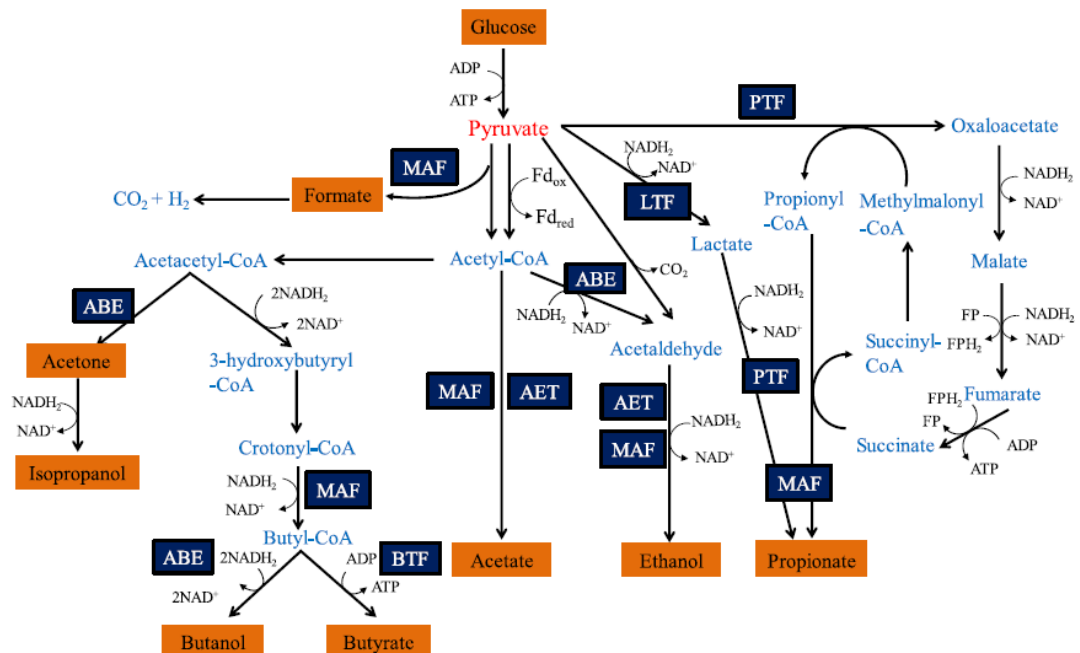
Figure 2.2. Metabolic pathways for acidogenesis. Taken from [50].

(AET, acetate-ethanol type fermentation; ABE, acetone-butanol-ethanol; PTF, propionate-type fermentation; BTF, butyrate-type fermentation; MAF, mixed-acids fermentation; LTF, lactate-type fermentation).

The main VFA precursors for methane production are acetic, followed by butyric acids, and to a lesser extent propionic acid. It has been suggested that 65-95 % of the produced methane comes from the acetic acid pathway. Microorganisms reported producing acetic acid are *Acetobacter, Thermoanaerobacter, Acetomicrobium, Acetothermus* and *Clostridium*. Lesser amounts of propionic acid are usually found in AD since its conversion into methane is

thermodynamically less favourable in comparison to acetate and butyrate. Furthermore, the production of VFAs is dependent on the substrate composition and operating conditions, including bioreactor type and design, pH, temperature, retention time, and organic loading rate (OLR). Temperature is a key parameter for the reactions taking place in AD. For instance, the rise of temperature favours the solubility of carbohydrates and proteins, and consequently their hydrolysis. Although no correlation between temperature and the type of VFA produced is stated [51]. From a kinetic perspective, acidogenesis exhibits a rapid reaction rate, which makes it the quickest step in AD [49]. Acetogenesis accompanies acidogenesis, where VFAs and alcohols are further converted to acetic acid and hydrogen by anaerobic bacteria. However, the pH_2 partial pressure limits acetogenesis since the bacteria involved is inhibited by high concentrations of hydrogen. Thus, acetogens must have a synergistic relationship with the following step, methanogenesis, and particularly the hydrogen-consuming methanogens [52].

The two pathways for methane production involve acetic acid (acetoclastic methanogenesis), and carbon dioxide and hydrogen (hydrogenotrophic methanogenesis). The acetate intermediate via the acetoclastic pathway is the major contributor to biomethanation (up to 70 % of methane). The acetoclastic methanogens of the archaea genera *Methanosarcina* and *Methanosaeta* have been more extensively described, although these genera are unable to metabolise hydrogen [52]. Methanogenesis requires rigorous conditions since it is the slowest stage and limiting step in AD. At this point, most of the intermediary compounds that were not transformed into acetate are not utilised by the methanogens and thus accumulate in the digester [53]. Moreover, the growth rate of methanogens is slower than acetogens, thus, allowing the reactor enough time for the methanogens to consume the VFAs and produce methane and carbon dioxide is highly important [51]. Generally, a syntrophic balance between both acetogenesis and methanogenesis is essential. This creates the proper environment for consuming hydrogen, converting the VFA, producing methane, and finally obtaining an effective anaerobic digestion process [47,48].

The mono-digestion can exhibit insufficient macro and micro-nutrients, an imbalanced C/N ratio, and unfavourable organic loading rates (OLR). Whereas a properly balanced anaerobic co-digestion (AcoD) can provide synergistic effects by improving the methane yield and kinetic parameters [54]. Co-digestion of N-rich and C-rich substrates at an adequate C/N ratio could provide a proper amount of ammonia, which can supply the nitrogen requirements for microorganisms and buffer the pH changes due to acid products. However, when

adding N-rich substrates to a digester at unbalanced C/N ratios, high concentrations of free ammonia (NH_3) are often produced. Since acidogens are less sensitive to ammonia than methanogens, more VFAs are accumulated, and less methane is produced [55].

2.2.2 Limitations of anaerobic digestion

It is necessary to overcome the two major problems associated with AD, operational instability, and the quality of the digestate. The selected organic substrate is a determinant factor for the stability of AD since they often contain inhibitory compounds. Depending on the source, some inhibitors originally accompanying the biomass are furans, limonene, antibiotics, and metals. Also, intermediates of the original organic biomass, such as ammonia (NH_3), and ammonium (NH_4^+) generated from N-rich feedstocks (e.g., animal wastes) [16,17]. Suitable fermentation conditions for the digester are key for maintaining stability. The enzymatic machinery of acidogenic and methanogenic microorganisms function better at pH 5.5-6.5 and 6.5-8.2, respectively, with an optimum range at 6.8-7.4. Consequently, changes in the pH damage the growth and activities of the microorganisms involved in AD [51].

The stability of the AD process is influenced by pH changes and the equilibrium established between the three primary buffers involved: VFAs, bicarbonate and ammonia. The buffering capacity index (or buffer intensity) (B) is defined as the amount of strong acid or base required to change one unit of pH. The equilibrium during AD has been described by Georgacakis et al. [56]. They stated that a digester with a high accumulation of VFAs hinders the buffering capacity of the bicarbonate ions according to:

$$HAc + NH_4HCO_3 \rightarrow NH_4Ac + H_2CO_3 \qquad \text{Equation 2-1}$$
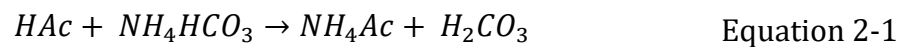
If ammonia is added to the digester or originated from a N-rich substrate, the bicarbonate taken from the CO_2 pool would form an ammonium salt:

$$NH_3 + H_2O \leftrightarrow NH_4^+ + OH^- \qquad \text{Equation 2-2}$$

$$CO_2 + H_2O \leftrightarrow H^+ + HCO_3^- \qquad \text{Equation 2-3}$$

Resulting in:

$$NH_4^+ + OH^- + H^+ + HCO_3^- \leftrightarrow (NH_4^+ + HCO_3^-)_{salt} + H_2O \qquad \text{Equation 2-4}$$
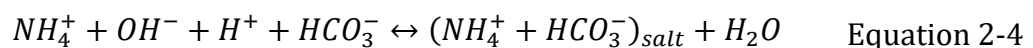
Figure 2.3 shows the schematic of changes in buffering capacity index with pH. A stable anaerobic digester should have a pH between the bicarbonate and ammonia buffer intensity peaks. This point is the safest zone given the equilibrium between the two buffers, illustrated by the deep valley which would require a force high enough to overcome the resistance. However, if the concentration of VFAs increases, there are two possible scenarios: (i) if the microbial community can convert the VFAs into methane, the bicarbonate buffering capacity increases and a stable digester is obtained; or (ii) if the microbial community is unable to transform the VFAs, the pH would continue to drop, and system failure will occur. In the second scenario, the increasing concentration of VFAs would attempt to move up the bicarbonate intensity curve according to **Equation 2-1**. If the concentration of VFAs continues to increase, the bicarbonate buffer intensity would be practically null due to the unavailability of the CO_2 that has returned to the CO_2 pool. Hence, the pH is reduced and located between the VFAs and ammonia peak buffer intensities. In this scenario, the biochemical stability of the digester is at the lowest point since it struggles to maintain pH and electroneutrality [56].
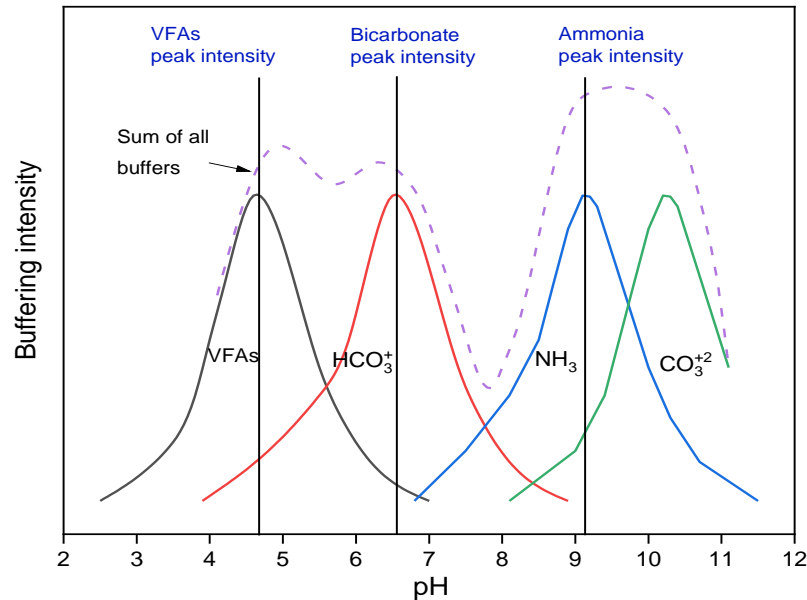
Figure 2.3. Schematic of changes in buffering capacity index with pH for primary buffers commonly found in anaerobic digesters. Adapted from [56].

If more VFAs are accumulated, the pH would further reduce towards the VFAs buffer intensity curve, if it overlaps with the bicarbonate curve, it will easily slip into the valley between the bicarbonate and VFAs intensity peaks resulting in the

instability of the digester due to the lack of the necessary buffering capacity to maintain a stable pH. Moreover, the increasing ammonia would act as a force that pushes the pH towards the ammonia buffer curve as more NH_4HCO_3 is formed (**Equation 2-4**). The microorganisms would not endure a pH within the ammonia buffer peak due to the ammonia toxicity. Therefore, it is imperative to maintain the pH between the bicarbonate and ammonia buffers to ensure stability [56].

Furthermore, the digestate slurry is a by-product of biomethane and heat generated by AD. The digestate contains a high proportion of nitrogen and other macro- and microelements useful for plant growth. The digestion process and the source feedstock materials influence the composition of the digestate. The digestate needs to meet certain standards of quality to be an effective fertiliser as stated by The British Standard Institution BSI PAS 110 [57]. Approximately 40-60 % of the carbon is converted into methane, while the rest is retained within the digestate fraction. From a sustainable point of view, it is necessary to consider the GHG emission potential of digestate (125 CO_2-eq/kg waste). However, the optimisation of AD is generally focused on enhancing biogas production while leaving digestate quality aside. Underestimating the role of the digestate defeats the objective of organic waste treatment. Therefore, it is suggested for the optimisation of AD to consider both enhancing methane yields and also digestion quality [58]. Some of the reported approaches for improving AD include operational conditions optimisation, bio-stimulation, co-digestion, biogas upgrading, two-phase process, the addition of trace elements, and the amendment by the addition of adsorbent materials, and cell immobilisation [48].

Coupling thermochemical biomass conversion and AD for enhancing energy performance and digestate quality is an area of great interest. Different pathways can achieve the complementation of these technologies. First, adding biochar to the AD reactor could stabilise the biological processes and enhance the retention capacity of the digestate. Second, employing the AD digestate as a feedstock for thermochemical treatment. Third, using the aqueous phase from the thermochemical processes as a feedstock for AD. Fourth, high recovery and reuse by thermochemical treatment of the digestate and application of the solid and liquid products as stabiliser and feedstock for AD [22]. For this work, the discussion will base principally on the first scenario, the addition of chars to anaerobic digestion.

2.3   Biochar and hydrochar

2.3.1   Char overview

Char is a solid carbonaceous material obtained from the thermochemical processing of organic matter. A wide range of biomass feedstocks is commonly used for the production of char, including wood materials, agricultural residues, paper residues, and food wastes [30]. **Table 2.4** outlines the thermochemical technologies used for the transformation of biomass, including slow pyrolysis, intermediate pyrolysis, fast pyrolysis, torrefaction (pyrolysis at low temperature), gasification, hydrothermal carbonisation (HTC), and flash carbonisation [59]. The chemical reactions involved in these processes include decarboxylation, dehydration, decarbonylation, intermolecular rearrangements, condensation, and aromatisation. There is no specific order for these reactions, as they can take place simultaneously, usually involving the degradation and decarboxylation reactions over the biomass polymers along with the formation of the chars by condensation and aromatisation reactions. Also, it has been stated that the nature and predominance of these reactions are governed by the operating conditions of each thermochemical treatment, thus each treatment leads to products with different yields, and chemical and physical characteristics [60].

Table 2.4. Thermochemical processes for the transformation of biomass

Thermochemical Process	Pressure	Temperature (°C)	Heating Rate (°C/min)	Residence Time	Primary Product
Torrefaction	Atmospheric	200-300	<50	10 – 120 min	Brown/black solid biomass
Slow pyrolysis	Atmospheric	300-700	1-30	h-week	Biochar
Fast pyrolysis	Vacuum-Atmospheric	400-600	10-200	<2 s	Bio-oil
Flash pyrolysis	<20 MPa	400-950	10^3-10^4	<0.5 s	Bio-oil
Hydrothermal carbonisation	2-10 MPa	180-250	5-10	1-12 h	Hydrochar
Gasification	Atmospheric-Elevated	750-1800	50-100	10-20 s	Gas

Hydrothermal carbonisation (HTC) consists of the conversion of biomass within compressed water at elevated temperatures, while pyrolysis consists of the dry

carbonisation of organic matter under anoxic conditions. These two thermochemical processes are described in more detail later in this chapter. Torrefaction is considered a mild process for slow pyrolysis that employs temperatures of 200-300 °C, slow heating rates (<50 °C/min), and anoxic atmosphere and ambient pressure conditions [61]. The mild conditions of torrefaction comprise only the beginning of pyrolysis, hence it is not possible to use the term biochar. The physicochemical properties of the solid product are found between the untreated biomass and the pyrolysed biochar. Torrefaction is considered a promising step for improving the physicochemical properties of biomass for further combustion and production of bioenergy. Therefore, the practical interest of torrefaction is not the production of carbon solids but to pre-treat biomass [60].

The thermochemical process of gasification employs high temperature and short residence time for the partial combustion of biomass, leading to the main product named syngas. The gasification is not employed when biochar is the product of interest since the amount of biomass destined to produce the solid fraction comprises less than 10 %. In addition, the solid fraction possesses a high concentration of heavy metals and organic pollutants (e.g., polyaromatic hydrocarbons) resulting from the high-temperature reactions. Just as torrefaction, given the physicochemical properties of the solid carbonaceous fraction obtained by gasification, it cannot be called biochar [60]. Therefore, it can be concluded that neither torrefaction nor gasification is suitable for thermochemical processes when the product of interest is the char. On the other hand, pyrolysis and hydrothermal carbonisation are suitable technologies to produce carbonaceous materials, as further discussed.

The process conditions of each technology differ, and in consequence the yield and proportion of the end-products. The products from thermochemical treatments are divided into three phases: solid, liquid and gas. Firstly, the solid phase, or char, corresponds to the carbon-rich residue remaining after the loss of volatile matter and a series of chemical reactions. The solid product from pyrolysis is known as biochar, while the solid from HTC is named hydrochar. Given the different reactions taking place during each process; the physical, chemical and functional properties of chars differ significantly. BC is a porous solid with a large surface area (SA), aromaticity and surface functionality. Whereas HC possess a sphere shape with reduced porosity and SA, but greater content of surface functional groups [60]. The properties of the chars are described in detail in further sections.

Secondly, the dark-brown liquid phase is called bio-oil when obtained from pyrolysis and process water when obtained from HTC. The highest yields of bio-oil are obtained by fast and flash pyrolysis processes. The liquid phase is formed by the rapid cooling of the gaseous products formed by the degradation of the organic fraction of the biomass [62]. The bio-oil is a mixture comprised of water (15-35 % wt), and a wide range of organic compounds, such as acids, alcohols, ketones, phenols, aldehydes, ethers, esters, furfurals, sugars, alkenes, and suspended solid particles [29]. The suspended solid particles are composed of fragments of the decomposed biomass [62]. The bio-oil can be directly used for gas turbines, boiler systems, diesel engines and Stirling engines or upgraded into light hydrocarbons and aromatics by reforming, cracking, catalytic esterification and hydrotreatment [63]. The HTC process water is a complex mixture of compounds solubilised in water, including organic acids (acetic, formic, levulinic and glycolic acid), hydroxyl-methyl-furfural (HMF), organic carbon and inorganic compounds [64,65]. Among the applications of HTC process waters, their integration with other technologies, such as AD, is reported to enhance energy yields [66].

Thirdly, gas fraction or syngas is formed by the non-condensable products formed from biomass degradation, including CO, CO_2, CH_4, H_2, and some non-methane hydrocarbons [62]. It has been reported that the primary components of the gaseous phase, CO_2 and CO, originated from the decomposition and reforming of carbonyl (C=O) and carboxyl (COO^-) groups, respectively. The secondary component CH_4 is the result of the decomposition of methoxyl (-O-CH_3) groups, methylene (-CH_2-) groups, and oxygenated compounds, while the H_2 is formed by the decomposition of aromatic (C=C) and methyl (C-H) groups. The applications of the syngas include the direct production of heat or electricity, or the further upgrade into individual gases (e.g., CH_4 and H_2), and liquid biofuels [29].

2.3.2 Pyrolysis

Pyrolysis is defined as the thermochemical decomposition of biomass in non-oxidative conditions that lead to the production of liquid bio-oil, solid biochar, and non-condensable gas products. Depending on the process conditions, pyrolysis can be divided into slow pyrolysis, fast pyrolysis and flash pyrolysis (**Table 2.4**) [29]. The low temperature and slow heating rate of slow pyrolysis favour biochar production, achieving yields of 25-35 % [60]. Fast pyrolysis uses high heat transfer rates, high temperatures, and short residence times that prevent the further cracking of the products into non-condensable compounds,

obtaining thus higher oil yields [62]. During fast or flash pyrolysis, the biomass is rapidly heated accompanied by the rapid cooling of the condensable volatiles for avoiding the cracking into gases or polymerisation into biochar [67]. Nevertheless, slow pyrolysis is usually preferred for obtaining biochars with notable functional properties [68].

2.3.2.1   **Pyrolysis pathway**

The pyrolysis of biomass is generally described under three parallel pathways, divided by the most significant end-products. The pathway of biochar and gas formation, the pathway of liquid and tar formation, and the pathway of gasification and carbonisation. The rate of these three pathways is primarily determined by the pyrolysis conditions of highest heating temperature (HHT), volatile removal rate and particle residence time [61]. First, the biochar and gas formation pathway develops below 300 °C. The biomass starts to decompose, water is released and starts the formation of free radicals, and carbonyl and carboxyl groups, which are subsequently reduced to CO and CO_2, respectively. Second, the tar (condensed volatiles) and liquid formation pathway develop between 300-600 °C. The liquid or bio-oil has an organic phase that can be used as a fuel, while the main components of the tar are anhydrosugars, which are volatilised or degraded. Third, above 600 °C, the production of gas dominates the pyrolysis, while the formation of tar, liquids, and char is drastically reduced, and even the biochar formed in the early stage of pyrolysis is further carbonised [61,62]. Nevertheless, these three steps are not consecutive as they occurred intermixed during pyrolysis [29].

Temperature determines the reactions taking place during pyrolysis. Below 200 °C, free and bound water is released, whereas above 200 °C, starts the degradation of the complex organic compounds, such as proteins, lipids and carbohydrates [68]. The most significant compositional changes of biomass take place at a temperature range of 200 to 400 °C. The initial steps of pyrolysis include the detachment of low-energy bonds, such as acidic hydrogen and oxygen-containing groups (e.g., carboxyl, hydroxyl and formyl groups). This detachment results in unpaired negative charges with the ability to accept protons and a more basic structure [67]. The carbonisation of biomass is not achieved at low temperatures. By increasing at 300-400 °C, the O-alkyl C and carbonyl C structures disappear while the presence of alkyl C structures intensifies [63]. Biochar formation generally occurs in the primary stage at temperatures of 200-400 °C where most of the mass loss takes place [29]. Although it is until 500 °C that the alkyl C structure is further destroyed, resulting

in a more aromatic BC. It has been suggested that biochars produced above 500 °C are mostly constituted by aromatic C structures [63]. As pyrolysis temperature raise, the graphitisation degree of the chars increases due to the dehydrogenation and deoxygenation reactions and consequently generation of stable condensed ring compounds [68]. Thus, the rise in temperature leads to biochar with lower H and O content, enhanced aromaticity, aromatic ring condensation and a more basic nature [69].

Biochar is formed by the alteration of the biomass structure due to the mass loss, microstructure arrangements, attrition, and the formation of pores. The initial changes involve the removal of water and carbon mass. This creates shrinkage stress that breaks and cracks the biomass structure, and since the surface of the material decomposes faster than its interior, the result of these changes is the creation of pores. The pores can be formed in different sizes, including micropores (<2 nm), mesopores (2-50 nm) and macropores (>50 nm). It is worth noting that the original carbon structure and mineral content of the raw biomass is retained to a certain degree since the mass loss is mostly attributed to volatile organic compounds [25]. The development of the pore network and final structure of the biochar is mainly determined by the process HHT and the biomass nature.

Moreover, the inherent surface functional groups of biomass are lost along with the volatile matter via dehydration, decarboxylation, and condensation [68]. The loss of functional groups is enhanced by increasing the severity of the treatment [67]. Thereby, it can be implied the importance of the process conditions in the structure and characteristics of biochar, as well as the yield of the by-products [69].

2.3.2.2 Biochar

The International Biochar Initiative (IBI) has proposed a standard definition for biochar, as 'the solid material obtained from the thermochemical conversion of biomass in an oxygen-limited environment' [70]. The amorphous structure of BC is comprised of graphite-like layers turbo-strategically arranged with a void space between them. BC is composed of two phases, the conducting and the non-conductive. The conducting or crystalline phase consists of highly conjugated polyaromatic sheets forming conductive crystalline ordered areas that resemble the structure of graphene. The non-conductive or amorphous phase consists of a complex and randomly organised structure. This phase is formed by aromatic rings and aliphatic organic compounds, including the residual volatiles and the mineral compounds (inorganic ash) [25].

Biochar has a heterogeneous structure formed by pores of different sizes and surface functional groups, as illustrated in **Figure 2.4**. The physical structure of biochar is represented by the porosity degree, which is influenced by the pyrolysis process [71]. The heterogeneous surface exhibits diverse functional groups, including hydroxyl, ketone, aldehyde, amino, ester, nitro, carboxylic and phenolic. These groups donate to BC the ability to exhibit acid/basic and hydrophobic/hydrophilic properties [60]. Low-temperature BC exhibits a large content of aliphatic functional groups and volatile matter (VM), while those produced at high-temperature exhibit a lower content of VM and functional groups, and higher aromaticity. As the aromaticity increases, other transformations take place, affecting the crystallinity, surface area and the microcrystalline structure of char [69]. The conductivity of BC increases with pyrolysis temperature due to the decrease of functional groups and the formation of conjugated double bonds [67].
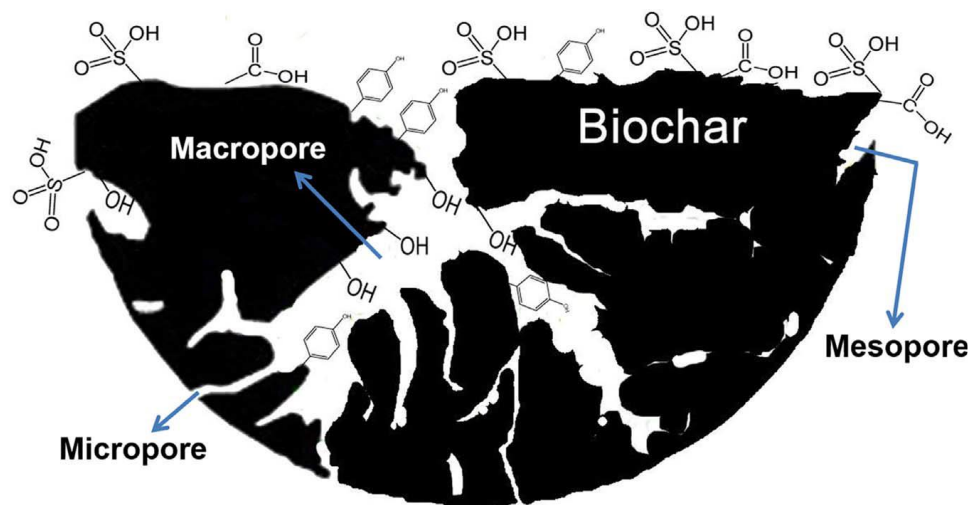
Figure 2.4. Illustration of the physicochemical structure of biochar, meso- and microporosity and the presence of functional groups. Taken from [31].

The influence of process conditions -highest heating temperature (HHT) and residence time- and feedstock composition on the final properties of biochar has been extensively studied. Zhao et al. [32] stated the importance of both parameters, although suggested that each is inclined to a different set of properties. The nature of the feedstock has a greater impact on the total organic carbon, fixed carbon, and mineral elements of BC. While the HHT is the determinant parameter for the development of surface area and pH. Santos et al.

[71] stated the role of increasing HHT to enhance pore size and SA. On the other hand, there are contradictory statements regarding the influence of residence time. Some reports have stated an inconsequential effect of residence time over BC chemical composition. Whereas others have stated that a prolonged residence time supports the polymerisation of volatile organic compounds, and the formation of secondary BC, enhancing thus the BC yield [67].

For understanding the role of biomass on the properties of biochar, it is important to outline the thermal degradation of its main components. In the case of lignocellulosic biomass, cellulose and hemicellulose degrade faster than the more complex lignin. Thus, the formers have a more relevant role in gas and liquid fractions whereas lignin mostly remains in the solid fraction [67]. For lignocellulosic biomass, it has been suggested that pyrolysis could be divided into two general steps. Below 600 °C, the degradation of the lignocellulosic fibre is linked to the net loss of the aliphatic fraction, whereas at higher temperatures, a reorganization of bonds takes place leading to the conjugation of aromatic bonds and finally, the rise of the aromaticity and aromatic ring condensation [69].

On the other hand, biomass rich in protein or lipids exhibits a more complex pyrolytic behaviour. During pyrolysis, the N atoms are integrated into the carbon matrix of BC by the formation of pyrrolic-N (N-5), pyridinic-N (N-6) and quaternary-N (N-Q) species [68]. Generally, N-content increases with temperature since the devolatilisation reactions reduce the concentration of other components. However, there are reports of N-content reduction on feedstocks like animal waste and sewage sludge due to the protein degradation and devolatilisation of ammonium nitrogen from the biomass structure [67]. Furthermore, biomass with a high content of ash usually produces more alkaline and aromatic biochars. It has been suggested that the presence of metals contributes to the alkalinity and aromatisation reactions. By increasing the pyrolysis temperature, the ash content concentrates as a result of organic matter loss, consequently, the alkalinity of the BC also increases [68].

The pyrolysis conditions and the nature of the biomass determine the chemical composition of biochar and the concentration of its principal elements C, H, O and N [72]. Regardless of how BC is produced, the C-content is found in a range of 175-905 g/kg, the N-content in a range of 1.8-56.4 g/kg, and the pH between 4 and 12. These large variabilities are due to the nature of the biomass and the pyrolysis conditions. It has been observed that even biochars produced from the same type of feedstock will have a different composition due to the process

conditions, especially regarding the N and S content [73]. Moreover, by increasing the reaction severity, particularly pyrolysis temperature, the volatilisation of C, H and O intensify resulting in lower H:C and O:C ratios and higher ash concentration [61,72]. Hence, there is a direct response to temperature regarding compounds containing carbon and oxygen. Hydrolysis starts at temperatures as low as 150 °C, reducing thus the content of OH and CH$_3$. At 300-400 °C, further loss of O and H is observed as biochar is partially carbonised. Although pyrolysis requires higher temperatures (up to 500 °C) to drastically reduce these compounds, and increase the content of C=C, due to the transformation of aliphatic compounds into aromatic structures. At 550 °C, the ratio of H:C and O:C decrease even more due to increased aromaticity, while at a higher temperature, the BC is mainly carbonised [73].

2.3.3 Hydrothermal carbonisation

It has been over a century since the HTC process was introduced as a method for the simulation of natural coalification. In recent years, the processing of biomass by HTC has gained a lot of attention by being considered an environmentally friendly treatment for wet biomass. Among the advantages of HTC are ease of operation, process energy efficiency, and the production of end-products with a stable nature, non-toxicity, and ease to handle and store. Additionally, HTC provides the possibility of employing different types of biomasses, without the necessity of the energy-intensive and costly step of drying. The HTC process consists of the thermochemical conversion of biomass at elevated temperatures, usually 180-250 °C, in the presence of water under saturated pressure conditions. The biomass is transformed by a series of reactions into a carbonaceous solid, called 'hydrochar', a gas phase, and a liquid phase, also known as 'process water' [19].

2.3.3.1   Hydrothermal carbonisation pathway

The sub-critical water facilitates the rapid depolymerisation and degradation of the polysaccharides (e.g., cellulose and hemicellulose) by acting as an acid/base catalyst, and as a non-polar solvent for the organic and gaseous components of the biomass [60,74]. From a general view, several chemical reactions take place during HTC, including hydrolysis, dehydration, decarboxylation, condensation, polymerisation, and aromatisation. They do not take place in consecutive order, but rather form a parallel network of different reaction paths determined by the type of biomass and process conditions [19]. First, the main components of biomass are degraded into their smaller fraction compounds. The lipids are

depolymerised into fatty acids and glycerol, the carbohydrates to monosaccharides, whereas the peptide bonds of protein are broken down into their compositional amino acids. Subsequently, the monomers decompose via dehydration, cleavage, decarboxylation, and deamination reactions. Afterwards, fragments with free radicals suffer recombination generating thus larger stable molecules, including the polyaromatic hydrochar [68].

A detailed mechanism for the formation of HC from carbohydrates has been proposed by Sevilla and Fuentes [75]. Firstly, the hydrolysis of biomass involves different reactions, primarily the cleavage of ether and ester bonds that form a wide range of compounds, including oligo and monosaccharides from cellulose, and phenolic fragments from lignin, and further hydrolysis of the resulting fragments. Secondly, different chemical reactions or physical processes (dewatering) are involved in the reduction of the water content. Hence, dehydration includes the elimination of hydroxyl groups and to a lesser extent, the condensation of hydrolysed fragments. While monosaccharides suffer dehydration, the fragmentation begins with the opening of rings, breaking of C-C bonds, and the formation of soluble compounds, including furfural, 5-hydroxymethylfurfural, 5-methylfurfural, 1,2,4-benzenetriol, acids and aldehydes. Simultaneously, the different furfural-based decomposed into acids/aldehydes and phenols [19,75].

Thirdly, at temperatures above 150 °C, carboxylic and carbonyl groups are rapidly eliminated as CO_2 and CO, respectively. It has also been proposed the production of CO_2 via the cleavage of intramolecular bonds, during condensation reactions, and by the thermal decomposition and action of water as an oxidising agent at elevated temperatures. Fourthly, the monosaccharides and/or their decomposition products undergo a process of polymerisation or condensation, leading to the formation of soluble polymers. Simultaneously, the decarboxylation of biomass creates unsaturated compounds that easily polymerise via condensation, particularly aldol condensation while producing some highly reactive fragments. Nonetheless, the detailed mechanisms of the decarboxylation paths during HTC are not entirely understood. Fifth, the soluble polymers suffer an aromatisation, which involves the formation of C=C groups, mainly a result of keto-enol tautomerism (**Equation 2-5**) or intramolecular dehydration (**Equation 2-6**). Finally, the condensation of aromatised molecules leads to the formation of aromatic clusters, which are the base for the microsphere formation (**Equation 2-7**) [19,75,76].

Equation 2-5

Equation 2-6

Equation 2-7
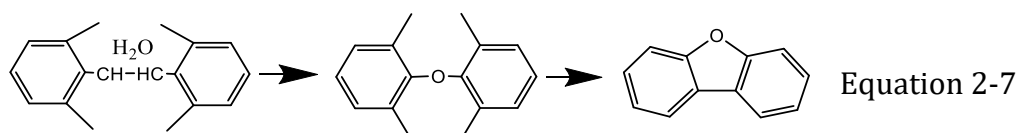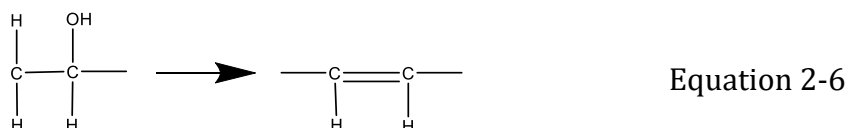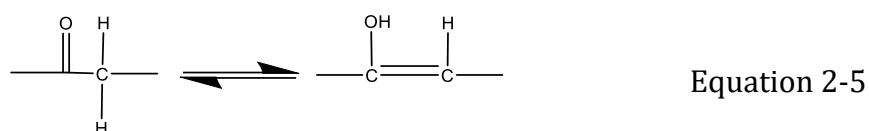
Furthermore, Sevilla and Fuertes [75] proposed that the formation of the HC microspheres undergoes a nucleation-growth mechanism as described by the La Mer model [77]. Hence, as the formation of aromatic clusters reaches a point of critical saturation, the process of burst nucleation starts. An aromatic nucleus is formed and grows by diffusion, as the chemical species present in the bulk solution are linked to the reactive oxygenated functional groups (OFGs) from the surface of the microsphere. These multiple reactions lead to the formation of stable oxygen groups, such as ester and pyrone, that remain in the core of the microsphere. Finally, the end products include the insoluble carbonaceous microspheres containing a core-shell chemical structure, and some soluble organic compounds, such as acids, aldehydes, and furfurals. Both the degree of aromatisation and the diameter of the microspheres enlarge with the higher reaction temperature, reaction time and carbohydrate concentration [75].

Table 2.5 outlines the effect of the processing conditions during HTC. Ionic reactions prevail at low temperatures, favouring the production of solid carbon products. Whereas at a higher temperature, homolytic bond cleavage reactions, and extensive dehydration and condensation of the biomass increases the gas yield. For instance, at HTC conditions ≤220 °C and 20 bar, most of the organic biomass is transformed into solids, while the gas production is approximate at 1-5 %. Increasing temperatures decreases the ion exchange capacity and reduces the O and H content of HC and in consequence the OFGs. The residence time is another important factor to determine the reactions undertaken during HTC and the obtained products. Prolonged residence time allows the ongoing polymerisation of the solved fragments from the liquid phase that finally precipitate, increasing the solid HC yield. For instance, it has been reported that as the residence time increases, the OFG content decreases, whereas the lactone

(C=O), and carboxyl (COOH) content increase. The OFG content reduction may be related to excessive dehydration and carbonization of the solid carbon and the gasification of surface OFGs [76].

Table 2.5. Summary of the effect of processing parameters on HTC reactions and products.

Increasing temperature (>220-350 °C)	Extending residence time (>1-12 h)	Increasing solid load (>16 %, w/v)
▪ More homolytic bond cleavage reactions take place	▪ OFG content decreased	▪ The liquid product is negligible affected
▪ Higher gas yields	▪ Reduced O:C and H:C ratios	▪ Poor hydrolysis
▪ Lower O:C and H:C ratios	▪ Lactone (-C=O), and carboxyl (-COOH) content increase	▪ Less condensed products
▪ Decrease of ion exchange capacity	▪ Excessive polymerisation	▪ Larger size microspheres
▪ OFG content decreased	▪ Larger size microspheres	▪ High O:C and H:C ratios
▪ Larger size microsphere	▪ Higher hydrochar yield	▪ High OFG content at high residence time and temperature
▪ Lower hydrochar yield		

The highest reaction temperature is the primary factor governing the final properties of the char, such as shape, diameter, particle size distribution, and aromatisation degree. All the reactions involved in the degradation of the biomass, the release of volatiles and the formation of intermediate compounds are dependent on temperature. The heating rate is the second most influential process parameter since it determines the heat mass transfer and rate for the formation of volatile compounds and other intermediates [60]. For instance, at 180 °C, the hemicellulose is completely hydrolysed, while at 200 °C a major fraction of lignin is hydrolysed. On the other hand, is not until 220 ° C, that cellulose starts to significantly hydrolyse. Moreover, the solid load represents the ratio of biomass to water and is a parameter that influences the HTC of biomass. It has been observed that raising the initial solid load leads to a larger fraction of solid material, as a major concentration of monomers in the liquid phase increase the possibilities of polymerisation [19].

The biomass composition also plays a role in the yields and composition of the HTC products. For instance, cellulose is first hydrolysed into oligomers, such as cellobiose, cellotriose, cellotetraose, cellopentaose and cellohexose that subsequently degrade into a variety of acids (acetic, formic, lactic and levulinic) and acetaldehyde. Glucose isomerised into fructose, thus both sugars react into

erythrose, glycolaldehyde, hydroxyacetone or 5-hydroxymethylfurfural. HMF and furfural structures can poly-condensate and be polymerised into the HC [78]. Lignin is only partially hydrolysed; hence it preserves part of the initial biomass macrostructure on the HC. The lignin fraction interferes with the hydrolysis of the cellulose and hemicellulose polymers. Lignin also contributes to the overall content of OFGs of the HC. Moreover, it has been suggested that crystalline carbon biomass leads to hydrochar with less porosity, in comparison to amorphous biomass. The structure of the biomass precursor has a direct role in the creation of the hydrochar porosity [76].

Knežević et al. [74] proposed a model for the conversion of glucose during HTC (**Figure 2.5**). Generally, glucose initially decomposes into the liquid phase, where it suffers further reactions that lead to the formation of char and gas. Glucose is decomposed into water-soluble primary products, including fructose, levoglucosan, dihydroxyacetone, 5-HMF, furfural, erythrose, glyceraldehyde, glycolaldehyde and formaldehyde. These products suffer polymerization reactions to form the solvent-soluble part in the hydrophobic phase, which later comprises the PW and HC. Excluding formaldehyde, all primary decay products are involved in the production of hydrochar. Based on this, they proposed that the compounds found in the process water and the hydrochar are essentially the same. They differed in the higher molecular weight for the HC compounds due to a higher polymerisation degree. The gas fraction, on the other hand, involves small secondary and tertiary decay products (e.g., formic acid and formaldehyde) that are further reduced to CO_2, CO, CH_4 and H_2.

2.3.3.2   Hydrochar

Hydrochar is a carbon sphere formed by a highly aromatic core-shell structure of approximately 0.4-6.0 µm in diameter. HC is composed primarily of furan rings cross-linked by domains of short aliphatic chains as illustrated in **Figure 2.6** [75]. The structure of the HC is very similar to the coal obtained by natural coalification, although with a higher OFG content. The HC exhibits a less hydrophilic nature than the starting material because the process of HTC eliminates several hydroxyl and carboxyl groups from the biomass [19].
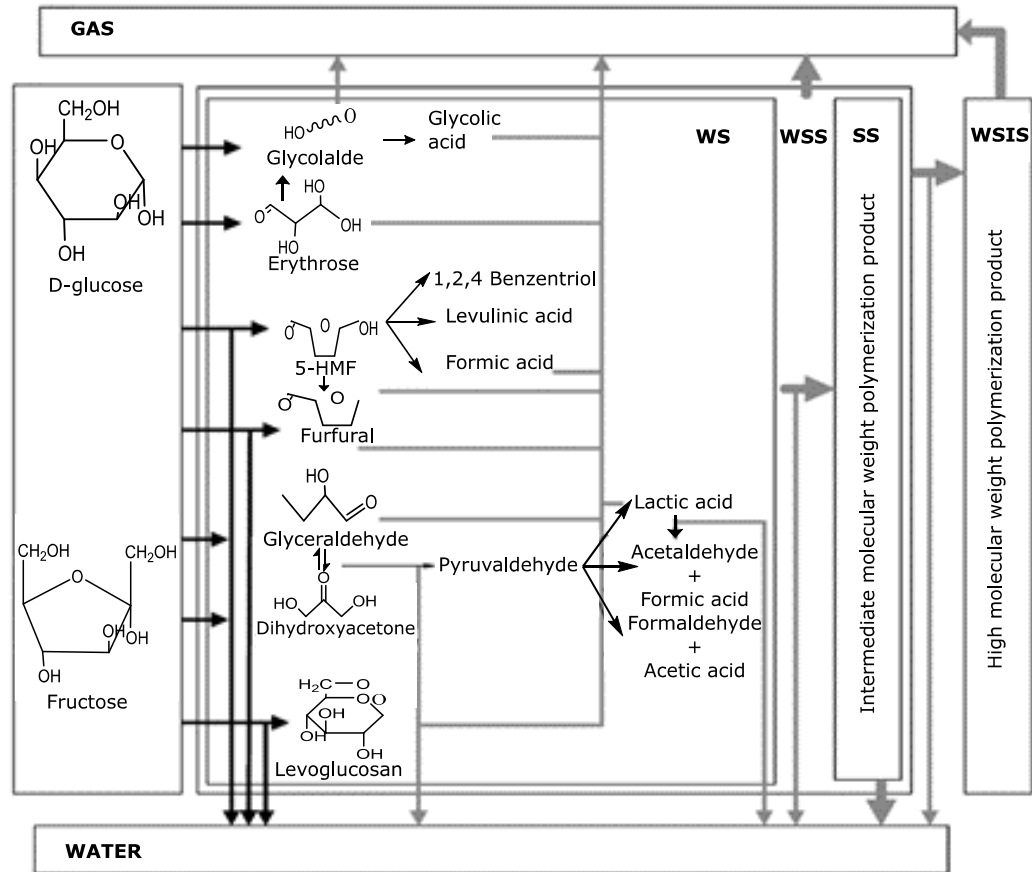
Figure 2.5. Reaction pathway model for the HTC of glucose as proposed by Knežević et al. [74].

WS water-soluble, SS solvent-soluble, WSS water-solvent soluble organics (process water), WSIS water-solvent insoluble organics (hydrochar).

It has been proposed that lignocellulosic biomass follows multiple routes for the formation of char. First, part of the solid biomass is directly transformed into char, named primary char. Second, the dissolved monomers generated by the biomass decomposition suffer polymerization or condensation reaction that led to the formation of secondary char. The mechanism for the conversion of biomass into char is complex and the routes above mentioned are just a generality. Moreover, the structure of the biomass precursor has a direct role in the creation of the hydrochar porosity. For instance, it has been reported that crystalline carbon biomass leads to hydrochar with less porosity, in comparison to amorphous biomass. In addition, the presence of lignin is suggested to interfere with the hydrolysis of the cellulose and hemicellulose polymers. Given its recalcitrant nature, it slows down the decomposition of the polysaccharides. Therefore, as lignin is only partially hydrolysed, its presence preserves the initial macrostructure of the biomass [76].
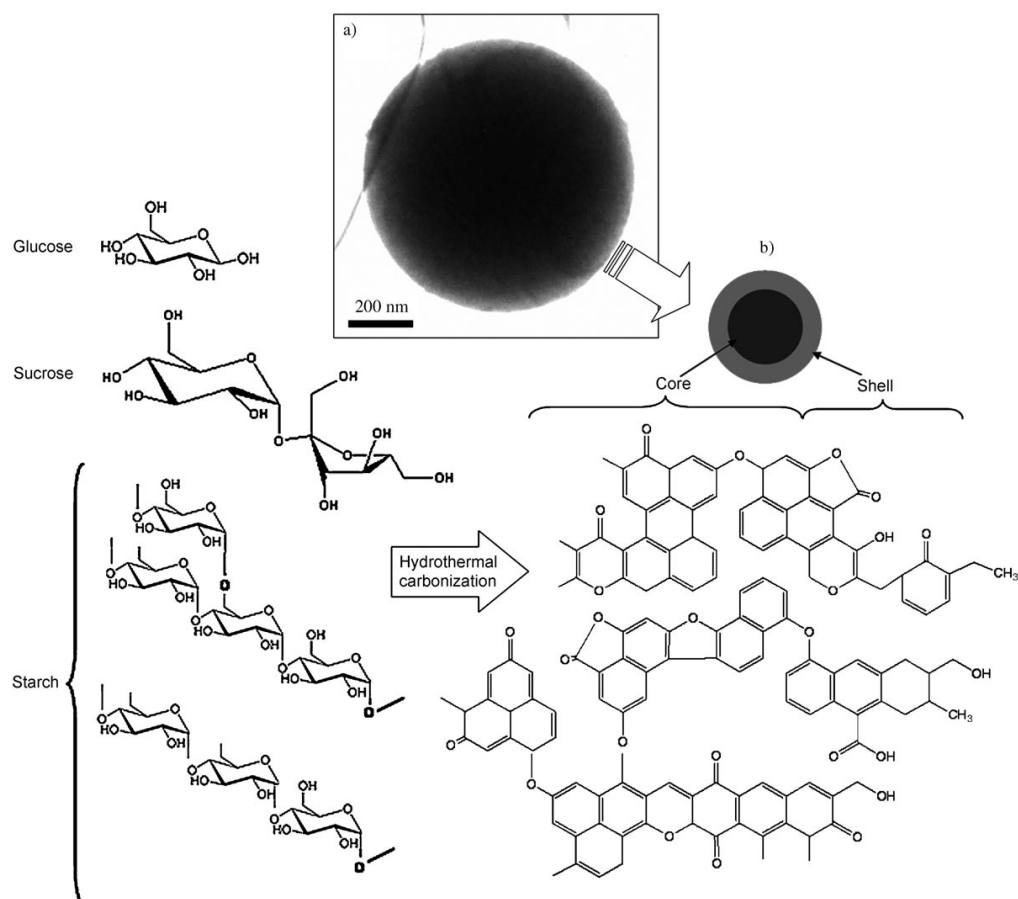
Figure 2.6. TEM image of the microsphere and schematic illustration of the core-shell chemical structure of hydrochar. Taken from [75].

2.3.4 Surface functionality of biochar and hydrochar

The surface chemistry of the chars exhibits hydrophilic, hydrophobic, acidic, and basic properties directly related to their heterogeneous composition. These properties contribute to the reactivity of the chars and are dependent on the nature of the biomass, the thermal degradation process, and the conditions used. The diversity of functional groups is formed by H, O, N, P, and S heteroatoms incorporated into the carbon structures and aromatic rings. The electronegativity of these heteroatoms relative to the C atoms determines the chemical heterogeneity of the chars. The nature of the functional groups on the surface of the chars includes electron donors, electron acceptors, and acidic and basic nature. The electron donor groups possess α or π electrons, such as OH, NH_2, OR or $O(C=O)R$. The electron acceptors with empty orbitals include $(C=O)OH$, $(C=O)H$ or NO_2 groups. The acidic groups include strong Brønsted acids (e.g., carboxyl groups) and less acidic groups (e.g. phenols and carbonyls), whereas the basic groups are conformed by pyrones and chromenes groups [61].

Figure 2.7 illustrates the interaction of biochar functional groups with phenolic groups. The sorption of the char surface is influenced by the functional groups and their surface charge nature and availability of π electrons. The charge of the functional groups is dependent on the pH and consequently the sorption of many functional aromatic molecules. For instance, the sorption capacity of phenols and anilines is stronger at pH solutions close to their points of zero charge. The chars with oxide surfaces exhibit pH-dependent amphoteric sites that under acidic conditions will be positively charged whereas under basic conditions will be negatively charged [61].
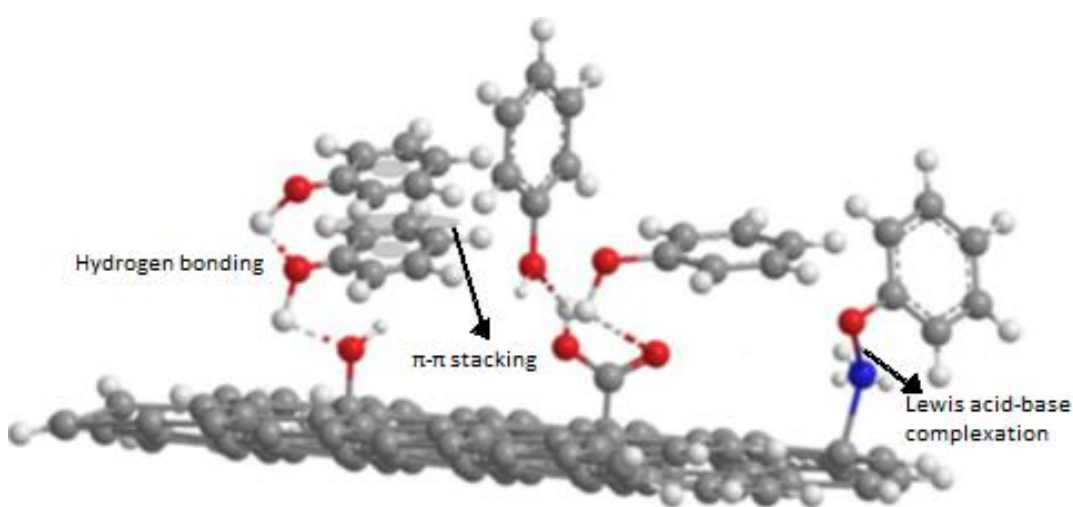
Figure 2.7. Modelling of the interaction between the functional groups from the surface of biochar and phenolic groups. Taken from [79].

The surface functionality of the chars is responsible for most of their interaction with organic matter. OFGs, such as C-O, C=O, OH and COOH, are the predominant and most important features of surface chemistry. OFGs are responsible for enhancing the hydrophilicity of the chars and thus their interaction in aqueous systems. They are also responsible for the interaction with metals via hydrogen bonding and complexation [63]. The OFGs serve as anchoring and interaction sites for the biomolecules. Therefore, these characteristics are of interest for their application in catalysis as an adsorptive or support material for the immobilisation of biomolecules [80]. The number of functional groups is dependent mainly on the carbonisation temperature, biomass composition, the heating rate, and if applicable, the post-treatment method (activation) [61]. Hence, a great advantage of the chars depends on the possibility to tailor their

functionality and chemical properties by adjusting the mentioned parameters [31].

The surface functionality of the biochar is highly influenced by the pyrolysis treatment. Slow pyrolysis BCs consist mainly of aromatic C-H groups and to a lesser extent hydroxyl and carboxylic groups, whereas fast pyrolysis BCs are comprised mainly of hydroxyl and carboxylic groups. It is important to outline that the capacity of BC to exhibit an acidic or basic character in an aqueous dispersion is related to the oxygen content. BC with a high OFGs content will exhibit an acidic pH, while those with low OFG content are attributed to basic surface properties and anion exchange behaviour [61]. On the other hand, BCs derived from N-rich biomass usually contain nitrogen functional groups (NFGs). The fate of NFGs is mostly determined by the pyrolysis conditions. At lower temperatures, pyrrolic and pyridinic amines are present, whereas at higher temperatures pyridinic and quaternary groups are predominant [61].

Hydrochar exhibits an even greater content of OFGs than BC, formed by more complex oxygenated aromatics and polymeric compounds, such as ether, phenolic, and esters [81]. Particularly, the OFG content from the core and shell of the HC microspheres differ. The oxygen located in the core of the HC is within more stable groups (e.g., ether, quinone, and pyrone); while the oxygen from the shell consisted of more reactive hydrophilic groups (e.g. hydroxyl, carboxylic, carbonyl, and ester) [75]. Increasing HTC temperature led to extensive dehydration and condensation of the biomass, reducing the OFGs. Jain et al. [76] observed an increasing content of OFGs with temperature until reaching a maximum point at 275 °C, followed by a drastic reduction at 315-350 °C due to the high decomposition and gas formation.

2.3.5 Comparison between biochar and hydrochar

Biomass can be classified based on its initial moisture content as wet-biomass (>30 %) and dry-biomass (<30 %). The biomass feedstock used for pyrolysis and HTC must meet the requirements for each technology. Drying wet biomass is an energy-intensive and economically inefficient process, hence the use of this type of biomass in HTC avoids the requirement of this step. Examples of wet biomass suitable for HCT include freshly harvested vegetable waste, animal waste, sewage sludge, and algae. Pyrolysis, on the other hand, is a more appropriate treatment for dry biomass, such as agricultural and wood waste [60].

Given the different reactions taking place during each process, the physical, chemical, and functional properties of BC and HC differ significantly. The HC

generally exhibits a lower ash content than the original untreated biomass. This behaviour results from the hot pressurised water that facilitates the demineralisation of ash. Whereas, during pyrolysis, the ash content is enhanced since the BC retains and concentrates most of the inorganic constituents while the organic fraction is volatilised. The transformations of the biomass carbohydrates follow different pathways in each process. It is important to outline the importance of water in HTC and its extensive reactive role. For instance, the decomposition of hemicellulose is faster during HTC than slow-pyrolysis. The thermochemical treatment of biomass reduces both O:C and H:C ratios, although to a different extent. HC generally exhibits higher O:C and H:C ratios than BC. This suggests a predominant role of decarboxylation and dehydration reactions during HCT, while pyrolysis display more aromatisation. The fundamental molecular structure was described for each char. The spherical core-shell structure of HC contributes to a reduced porosity and SA. Whereas the BC exhibits a greater porosity and SA due to the reactions of mass loss and microstructure arrangements taking place during pyrolysis that promote the formation of pores [60].

2.4 Current applications of biochar and hydrochar

The biotechnological application of the products of pyrolysis and HTC are considered environmentally sustainable and cost-effective. Anthropogenic carbon dioxide taken from the atmosphere by plants can be further used as biomass for pyrolysis and HTC. Hence, this carbon dioxide can end up in the carbonaceous structure of the chars, which can be used as functional materials or carbon storage. Additionally, pyrolysis bio-oil and gas can be employed as a biofuel, which could also counterbalance the carbon dioxide emissions from fossil fuels [63]. Whereas HTC process water is reported to be used as a feedstock in the recycling for consecutive HTC runs, production of methane by AD, fertiliser, and disposal at a WWT plant [64]. Furthermore, the process waters contain some valuable compounds, such as levulinic acid, 2,5-hydroxyl-methyl-furfural (2,5-HMF) that are key blocks to producing further valuable chemicals.

The main scope of the HTC and pyrolysis solid products is carbon sequestration and the production of energy as an alternative to coal [82]. Alternative uses have essentially focussed on soil amendment, and as contaminant adsorbents in soil, water, and air. The addition of chars to the soil has proven to reduce the loss of nutrients and improve the production of crops [83]. Recently they have gained attention as advanced materials for other areas, including energy production,

agriculture, wastewater treatment, and bio-refinery [60]. Porous carbon materials are widely used for catalysis, energy storage, chromatography, gas separation, and water and air purification [84]. Carbon-based materials with a mesoporous structure are extensively applied as catalysts or catalyst supports in different industries. The interest in the chars as support materials for replacing the conventional carbon-based catalysts has been raised. The latter is due to the physicochemical properties of biochar and hydrochar, and the possibility of their tailoring by controlling the process conditions and their sustainable origin [31].

The advancement in research and technology for pyrolysis and HTC, in addition to the attractive and diverse properties of the chars, has broadened the application fields. For instance, biochar activated with sulphuric acid has been employed as an inexpensive catalyst to produce biodiesel [85]. Biochar enhances the yields in comparison to other commonly used catalysts, such as Zeolite Beta, niobic acid, Amberlyst-15, and sulphated zirconia [86]. Moreover, biochar is an economic option for the removal of tar, a necessary step to produce syngas by biomass gasification. The removal efficiency of biochar surpassed the reported for olivine and dolomite, commonly used materials. Thereby, the reports of the performance of biochar indicated its potential as an alternative and economic catalyst for different processes [31]. Additionally, biochar and hydrochar are reported to serve as immobilisation supports for purified proteins. For instance, Castro et al. [80] immobilised ConBr lectin on hydrochar reporting that non-covalent interactions were sufficient to maintain the protein structure and stability. Furthermore, González et al. [21] immobilised lipase from *Candida rugosa* onto biochar, observing an enhanced enzymatic activity. Khosla et al. [24] immobilised lipase on activated biochar for the transesterification of oil feedstocks. The immobilisation resulted in higher biodiesel productivity in comparison to the suspended enzyme. These studies used immobilisation by binding, supporting the potential of the chars as a support material.

Recently, it has been pointed out the positive outcome of the integration of char products from thermochemical processes with anaerobic digestion, for enhancing the digestibility of the organic fraction of municipal solid waste (OFMSW) and the production of methane. The chars are reported to promote the formation of biofilm, adsorbed toxic compounds, and work as a support material for the immobilisation of microorganisms. It has been reported the application of biochar as a heterogeneous catalyst for different purposes. There are several reports of the addition of biochar for enhancing methane yield and production rate. This improvement has been generally attributed to a series of biochemical

interactions and micro-environmental conditions. For instance, higher electrical conductivity, improved DIET processes, improved syntrophic VFA oxidation, and acid buffering [48]. Studying the potential of biochar and hydrochar as adsorbent materials in AD is part of the objectives of this work and will be discussed in detail in further sections.

2.4.1 Char addition in anaerobic digestion

It has been suggested that the addition of carbonaceous materials like BC, HC, activated carbon (AC), graphite, graphene, carbon nanotubes (CNTs), and carbon cloth may improve AD efficiency [48]. The advantages of using chars, BC and HC, over other adsorbent carbon materials include their low cost, the potential to use a wide range of biomass feedstocks for their production, their environmental sustainability, improvement of the digestate, and them having advantageous physicochemical properties that can be further tailored to fulfil desired characteristics [31].

There are reports of BC having a positive impact on AD performance. For instance, Sugiarto et al. [36] used 1 % (w/v) of pine sawdust BC produced at 650 and 900 °C in the AD of food waste. BC addition improved methane yield and production rate by 41-47 and 33-43 %, respectively. BC addition also accelerated acetic and butyric acid formation and further VFA degradation. They attributed this positive effect to the minerals contained within the BC that can support microbial metabolism by acting as micronutrients. They also observed that BC stimulated the growth of the acetoclastic *Clostridia* and the methanogen *Methanosaeta*. Mumme et al. [17] studied the impact of BC and HC addition at 2 % (w/v) in the AD of ammonium carbonate at variable concentrations (0, 500, 1500, 2500 and 5000 mg N/kg). The BC was produced by pyrolysis of paper sludge and wheat husks at 500 °C for 20 min, while the HC was obtained from the HTC of wheat straw digestate at 230 °C for 6 h. Both chars reduced the start-up phase and accelerated the growth phase, although there were differences regarding the stability of the chars. The values of labile carbon fraction were 0.6 and 10.4 % for BC and HC, respectively. The higher degradability of the HC suggests the presence of readily available carbons, such as sugars and volatile organic compounds. Particularly for BC, the digester was able to endure mild concentrations of total ammonium nitrogen (TAN) (≤ 500 mg/kg) without an inhibitory effect. At higher TAN concentrations, the methane yield was affected which indicate that the preventing ammonia inhibition provided by the BC had a limited capacity. They also evaluated the microbial consortia, suggesting that BC and HC might provide support for the growth of methanogenic microorganisms.

Another case study was performed by Luo et al. [87], where BC from fruitwoods pyrolysed at 800 °C was added to AD. The digestion conditions included a char load of 1 % (w/v), inoculum 1 g VS/L, and glucose at 4, 6 and 8 g/L. At this point is worth remarking on the limitations regarding the inoculum, as it was stored at very low temperatures (-80 °C), and no acclimatisation treatment was applied. Additionally, they employed considerably low inoculum to substrate ratios (ISR) with values of 1:4, 1:6 and 1:8. The latter could be accountable for the considerably large initial lag phase (10 to 20 days) observed for all treatments. Nonetheless, BC addition for the digestion of glucose at 4, 6 and 8 g/L reduced the lag phase (11.4, 30.3 and 21.6 %) and an improved methane production rate (86.6, 21.4 and 5.2 %) in comparison to the non-BC control, respectively. However, BC addition had no significant effect on methane yield, although it promoted the formation and degradation of VFAs with n-butyrate and acetate as major intermediates and minimal concentration of propionate. They also observed the establishment of methanogenic zones on the surface of the BC with *Methanosarcina sp* residing inside the pores and *Methanosaeta sp*. on the outer surface. They stated that BC promoted biofilm growth and the transfer of protons and electrons between cells.

Similar results were obtained by Wang et al. [88] as they tested two UASB reactors operated continuously for 100 days. The rice straw biochar was produced by pyrolysis at 500 °C. The reactors were inoculated at 3 g VS/L, sucrose 90 g/L, one with biochar 0.4 % (w/v) and the other without biochar, with gradually increasing COD. The BC reactor exhibited a lower accumulation of VFAs, a higher proportion of methane in the biogas, and enhanced methane yield (13 %) and lag phase (29 %) in comparison to the control. The BC addition also improved conductivity, granulation formation, and enhanced dominance of the archaea *Methanosarcina* and *Methanosaeta*. They attributed this positive effect to the tandem reaction of syntrophic acetate oxidation and hydrogenotrophic methanogens and suggested that BC could promote the conversion of CO_2 into CH_4 and reduce H_2.

In the literature, there are fewer reports of HC addition than BC in AD. Wang et al. [89] evaluated the impact of cellulose HC produced at 220 and 260 °C in AD. They suggested that HC addition could improve the acidification step by enhancing the production and accumulation of short-chain fatty acids (SCFA). HC also promoted substrate degradation and enhanced sludge solubilisation. They observed that HC inhibited the methanogenic activity of the archaea fraction. They partially attributed this to the competition of the humic substances and the methanogens for the electrons, decrementing the reaction of acetyl-CoA → 5-

methyl-THMPT and consequently a slower SCFA consumption. They reported an increase in the activity of the enzymes involved in hydrolysis and acidification. Furthermore, Codignole-Luz et al. [90] studied the use of spent coffee HC produced by HTC at 180, 220 and 250 °C as a substrate for AD. The HC produced at the lowest temperature exhibited the highest methane yield and production rate. This highlights the potential of mild HTC as a pre-treatment of biomass and suggests that more severe HTC conditions could result in less degradable and more stable HCs.

2.4.1.1 Biochar in syntrophic interactions

The proposed mechanism for explaining how BC facilitates methane generation is complex. The H_2 produced during acidogenesis increases the partial pressure of the system, thus the rapid response of H_2-utilising archaea and the subsequent production of methane is key. The interspecies electron transfer (IET) between fermentative bacteria and methanogens employs formate or H_2 as electron carrier via the hydrogenases and formate dehydrogenases (FDH) enzymes. This syntrophic IET relation can overcome the internal energy barrier (positive Gibbs free energy) required for the transformation of VFAs and acetate into methane [91].

Direct interspecies electron transfer (DIET) interactions are more thermodynamically favourable and efficient than IET because they do not depend on electron carrier diffusion. The mechanisms involved in DIET are bioelectric connections via biological compounds, such as conductive pili (e-pili), c-type cytochrome (OmcS) and electron transport proteins. However, it is necessary for the microorganisms involved in DIET to have an intimate direct contact with the electron transport proteins on the outer membrane to deliver the electrical contact. Remarkably, microorganisms can exhibit DIET not only through their conductive structure but also via exogenous non-biological conductive materials (CM), such as carbon-based or metal-based CM. Carbon-based CMs, such as chars, can mediate the DIET by emulating the function of pili or OmcS [91]. Though, it has been reported that the electrical conductivity of the BCs is not a rate-limiting factor for its role in the DIET process and other properties responsible for enhancing the methanogenic rate [48,91,92].

Chars catalyse the reductive reactions by facilitating the transfer of electrons from bulk chemical electron donors to a receiving organic compound. The role of the char in electron transfer catalysis could involve two types of redox-active structures, quinone-hydroquinone moieties and/or conjugated π-electron systems within the condensed aromatic sub-structures of the char. A correlation

between the carbonisation temperature and the redox properties of the chars has been proposed. The pool of redox-active moieties within the chars produced at low temperature (200-300 °C) is dominated by electron-donating phenolic moieties. Whereas intermediate (400-550 °C) and high temperature (>600 °C) chars are dominated by electron-accepting quinones and condensed aromatics, respectively. Furthermore, the redox states of the chars respond to changes in the external redox conditions, suggesting that the chars can also act as redox buffers [93]. It has even been suggested that conductive carbon may affect the gene expression and enzyme synthesis of bacteria, modifying then the metabolic rates of the pathways, although this requires more research [48].

The electrons involved in methanogenesis are generally destined to three mechanisms: (i) certain microorganisms use them to chance the ΔG° of the reaction; (ii) some methanogens use them for methane generation; (iii) some electron acceptors compete for them. Thus, the addition of CMs could capture more electrons for the second mechanism and generate more methane by triggering DIET and obtaining a more efficient syntrophic metabolism. CM, such as biochar, can replace the role of conductive pili or c-type cytochrome, facilitating thus the DIET between substrate-oxidation microorganisms and methanogens, and in consequence AD performance [91].

There are several reports of the addition of biochar for enhancing methane yield and production rate. This improvement has been generally attributed to the properties of the chars and a series of biochemical interactions and micro-environmental conditions. These properties are further described in this Chapter, whereas a detailed compilation and analysis of the reports of biochar addition in AD are discussed in Chapter 7.

2.4.1.2 Biochar as immobilisation support

It has been reported that BC can act as immobilisation support for the anaerobic sludge. The improvement in methane generation has been attributed to the proliferation and immobilisation of methanogens, such as *Methanosaeta* and *Methanosarcina*, onto the biochar [87]. Cell immobilisation in a digester often takes place by adsorption and biofilm formation over solid support. The immobilisation by physical adsorption is a reversible process performed via the direct interaction of the cells and the carrier. The binding is achieved through physical and chemical interactions. The physical interactions often include hydrophobic and Van der Waals interactions, while the chemical binding includes ionic and covalent bonding [94]. For achieving the formation of chemical bonds, the support must offer a large presence of functional groups. On

the other hand, the immobilisation by non-covalent interactions is simple and in aqueous-based media, these interactions can occur by themselves [80]. The transport of the nutrients from the bulk medium to the immobilised cells exhibits transfer efficiency [95]. Further advantages include biomass stability and retention, better substrate consumption under low HRT, and enhanced productivity [96]. One of the challenges of immobilisation techniques is the preservation of the fundamental properties of both support and cells. From the different immobilisation approaches, covalent bonding provides stability and reduces leaching problems.

Biochar exhibits desirable properties that made it suitable for immobilisation. Key physicochemical properties include surface area, particle size, pore structure and surface functional groups. The working surface area available for immobilisation involves the external surface area of the carrier minus the area of the micropores. The porous structure of the support facilitates the biomass transfer between the substrate on the bulk and the immobilised microorganisms [96]. Moreover, certain interactions between the cell and the support depend on the chemical characteristics of the surface of both. It has been reported the importance of OFGs on the surface of the support for the hydrophilic character, and the promotion of electrostatic interactions that lead to a greater immobilisation performance [27]. The surface chemistry of the support has shown a direct effect on the enzyme loading, bacterial population and the catalytic activity of the immobilised system [97].

2.4.2 Comparison of biochar with other materials

Carbon, metal, and mineral-based materials have been applied to improve AD performance by facilitating the syntrophic metabolism, increasing thus the acceleration rates and the thermodynamic and kinetic efficiencies. Among these materials are AC, BC, carbon fibre, CNTs, carbon cloth, graphite, graphene, zeolite (aluminosilicate minerals), hematite (Fe_2O_3), and magnetite (Fe_3O_4) [48,91]. Many of these materials have been reported to amend AD and improve methane yields and production rate (μ_m). It has also been stated their potential as supports for the immobilisation of the anaerobic sludge. In prolonged processes, such as AD, superior biomass retention and substrate utilisation has been related to the formation of biofilm and granular sludge. Reaching a high cell density in immobilised systems could increase the efficiency of the production, reduce the fermentation time, facilitate product recovery, and provide protection and re-utilisation of cells [98]. These materials should have a well-developed porous structure, and an affinity for the cells to immobilise to guarantee the maximum

activity possible. In addition, the cost of the supporting materials must be reasonable, they must have a long-life endurance, inertness and thermo-stability [99]. Therefore, in this section, the implementation of other additives in AD is reviewed and compared to the BCs.

Carbon materials are recognised as the most promising materials for AD given their high surface area, porosity, superior textural properties, and adsorption capacity. There are several reports of the positive effect of different carbon materials in AD. For instance, Yan et al. [100] improved the stability and performance of thermophilic AD of glucose by adding granular activated carbon (GAC) and CNTs. The addition of these materials promoted the enrichment of microorganisms involved in the DIET process, and almost doubled μ_m. Lin et al. [101] evaluated the addition of 0.05-0.2 % of graphene in the AD, resulting in similar μ_m, reduced λ and slightly improved the BMP yield to the control, with the best performance of a graphene load of 0.1 %.

Shanmugam et al. [28] compared five BCs and two AC, GAC and powdered activated carbon (PAC). The addition of the additives resulted in considerably higher BMP than the control, although the BC systems surpassed the AC. It is important to distinguish the differences between these materials. BC is produced by the pyrolysis of biomass at 400-600 °C. Whereas AC is produced by the carbonisation of coal, asphalt, or biomass at 700-1000 °C, accompanied by physical or chemical activation. There are similarities between BC and AC, as both possess an amorphous structure with large porosity. Nevertheless, BC usually exhibits a lower carbon content and significantly higher presence of functional groups than AC [63]. Nonetheless, the production of BC is relatively cheaper than other adsorbents because BC is produced at lower temperatures and does not require activation [16].

Other non-carbon materials have also demonstrated a positive impact on AD. Suanon et al. [102] studied the effect of two iron nanoparticles in AD, nanoscale zero-valent iron (nZVI) and magnetite. They observed more methane content with the addition of both nanoparticles, attributed to facilitated DIET in syntrophic methanogenesis. Although the concentration of the magnetite nanoparticles affected the yields since at 0.5 % the methane production was improved whereas at 1 % it was strongly inhibited, suggesting a toxic effect. On the other hand, they suggested that nZVI could serve as an electron-donor for methanogens and facilitate the release of hydrogen during corrosion/oxidation, resulting in a better methane yield.

Achi et al. [34] compared the addition of BC and zeolite as adsorbent materials for the AcoD of cassava wastewater and livestock manure. Zeolite improved BMP, whereas BC reduced λ and accelerated methane production. Shao et al. also compared zeolite with wood BC prepared at 900 °C, with the addition of an external voltage for the AD of acetate. The reactors underwent 4 consecutive cycles, where more substrate was added after the depletion of the acetate. For the first cycle, neither additive of voltage had an effect. For the second cycle, the mixture of BC and voltage enhanced the BMP, whereas the zeolite offered no difference in comparison to the control. For the third cycle, both adsorbents in the presence of the voltage improved AD, whereas the adsorbents by themselves had no effect. They stated that the adsorbents, especially BC, could amend only reactors under stressful conditions.

The use of BC as a heterogeneous and inexpensive catalyst has been reported for different purposes. For instance, BC treated with H_2SO_4 has been compared to other catalysts to produce biodiesel. BC has resulted in a better performance in comparison to zeolite, niobic acid, Amberlyst-15, sulphated zirconia, and $Al(HSO_4)_3$. Moreover, BC has also been employed as an economic option for the removal of tar, a necessary step to produce syngas by biomass gasification. The tar removal efficiency of BC surpassed the reported for olivine and dolomite, commonly used materials. Thereby, the reports of the performance of biochar indicated its potential as an alternative and economic catalyst, not only for AD but for different processes [31].

Chapter III

Materials and methods

3.1 Introduction

The scope of the project covered the production of chars from different feedstocks and their application as additives and immobilisation materials in fermentative processes. This chapter provides information about the feedstock materials, equipment, analytical techniques, and experiments used throughout the PhD research. For facilitating the connection with the results from further chapters, this chapter was divided into three stages as outlined in **Figure 3.1**. Firstly, a description of the feedstocks and the methods used for pyrolysis and hydrothermal carbonisation. This is followed by a detailed discussion of the methods used for the chemical, physical and functional characterisation of the chars. Secondly, information on the source of digestate inoculum and substrates employed in anaerobic fermentations is provided with a description of the equipment used for anaerobic digestion. The experimental methodology that was used for char addition to anaerobic digestion is described. Thirdly, the anaerobic digestion results originated from this work are compared to the literature via factor analysis. The tests, software and methods used for this comparison and other statistical tools used throughout this thesis are discussed in this section.

All chemicals used for these methodologies were of analytical grade and used as received.
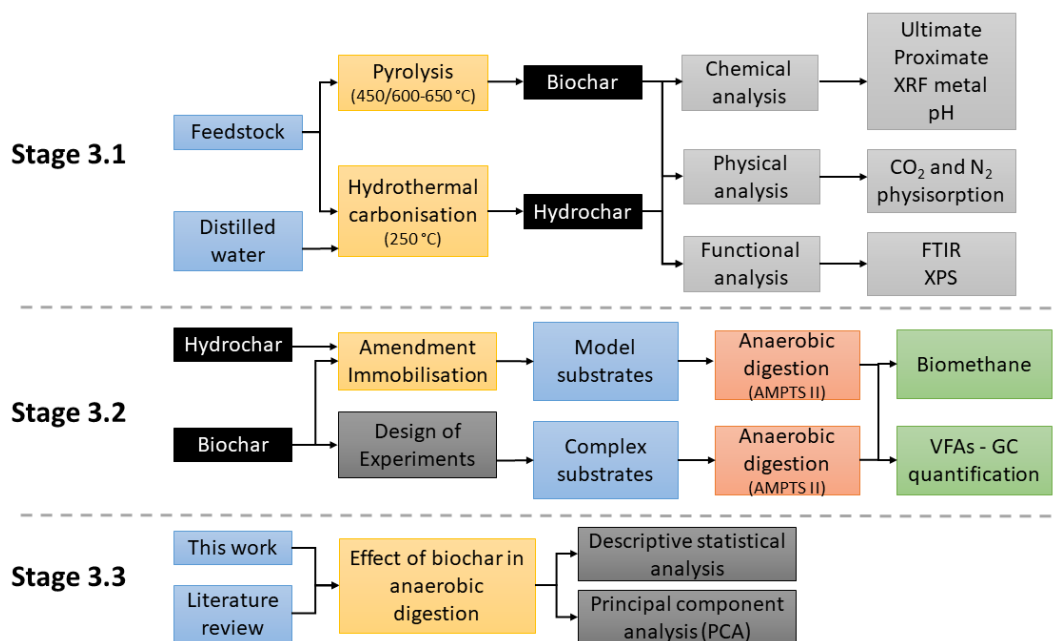
Figure 3.1. Flow chart outlining the three method sections and analytical techniques used during this thesis work.

Blue: material and data; black: chars; yellow: treatment; orange: anaerobic digestion experiments; grey: characterisation methodology; dark grey: statistical methods; green: fermentation products biomethane and volatile fatty acids quantified by gas chromatography.

3.2   Thermochemical processing and char characterisation

3.2.1 Feedstock description

A range of organic wastes from agricultural and invasive sources was employed as feedstocks for the pyrolysis and hydrothermal carbonisation processes. The selection was based on the compositional differences between them given their nature and origin. Thus, the selected feedstocks comprised oak wood, water hyacinth, and saw wrack. Holm oak (*Quercus ilex*) wood was obtained from a clean forestry holm oak wood residue. The seaweed saw wrack (*Fucus serratus*) was collected from the shores of Aberystwyth, Wales. This biomass was subsequently air-dried and milled down as provided by Aberystwyth University. Water hyacinth (*Eichhornia crassipes*) was collected from Lake Victoria in Uganda and provided via a collaboration with the Centre for Research in Energy and Energy Conservation (CREEC) at Makerere University. WH was dried and milled before its shipment to the UK. The characteristics of the feedstocks could be altered during storage due to their composition, and the storage conditions, such as duration, climate, container configuration and the presence of air.

Biomass can lose mass in the form of moisture, volatile chemicals, and dry matter. The stored biomass needs to have a low content of moisture since water is linked to biological degradation and loss of dry matter, especially when stored. Storage at an optimal temperature for fungal activity (20-30 °C) is problematic if the biomass has a considerable moisture content. The loss of mass and compositional changes of biomass are more significant when stored in uncovered conditions [103]. To minimise the above mentioned, all samples were stored in a solid container in a dark cupboard at room temperature. Biomass collected in different periods will exhibit different compositions due to seasonal variations. Thus, the feedstocks used for producing the chars corresponded to the same batch.

3.2.2 Pyrolysis

Oak wood biochars were produced by Proininso S.A. (Malaga, Spain) via slow pyrolysis in a mono retort reactor from a bark-free holm oak wood residue, in the absence of oxygen at 450 and 650 °C. They are referred to as OW-BC450 and OW-BC650, respectively. The biochars were provided with particle sizes ranging from approximately 5–50 mm.

Pyrolysis was performed at the University of Leeds in a laboratory-scale fixed-bed slow pyrolysis reactor shown in **Figure 3.2**. Between 50 and 150 g of sample was added to a stainless-steel tube and further placed inside a metal mesh basket of 82 mm internal diameter (ID). The feedstocks saw wrack and water hyacinth were pyrolysed at 2 HHT sets, 450 and 600 °C, and held constant for 1 hour. After this period the heater was turned off and allowed to cool down at a rate of 0.4-1.4 °C/min. The nitrogen flow was maintained for at least one hour during the cool-down period for removing the remaining evaporated material. The sample, pyrolysis oils and containers were weighed for yield calculation. Once cooled, the chars were stored in airtight containers.

The pyrolysis reactor consisted of a sealed tube furnace of 95 mm I.D. x 820 mm in length where the mesh basket containing the sample hung at the centre (**Figure 3.3**). A 1.2 kW tube furnace externally heated the reactor at a heating rate of 5 °C/min until reaching the desired highest heating temperature (HHT). A flow of nitrogen at 200 mL/min is fed through the top of the reactor to remove oxygen and volatile compounds and create an inert atmosphere. The addition of a nitrogen carrier begins 10 minutes before the heating commences for purging the oxygen from the system and assuring anoxic conditions. A condenser set at 4 °C cooled down the hot gases that originated from the furnace, removed the

condensable compounds, and further collected them in a catch pot below. The exhaust non-condensable gases were passed through two impingers to remove liquid or solid residues from the stream. The impingers were in series, the first one containing water and the second quartz wool.
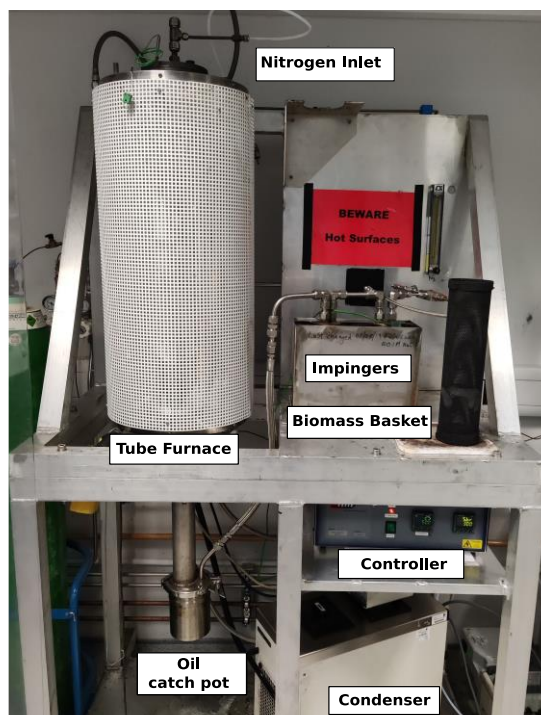
Figure 3.2. Bench pyrolysis reactor used for biochar production.
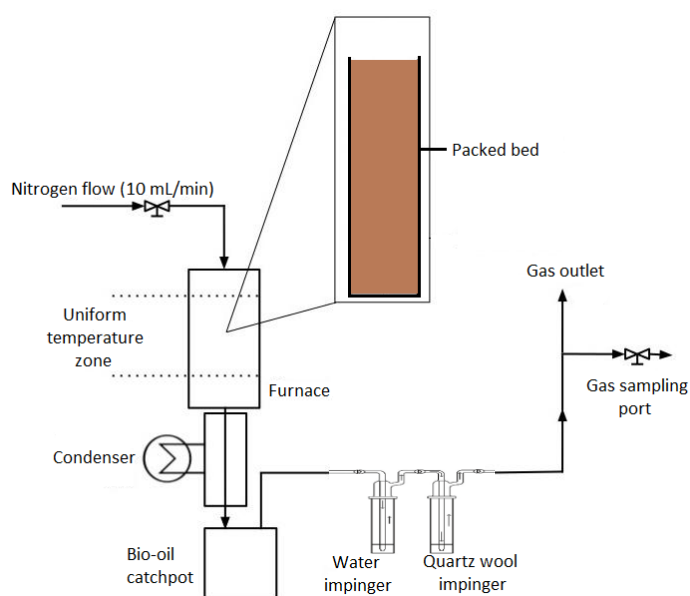
Figure 3.3. Schematic describing the components of the pyrolysis reactor.

3.2.3 Hydrothermal carbonisation

HTC was performed at the University of Leeds in a 2 L benchtop autogenic non-stirred reactor (Parr Instrument Company, USA) (**Figure 3.4**). 96 g of sample and 880 mL of distilled water were placed inside a weighed glass liner, sealed, and inserted into the HTC reactor. A heating jacket surrounding the vessel heated the reactor using a ramped proportional-integral-derivative (PID) controller at a heating rate of approximately 8 °C/min. Once the HTC reactor reached an HHT of 250 °C, it was held for 1 h, while the pressure was increased up to approximately 40 bar. The reactor temperature was measured with two thermocouples, one located on the inner wall of the reactor and the other at the centre of the reactor. At the end of the residence time at the desired HHT, the heating was turned off, and the reactor was allowed to cool down. The reactor was opened once it reached room temperature, the gaseous phase was vented through the fume cupboard and the reactor liner containing the solid and liquid phase was taken out and weighed. Liquid and solid phases were separated by vacuum filtration using 150 mm filter paper (Whatman, UK). The obtained hydrochar was first allowed to air dry in a ventilated fume cupboard and then oven-dried at 60 °C overnight. The mass balances of materials and containers are registered for further calculating product yields.
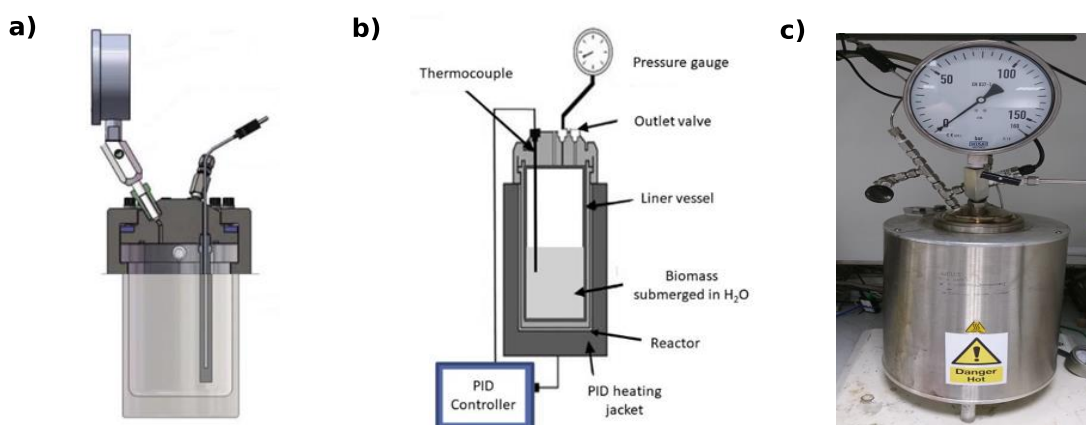
Figure 3.4. Schematic describing the 2000 mL HTC Parr reactor. a) HTC reactor design; b) components of the HTC system; c) HTC reactor used for hydrochar production. Modified from Kottatep et al. [104].

3.2.4 Biochar activation

Activation treatment modifies the essential properties that govern the catalytic activity of carbon material, such as surface area, pore-volume, pore size, and

functionality. In the chemical activation process, the raw material is impregnated with the reagent and subsequently pyrolysed. Chemical activation is preferred over physical activation since it results in higher yield, more porous biochars and allows the use of lower pyrolysis temperature and time of treatment, thereby reducing energetic requirements [105]. However, the utilisation of chemical agents creates pollution concerns [106].

The chemical activation of biochar with the metal magnesium followed the methodology described by Zhang et al. [107]. The same holm oak wood biomass used for producing the OW-HC250 by HTC was selected for this methodology. 10 g of untreated wood flakes were mixed with an $MgCl_2$ solution, where 40 g of $MgCl_2 \cdot 6H_2O$ were dissolved in 60 mL of distilled water. This mixture was stirred thoroughly, left to stand for 2 h at room temperature, and dried in an oven overnight at 100 °C. Afterwards, the biomass impregnated with $MgCl_2$ was pyrolysed at 450 °C in the slow pyrolysis reactor at the University of Leeds, as described in section 3.2.2. The resulting biochar was designated as OW-BC450-MgCl.

3.3 Analysis of the feedstocks and chars

Figure 3.1 shows a flow diagram of the analysis used for the untreated biomass and chars. The materials were homogenised into fine powder by mortar and pestle before analysis, except for the adsorption isotherms. It was important for this method to maintain the innate physical structure of the chars. Biochar suffers a mild and slow oxidation process at ambient temperature, that exacerbates by being exposed to atmospheric conditions and warmer temperatures. Atmospheric ageing incorporates moderate amounts of oxygen onto the biochar by increasing the OFGs. Photochemical transformation of biochar induces the generation of active oxygen species, such as hydroxyl radical (•OH), singlet oxygen (O_2), and superoxide (O_2^-) [108]. To minimise the above mentioned, all samples were stored in a solid container in a dark cupboard at room temperature.

3.3.1 Proximate composition

The untreated feedstocks and produced chars were analysed for moisture content (M), volatile matter content (VM), fixed carbon content (FC) and ash content (**Figure 3.5**). The proximate composition was determined via a thermogravimetric analyser (TGA) (Mettler Toledo TGA/DSC 1). Approximately 10 mg of the homogenised sample was placed into an Alumina 70 µL ceramic

crucible. The sample was compacted and flatted by carefully tapping on the worktop, weighed, covered with a stainless-steel lid to protect from atmospheric moisture, and then placed in the TGA. The equipment automatically took the sample, removed the lid, and performed the analysis. The analyser was set from 25 to 900 °C with a heating rate of 25 K/min and under a constant flow of nitrogen (50 mL/min). The program followed a temperature ramp: (1) linear heating from 25 to 105 °C; (2) held at 105 °C for 10 min for moisture removal; (3) linear heating from 105 to 900 °C; (4) held at 900 °C for 10 min for volatile matter removal; and (5) held at 900 °C for 15 min while switching nitrogen flow to airflow for promoting complete combustion of fixed carbon. The remaining product comprised just the inorganic fraction (ash). The difference in mass loss during the heating stages allowed for calculating the percentage for moisture, volatile matter, fixed carbon and finally ash.
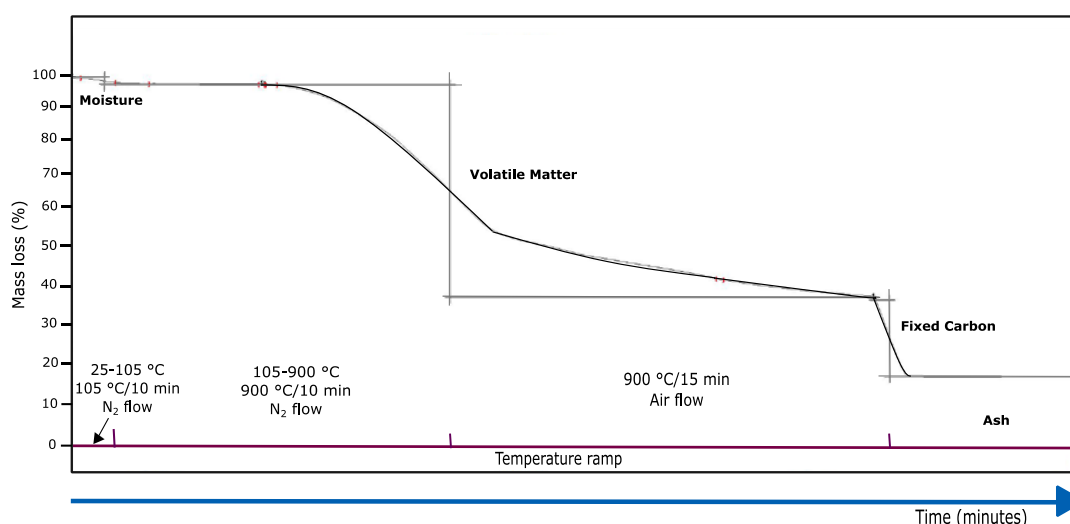
Figure 3.5. Example of a proximate analysis curve produced by TGA analysis, noting the division of sections.

3.3.2 Ultimate composition

The aim of the ultimate analysis is the quantification of the elemental composition of biological materials: carbon, hydrogen, nitrogen, sulphur, and oxygen (CHNSO). The principle of the method is the flash combustion of the sample via the elemental analyser 'Thermo Instruments Flash EA 1112 Series'. 2.5-3.0 mg of sample were weighed inside tin foil capsules (Elemental Microanalysis D1009) with a dimension of 8 x 5 mm, crimped for removing the presence of air, and finally analysed in duplicate. The encapsulated sample was

combusted at 1000 °C inside the reaction zone of the elemental analyser and within a helium atmosphere and a known amount of oxygen. The elemental composition of the samples was calculated by the conversion of carbon to CO_2, nitrogen to NO_x, sulphur to SO_2 and hydrogen to H_2O. These gases were then passed through gas chromatography coupled to a thermal conductivity detector (TCD), which identified the composition according to their chromatogram. The instrument was calibrated, and the analysis was verified by running standards and certified biomass reference materials (Elemental Microanalysis, Devon, UK) in parallel to the samples (**Table 3.1**).

The values for CHNS are expressed as the percentage of total dry weight, with total oxygen (O) determined by difference as follows:

$$O\,(\%) = 100 - C(\%) - H(\%) - N(\%) - S(\%) - ash\,(\%) \qquad \text{Equation 3-1}$$

Table 3.1. Known composition of the standards used for ultimate analysis

Standard	Description	Ultimate (% wt, db)				
		C	H	N	S	O
B2044 BBOT	2,5-Bis(5-tert-butyl-2-benzo-oxazol-2-yl) thiophene (BBOT) OAS	72.53	6.09	6.51	7.44	7.43
B2276 Oatmeal	Oatmeal Organic Analytical Standard	47.76	5.72	2.09	0.16	-
B2306 Coal	Coal Standard Sulphur Range 2.04%	-	-	-	2.03	-
B2322 Coal	Ultimate coal standard	45.14	3.39	0.91	2.27	5.40

The standards were acquired from Elemental Microanalysis, UK.

3.3.3 Inorganic analysis

X-ray fluorescence (XRF) is a non-destructive elemental analysis technique that provides quantitative chemical information about a given material. XRF allows the quantification of the absolute concentration of inorganics from XRF signals. It consists of the bombardment of a specimen with X-rays, where a high-energy incident, also called primary X-rays, collide with the atom disturbing their stability, and resulting in changes in the electrons of the orbitals of the atom. An electron from a low-energy level is ejected leaving a space that is subsequently filled by an electron from a higher energy level. The difference in energy produced by the movement of electrons is called secondary X-rays and is characteristic of each atom. The resulting characteristic fluorescence spectra are collected and analysed for quantification [109].

XRF was used to determine the inorganic elemental composition of the chars and untreated samples. Before analysis, the homogenised samples were prepared by calcination in a furnace muffle (Nabertherm B80), the heating rate was not determined, and the atmosphere was not controlled. The samples were first heated at 550 °C for two hours and then a further treatment at 850 °C for two hours. The ashes were collected, ground with mortar and pestle for homogenisation, and stored in a desiccator. 0.7 g of ash was accurately weighed and mixed with 6.3 lithium borate flux into a platinum crucible. This mixture was heated at 1100 °C and melded back into the crucible using a Katanax K1 automated fusion system. The fused beads were then analysed by wavelength dispersive X-ray fluorescence (WDXRF) on a Primus WDXRF 1 (Rigaku, Japan).

3.3.4 pH measurement

The pH measurement of the chars was performed by following the methodology suggested by Singh et al. [110]. 5 g of air-dried biochar (<2 mm) were weighed into a 100 mL centrifuge bottle, with 50 mL of distilled water. The mixture was stirred for 1.5 h at room temperature. Afterwards, the suspension was allowed to stand for 30 min and the pH was measured.

3.3.5 Gas physisorption for surface area and pore size distribution

Gas adsorption (physisorption) measurements are implemented for the analysis of the surface area (SA) and pores size distribution (PSD) of solid materials. The term 'physisorption' refers to the process where an adsorbable gas (N_2 or CO_2), named the adsorptive, gets into contact with the surface of solid material, named the adsorbent. The intermolecular forces involved in physisorption include attractive dispersion and short-range repulsive forces. Additionally, the geometric and electronic properties of both adsorbent and adsorptive lead to some specific molecular interactions, such as polarisation, field-dipole, and field gradient-quadrupole. Hence, the mechanisms behind physisorption are also dependent on the properties of the gas (adsorptive), and the shape of the pores. The complete accessible volume inside micropores is considered the adsorption space that can be filled with gas (micropore filling). Whereas in the case of mesopores, the physisorption comprises more stages, including monolayer-multilayer adsorption and capillary condensation. On the other hand, the gas adsorption on the walls of macropores only comprises surface coverage [111].

The adsorption isotherms represent the relationship between the amount of gas adsorbed and the equilibrium pressure of the gas at a constant temperature. The

adsorption isotherm is determined by a static volumetric method at a constant temperature. Thus, a known amount of pure gas is introduced into a confined volume of the adsorbent, and as adsorption develops, the pressure of the confined system falls until reaching equilibrium. At equilibrium pressure, the amount of gas admitted corresponds to the difference between the amount of gas adsorbed and the necessary amount of gas for filling the space that surrounds the adsorbent (dead space). The measurement of the admitted gas is taken point by point, while successive dosing of gas is administered, these points are used for the formation of the adsorption isotherm [111].

The physisorption isotherms are obtained by plotting the volume of gas adsorbed against the relative pressure $p/p°$ and can be grouped into six types (**Figure 3.6**). The reversible Type 1 isotherm is concave against the $p/p°$ axis until $p/p°{\rightarrow}1$, where n reaches a limiting value. The reversible Type II isotherm suggests unrestricted monolayer-multilayer adsorption with a marked Point B, which indicates the beginning of the linear section of the isotherm, representing thus the point where the monolayer coverage is complete, and the multilayer adsorption starts. The Type II isotherm is characteristic of both non-porous and macroporous adsorbent materials. The reversible Type III isotherm is convex against the entire p/p_0 axis; thus, it does not present a Point B and is not found for most adsorbents. The initial section of the Type IV isotherm exhibits the same pattern that Type II isotherm, which is attributed to monolayer-multilayer adsorption. In addition, the Type IV isotherm follows a characteristic hysteresis loop, associated with capillary condensation in the mesopores, and produces a gas uptake limitation over higher p/p_0. The Type V isotherm is related to the Type III isotherm, as the interaction between the adsorbent and the adsorbate is weak. The Type V isotherm is also uncommon, except for certain porous adsorbents. Finally, the Type VI isotherm follows a stepwise multilayer adsorption pattern, with a step height that represents the monolayer capacity of each adsorbed layer. The sharpness of the steps depends on the system and the temperature and it is common to have only two or three layers. However, the Type VI isotherm is commonly reported only when using argon or krypton as adsorptive. Furthermore, the interpretation of physisorption isotherms starts with the identification of the type of isotherm, followed by the identification of the adsorption processes that may be taking place (monolayer-multilayer adsorption, capillary condensation or micropore filling). Afterwards, an empirical model is used for the quantification of the surface area and pore size distribution [111].
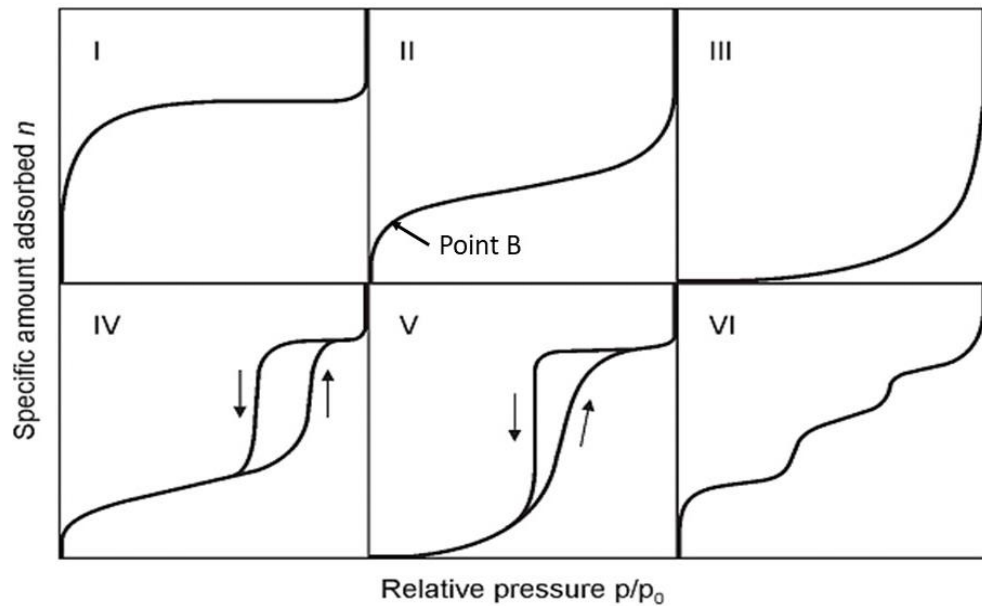
Figure 3.6. Physisorption isotherm types. Adapted from [111].

I) microporous solids; II) nonporous or macroporous solids; III) no identifiable monolayer formation; IV) mesoporous solids; V) hydrophobic micro and mesoporous materials; VI) highly uniform nonporous solid.

The surface area and porosity of porous materials are typically obtained by N_2 adsorption at 77 K. However, this bears certain diffusion limitations due to the inability of N_2 to reach micropores that could underestimate the surface area. This problem could be overcome by using another adsorptive, such as CO_2 at 272 K. At this temperature, the CO_2 molecules exhibit higher kinetic energy and smaller kinetic diameter (3.64 Å) that allow them to enter into narrow pores [67].

Many models consider different characteristics of carbon materials, such as geometry, energetic heterogeneity of pore walls, the influence of neighbouring pores or the presence of pit defects on the carbon surface. However, in practice, using a simple slit-shape model is more appropriate because for considering the characteristics mentioned above, some assumptions must be taken distressing thus their justification. Even though the Brunauer-Emmett-Teller (BET) model is the most used for SA and PSD evaluation, it was not suitable for the isotherms obtained for the chars. Therefore, the nonlocal density functional theory (NLDFT) model was selected due to its compatibility with microporous materials [112]. NLDFT assumes pores to be infinite slits with graphite walls, meaning a solid structure and pore topology, where all the pores, despite the size, exhibit the same shape, and at the same time, each pore behaves independently [113].

Density functional theory (DFT) accompanied by computer simulation methods measures equilibrium density profiles for the adsorption of fluid on the surface and inside the pores, while calculating the PSD of meso- and microporous materials. Particularly, NLDFT simulation provides a highly accurate description of the fluid density profile inside narrow micropores. NLDFT calculates isotherms for a set of pore sizes by integrating the equilibrium density profiles of the fluid over the analysed system [114]. The superiority of NLDFT and its compatibility with the properties of carbonaceous materials and both adsorbates, N_2 and CO_2, make this method one of the most accepted and reliable.

The samples were outgassed before analysis to remove all the physically adsorbed species. The outgassing was achieved by applying a high vacuum at elevated temperatures. Increasing stepwise heating of 50 °C every 30 minutes until reaching 150 °C for HCs and 200 °C for BCs, and held for 1.5 h. Immediately before analysis, the samples were flushed by 30 minutes of nitrogen flux at room temperature. The selection of the temperature took into consideration the prevention of char decomposition. The analysis was performed in a Quantachrome Nova 2200. Two adsorptive gases were tested, N_2 at -196 °C (77 K) maintained with liquid nitrogen, and CO_2 at 0 °C (273 K) maintained with ice. Density functional theory (DFT) models for CO_2 and N_2 on slit-pore carbon were used for the pore size distribution (PSD) analysis on the Micromeritics software. The NLDFT models for infinite slit carbonaceous materials for CO_2 at 273 K and N_2 at 77 K were selected for the analysis of pores with 0.35-1.0 and 0.35-100 nm, respectively [115,116].

3.3.6 Attenuated reflectance Fourier transform infrared spectroscopy (ATR-FTIR)

Fourier Transforms Infrared (FTIR) spectroscopy provides qualitative information on the surface functional groups of a given sample. Of the different methods reported for FTIR, attenuated total reflectance (ATR) is the most used for char analysis. In ATR, the sample is placed in direct contact with an internal reflection element (IRE), such as a diamond crystal, with a higher refractive index than the sample and the surroundings. A specimen is irradiated with a continuous spectrum of infrared energy to reach the first vibrationally excited state, while the absorbed light quanta are measured. The spectrum obtained in the interferogram shows an absorption band at a frequency of the vibrations. Afterwards, the spectrum was calculated using the fast Fourier transform technique and correlated for the identification of compounds [117]. Each

material exhibits a unique spectrum since it absorbs and transmits different ranges and levels of light. Nonetheless, peak assignment for the stretching vibrations is largely reported for char materials.

The equipment employed for the ATR-FTIR analysis was an *iS10 Nicolet* ATR-FTIR spectrophotometer fitted with a diamond crystal. An approximate 34-36 scans were taken over a range of 4000–400 cm^{-1} and a resolution of 4 cm^{-1}. The readings were collected every 5 minutes for background, and the sample spectra data was automatically subtracted to minimize the interferences from atmospheric carbon dioxide.

3.3.7 X-ray Photoelectron Spectroscopy (XPS)

XPS identifies the elemental surface composition of a material by assessing the oxidation state of the elements and the dispersion of each element. The system involves a source of primary radiation (sample of study), an ultra-high vacuum chamber with an electron energy analyser, and the source of X-ray [118]. The specimen is irradiated by a soft X-ray beam (~15 keV) for the excitation of the atoms within the X-ray penetration depth and posterior relaxation from their excited state by the emission of low-energy photoelectrons (20-2000 eV). The emission of photoelectrons leaves an energy spectrum corresponding to the structure of the energy levels characteristic of the atoms from which they were originally emitted. Thus, the photoelectron spectrum allows the identification of the atomic species present in the near-surface region of the analysed specimen [119].

The generation and detection of photoelectron by XPS can be divided into three main steps: excitation, relaxation, and transport of the photoelectron to the surface. First, the atoms near the surface absorb energy (*hv*) from an incident X-ray photon, which leads them to an excited state. Second, the emission of photoelectron from the excited atom at an energy level of original binding energy E_B leads to a relaxation state. Third, the photoelectron travels through the material up to the surface, where they are emitted. The photoelectrons contribute to the spectrum intensity [119].

XPS measures the energy emitted by the electrons of a sample, the transitions of the observed photoelectrons are described according to their quantum numbers. The transitions are labelled by the scheme nl_j. First, n comprise the principal quantum number, with values of 1, 2, 3, etc. Second, the notation l corresponds to the quantum number for the orbital angular momentum of the electron, with values of 0, 1, 2, 3, or more than the commonly used letters (0=s, 1=p, 2=d, 3=f).

The peaks observed in the XPS spectra are derived from orbitals with an angular momentum quantum number greater than zero and usually split into two. The latter results from the interaction of the electron angular momentum resulting from its spin with its orbital angular momentum. Each electron possesses a quantum number related to its spin angular momentum (s2), with values for s of +1/2 or -1/2. Third, the quantity j comprises the vectorial addition of the two angular momenta (i.e., j= |1+s|) [118]. The photoemission detected in XPS spectra is presented thus as counts vs electron energy as follows:

$$E_B = h\upsilon - E_K - \varphi$$
                                                              Equation 3-2

Where E_B is the binding energy of the electron. This parameter is responsible for the identification of the electron by both the parent element and atomic energy level. E_K is the kinetic energy of the electron experimentally measured by the spectrometer. The value for E_k is not intrinsic to the material since it depends on the photon energy of the X-ray employed. Additionally, *hv* is the photon energy and φ is the spectrometer work function.

Therefore, the peaks on the spectra correspond to the electrons that were excited and escaped without energy loss. On the other hand, the background of the spectrum comprises the electrons that undergo inelastic scattering and energy loss. [118]. It is necessary to subtract the background of the spectrum for estimating the area of the peak intensity. Tougaard is one of the most employed methods [120].

XPS analysis of biochars was acquired using a Specs system with high-intensity XR50 X-ray monochromatic Al Kα radiation of 1486.71 eV and a Phoibos 150 hemispherical electron analyser (**Figure 3.7a**). The analysis of biochar took place at an ultrahigh vacuum of 10^{-9} Pa, the survey XPS spectra were acquired in a single sweep with a pass energy of 25 eV, in steps of 0.1 eV and dwell time of 0.1 s. High-resolution C 1s and O 1s spectra were obtained with a pass energy of 3 eV. On the other hand, XPS analysis of hydrochar was acquired using an EnviroESCA system at near ambient pressure (NAP), under an argon atmosphere at a gas flow of 2 mL/min (**Figure 3.7b**). The hydrochar XPS spectra for the survey and the high-resolution spectra, C 1s and O 1s, were obtained with a pass energy of 100 and 50 eV, respectively.

Figure 3.7. XPS equipment used for analysing the surface chemistry of the chars. a) ultra-high vacuum XPS Specs system; b) near ambient pressure EnviroESCA system.

Curve fitting and semi-quantification were performed using Casa XPS software with the Tougaard background subtraction for all components of the same peak. The C 1s, O 1s and N 1s binding energy were assigned at 284, 532 and 399 eV, respectively. The Tougaard method was selected for the analysis of the peaks given its simplicity and reliability when analysing several materials with different chemical compositions. It is common for experimental data to exhibit a chemical shift in the binding energy axis due to the differences in sample, measuring conditions and analytical techniques [120]. Therefore, a chemical shift correction based on theoretical and experimental calculations previously reported for equivalent material was performed [121]. Assignment of XPS peaks to chemical elements found on the surface of the chars was based on literature reports for similar materials.

3.4 Anaerobic digestion

3.4.1 Inoculum

The anaerobic sludge was obtained from an anaerobic digestion reactor operated at 37 °C at the wastewater treatment (WWT) plant Esholt in Bradford, West Yorkshire. The collected inoculum was stored at 4 °C until required, and replaced every three months to ensure the quality, as advised by Holliger et al. [122]. Before use, the particle size of the inoculum was homogenised by passing

it through a 1 mm mesh. The TS and VS content of the initial inoculum was measured and adjusted to achieve the desired inoculum to substrate ratio (ISR).

3.4.2 Substrate

Cellulose is often employed as a reference substrate in AD. According to the literature, 80-90% of the cellulose is directed to methane generation, whereas the rest is directed to cell metabolism and the formation of new cells [123].

The microalgae *Chlorella vulgaris* was used as a co-substrate in AD. Autotrophic *C. vulgaris* was produced and dried in China and cracked in a ball mill at the University of Leeds. The exact strain, growth media, conditions and location are unknown for this substrate, nonetheless, its chemical composition was determined. *C. vulgaris* had a proximate composition of moisture 7.06 %, volatile matter 71.69%, fixed carbon 13.28 % and ash 7.98%; and an ultimate composition of C 54.59 %, H 8.05 %, N 9.27 %, and O 20.11 %.

3.4.3 Total and volatile solids

The values for total solids (TS) and volatile solids (VS) were quantified gravimetrically according to APHA (2005). First, the clean evaporating dishes were ignited at 550 °C for 1 hour in a muffle furnace, after cooling down, they were transferred to a desiccator, and weighed (W_{Dish}). On the dried evaporating dishes, from 25 to 50 g of sample was placed and weighed (W_{Sample}). Afterwards, the samples were dried in an oven at 105 °C overnight, cooled in a desiccator for balancing the temperature, and weighed ($W_{DryMatter}$). The remaining mass balance of the sample corresponds to the TS (**Equation 3-3**). The residual dry matter was then placed in a muffle furnace at 550 °C for 2 h, and once more, cooled in a desiccator and weighed (W_{Ash}). The remaining mass balance after the calcination corresponds to the ash content of the sample (**Equation 3-4**). Finally, the values for VS were according to **Equation 3-5**.

$$\% \, TS = \frac{W_{DryMatter} - W_{Dish}}{W_{Sample} - W_{Dish}} * 100 \qquad \text{Equation 3-3}$$

$$\% \, Ash = \frac{W_{Ash} - W_{Dish}}{W_{Sample} - W_{Dish}} * 100 \qquad \text{Equation 3-4}$$

$$\%VS = \%TS - \%Ash \qquad \text{Equation 3-5}$$

3.4.4 AMPTS II equipment

Figure 3.8 shows the Bioprocess™ Automatic Methane Potential Test System (AMPTS II) used for the assessment of biomethane production during AD. The system encompasses three units: a thermostatic water bath, a carbon dioxide fixing unit, and a device for measuring gas volume. The AMPTS II accepts fifteen reactors of 500 mL volume, consisting of 400 mL working volume and 100 mL of headspace. The reactors are introduced in the water bath for adjusting the temperature and individually fitted with an automatic agitator for mixing the media for 60 seconds every 10 minutes. The biogas generated in each reactor passes to its designated CO_2 fixing unit containing 80 mL of an alkaline solution (3M NaOH). Several acid gasses fractions, such as CO_2 and H_2S, are retained by reacting with the NaOH, allowing only the passage of CH_4 or H_2 through the gas volume measuring device. This device measures the volume of CH_4 and H_2 according to the principle of liquid displacement and buoyancy via a multi-flow cell arrangement with an accurately calibrated volume of approximately 10 mL. The gas measured is automatically normalised to standard conditions (0 °C, 1 atm, and no humidity), and quantified since the gas volume generates a digital pulse that is integrated by a data acquisition system.
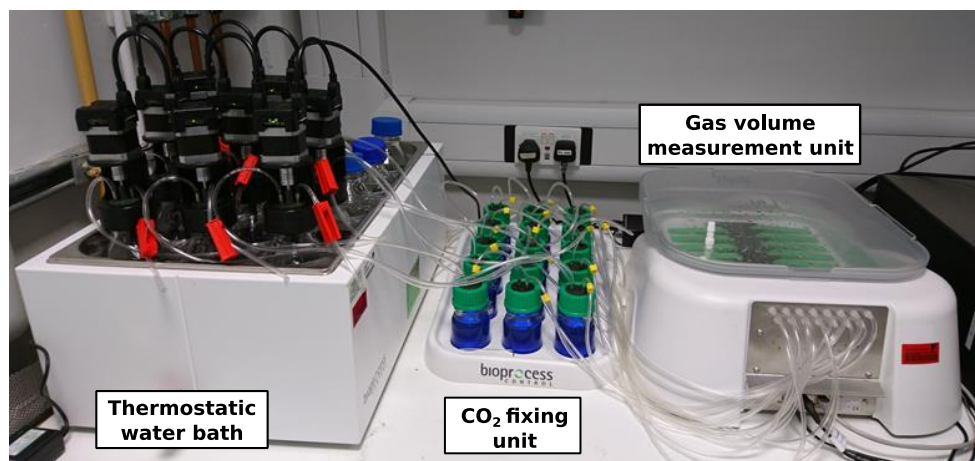
Figure 3.8. Automatic Methane Potential Test System (AMPTS II) used for anaerobic digestion experiments.

3.4.5 Biochemical methane potential

The biochemical methane potential (BMP) measurement was performed using the AMPTS II systems. The cumulative volumetric BMP values obtained for each experimental treatment were calculated according to **Equation 3-6**. A blank

reactor only containing inoculum was run in parallel to account for residual methane emissions.

$$BMP = \frac{Volume\ CH_4\ from\ sample\ (mL) - Volume\ CH_4\ from\ blank\ (mL)}{g\ VS\ of\ substrate\ fed\ in\ digester} \quad \text{Equation 3-6}$$

3.4.6 Theoretical biochemical methane potential

The potential BMP yields can be estimated from the chemical composition of the substrate. The conversion of carbon matter during AD follows **Equation 3-7**, according to Buswell and Mueller [124].

$$C_aH_bO_c + \left(a - \frac{b}{4} - \frac{c}{2}\right)H_2O \rightarrow \left(\frac{a}{2} + \frac{b}{8} - \frac{c}{4}\right)CH_4 + \left(\frac{a}{2} - \frac{b}{8} + \frac{c}{4}\right)CO_2 \quad \text{Equation 3-7}$$
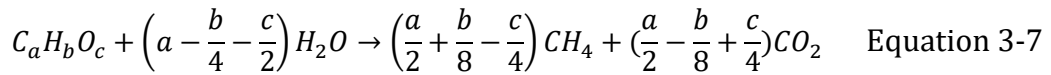
This model has a certainty of 95 %, is time-independent, and considers the mixed culture and multiple metabolic pathways followed in AD. Although it does not take into consideration the necessary energy for cell mass growth and maintenance.

The theoretical biochemical methane potential (BMP$_{Th}$) of the substrates of study has been calculated based on Boyle´s equation (**Equation 3-8**), where c, h, o and n represent the molar fractions of C, H, O and N, respectively [124,125]. This equation assumes a substrate breakdown efficiency of 100 % and considers only the products CH$_4$ and CO$_2$. The ash content was subtracted from the calculation and only the biodegradable fraction was considered, hence the BMP$_{th}$ is expressed as mL CH$_4$/g VS.

$$BMP_{th} = \frac{22400 * \left(\frac{c}{2} + \frac{h}{8} - \frac{o}{4} - \frac{3n}{8}\right)}{12c + h + 16o + 14n} \quad \text{Equation 3-8}$$

During the anaerobic co-digestion (AcoD) of two substrates, the BMP$_{th}$ is calculated based on the BMP$_{Th}$ and ratio of each substrate used for the experiments according to **Equation 3-9**.

$$BMP_{th} = (BMP_{th,a} * C_a) + (BMP_{th,b} * C_b) \quad \text{Equation 3-9}$$

where $BMP_{th,a}$ and $BMP_{th,b}$ are the theoretical gas yield, and C_a and C_b are the mass fraction of substrate a and substrate b, respectively.

3.4.7 Anaerobic biodegradability

The anaerobic biodegradability (BD) of methane depends on the degradability degree of the substrate used for AD. The BD was calculated based on the BMP_{Th} of the substrate and the final experimental BMP yield (BMP_{Exp}) for each treatment of study (**Equation 3-10)** [125].

$$BD\ (\%) = \frac{BMP_{Exp}}{BMP_{Th}} * 100$$
Equation 3-10

3.4.8 Kinetic models

The experimental BMP values were fitted to the modified Gompertz model equation according to **Equation 3-11** [126].

$$BMP(t) = BMP_{max} \cdot exp\left\{-exp\left[\frac{\mu_m \cdot e}{BMP_{max}}(\lambda - t) + 1\right]\right\}$$
Equation 3-11

where BMP(t) is the cumulative methane yield (mL CH_4/g VS) at time t (day), BMP_{max} is the maximum methane yield (mL CH_4/g VS), μ_m is the methane production rate (mL CH_4/g VS·day), λ is the lag phase (days), and e is the exp(1). By fitting the experimental data into the Gompertz equation, a coefficient of determination (R^2) is obtained to validate the model. The data of each experimental run is fitted into the model, and the values reported throughout this work correspond to the average between the runs. These calculations were obtained using the SPSS Statistics 26 software.

3.4.9 Char addition in anaerobic digestion

The standard processing conditions for AD experiments on the AMPTS II systems included inoculum 5 g VS/L, carbon substrate (cellulose) 5 g VS/L, ISR ratio of 1:1, biochar 3 % (w/v). First, the solids (substrate and chars) were weighed into the bottles. The concentration of the sieved inoculum (1 mm) of known VS was adjusted with distilled water to double the desired VS value (10 g VS/L), 200 mL of this inoculum were added to each reactor. The final working volume of the reactors (400 mL) was adjusted with distilled water, obtaining thus the final inoculum concentration (5 g VS/L). The pH was measured but not adjusted. All reactors were flushed with nitrogen gas for ensuring anaerobic conditions. To achieve this, a bag filled with N_2 gas was connected to each of the reactors and

flushed to remove the air. Afterwards, the reactors were incubated at 37 °C for 30 days and stirred automatically for 60 s every 10 min. Blank reactors containing only inoculum ran in parallel to account for residual methane emissions, always in duplicate. All treatments were performed in duplicate, or triplicate as stated for each case.

The AD conditions used in the experiments correspond to the standard conditions unless stated otherwise. Other inoculum concentrations, ISR, char load and substrates were employed while maintaining the standard procedure with minor modifications. For instance, if a final inoculum concentration of 10 g VS/L was employed. The inoculum was first adjusted at a concentration of 20 g VS/L, of which 200 mL were taken to seed the reactors at a final concentration of 10 g VS/L.

3.4.10 Immobilisation of anaerobic sludge on biochar

The potential of the chars to immobilise the anaerobic sludge, followed by the capacity of the attached cells to produce methane during AD was investigated. Two consecutive AD batches were performed using the standard AD conditions described above with the chars OW-HC250, OW-BC450 and OW-BC650. Firstly, digestion with the inoculum 5 g VS/L and 3 % (w/v) of chars at 37 °C for 48 h without substrate addition. Due to the absence of substrate, no further bacterial growth was assumed. This first digestion aimed to promote the immobilisation/adsorption of the AS to the chars. After 48 h of the first digestion, the chars were collected, and the supernatant discarded. The biochar was placed on a sieve and gently washed with distilled water to remove the excess sludge that was not incorporated and/or immobilised onto the biochar materials. Secondly, the collected chars were employed as the source of both char and inoculum for seeding a second AD batch. Substrate (cellulose at 5 g VS/L) was added to the digesters, oxygen was removed with N_2 for promoting an anaerobic environment. The digesters were incubated at 37 °C for 40 days. The amount of inoculum was not fixed for the second run, thereby it was not possible to state the ISR. The char runs were not performed in replicates, while a duplicate blank control was run in parallel to account for residual methane emissions.

3.4.11 Volatile fatty acids analysis

Total volatile fatty acids (VFAs) were determined in the liquid fraction after the fermentative digestion. The samples were centrifuged and filtered using a 0.2 μm syringe filter and then analysed by gas chromatography (GC). The analysis was

performed with an Agilent 7890A GC, fitted with a DB-FFAP column (30 m × 0.32 mm, film thickness of 0.5 μm) and a flame ionisation detector (FID). An autosampler injected 10 μL of the sample at a 5:1 split ratio with the inlet port. The GC-FID operating conditions were 150 °C inlet temperature, 200 °C FID detection temperature, nitrogen as make-up gas, and helium at 10 mL/min as the carrier gas. The column oven program started at 60 °C and was held for 4 min, then increased to 140 °C with a ramp of 10 °C/min. Afterwards, the temperature was raised to 200 °C with a ramp of 40 °C/min and held for 5 min. The comparative standards used were a volatile acid standard mix (Supelco) and alcohols made from high purity single reagents. An example of a chromatogram and standard report for the quantification of volatile fatty acids via gas chromatography is shown in the Appendix **Figure B.1**. Data was acquired with ChemStation software.

3.4.12 Design of experiments

Design of experiments (DOE) is a systematic technique for planning and analysing by statistical tools the information obtained from an experiment. A mathematical model is then created, which is used to understand the influence of the experimental parameters on the variables of response. Factorial designs are commonly used in DOE when more than one factor is evaluated. The effect of a factor, also known as the main effect, is defined as the response change due to variations in the level of the factor. While the interaction between factors is a form of curvature on the response surface model. The linear regression method is used for fitting models to the experimental data. For instance, a two-factor model can be represented as outlined in **Equation 3-12**.

$$Y = \beta_0 + \beta_1 X_1 + \beta_2 X_2 + \beta_{12} X_1 X_2 + E \qquad \text{Equation 3-12}$$

Where Y is the response variable, β_0 is the overall mean effect, β_1 is the effect of factor X_1, β_2 is the effect of factor 2, β_{ij} is the interaction between factors X_1 and X_2, E is the random error component [127].

Analysis of variance is used to analyse the variation between groups. The hypothesis tested for the full model, comprising main effects and interactions is shown in **Equation 3-13**.

$$H_0: \beta_1 = \beta_1 = \beta_2 \ldots = \beta_k = 0$$

$$H_1: \beta_j \neq 0 \; for \; at \; least \; one \; j$$

Equation 3-13

The F-test is used to determine the statistical significance of the model at a p<0.05. When the F-value> F-critical, it can be concluded that at least one of the variables contributes significantly to the model, thereby the null hypothesis (H_0) is rejected. Then, the significance of each factorial effect is tested using the F-statistic [128].

Minitab 27 software was used for creating the factorial design and analysing the response variables, models, and optimisation. Comparison of the effect of the factors over response variables was performed by analysis of variance (ANOVA) and linear regression at a confidence level of $p < 0.05$ by using the software SPSS Statistics 26.

3.4.12.1   Anaerobic co-digestion of *Chlorella vulgaris* and cellulose

A full factorial 2^3 DOE with three independent factors at two levels, C/N ratio (7 and 25), ISR (1 and 2) and BC load (0 and 3 %) with 3 replicates and 3 centre points (C/N 16, ISR 1.5 and BC load 1.5 %) was performed (**Table 3.2**). The OW-BC450 was selected, and the inoculum was fixed at 10 g VS/L, whereas the amount of substrate added ranged from 5 to 10 g VS/L for achieving the corresponding ISR. The amount of *C. vulgaris* and cellulose added for each C/N ratio and ISR were calculated based on their chemical composition. For achieving the C/N ratio of 7, 16 and 25, the ratio of *C. vulgaris* to cellulose were 0.8:0.2, 0.3:0.7 and 0.2:0.8, respectively. A factorial regression model was used for analysing BMP yield and the kinetic parameters obtained from fitting the modified Gompertz model. Contour plots were produced for the graphical representation of the DOE conditions over the response variables. The desirability (D) function was used for optimising the AcoD conditions based on maximising the BMP_{Exp}, BMP_{max} and μ_m.

3.4.12.2   Anaerobic digestion of water hyacinth

A full factorial 2^2 DOE was performed to evaluate the effect of OW-BC450 and ISR. The DOE consisted of two independent factors at two levels, ISR (1-2) and BC load (0-3 %) with 3 replicates and 3 centre points as shown in **Table 3.3**. The sample WH-VBU was selected as substrate, and the inoculum was fixed at 10 g VS/L, whereas the amount of substrate added ranged from 5 to 10 g VS/L for achieving the corresponding ISR. Like above, a factorial regression model was used for analysing and contour plots were produced for evaluating the influence of the experimental factors on the variables of response. This is followed by the optimisation with the desirability (D) function for maximising the BMP_{Exp}, BMP_{max} and μ_m.

Table 3.2. Full factorial 2^3 experimental design used for the anaerobic co-digestion of *Chlorella vulgaris* and cellulose

Run		Levels			Actual value		
Std Order	Run Order	C/N	ISR	BC load	C/N	ISR	BC load (%)
1	27	-1	-1	-1	7	1	0
2	26	1	-1	-1	25	1	0
3	5	-1	-1	1	7	1	3
4	14	1	-1	1	25	1	3
5	22	-1	1	-1	7	2	0
6	8	1	1	-1	25	2	0
7	21	-1	1	1	7	2	3
8	20	1	1	1	25	2	3
9	7	-1	-1	-1	7	1	0
10	19	1	-1	-1	25	1	0
11	25	-1	-1	1	7	1	3
12	10	1	-1	1	25	1	3
13	13	-1	1	-1	7	2	0
14	2	1	1	-1	25	2	0
15	4	-1	1	1	7	2	3
16	9	1	1	1	25	2	3
17	11	-1	-1	-1	7	1	0
18	24	1	-1	-1	25	1	0
19	18	-1	-1	1	7	1	3
20	16	1	-1	1	25	1	3
21	1	-1	1	-1	7	2	0
22	6	1	1	-1	25	2	0
23	3	-1	1	1	7	2	3
24	23	1	1	1	25	2	3
25	17	0	0	0	16	1.5	1.5
26	12	0	0	0	16	1.5	1.5
27	15	0	0	0	16	1.5	1.5

Table 3.3 Full factorial 2^2 experimental design used for the anaerobic digestion of water hyacinth

Run		Levels		Actual value	
Std Order	Run Order	ISR	BC load	ISR	BC load (%)
1	13	-1	-1	1	0
2	2	1	-1	2	0
3	12	-1	1	1	3
4	15	1	1	2	3
5	5	-1	-1	1	0
6	7	1	-1	2	0
7	11	-1	1	1	3
8	6	1	1	2	3
9	10	-1	-1	1	0
10	1	1	-1	2	0
11	14	-1	1	1	3
12	8	1	1	2	3
13	3	0	0	1.5	1.5
14	4	0	0	1.5	1.5
15	9	0	0	1.5	1.5

3.4.13 Statistical analysis

The BMP values were statistically evaluated under an interval of confidence of 95 %. The Shapiro-Wilks test was employed to demonstrate normality ($p>0.05$). Comparison of the char addition over the BMP was achieved by an analysis of variance (ANOVA), whereas a *Tukey post-hoc* test was used to determine the significance of each char and interaction. A T-test was used for comparing the BMP with its corresponding control. All analyses were performed at a confidence level of $p<0.05$ using the SPSS Statistics 26 software.

3.5 Comparative analysis

3.5.1 Biochar effect on anaerobic digestion

To establish the effect of biochar addition on AD performance the changes in the kinetic parameters were calculated in comparison to their corresponding non-BC control as follows:

$$BMP_{BC}(\%) = \frac{(BMP_{max,BC} - BMP_{max,C}) * 100}{BMP_{max,C}} \qquad \text{Equation 3-14}$$

$$\mu_{m,BC}(\%) = \frac{(\mu_{m,BC} - \mu_{m,C}) * 100}{\mu_{m,C}} \qquad \text{Equation 3-15}$$

$$\lambda_{BC}(\%) = \frac{(\lambda_C - \lambda_{BC}) * 100}{\lambda_C} \qquad \text{Equation 3-16}$$

Where BMP_{max} is the maximum methane yield (mL CH_4/g VS added) at time t; μ_m=maximum specific methane yield per day (mL CH_4/g VS added·day); λ=lag phase (days); the denotation BC and C correspond to systems supplemented with biochar and the non-biochar control, respectively.

The obtained values for this work and the literature reports compilation are shown in the Appendix **Table B.1**. These effects were expressed as % of variation where 0 % represents the value obtained as the same as the control, while 100 % states that the BC addition doubled the value obtained by the control. Moreover, a positive value states an improvement of that parameter, while a negative value states a detrimental effect due to BC addition. Each of these features is used for descriptive statistics and finally, employed for the PCA.

The descriptive statistical analysis included frequency tables and box plots for displaying the distribution of a large set of data through their quartiles. Individual comparisons of different quantitative variables, such as ISR, and biochar load, among others over the response variables BMP_{BC}, $\mu_{m,BC}$ and λ_{BC} were evaluated by analysis of variance at a confidence level of $p<0.05$. All analysis was performed using the SPSS Statistics 26 software.

3.5.2 Principal component analysis (PCA)

Principal component analysis (PCA) aims to determine the fewest number of variables that will explain most of the variance in the analysed data [129]. PCA is also known as a projection method, which principal objective is the explanation of large data into smaller and more informative components. **Equation 3-17** shows the general equation for PCA.

$$X = TP' + E \qquad \text{Equation 3-17}$$

where X is the original data, T are the scores obtained from the matrix of sample structure information, P is the loadings from the matrix of variable structure

information, and E is the matrix of residuals which cannot be explained by the PCA model. From a more general perspective, the equation transforms into DATA=MODEL + ERROR, where X is the data component analysed after analysing the variables, TP is the information explained by the model and E is the noise of the analysis which cannot be explained by the model [130].

Extraction communalities values are also useful for evaluating the PCA. The communalities indicate the relationship or amount of common variance of each variable with the entire set of data. High communalities are desirable since they indicate the extent of the variance being explained by the variable [129]. The information of the dataset is separated by the PCA into sample information (scores) and variable information (loadings). A score is the projection of each sample from the dataset on the PCA space, with values within both positive and negative regions along the PC axis. It contains the sample information, and its distribution along the PC axis indicates how much of that information is contained in the PC. The PCA loadings indicate the contribution placed on each variable to describe the PCs and are shown in the PCA plot as the orthogonal projection of a variable onto a PC axis. The loadings indicate the association strength between variables. The information provided by the PCA scores, and loadings provides an extensive insight into the dataset and the variable relationships [129,130].

The PCs represent the most important sources of variability and explain a certain amount of information within the original data. Eigenvalues and scree plots can be used to determine the number of PCs to represent the dataset. PCs with eigenvalues greater than one are considered important and are thus retained for the analysis. The eigenvalues plotted against the number of variables of the dataset are illustrated on the scree plot (**Figure 3.9**). The PCs displaying a sharp change in the slope of the line connecting to adjacent PCs are the ones to be maintained for the PCA.
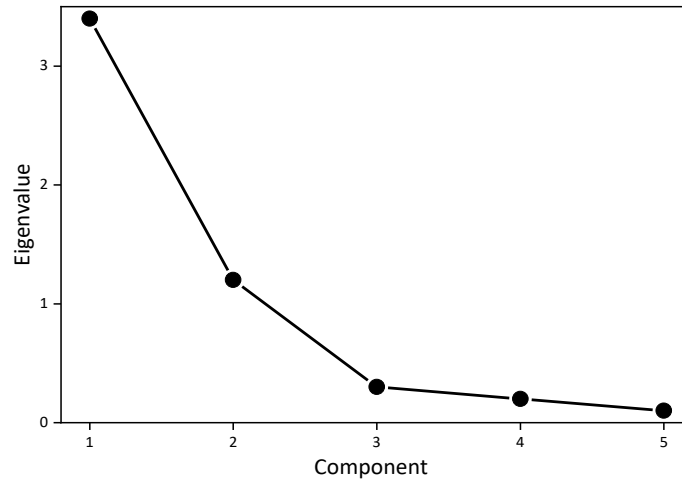
Figure 3.9. Example of a scree plot for principal component analysis.

The first PC contains the greatest source of information explaining the data set, whereas each subsequent PC contains less information than the previous one. The first PC is usually plotted as the x-axis, and it describes the greatest elongation of the data. The next PC estimated from the remaining variance is orthogonal to the first. Plotting combination of PC1 and PC2 forms a 2-dimensional plane, named score plot, containing the data. Interpretation of the PCA is carried out by visualisation of the component scores as displayed in **Figure 3.10**. A score is the orthogonal projection of each sample data onto the axis of the PC. The scores indicate the importance of the sample in describing the variability of the data set. The distance of the samples distributed along the axis is an indication of how much of their information is contained within the PC. Scores close to the origin show the least variability and could be considered unimportant and not well described by the PCA model. While those at the extremes of the PC axis show most of the variability and are well described by the PCA model [130].

Moreover, information about the correlation between the variables can also be deduced from the plot. Such correlation is described by the cosine of the angle between the loading vectors. Thus, smaller angles lead to a higher correlation between variables. Conversely, uncorrelated variables are usually orthogonal (perpendicular) to each other [131]. Variables positively correlated are in a similar direction, while opposite directions indicate a negative correlation [132]. Furthermore, any relationship identified between variables must be evident in all the retained PCs.
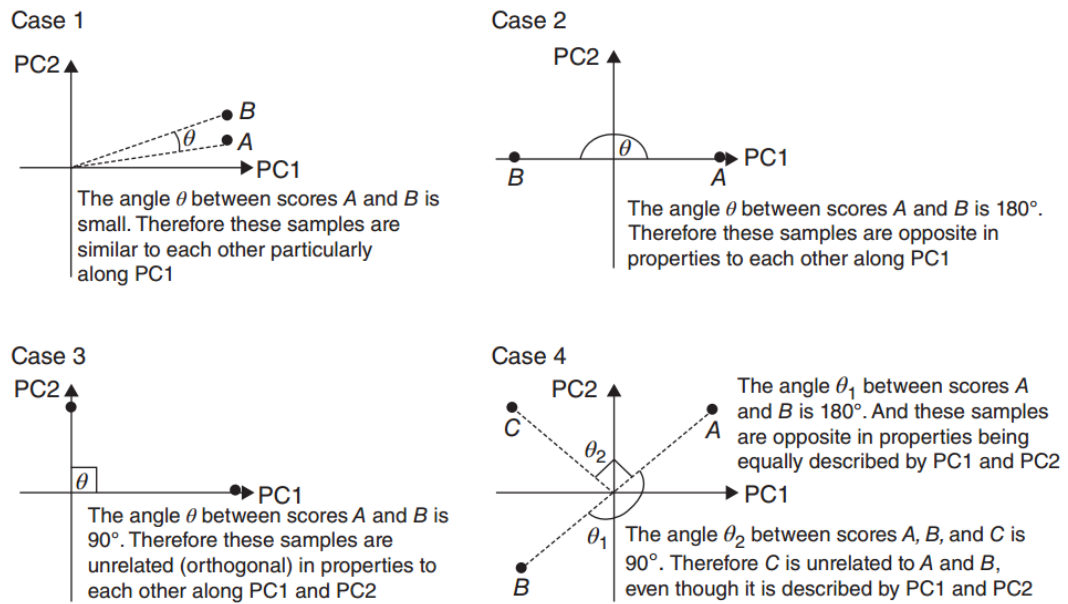
Figure 3.10. Relationship between samples along the PC axis of a principal component analysis (PCA). Extracted from [130].

For this PCA analysis, the parameters pyrolysis temperature, ash content of biochar, biochar O:C atomic ratio, biochar load, BMP_{BC} yield, methane production rate ($\mu_{m,BC}$) and lag phase (λ_{BC}) were selected. The parameters BMP_{BC}, $\mu_{m,BC}$ and λ_{BC} were calculated based on the comparison to their corresponding control as described in the previous section and listed in Appendix **Table B.1**. Therefore, using PCA, the relations between the nature of the biochars and changes in AD performance can be associated with their dynamics by evaluating the score and loadings.

Unlike other mathematical analyses (e.g., linear regression) that the use of variables with different units is widespread. The criterion of PCA based on variance is highly dependent on the measurement units, hence the necessity to standardise the data [129]. To avoid the effect of different scale units, the initial data values were re-scaled. Hence, the variables were mean centred and divided by their standard deviations [130]. The re-scaled dataset based on the difference between the control and standardised as above described are listed in Appendix **Table B.1**, and the original dataset is listed in Chapter 7.

The dataset was analysed by PCA with the software IBM SPSS Statistics 26. Oblique rotation was selected as a factor rotation strategy given the assumption of a correlation between the variables. The regression method was selected for calculating the factor scores, which were subsequently used for the discernment function analysis. To validate the adequacy of PCA for the dataset, the Kaiser-

Meyer-Olkin (KMO) method was applied. KMO values are found between 0 and 1 and can be categorised as average 0.5-0.7, good 0.7-0.8, great 0.8-0.9, and perfect >0.9. The correlation between the variables was validated with Bartlett´s test of sphericity for establishing significant differences (p<0.05). It is not desirable for the correlations to be extremely low or non-existent or to be extremely high because these might indicate a lack of variation in the data [129]. Commonalities among the variables were also considered in the evaluation.

Chapter IV

Characterisation of the chars

4.1 Overview

Thermochemical processing of biomass produces a carbon solid product known as 'char'. The char can be combusted for heat and power, further gasification or used in several adsorption applications such as soil remediation, carbon sequestration, and as an additive in anaerobic digestion. The uses given to the chars are based on their advantageous physical and chemical characteristics. Even though the correlation between such properties and their potential applications remains unclear, it is important to provide an understanding of these relationships. First, to assess the properties of the chars based on the thermochemical processing and the feedstock of origin. This can be accomplished by analysing the chars using a complementary series of chemical, physical, and functional characterisation techniques. This chapter describes chars from slow pyrolysis and hydrothermal carbonisation (HTC) of oak wood (OW), water hyacinth (WH), and saw wrack (SW). Biochars from WH and SW produced at low (450 °C) and high temperature (600 °C) pyrolysis and two commercial oak wood biochars produced at 450 and 650 °C were characterised. Hydrochars from the same three feedstocks produced by HTC at 250 °C were also characterised. These char materials were evaluated in the following chapters of this work. The augmentation of biochars and hydrochars on anaerobic digestion of model substrate cellulose was evaluated in Chapter 5. The effect of biochar augmentation on the anaerobic digestion of complex substrates, such as microalgae and water hyacinth, is described in Chapter 6. The properties of these biochars and their effect on anaerobic digestion discussed in Chapters 5 and 6, in addition to literature reports were further statistically evaluated by principal component analysis in Chapter 7.

To establish the most important variables affecting both biochar and hydrochar properties. To evaluate these materials, the thermochemical processing conditions of temperature, and the composition of the biomasses were considered. According to the International Biochar Initiative, oak wood chars possessed the highest C content, resulting in Class 1 (≥60 %). Whereas water

hyacinth and saw wrack chars were categorised as Class 2 (≥30 and <60 %). The greatest differences between these three feedstocks relied on the nature of their carbohydrate fraction and the degradability during pyrolysis and HTC. The lignocellulosic nature of oak wood chars influenced their higher loss of volatile matter and more developed surface area and porosity. The aquatic biomasses WH and SW suffered a dramatic loss of volatile matter and considerably lower surface area. These chars also exhibited more nitrogen and a large content of inorganic elements, principally Cl, Na, K, Fe, Ca, S, and Mg. The XPS analysis allowed the evaluation of the surface chemistry of the chars, comprised principally of -C-C-, C-O and C=O functional groups. Both temperature and biomass feedstock influenced the oxygenated and nitrogen functional groups of the chars. Higher-temperature BCs generally transformed the biomass towards more stable and ordered structures as showed by the enhancement of the proportion and peak intensity of C-C groups, reduction of oxygenated functional groups, and increasing proportion of pyridinic-N and quaternary-N. Detailed insight into the transformations of the biomass, obtained during the pyrolysis and HTC conversion, revealed the major role of reaction temperature and composition of the feedstocks.

The work within this chapter has been published in Bioresource Technology Journal, please see: J Quintana-Najera, AJ Blacker, LA Fletcher and AB Ross "The effect of augmentation of biochar and hydrochar in anaerobic digestion of a model substrate" *Bioresource Technology* 321 (2021): 124494.

4.2 Introduction

The reactions taking place during the thermal degradation of biomass are influenced by the process conditions, primarily temperature, and the nature of the feedstock. Even though the chemical reactions involved in pyrolysis and HTC largely differ, they generally involve the simultaneous degradation and decarboxylation of biomass polymers with the formation of the chars by condensation and aromatisation. The rate and predominance of these reactions are governed by the operating conditions of each thermochemical treatment; thus, each treatment leads to products with different yields, and chemical and physical characteristics [60].

The chars were obtained via pyrolysis and hydrothermal carbonisation (HTC) of oak wood (OW), water hyacinth (WH), and saw wrack (SW). The OW biochars produced at 450 and 650 °C were purchased from a commercial pyrolysis plant (Proininso) produced using a traditional kiln reactor. The WH and SW biochars

were produced at the University of Leeds in a fixed bed pyrolysis reactor at 450 or 600 °C held for 1 h. All BCs were classified as low-temperature (450°C) and high-temperature (600-650 °C). Hydrochars derived from each feedstock were produced in a 2 L batch high-pressure reactor (Parr USA) at 250 °C held for 1 h. The chemical, physical and functional properties of the resulting chars were determined by a series of methods.

The chemical composition of the feedstocks and chars was evaluated by proximate, ultimate, inorganic analysis and pH measurement as described in section 3.2.5. Proximate analysis was determined via thermogravimetric analysis (TGA), which allows the calculation of volatile matter (VM), fixed carbon (FC), ash, and moisture. Ultimate analysis of the main elements (CHNOS) also allowed the calculation of H:C and O:C ratios. X-ray fluorescence (XRF) was used to determine the inorganic content, and pH was measured using a pH meter following the addition of a known mass of char to distilled water. Pore volume and surface area were determined using the gas adsorption method with N_2 and CO_2 as adsorbate. To evaluate the functional groups located on the surface of the chars, Fourier transform infrared spectroscopy using attenuated total reflectance (ATR-FTIR) and X-ray photoelectron spectroscopy (XPS) were performed. This series of techniques allowed the examination of the effects of the thermochemical treatment and feedstock on the characteristics of pyrolysis and HCT solid products. The investigation of these properties provides an understanding between process variables used in their production and the final properties of the chars and their possible further applications.

4.3 Chemical composition

4.3.1 Untreated biomass

The composition of terrestrial plant biomass is comprised of cellulose, hemicellulose, lignin, and protein, with smaller quantities of other components, such as inorganics, phosphorous, sulphur, and trace minerals [133]. Free-floating macrophyte aquatic plants exhibit rapid growth in warm climates by adsorbing the nutrients from water bodies. These plants are composed mainly of starch, sugar, pectin, proteins and lipid, with a considerably high ash fraction, partially composed of alkali metals [134]. Aquatic biomass such as macroalgae has a different composition including a range of hydrocolloids (alginates, laminarin and mannitol), protein and mineral matter and smaller quantities of other components such as polyphenols, and sulphated carbohydrates [30].

Factors such as botanical species, plant fraction, and climatic conditions can influence the final composition of all types of biomasses. The inherent heterogeneous composition of biomass presents a challenge for the design and standardisation of their processing. Thus, when subjecting it to thermal conversion, it is imperative to characterise the original feedstocks to correlate and further predict the composition of the char products [135].

The selected feedstocks oak wood, water hyacinth and the seaweed saw wrack have different origins and compositions. The growth environments for OW, WH and SW were forestries, freshwater and marine, respectively. Although both OW and WH are plant biomass, and both WH and SW are aquatic biomass, their structure and characteristics differ significantly. Firstly, OW (*Quercus ilex*) is recalcitrant lignocellulosic biomass composed mainly of cellulose (44 %), hemicellulose (24%) and lignin (24%), with negligible protein content [136]. Oak waste is usually used as a model feedstock for typical lignocellulosic biomass given its lack of potentially hazardous elements and toxic compounds, such as heavy metals [137]. Secondly, WH (*Eichhornia crassipes*) is an aquatic perennial free-floating plant and invasive macrophyte. The flexible morphology of WH allows the hyper-accumulation of nutrients, adaptation to variable growing conditions and invasive potential [138]. The adaptive phenology characteristic of such behaviour influences the chemical composition of WH. Nonetheless, WH belongs to cellulosic biomass given its considerable content of cellulose and hemicellulose, consisting of approximately 18-33 and 22-43 % (db), respectively. The lignin content of WH is considerably lower (7-8 %) than the reported for OW [139–141]. Moreover, WH is also rich in nitrogen and has significant protein and inorganics, such as P and K [142]. Thirdly, SW (*Fucus serratus*) is a brown seaweed composed of up to 55 % of carbohydrates, mainly alginate, laminarin and mannitol, with considerable amounts of nitrogen and protein and high levels of mineral matter, principally Na, K, Ca and Mg [143]. The results from the proximate and elemental analysis of the untreated feedstocks are shown in **Tables 4.1** and **4.2**.

Table 4.1. Proximate composition of biomass feedstocks and chars expressed on a dry basis.

Material	Char yield (%)	Volatile matter (%) db	Fixed carbon (%) db	Ash (%) db	pH
Oak wood					
Untreated	-	72.5	24.7	2.9	-
OW-HC250	59.5	57.9	38.5	3.8	3.9
OW-BC450	-	21.1	67.2	11.7	9.9
OW-BC650	-	11.8	73.9	14.3	9.3
Water hyacinth					
Untreated	-	85.6	0.02	14.6	-
WH-HC250	28.4	56.8	22.8	20.6	5.6
WH-BC450	59.4	30.9	35.2	33.9	9.1
WH-BC600	54.2	21.5	35.9	42.6	10.6
Saw wrack					
Untreated	-	74.5	11.3	14.2	-
SW-HC250	37.9	64.0	21.6	14.3	6.2
SW-BC450	39.8	48.4	18.8	33.3	11.1
SW-BC600	37.3	36.1	29.3	34.6	12.1

Table 4.2. Ultimate composition and atomic ratios of biomass feedstocks and chars expressed on a dry basis.

Material	C (%) db	H (%) db	N (%) db	O (%) db	S (%) db	O:C	H:C	N:C
Oak wood								
Untreated	50.8	7.4	1.5	37.4	0.0	0.55	1.74	0.03
OW-HC250	62.0	5.0	1.2	29.4	0.0	0.36	0.96	0.02
OW-BC450	65.7	2.7	0.6	19.3	0.0	0.22	0.49	0.01
OW-BC650	76.5	1.4	0.8	7.0	0.0	0.07	0.22	0.01
Water hyacinth								
Untreated	38.7	3.4	2.7	40.8	0.2	0.79	1.04	0.06
WH-HC250	50.8	4.3	3.4	20.2	0.1	0.30	1.01	0.06
WH-BC450	26.1	1.4	1.7	36.9	0.2	1.06	0.65	0.05
WH-BC600	37.8	1.0	2.0	14.9	0.0	0.30	0.31	0.05
Saw wrack								
Untreated	44.2	6.1	1.4	37.2	1.6	0.55	0.38	0.03
SW-HC250	54.9	4.6	2.4	22.7	1.1	0.31	0.99	0.04
SW-BC450	39.2	1.8	2.4	21.6	1.7	0.41	0.56	0.05
SW-BC600	40.4	0.9	2.3	21.6	0.3	0.40	0.27	0.05

As expected, the volatile matter (VM) is generally high ranging between 72.5-85.6 %. OW showed the lowest ash content of 2.9 %, highest FC of 24.7 %, low N of 1.5 % and O:C atomic ratio of 0.55 in agreement with other reports [144]. WH exhibited a considerable higher ash content of 14.6 %, low FC of 0.02 % and an O:C ratio of 0.79, similar to the one reported by Ye et al. [142]. Whereas the seaweed SW also exhibited a considerable ash content of 14.2 %, but O:C ratios of 0.55, the values here observed were within ranges reported elsewhere [66,145].

4.3.2 Proximate analysis

4.3.2.1 Biochars

The characteristics of the biochars derived from different feedstocks and pyrolysis conditions are shown in **Table 4.1**. The VM content gradually reduces, and the ash is enhanced by increasing pyrolysis temperature. Among the different BC types, the OW-BCs exhibited the highest reduction of VM, lowest ash content and highest FC. The WH-BCs exhibited a similar reduction of VM, whereas the ash and FC enhanced to similar values for both BCs. Conversely, the SW-BCs showed less VM reduction, but similar ash concentration with increasing pyrolysis temperature to the other BCs. These results agree with previous reports where increasing pyrolysis temperature results in biochars with reduced VM and enhanced FC and ash content (**Figure 4.1**). These changes are a consequence of the volatilisation of organic matter, the reduction of OH and CH_3 functionality and an increase in C=C, resulting from an increase in carbon content and aromaticity [73].

The most significant loss of VM and compositional changes of biochar often take place at a temperature range of 200 to 400 °C [67]. Notwithstanding, some lignocellulosic BCs could exhibit a high VM at relatively low pyrolysis temperature (**Figure 4.2a**). The VM content is related to the degradation of their main components, cellulose, hemicellulose, and lignin, which differ with pyrolysis temperature. Hemicellulose is easily decomposed at 200-260 °C, whereas cellulose and lignin start at 240-350 and 280-500 °C, respectively [152]. Hence, at 450 °C and below, lignocellulosic, and herbaceous - particularly OW-BCs and WH-BCs - suffered an extensive decomposition of the predominantly cellulosic fraction, accompanied by a degree of carbonisation. Above 500 °C further dehydration, condensation and decarboxylation reactions predominate, hence biochars produced at higher temperatures underwent more conjugation, aromaticity and carbonisation [73]. WH suffered a considerable loss of VM, due

to its easily degradable starch, cellulose and hemicellulose fractions [153]. Both cellulose and starch are polysaccharides formed by the monomer glucose linked via β-(1-4) and α-(1-4) linkages, respectively [154]. In comparison to cellulose, starch is less crystalline, less polymerised, and thus more easily degraded.
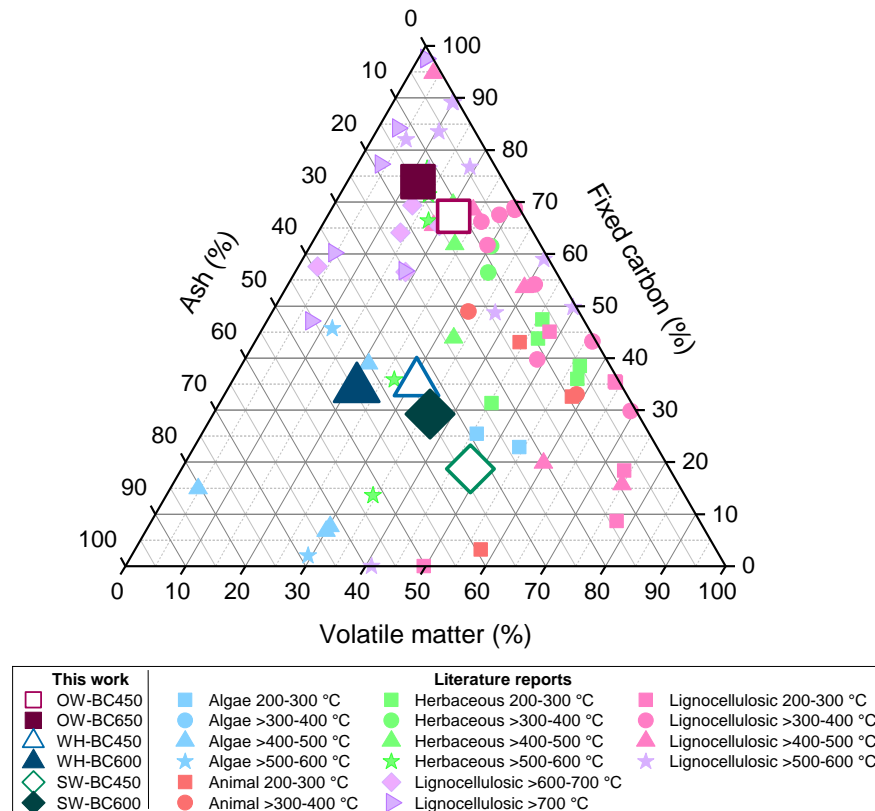
Figure 4.1. Triangle plot of the ash, volatile matter, and fixed carbon composition of the obtained biochars and literature reports [21,28,151,69,88,144,146–150].
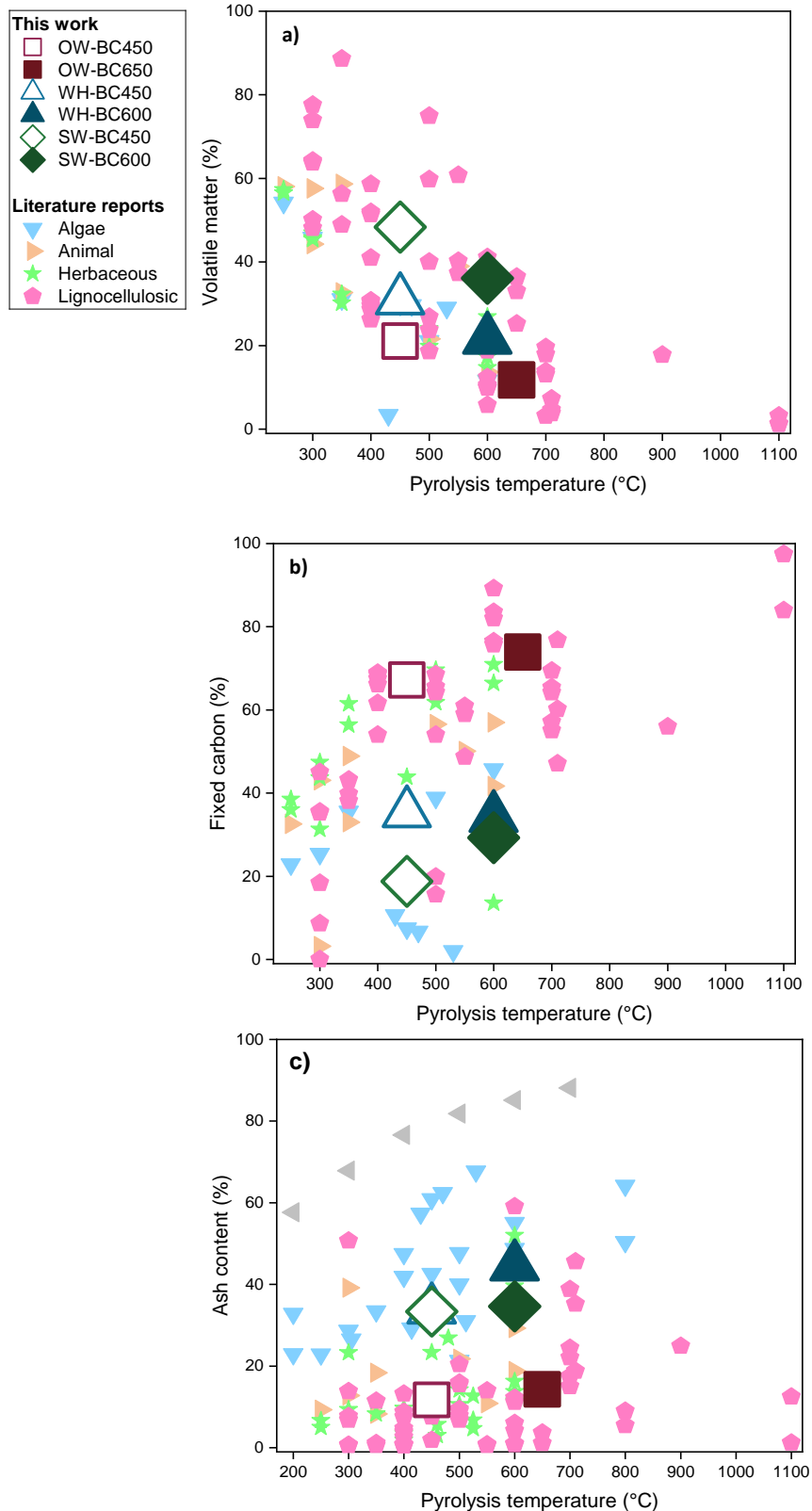
Figure 4.2. Correlation of feedstock and pyrolysis temperature on the proximate composition of the obtained biochars and comparison to literature reports [21,28,151,69,88,144,146–150]. a) Volatile matter; b) Fixed carbon; c) Ash content.

The VM content of algal BCs also decreased with increasing pyrolysis temperature but to a lesser extent than the other BCs as shown in **Table 4.1** and **Figure 4.2a**. Algal biomass is comprised of carbohydrates, protein, lipids, and unsaturated fatty acids. The fraction of these constituents is dependent on the species, season, location and cultivation technique [155]. Brown seaweed like SW is comprised principally of the carbohydrates laminarin, mannitol and alginic acid, and lesser amounts of protein and lipids [156,157]. The pyrolysis degradation of algae carbohydrates differs significantly from cellulosic biomass. Anastasakis et al. [158] investigated the pyrolytic behaviour of the main constituents of brown algae, alginic acid, mannitol, laminarin and fucoidan by TGA and Py-GC/MS. They demonstrated that each of these compounds follows a different degradation pathway. The devolatilization of laminarin and fucoidan occurs over two steps, the first at 342 and 202 °C, and the second at 540 and 710 °C, respectively. Most of the weight loss of alginic acid arises at 200-350 °C and practically ends at 555 °C. The maximum devolatilization of mannitol takes place at 336 °C and ends at 400 °C [158]. Hence, the SW-BCs suffered a considerable devolatilization of all its carbohydrate components, and in consequence, VM intensified for SW-BC600.

The FC of raw biomass feedstocks falls within a range of 0-24.7 % and increases up to 18.8-73.9 % (**Table 4.1**) after subsequent pyrolysis at 450-650 °C. The FC comprises the carbon content remaining in the solid char after the volatilisation of organic compounds. As the pyrolysis temperature increases, VM is volatilised, and the graphitisation degree of the chars increases due to the dehydrogenation and deoxygenation reactions resulting in the generation of stable condensed ring structures [68]. The pyrolysis of biomass originates BCs with higher FC than the untreated feedstock. This enhancement was greater for OW-BCs and WH-BCs and to a lesser extent for algal SW-BCs (**Figure 4.2b**). The greatest rise of FC took place after treating the feedstocks at 450 °C since below this temperature is where most changes took place and VM is lost. Whereas further increasing the pyrolysis temperature to 600-650 °C slightly enhanced FC for OW and WH-BCs and considerably more for SW-BCs. Enders et al. [159] reported that increasing the pyrolysis temperature enhances the FC fraction for low-ash biomass, such as lignocellulosic biomass. In contrast, the FC could maintain unaltered or even decrease for BCs with more than 20 % ash, as observed for WH. They suggested that interactions between the organic matter and the inorganic constituents during pyrolysis affected the formation of aromatic C-structures and thus the FC fraction. Furthermore, it is worth relating the raise on FC for SW-BC600 with the two-step devolatilisation of algae constituents previously mentioned [158].

Another major difference among the biochars produced from the different feedstocks relies on their ash content (**Figure 4.2c**). The loss of organic matter leads to the concentration of the inorganic constituents for all BCs in comparison to the untreated biomass. Like FC, most VM volatilisation and ash concentration takes place below 450 °C. By increasing pyrolysis temperature from 450 to 600-650 °C, the ash content slightly increased for all BCs. OW-BCs exhibited considerably lower ash content than WH and SW-BCs, although these latter reached similar values. These results agree with previous reports stating that the inorganic content of BC produced from woody biomass is significantly lower than BC from herbaceous (e.g., corn cops and stovers, wheat straws and grass) and hydrophyte (waterweeds and algae) biomass [63]. Biochars derived from lignocellulosic sources generally exhibited lower ash content than those produced from other sources.

4.3.2.2   Hydrochars

Table 4.1 lists the chemical composition of oak wood, water hyacinth and saw wrack hydrochars produced by HTC at 250 °C. HC samples exhibit different properties to BCs, including a significantly higher VM, and lower FC and ash content. The HTC of the different biomasses reduced the VM from 72.5-85.4 % to 56.4-64.1 %, although the net loss of VM for each substrate differed. Greater differences were observed for the FC, which increases from 0-24.7% for the untreated feedstocks to 21.6-38.5 % for the HCs. HTC of WH results in the greatest enhancement of FC content from 0 to 23.0 %. Moreover, the ash content of untreated OW and SW showed little variation after the HTC treatment. Conversely, the ash content of WH-HC further increased up to 20.6 %. Accordingly, with the feedstock, the extent of VM loss, FC enhancement and ash concentration followed the order WH>OW>SW. Since all HCs were produced under standard conditions, the differences in the proximate composition are attributed to the nature of the original biomass.

Oak wood is composed of hemicellulose, cellulose, and lignin. Under subcritical water conditions, hemicellulose is completely hydrolysed at approximately 180 °C, whereas cellulose and lignin hydrolysis start at 220 and 200 °C, respectively. Cellulose and hemicellulose are degraded into a series of intermediate poly- and monosaccharides, acids, furfurals and hydroxymethylfurfural. The furfural structures suffer further reactions of condensation, polymerisation and aromatisation to form the hydrochar [60]. Lignin possesses greater thermal stability than cellulose and hemicellulose. It has been suggested that at 250 °C only a small fraction of lignin is hydrolysed into phenolic fragments that

subsequently polymerise [78,160]. In addition, the recalcitrant nature of lignin is reported to interfere with the hydrolysis of both cellulose and hemicellulose polymers, by slowing down their decomposition [76]. The latter suggests that while cellulose and hemicellulose fractions were greatly degraded during HTC at 250 °C, most of the lignin remained to form part of the solid fraction. Hence, the reduced loss of VM for OW derived hydrochar could be due to the recalcitrance of the lignin fraction.

Conversely, water hyacinth derived HC produced the greatest loss of VM content. This could be attributed to the easily degradable composition of WH, comprised principally of starch, cellulose and hemicellulose [153]. Hemicellulose is easily hydrolysed, which makes it a major contributor to the formation of HC microspheres. Even though the hydrolysis of cellulose is limited by the solubilisation of its crystalline fraction, most of the cellulose is expected to degrade under the HTC conditions here employed [161]. Starch is more easily degraded than cellulose. During HTC the crystalline structure of starch is destroyed by melting, swelling and collapse, leaving glucosyl units that further dehydrate into a furan-like compound, that contribute to HC formation [162,163]. Unlike OW-HC, the low levels of lignin of WH could interfere less in the degradation of the cellulosic polymers. Therefore, the greater loss of VM content for WH-HC could be attributed to the degradability of its components.

Similarly, saw wrack (*F. serratus*) biomass is reported to efficiently degrade into an HC structure, even at low HTC temperatures, such as 200 °C [145]. Like most biomasses, SW seaweed has a complex structure characterised by its protein, carbohydrate (alginic acid, laminarin, mannitol and methyl pentoses) and lipids content [143]. During HTC, the usually acidic pH promotes the hydrolytic cleavage of the alginate polymer into the more easily degradable monomers, D-mannuronic acid and L-guluronic acid [164]. In comparison to lignocellulosic biomass, the conversion of algal materials can take place under milder HTC conditions due to the absence of cellulose and lignin [165]. Hence, the differences in loss of VM and changes in chemical composition for WH and SW hydrochar could be attributed to their composition, particularly the easily degraded carbohydrates.

During HTC, not only volatile matter is degraded into water-soluble compounds, but the acidic nature of subcritical water also solubilises some inorganic elements into the liquid phase, reducing then the overall ash content of the HC [60]. Therefore, the remaining solid HC partially retains both organic and inorganic fractions, which could explain why the ash concentration of OW-HC

and SW-HC remained, like the original biomass. Whereas the ash content for WH-HC raised from 14.6 to 20.6 %. Although this HC suffered the greatest VM loss, which could explain why the inorganic fraction was concentrated. In agreement with the ash content of the untreated feedstocks, the HCs derived from WH and SW also exhibited a higher inorganic content than the terrestrial OW.

4.3.3   Ultimate analysis

4.3.3.1   Biochars

Table 4.2 and **Figure 4.3a** show the ultimate analysis of the untreated biomass and chars determined by the CHNOS content on a dry basis (db). Due to the ash content variation between the different materials, the CHNOS expressed on a dry ash-free basis (daf) was also outlined for facilitating the direct comparison between the organic compositions of the chars. The CHNOS daf values are listed in Appendix **Table A.1** and outlined in **Figure 4.3b**. As the pyrolysis temperature was raised, the content of C and N was enhanced, while O and H were reduced for WH-BCs and more substantially for OW-BCs. Both SW-BCs exhibited similar CHNOS daf composition, with a little increased C content in comparison to the untreated feedstock. The CHNOS values indicate how the graphitisation degree of the chars increased due to the dehydrogenation and deoxygenation reactions, which in consequence generates more stable condensed ring compounds. Hence it is expected for the biomass to lose O and H while increasing the C content during biochar formation. OW-BCs and WH-BC600 followed this behaviour, while WH-BC450 and SW-BCs to a lesser extent.

The elemental composition of the different untreated feedstocks and biochars produced in this work along with literature reports were visualised by a Van Krevelen diagram plotting O:C vs H:C atomic ratios (**Figure 4.4**). The evolution of the O:C vs H:C ratios facilitate information retrieval from the extent of pyrolysis, degree of aromaticity and the type of reactions that predominate during pyrolysis as shown in the bottom right of the diagram. The process of carbonisation changes the chemical structure of biomass, mostly due to the detachment of functional groups containing O and H. BCs produced at 200-400 °C resembled the energy density of peat, lignite, and brown coal. These values indicate an early stage of carbonisation and suggest the presence of uncharred fractions of the primary components of the biomass, such as carbohydrates.
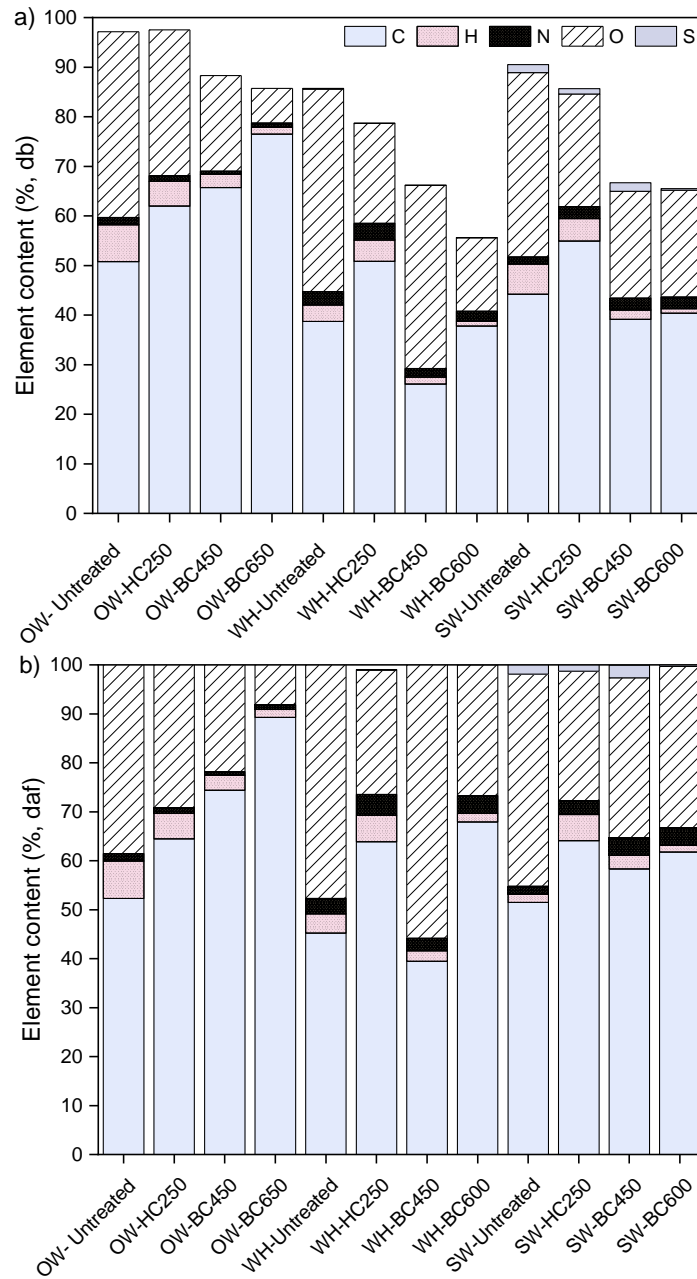
Figure 4.3. Correlation analysis of elemental CHNOS and corresponding feedstock and char. a) expressed in dry basis (db); b) expressed as a dry ash-free basis (daf).
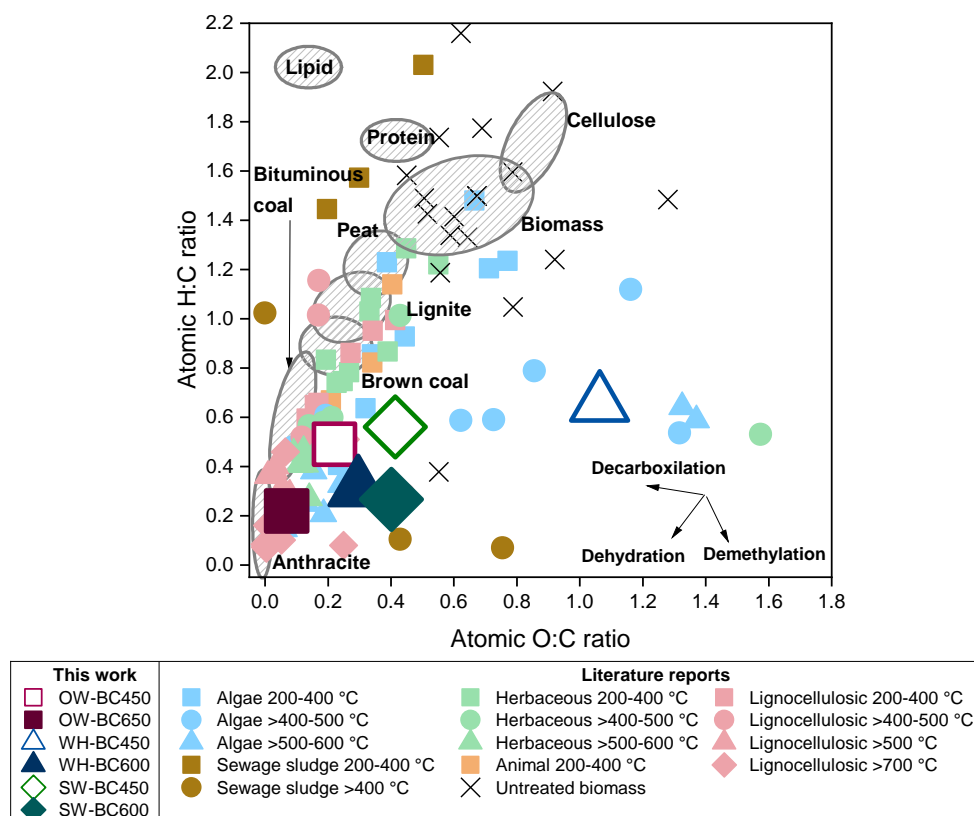
Figure 4.4. Van Krevelen diagram of O:C and H:C atomic ratios of untreated feedstocks and obtained biochars in comparison to literature reports [21,28,151,69,88,144,146–150]. Biomass and coal classification adapted from [166–168].

The decrease of the H:C and O:C ratios with increasing pyrolysis temperature were comparable to the coalification process of biomass. The decarboxylation and dehydration reactions intensified with temperature for all feedstocks. Most BCs produced >400 °C resembled brown and bituminous coal, including OW-BC450 and SW-BC450. Whereas those produced ≥ 600 °C, including OW-BC650, SW-BC600 and WH-BC600, reduced the H:C ratio below 0.4 and resembled anthracite. On the other hand, WH-BC450 exhibited an average H:C ratio, similar to other reports [169,170]. Although an exceptionably high O:C ratio suggests a lower degree of carbonisation than the rest BCs and a predominance of demethylation reactions. Notwithstanding, the decrease of H:C and O:C ratios with temperature indicated the conversion of organic materials to aromatic C structures with reduced carboxyl and hydroxyl groups [167].

Figure 4.5 shows the effect of pyrolysis temperature on the atomic N:C ratio of BCs and compares it with several reports found in the literature. Regardless of the pyrolysis temperature, lignocellulosic BCs exhibited a very low N:C ratio, while herbaceous BCs showed a greater variation. Feedstocks with intrinsic

higher protein and thus N content, including algae, animals, and sludge, suffered the greatest reduction of the N:C ratio when increasing the pyrolysis temperature. This change could be attributed to the intensified loss of VM and carbonisation taking place under more severe pyrolysis conditions.
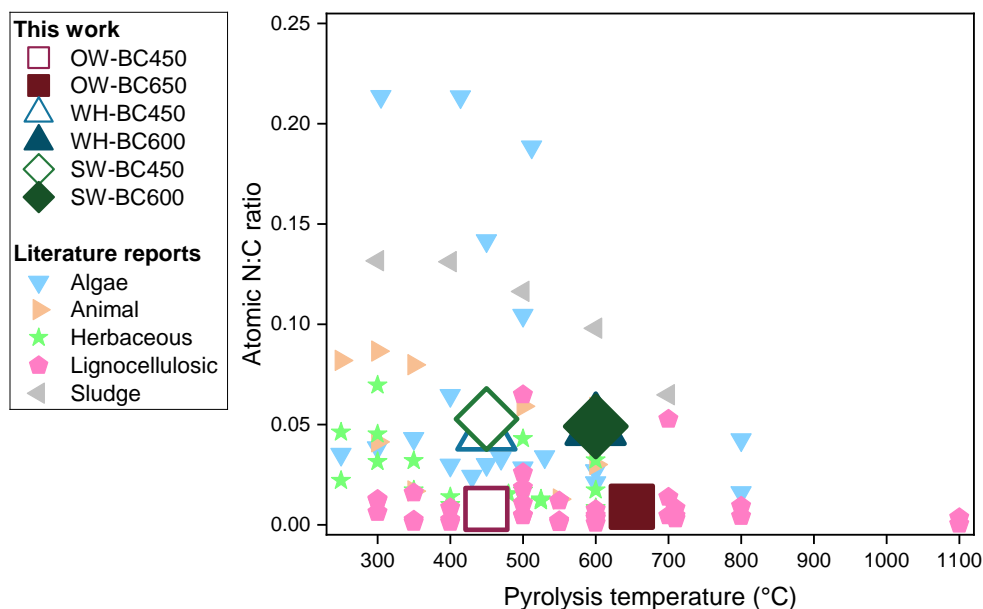
Figure 4.5. Correlation of feedstock and pyrolysis temperature on N:C ratio of obtained biochars in comparison with literature reports [17,21,173–181,38,69,87,144,149,151,171,172].

On the other hand, OW, WH and SW BCs produced at either 450 or 600-650 °C showed similar N:C ratios. It has been stated that pyrolysis temperature determines the fate of N since nitrogen species tend to be converted into more stable structures. As the temperature increases, the compositional changes are accompanied by some N loss due to the protein degradation and devolatilization of ammonium N from the biomass structure. Further pyrolysis promotes condensation reactions that convert C=N and C=O groups into heterocyclic compounds containing C-N groups [182]. Nonetheless, it is also possible to observe either an increase or no changes in N-content since the concentration of other components is reduced due to devolatilization [67].

4.3.3.2   Hydrochars

Table 4.2 and **Figure 4.3a** show the CHNOS of the hydrochars produced by HTC at 250 °C for 1 h on a dry basis. In comparison to the untreated feedstocks, the hydrochar products exhibited a higher C-content accounting for 50.8-62.0 % of

their composition, while the O-content reduced to 20.2-29.4%. The N content considerably enhanced for WH and SW HCs, while it slightly decreased for OW-HC. The H content was reduced for OW and SW HCs, whereas it slightly increased for WH-HC. From all HCs, WH biomass suffered the greatest loss of O and enhancement of C and N content. This behaviour agrees with the observed volatile matter since WH was the biomass that suffered the greatest net loss of VM during HTC.

Figure 4.3b shows the changes of CHNOS of HCs on a dry ash-free basis. The behaviour was similar when comparing the CHNOS composition in daf and db. These HCs also exhibit different properties from the BCs. The C-content was typically higher than the intermediate temperature (450 °C) BCs, although they contained similar or lower levels of O. The loss of H and O and the rise of C-content in HCs were mainly due to dehydration, deoxygenation, and decarboxylation reactions. The reaction mechanisms taking place during HTC are also dependent on the feedstock nature and in consequence their main components.

Elemental molar ratios of O:C vs H:C of biomass and hydrochars produced in this work alongside literature reports are displayed in a Van Krevelen diagram (**Figure 4.6**). The diagram illustrates the chemical transformations that predominated during HTC resulting in carbon-rich products. The decrease of the H:C and O:C ratios with increasing HTC temperature were comparable to the coalification process of biomass. Most HCs produced at ≤ 225 °C resembled peat, while those produced at 250 °C resembled lignite and brown coal. The ratios for OW-HC, WH-HC and SW-HC were very similar and resembled lignite. Nonetheless, most HCs showed 'coal like' O:C ratios and higher H:C ratios suggesting the predominance of dehydration and decarboxylation reactions. All HCs exhibit a reduction of O:C and H:C ratios, except for the H:C ratio for SW-HC which increased. As the HTC severity intensifies, dehydration reactions break hydroxyl and carbonyl groups, and the formation of aromatic ring carbons is enhanced. At high HTC temperature, free-radical reactions become involved in the cleavage of aliphatic C-C groups, resulting in extensive dehydration and condensation that reduced the O:C and H:C ratios [78]. The observed reduction of O:C and H:C ratios with increasing temperature, supports the predominant influence of the HTC temperature in the process of carbonisation.
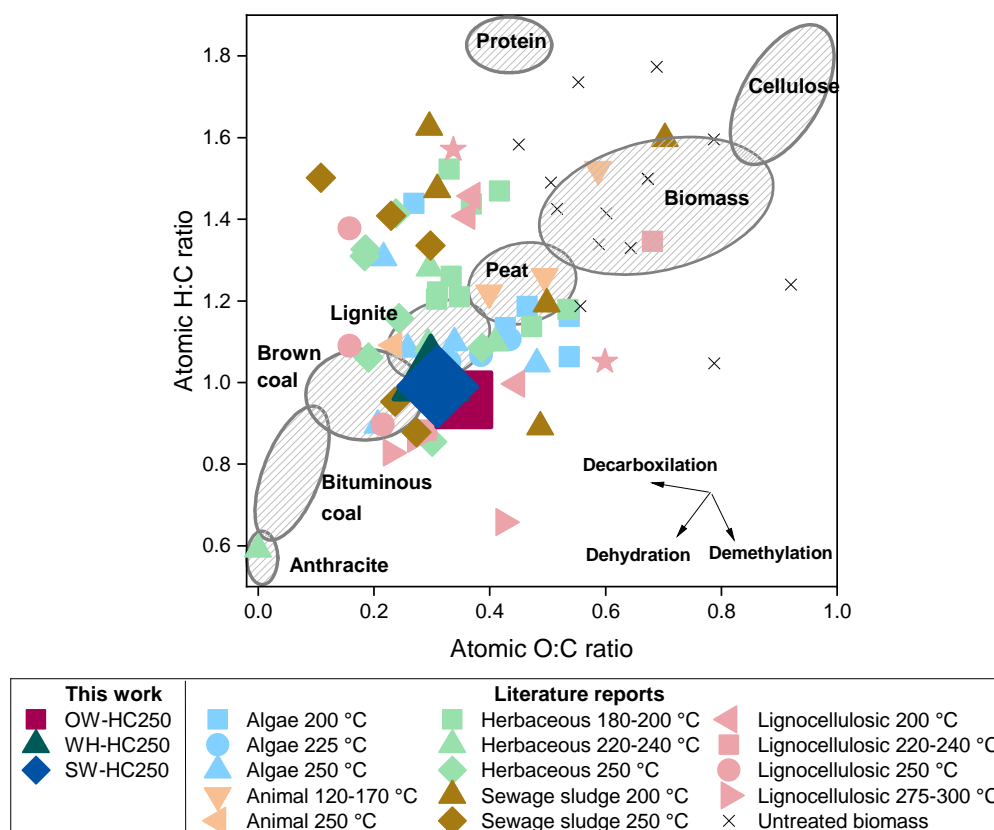
Figure 4.6. Van Krevelen diagram of O:C and H:C atomic ratios of untreated feedstocks and obtained hydrochars in comparison to literature reports [17,66,189,190,145,146,183–188]. Biomass and coal classification adapted from [166–168].

The fate of N during HTC differed among the analysed HCs (**Table 4.2**). In comparison to the untreated feedstock, the N content of OW-HC reduced from 1.5 to 1.2 %, while WH-HC and SW-HC were enhanced from 2.7 and 2.4 % to 3.4 and 2.4 % db, respectively. **Figure 4.3** visualises the fate of N after the HTC treatment, showing a similar behaviour in both db and daf. During HTC, part of the N is decomposed by hydrolysis resulting in deamination reactions, hence, a fraction of the N is solubilised in the liquid fraction. The extent of N solubilisation is influenced by processing conditions and feedstock principally by the reaction temperature [191]. Increasing temperature enhances the solubilisation of N, although the N species found in HC are strongly related to the biomass of origin. Still, most of the N is solubilised during HTC, whereas a fraction remains or is further incorporated into the solid HC in the form of more stable heterocycles N species. The latter is due to chemical, precipitation and crystallisation reactions, usually favoured by increasing HTC temperature [192].

Figure 4.7 shows the effect of HTC temperature on the atomic N:C ratio of HCs and compares it with literature reports. In agreement with the ultimate composition, the N:C ratio of the HCs exhibited the following trend WH>SW>OW as listed in **Table 4.2.** In a similar way to BCs, lignocellulosic HCs exhibited the lowest N:C ratios, while herbaceous HCs varied. Both sludge and algae show the highest N:C ratio in agreement with their higher protein content. Nonetheless, the trend for most HCs was to reduce the N:C ratio with increasing reaction temperature. Biomass with higher N content is reported to be more susceptible to N solubilisation.
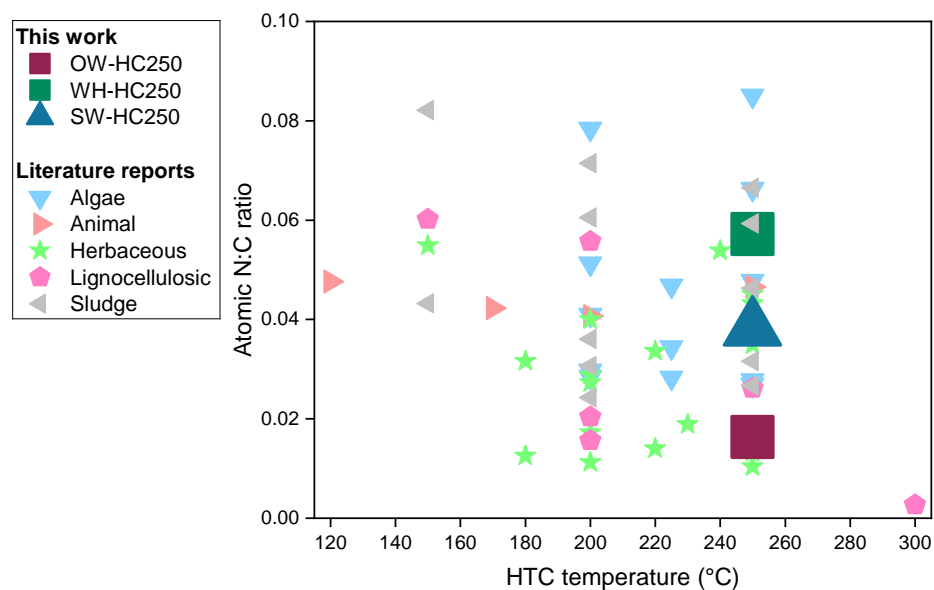
Figure 4.7. Correlation of feedstock and pyrolysis temperature on N:C ratio of obtained hydrochars and comparison with literature reports [17,66,188,193,134,145,146,183–187].

Similarly, Kruse et al. [191] compared the HTC at 180, 220 and 250 °C and reaction time of 1-12 h of the protein-rich *Chlorella,* and carrot green biomass with low N content. They observed a considerable reduction of N content in the *Chlorella*-HC, which increased with temperature and reaction time. Whereas for the carrot green-HC, the N content slightly enhanced with temperature but decreased with reaction time.

4.3.4 Inorganic composition

4.3.4.1 Biochars

Figure 4.8 shows the major inorganic elements within the untreated feedstocks and the chars, while the values for all the inorganic elements are listed in Appendix **Table A.2**. Analogous to the TGA analysis, lignocellulosic OW materials showed the lowest inorganic content, comprised mainly of Ca, Mg, and Fe. Conversely, WH materials exhibited a wider variety of inorganics, including Si, Ca, S, Fe, Al, Na and K, in agreement with other reports [189].
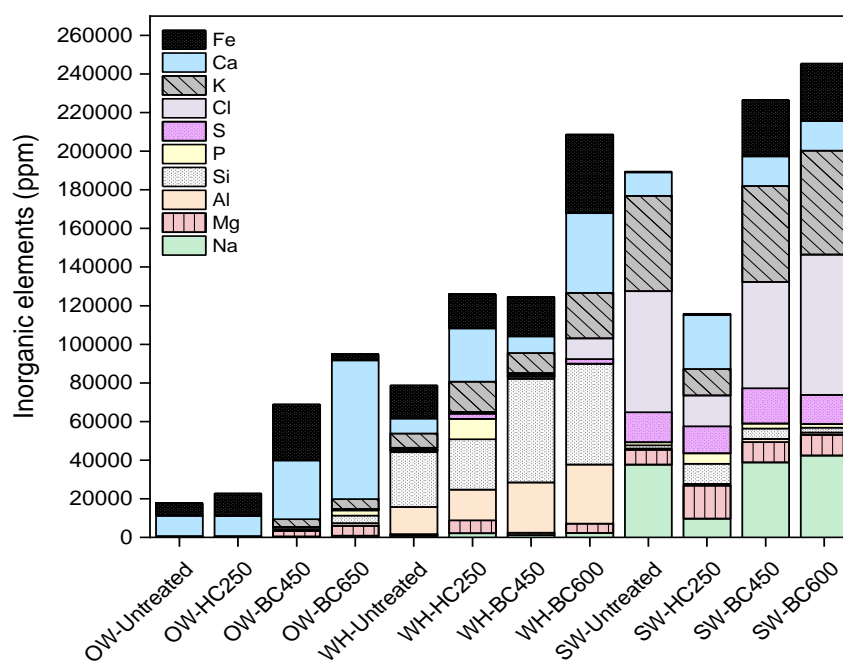
Figure 4.8. Content of main inorganic elements of untreated feedstocks and chars obtained by X-ray fluorescence (XRF).

The chemical composition of WH is highly dependent on its growing environment, which in this case was collected from Lake Victoria where it was exposed to wastewater discharge and other sources of contamination. WH is reported to remove heavy metals from water, hence its substantial content of inorganics and potential for sustainable phytoremediation of water [194]. SW materials exhibited the highest inorganic content, comprised principally of Cl, Na, K, Fe, Ca, S, and Mg. Seaweeds usually exhibit a greater abundance of inorganics, principally Na, K and Ca bonded to carbonate ions and also considerable amounts of Si [195]. The chemical composition of SW is also influenced by the growing environment, thus the salinity of the seawater could

also contribute to the high content of Na and Cl. The latter suggests that the amount and distribution of mineral ash in the chars were greatly determined by the feedstock.

The inorganic composition of chars was also influenced by the thermochemical processing conditions, principally temperature. For all BCs, the ash content is concentrated with the pyrolysis temperature due to the loss of C, H and O by volatilization (**Table 4.2**). Notwithstanding, inorganic elements can form a bond with organic volatiles, be released by vaporisation and end up in the bio-oil. The elements that largely remain within the solid biochar are alkali earth metals (Ca, Mg), transition metals (Fe, Cu, Ni, Cd, Cr, Co, Mn, Zn) and post-transition metals (Al, Pb) [196]. At low pyrolysis temperature, some labile ions (K and Cl) can vaporise, while others require more severe conditions (Ca, Mg, P, S and Si) [61]. The alkali metals Na and K can undergo both pathways, their principal destiny is to remain within the biochar, although notably amounts can also be transferred with the organic volatiles to the oil fraction. The concentration of K, Cl, Ca, Mg, S and Si for the BCs remained unaltered or even concentrated when increasing temperature. For all BCs, the content of Fe increased after the treatment, except for OW-BC650, which unexpectedly reduced. Fe is strongly retained in the solid char during thermal treatment, although a low transfer of Fe to pyrolysis oil has also been reported [196]. The loss of organic matter concentrated the inorganic fraction, thus, the pyrolysis conditions for BCs produced from the same feedstock were reflected in the inorganic composition.

4.3.4.2   Hydrochars

The content of inorganic elements within HCs was lower than the BCs produced from the same feedstock (**Figure 4.8**). These variations reflect the different reactions taking place during each thermochemical treatment. The subcritical acidic conditions of HTC promote the solubilisation of some inorganic elements, although the majority often remained in the HC structure [68]. The removal of inorganic elements bound by ionic bonds to organic structures within the biomass is facilitated by HTC. The subcritical conditions increase the ionic dissociation constant and lower the pH of the subcritical water resulting in ion exchange and the dissolution of inorganic salts. The reason for either the decrease or enhancement of ash content in HC is determined by the specific ash chemistry of the feedstock. HTC generally reduces the ash content of biomass; however, it does not always reflect on the compositional values due to the simultaneous loss of C, O and H. Despite the loss of inorganic elements into the

liquid phase, the overall concentration of inorganics within the HC can still increase [183].

The concentration of inorganic elements for the HCs exhibited the following order WH>SW>OW from higher to lower, comprised principally of Ca, Fe, Si, K, P, S and Mg (**Figure 4.8**). Firstly, the inorganic content of the OW-HC consisted mainly of Ca and Fe, with values slightly higher than the untreated OW. Similarly, Smith et al. [183] reported that the inorganic fraction of OW biomass is comprised principally of Ca, K and Mg. After its treatment by HTC at 250 °C, they observed that the concentration of Na, Mg, P and Fe in the HC remained close to the untreated biomass, although the overall ash content was reduced. Secondly, WH-HC increased the concentration of inorganics by 63 % compared to the untreated WH. From the analysed HCs, WH-HC exhibited the greatest concentration of the ash fraction from 14.60 to 20.55 %, due to a greater loss of VM (**Table 4.1**). Nonetheless, some inorganic elements exhibited no significant variation (Si, Al, and Fe), while others enhanced (Mg, P, K, Ca, and S). Accordingly, it has been reported that feedstocks rich in Si and Fe often lead to HC with higher ash content [183]. Besides, WH-HC was largely comprised of not easily removed inorganic elements, such as Mg, Ca, P and Si [142]. Thirdly, the HTC of SW reduced the inorganic concentration of some elements (Na, Cl and K), while increasing others (Mg, Si and Ca) in agreement with other reports [143]. Alkali earth chlorides comprised of Na, K and Cl are reported to be easily dissolved into the liquid phase, whereas the removal of P and alkaline earth metals Mg and Ca is more limited. Furthermore, it has been suggested that the HTC of biomass containing alginate, such as SW, could incorporate divalent cations (Ca and Mg) into the HC by promoting cross-linking of alginate oligomers, thus limiting the removal of these elements [183].

4.3.5 pH

The pH of the BCs and HCs ranged between 9.1-12.1 and 3.9-5.6, respectively (**Table 4.1**). As expected, the HCs were acidic while BCs were alkaline. The nature of the feedstock also influenced the pH of the chars in the following order OW<WH<SW. In the case of BCs, the pyrolysis temperature is the main factor affecting the pH, followed by the chemical composition. The functional groups detached during pyrolysis are generally acidic (e.g., carboxyl, hydroxyl, and formyl groups) resulting in a more basic structure. The concentration of ash is another large contributor to enhancing alkalinity [67]. The ash, as well as the total base cations and carbonates content of BCs, enhances with pyrolysis temperature, influencing the pH [197]. The latter agrees with the higher values

observed for the SW-BCs (pH 11.1-12.1) and WH-BCs (pH 9.1-10.6) in comparison to OW-BCs (pH 9.3-9.9). Conversely for HCs, many organic acids (e.g., acetic, lactic, formic and levulinic acids) formed during the HTC reduce the pH of the system. Even though the process of HTC eliminates several hydroxyl and carboxyl groups, the HCs still exhibit an acidic pH [76].

4.4 Surface area and porosity

4.4.1 Nitrogen isotherms

The N_2 adsorption isotherms for the chars are outlined in **Figure 4.9**. The amount of adsorbed nitrogen was very low for most chars, with only OW-BC450 and OW-BC650 showing some uptake at low partial pressure. It was not possible to obtain an isotherm with meaningful and positive values for SW-BC450, which could be related to the inability of N_2 to access the narrow microporosity of some chars [198]. Nonetheless, the N_2 adsorption isotherm for most BCs showed a similarity with the Type III, and given the hysteresis, also to isotherm Type V. The shape of Type III isotherm indicates weak adsorbent-adsorbate interactions and an accumulation at the nonporous and macroporous sites of the material due to condensation [199]. This accumulation results in isotherms with a resilient rise of the adsorbed amount even near the saturation pressure. The hysteresis loop is considered an indicator of mesoporosity and is attributed to the filling and voiding of the mesopores [114]. However, the hysteresis for the N_2 isotherms of most BCs and HCs started below p/p_0 of 0.4 and there was no defined closure. This behaviour has been related to the presence of low-pressure hysteresis due to the swelling of the non-rigid porous structure or the irreversible accumulation of molecules in pores [200].

Even though N_2 adsorption at 77 K is the most used technique, its routine application on heterogeneous materials often provides erroneous information. The N_2 isotherms obtained for the chars corroborated the influence of the mentioned limitations. For instance, the inability to obtain an isotherm for SW-BC450, the weak adsorbent-adsorbate interaction and condensation of the N_2 supported by the Type III isotherm profile. The SA values are a function of the selective adsorptive, hence the importance to consider the limitations. The adsorption with N_2 at 77 K is often reported as unable to obtain correct measurements for the SA of chars [67]. Hence, it can be stated that the N_2 adsorption/desorption isotherms for the chars here tested do not correspond to the real SA of the materials.
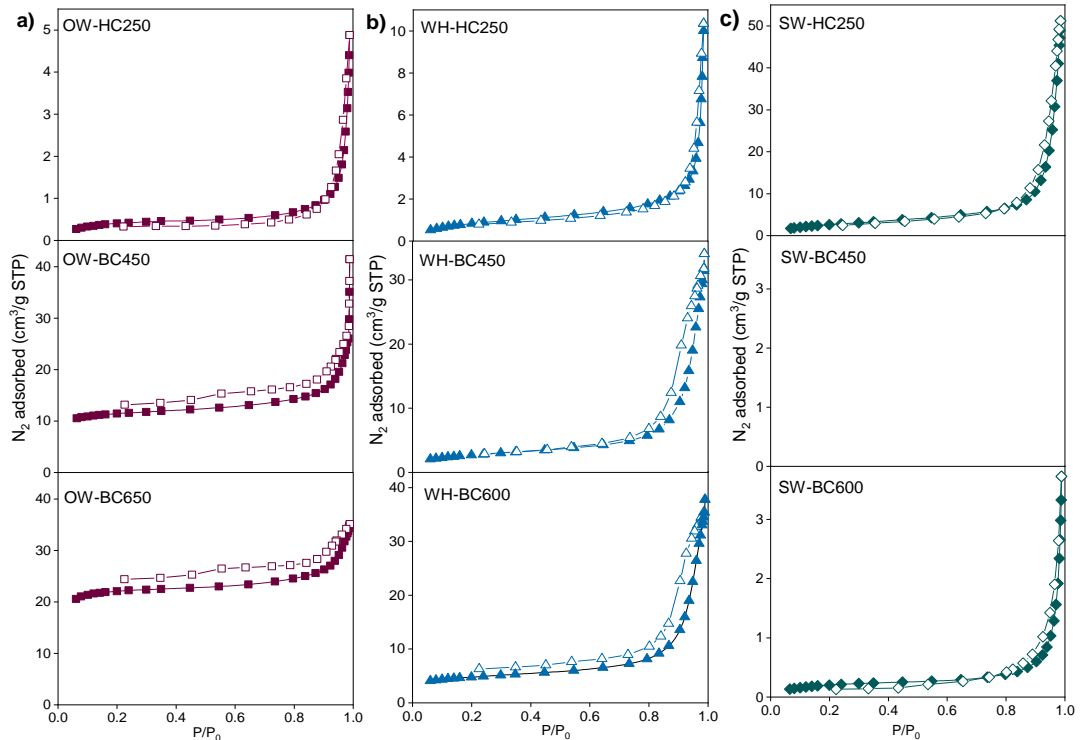
Figure 4.9. Nitrogen (N_2) gas adsorption (●)/desorption (○) isotherms for the char materials: a) oak wood; b) water hyacinth; c) saw wrack.

4.4.2 Carbon dioxide isotherms

The use of CO_2 as an adsorptive overcomes some of the inherent problems of N_2. At 273 K, the kinetic energy of the CO_2 molecules is larger in comparison to N_2 at 77 K, improving the ability of CO_2 to reach narrow pores, overcoming thus the diffusional problems of N_2 [198]. The CO_2 adsorption isotherms of all BCs and HCs resembled isotherm Type II, except for OW-BC650, which resembled Type I isotherm (**Figure 4.10**).

The Type II isotherm is characteristic of both nonporous and macroporous materials, which in this case suggested a wide microporosity [111]. Reversible Type I isotherm, on the other hand, is characteristic of microporous solids with small external SA. The shape of the Type I isotherm is concave against the $p/p°$ axis, where the adsorbed amount has a steep uptake and approaches a limiting value at very low relative pressures, which is related to the accessibility of the micropores rather than the internal SA. Moreover, the shape of the OW-BC650 isotherm is Type I(b), which is an indication of a wider range of pores containing not only micropores but also mesopores [199].
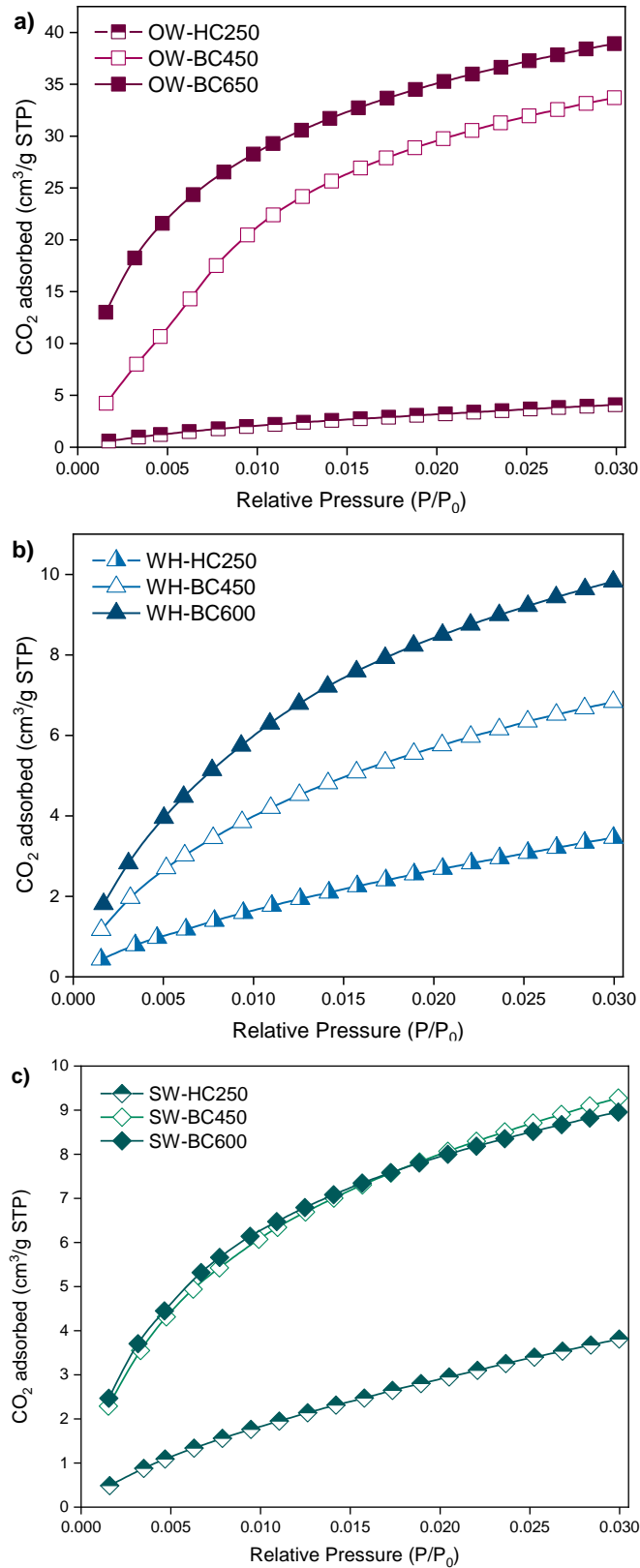
Figure 4.10. Carbon dioxide (CO_2) gas adsorption isotherms for the char materials: a) oak wood; b) water hyacinth; c) saw wrack.

4.4.3 Surface area

The SA and pore volume (PV) values for the chars were obtained with the NLDFT model (**Table 4.3**). The SA was considerably low with the N_2 adsorption (2.28 to 18.35 m^2/g), in agreement with the limitations previously mentioned. Conversely, the SA of BCs and HCs obtained by CO_2 adsorption were considerably higher in a range of 39-221 and 37-58 m^2/g, respectively. The physical structure of BC and HC differ largely. HCs exhibit the morphology of a dense sphere, whereas BC resembles the original morphology of the biomass accompanied by a degree of aromaticity [25].

Table 4.3. Surface area and pore volume of biochars and hydrochars from the analysis of N_2 at 77 K and CO_2 at 273 K adsorption/desorption isotherms.

Char	N_2 adsorption at 77 K		CO_2 adsorption at 273 K	
	SA (m^2/g)	PV (cm^3/g)	SA (m^2/g)	PV (cm^3/g)
Oak wood				
OW-HC250	0.438	0.0067	44.02	0.0109
OW-BC450	3.356	0.0464	221.00	0.0776
OW-BC600	2.441	0.0513	237.00	0.0900
Water hyacinth				
WH-HC250	1.343	0.0158	37.14	0.0094
WH-BC450	5.003	0.0489	38.69	0.0188
WH-BC600	5.338	0.0540	89.90	0.0264
Saw wrack				
SW-HC250	6.794	0.0784	40.55	0.1040
SW-BC450	-	-	71.51	0.0230
SW-BC600	0.316	0.0047	63.51	0.0215

- Adsorption isotherm not obtained

Hence, BCs exhibited a considerably higher SA than HCs, which was enhanced by increasing the pyrolysis temperature. OW-BC450 and OW-BC650 were the chars with the highest SA, with values of 221 and 237 m^2/g, respectively. Although, the other BCs exhibited lower SA with values of 39, 90, 72 and 64 m^2/g for WH-BC450, WH-BC600, SW-BC450 and SW-BC600, respectively. These differences agree with reports found in the literature where lignocellulosic BCs generally exhibited significantly higher SA than BCs from other sources, such as herbaceous, algae, animal, and sludge (**Figure 4.11**). The SA of the BCs produced in this work along with literature reports were found in a wide range.

Nonetheless, the general trend was an enhancement of SA with increasing pyrolysis temperature up to a certain point.
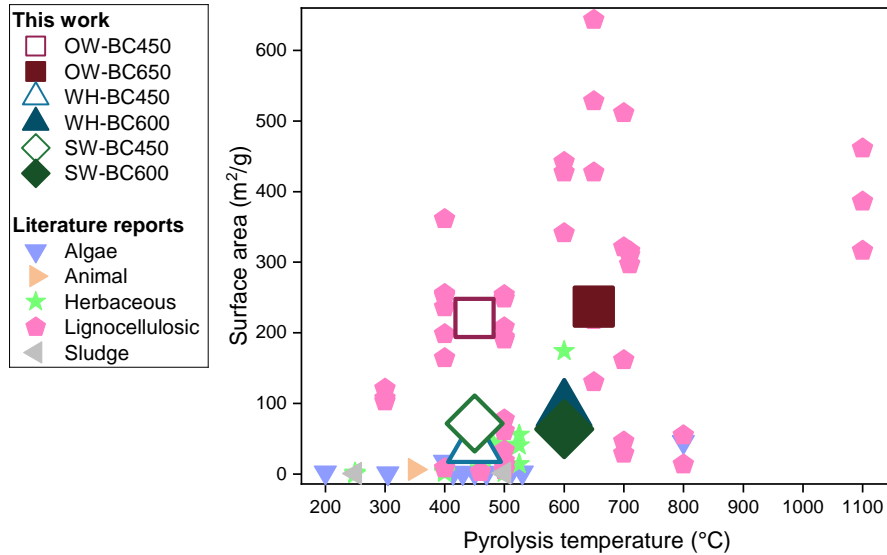
Figure 4.11. Correlation of feedstock and pyrolysis temperature on the surface area of the obtained biochars and comparison to literature reports [28,35,175–178,181,201–204,37,38,69,92,146–148,173].

The higher SA for the OW-BCs could be attributed to their low ash content and lignocellulosic composition. Low content of ash is regarded as a positive factor for achieving greater SA since high ash concentration often leads to the loss and collapse of the structure due to the partial fusion and swelling of inorganics during carbonisation [25]. It has been established the role of lignin in maintaining the physical structure of biomass during pyrolysis. For instance, biomass rich in lignin is likely to develop macroporous BC, while biomass rich in cellulose develops a more microporous structure [197]. The lower SA obtained for both WH and SW BCs could be due to the cellulosic nature of the biomasses, and their high volatile matter and ash content. BC with high VM content is frequently reported to show low SA due to the decomposition and softening of certain volatile intermediates that could further melt into the structure of the BC and block the pores [25].

Increasing the pyrolysis temperature generally led to BCs with greater porosity. During pyrolysis below 350 °C, biomass suffers a rapid increase in porosity. At higher temperatures 400-600 °C, the porosity continues to increase, in the case of lignocellulosic feedstocks, lignin slowly decomposed contributing to porosity. At even higher temperatures (e.g., above 600 °C) the porosity is not significantly

enhanced, and in some cases, shrinking of the solid matrix takes place, affecting thus the final structure [67]. It has also been suggested that the burn-off of the carbon is the main responsible for the rise of the SA rather than the pyrolytic temperature [59]. Nonetheless, the porosity of BCs increased drastically at 400-600 °C partially due to the releasement of molecules of water by dehydroxylation [73].

In addition to pyrolysis temperature and the composition of biomass, other factors could influence the SA and porosity of BC. Such is the case of the process variables reactor type, heating rate, residence time, carrier flow rate (usual nitrogen), recirculation of gas product and the techniques used to cool and condense the hot volatiles from the reactor. According to the contact between gas and solid, conventional pyrolysis reactors can be classified into three categories: entrained beds (traditional retort kiln), fixed beds (muffle furnace) and fluidised beds. For instance, BC produced in a muffle furnace will contain more ash, fixed carbon, and less volatile matter than that produced in a retort kiln. Microwave-assisted pyrolysis is suggested to provide higher SA and PV than conventional pyrolizers. Microwave pyrolysis creates a smaller temperature difference between the surface and the core of biomass, resulting in a higher transfer rate and emptier micropores. Increasing the heating rate up to a certain point could increase these parameters [205].

A residence time of 60 minutes was employed for producing the BCs, allowing sufficient reaction time for releasing the volatile matter and develop thus the porous structure. Excessively prolonged heating rates and residence times could result in pore blockage and collapse. Increasing the carrier flow rate could favour the removal of volatile matter, although if it is too high it could decrease the temperature of biochar [205]. The recirculation of pyrolysis non-condensable product gas into the reactor increases the bio-oil yield affecting biochar [206]. Similarly, quenching condensation by circulating or spraying water is also reported to increase the bio-oil yield [207]. In summary, all these parameters must be taken into consideration during pyrolysis for obtaining biochars with desirable features, such as SA and PV.

As expected, the HCs exhibited lower SA than BCs made from the same feedstock, with values found in a narrow range of 37-44 m^2/g by NLDFT of CO_2 isotherms. All HCs were produced under standard HTC conditions, hence the minor differences in SA could be attributed to the nature of the different feedstocks. Even though there is a correlation between the different biomass components and the HTC products, the mechanisms of action for HC production are not

completely understood [19]. The presence of water in HTC leads to a different degradation pathway and reactions in comparison to pyrolysis. It has been reported by SEM studies that the fibrous structure of the biomass could be lost by increasing the HTC process severity leading to a smoother surface with a lower surface area [60].

4.4.4 Pore size distribution and pore volume

The adsorption technique also allowed the estimation of the pore size distributions (PSD) of the chars. CO_2 allowed the analysis of micropores (0.35-1.0 nm), while N_2 covered meso- and macropores (0.35-100 nm) [115,116]. The complementary analysis with both adsorptive covers a wider range of pore sizes and provides a more robust analysis. The PSD obtained from the N_2 isotherms by NLDFT analysis is displayed in **Figure 4.12**. The incremental PV curves allow the differentiation between sizes for the most prevalent pores, whereas the cumulative PV curves allow the estimation of the total PV of each char.

Figure 4.12 suggested that BCs made at different temperatures but from the same feedstock exhibited similar PSD, comprised mostly of mesopores (2-50 nm) and macropores (>50 nm). Firstly, both OW-BCs showed a wide distribution of mesopores (5-50 nm) and a significant macroporous presence (60-70 nm) in agreement with their higher SA. The significantly higher peak at 63 nm observed for OW-BC450 in **Figure 4.12a** and the sharp step in **Figure 4.12c** suggest a broad macroporosity for this material. Secondly, the PSD of the WH-BCs was similar, both comprised of a wide range of mesopores (8-40 nm), and particularly pores of 20 nm. The slightly higher PV for WH-BC600 supports the influence of higher pyrolysis temperature to obtain BCs with larger PV and PSD. Thirdly, since it was not feasible to obtain an N_2 isotherm for SW-BC450, it is not possible to evaluate the role of pyrolysis temperature on the PSD of seaweed BC. Hence, SW-BC600 exhibited the lowest PSD of all BCs, accompanied by a minor mesoporosity, with a slight macroporosity at 63 nm.
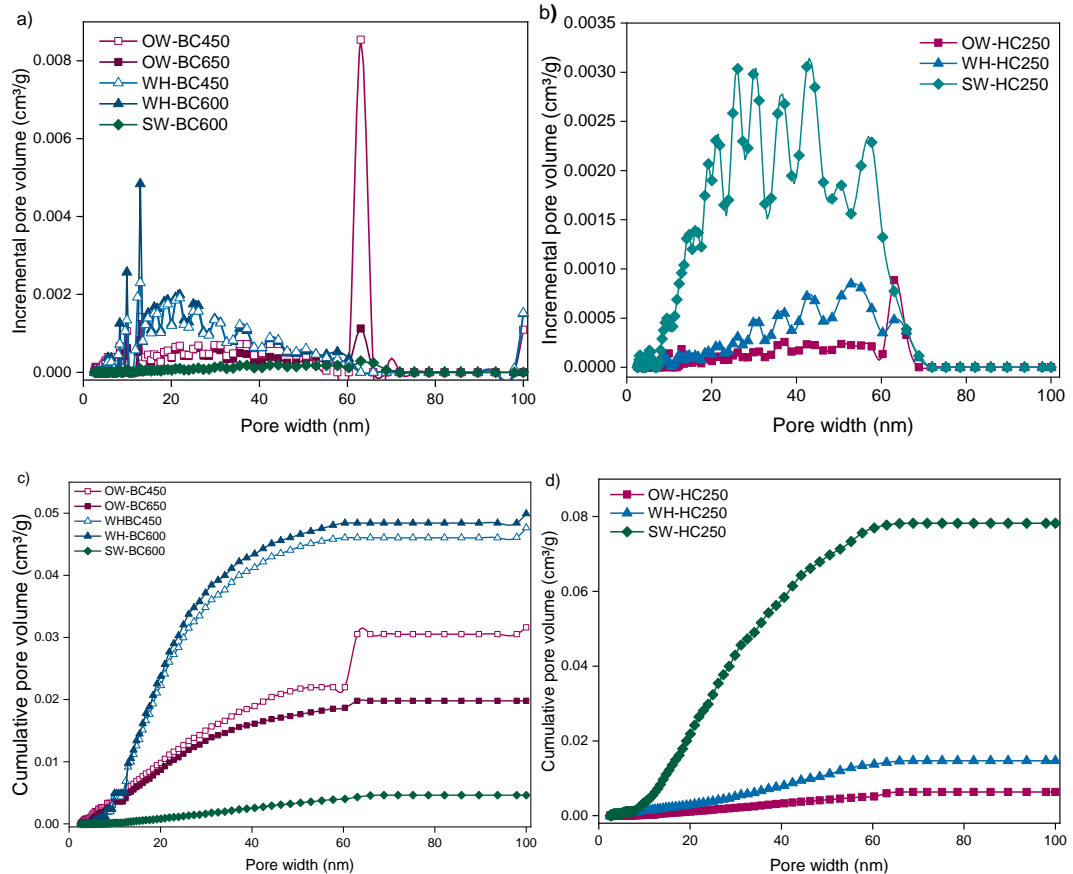
Figure 4.12. Pore size distribution calculated from nitrogen (N₂) gas adsorption isotherms: a) Incremental PSD of biochars; b) incremental PSD of hydrochars; c) cumulative PSD of biochars; d) cumulative PSD of hydrochars.

BCs exhibit a larger SA and porosity than HCs due to the differences in physical structure originating from the nature of each thermochemical treatment. During pyrolysis, the removal of water and carbon mass creates shrinkage stress and breaks the biomass structure. Since the surface of the material decomposes faster than its interior, the result of these changes is the creation of pores of different sizes. The physical structure of the original biomass is retained up to a certain extent, and more significantly for lignocellulosic materials, in agreement with the larger PSD obtained for OW-BCs [25]. On the other hand, HCs exhibit the morphology of a dense sphere with a highly aromatic core-shell and a more aliphatic outer shell. The density of the HC sphere structure results in low SA and PSD [19]. **Figure 4.12b** outlines the mesoporosity (2-50 nm), and a significant presence of macropores (50-70 nm) for all HCs. OW-HC exhibited a prevalent macropore peak at 63 nm, in agreement with the observed for the OW-BCs. WH-HC exhibited a low PSD, with a slight predominance at 40-60 nm. Contrary to the behaviour observed for the BCs, the SW-HC exhibited a larger and broader PSD

(20-60 nm) than the rest of the HCs. The cumulative PSD of SW-HC was more than four times larger than the obtained for OW-HC and WH-HC (**Figure 4.12d**).

For CO_2 adsorption, the BCs from the same feedstock but at different temperatures showed similar PSD (**Figure 4.13**). Most of the pores were found in a range of 0.45 to 0.70 nm categorised as ultramicropores, according to IUPAC [111]. In agreement with the SA and N_2 PSD, the OW-BCs showed a larger porosity than the others. Both OW-BC450 and OW-BC650 exhibited microporosity within a range of 0.45-0.60 nm. Conversely, SW-BCs and WH-BCs offered a very low microporosity.
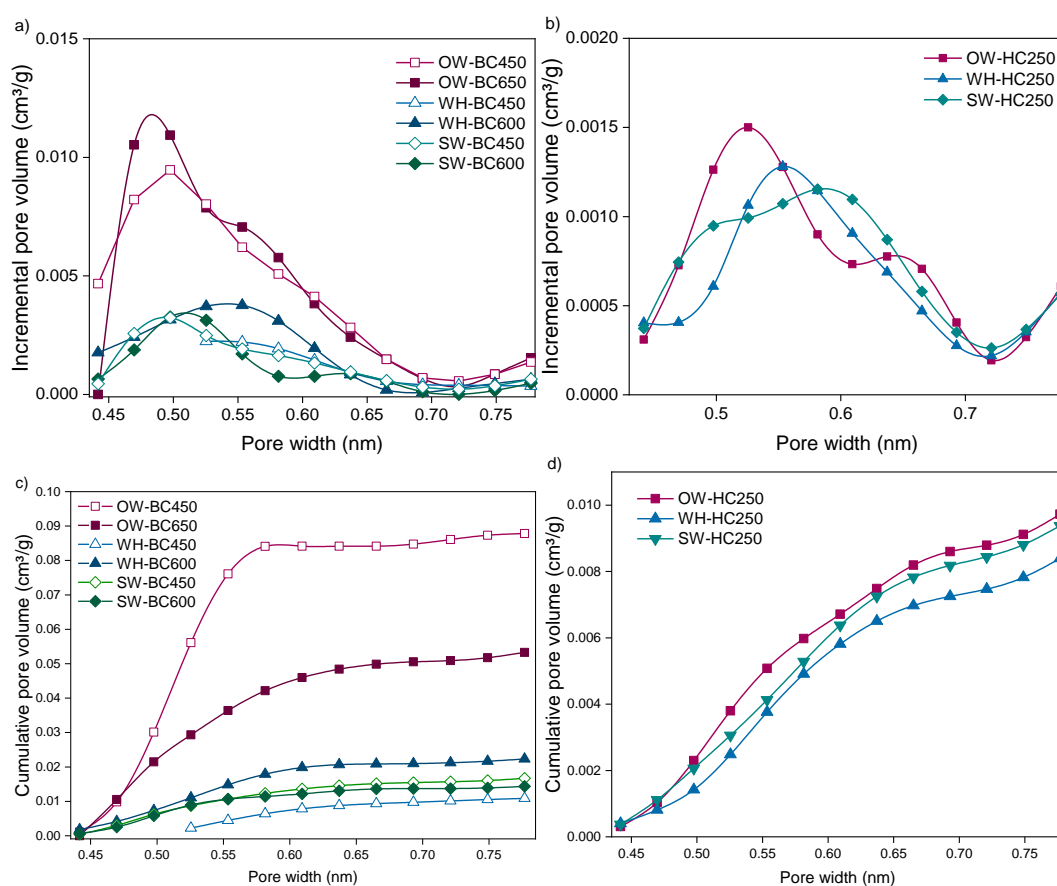
Figure 4.13. Pore size distribution calculated from carbon dioxide (CO_2) gas adsorption isotherms. a) Incremental PSD of biochars; b) incremental PSD of hydrochars; c) cumulative PSD of biochars; d) cumulative PSD of hydrochars.

Further, all HCs exhibited a similar PSD ranging from 0.45 to 0.72 nm, a maximum peak at 0.50-0.55 nm and a rise tailed near 0.75 nm, indicating some wider micropores. The pore volume (PV) of the chars was found in relatively similar ranges with both N_2 (0.005-0.078 cm^3/g) and CO_2 (0.009-0.104 cm^3/g)

adsorption methods (**Table 4.3**). Generally, the BCs showed a higher PV than HCs, except for SW-HC, which showed the greatest value (0.104 cm^3/g). However, it is important to be cautious with the N$_2$ adsorption data since the isotherms showed poor adsorption and it proved to be unsuitable for SA analysis.

4.5 Surface functionality

When analysing the properties of BCs and HCs, not only their bulk composition is relevant. The surface properties are crucial by taking into consideration that chars interact with their surrounding environment through their surface. The surface of a solid considers the outermost layer of atoms, which is divided from the bulk region by a layer of atoms known as the selvedge of the material. It is common for the surface and bulk region to differ in composition, in terms of atomic concentrations, chemical state and coordination number [119]. Surface chemistry is comprised of a diversity of functional groups formed by H, O, N, P, and S heteroatoms incorporated into the carbon structures and aromatic rings [61]. Nonetheless, the surface functionality of chars is composed predominantly of oxygenated functional groups (OFGs), including C-O, C=O, OH and COOH groups. These functional groups enrich the chars with attractive properties for further applications. For instance, in aqueous systems, the OFGs enhance the hydrophilicity of the chars and facilitate the interaction via hydrogen bonding and complexation with organic compounds and metals [63].

It has been reported that the concentration of the functional groups is dependent mainly on the biomass composition and processing conditions, such as temperature, the heating rate, the composition of the gas surrounding the biomass during the carbonisation, and the post-treatment (activation) [61]. Therefore, the surface chemistry of a given material influences its properties, such as catalytic activity, adhesive properties, wettability, contact potential, and failure mechanisms. It is important for the techniques employed for the analysis of surface chemistry to be extremely sensitive and at the same time efficient at filtering out the signals from a large number of atoms within the sample [118].

To confirm the influence of feedstock composition and thermochemical processing conditions on the surface functionality of the chars, two methods were employed. First, ATR-FTIR is commonly used for char analysis since it provides a spectrum that allows the identification of the surface functional groups. Among the advantages of FTIR are minimal sample preparation requirement, short time for analysis and sensibility to organic and inorganic
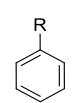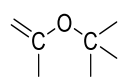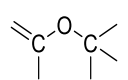
species [208]. Second, XPS provides a semi-quantification of the elemental composition of a material by assessing the oxidation state of the surface elements and the dispersion of each element. The principal advantage of using XPS for char characterisation is primarily directed to the analysis of OFGs by examining the C 1s and O 1s photoelectron lines [119]. XPS can also reflect chemical interactions at an atomic scale by elucidating the bonds between adjacent atoms and structural characteristics for amorphous surfaces with complex compositions [209]. Spectroscopic techniques, such as FTIR, have proven to be useful, however, they do not provide a quantification. XPS, on the other hand, is a powerful tool for the characterisation of the surface layers accompanied by a quantitative nature [121]. Even though XPS is not routinely employed, it has been gaining importance in this research area, while its complementation with FTIR could provide a more detailed analysis.

4.5.1 Attenuated total reflectance Fourier transform infrared (ATR-FTIR) spectroscopy

Analysis of the feedstock biomass and selected chars by ATR-FTIR was performed to determine the changes in the surface chemical composition resulting from the carbonisation treatments. **Table 4.4** summarises the FTIR adsorption regions for the identification of functional groups found on the different chars. The features of the char spectra are dependent primarily on the treatment temperature, heating rate, type of feedstock and the presence of inorganic constituents [208]. The presence of the functional groups is outlined in the spectra of the untreated feedstock and char materials produced from oak wood (**Figure 4.14**), water hyacinth (**Figure 4.15**) and saw wrack (**Figure 4.16**).

All untreated feedstocks exhibited strong vibrations for most of the groups outlined in **Table 4.4.** Functional groups associated with these peaks, therefore, change as the thermochemical treatment proceeds, in some cases with less intensity. Particularly lower for the broad peak between 3650 and 3200 cm^{-1} attributed to the stretching vibration of aliphatic OH found in alcohol, phenol, and carboxylic groups. Hence, the intensity of the polysaccharide region, hydroxyl, carbonate, and carboxylic groups reduced after the HTC and by increasing the pyrolysis temperature. The latter supports the dehydration and decarboxylation reactions taking place during the thermochemical treatments.

Table 4.4. Assignment of the Fourier transform infrared (FTIR) spectroscopy spectral band to the functional groups found on biochar and hydrochar surface. Spectra assignment based on [181,208,210,211].

Wavenumber (cm^{-1})	Description	Structure
3650-3200	Hydroxyl group	
2950-2920	Aliphatic v(CH) from -CH$_2$ groups	
2870-2840	Aliphatic v(CH) from -CH$_3$ groups	
1715-1695	Aromatic C=C aryl group	
1610-1550	Carboxylate anions	
1426-1410	Carbonate group	
1390-1310	Phenolic hydroxyl bend	
1275-1200	Ether group	
1160-1020	Polysaccharide region	
940-700	Out of plane hydroxyl bending	
840-790	Aromatic C-H bending	
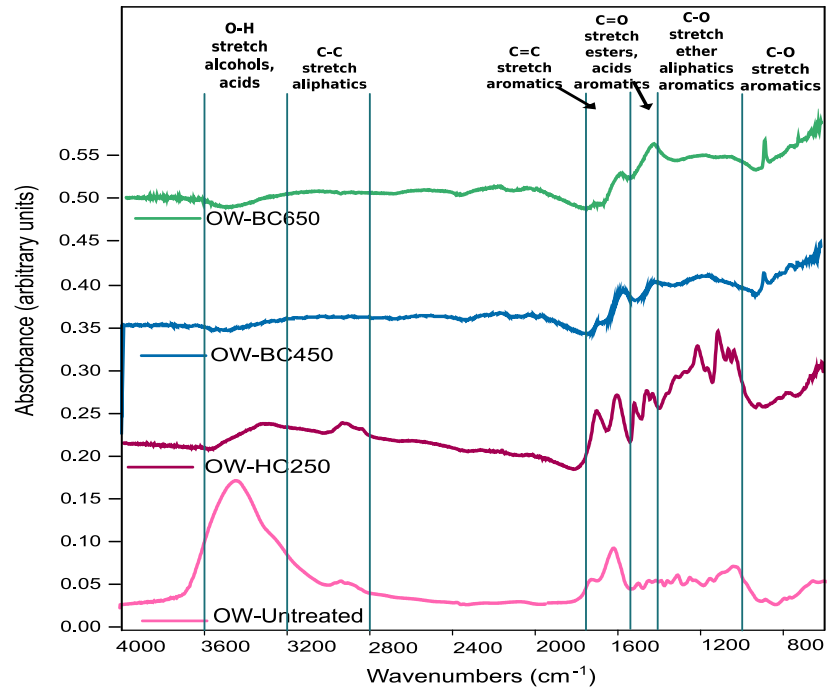
Figure 4.14. ATR-FTIR spectra of oak wood untreated feedstock and char materials.
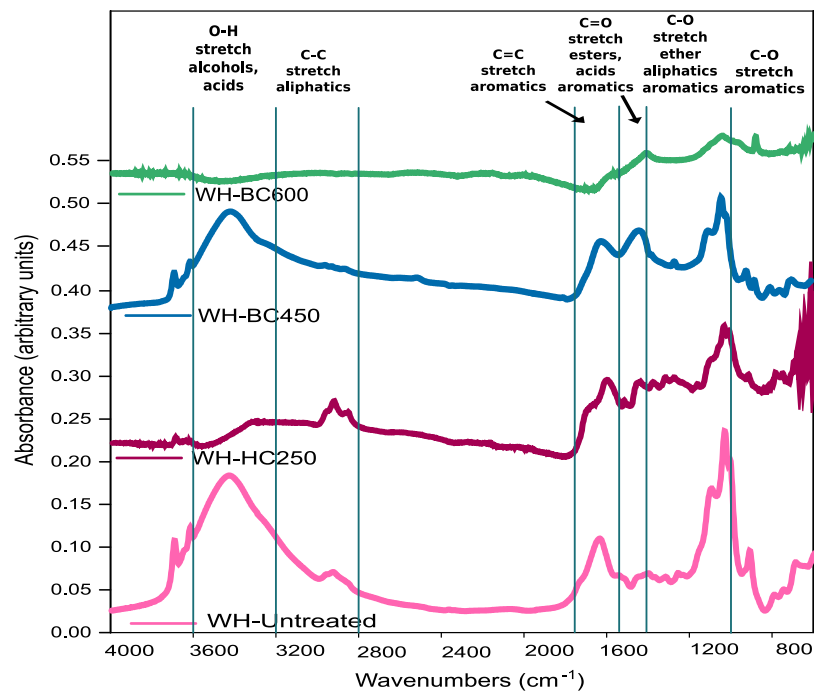
Figure 4.15. ATR-FTIR spectra of water hyacinth untreated feedstock and char materials.
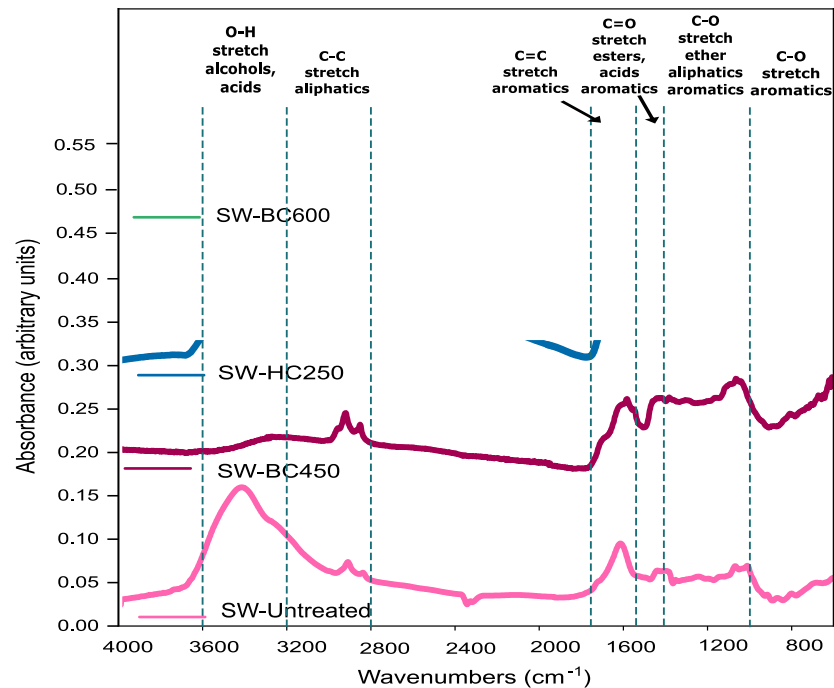
Figure 4.16. ATR-FTIR spectra of saw wrack untreated feedstock and char materials.

The stretching vibration of aromatic groups at 840-790 cm^{-1} increases with increasing temperature of thermochemical treatment suggesting an increase in aromatic character during carbonisation. The non-condensed and non-physically protected organic matter is not stable at temperatures such as 450 °C. Hence, biochars produced at higher temperatures are characterised by structural stability with high aromaticity. Thus, higher-temperature biochars are more refractory and during vibrational spectroscopy, they exhibit higher reflectance values and overall aromatic character [208]. Conversely, the stretching vibration of aromatic groups at 1715-1695 cm^{-1} was reduced for all chars. The aromatic C-H relative to the aromatic C=C could decrease after pyrolysis temperature above 500 °C due to the increased formation of condensed polyaromatic sheet structure [212]. Furthermore, mineral/inorganic impurities present in the char often result in intense absorption features. Inorganic constituents such as carbonate, silica, clay minerals, quartz and other ash components have a significant impact on the IR spectra of char [208]. Accordingly, WH and SW chars exhibited remarkably higher IR absorption than OW chars, possibly associated with their high concentration of inorganics.

In general, FTIR indicated that there were changes in structure with HTC and pyrolysis temperature and the selected feedstock. ATR-FTIR is a highly used sensitive tool for evaluating the variations in aliphatic and aromatic and

functional carbon materials. Nevertheless, the implementation of a second method, such as XPS, could complement the data obtained by FTIR and provide a more detailed and robust analysis of the changes that functional groups suffered during pyrolysis and HTC treatments [120].

4.5.2 X-ray photoelectron spectroscopy (XPS)

4.5.2.1 Survey spectra

Table 4.5 summarises the assignment of the peaks observed on the XPS survey and high-resolution C 1s, O 1s and N 1s spectra of the chars. The XPS analysis of the BCs was performed at ultra-high vacuum (UHV), whereas HCs analysis took place at near ambient pressure (NAP). These respective conditions were chosen based on the high carbonisation and stability of the BC that allowed the use of UHV, and the high degree of the volatile matter of the HC that required NAP. It is important, however, to reiterate the limitations of comparing BCs and HCs since they were analysed with different equipment and methodology.

Table 4.5. Assignment of X-ray photoelectron spectroscopy (XPS) peaks to chemical elements found on the surface of biochar and hydrochar. Peak assignment based on [118,120,213].

	Survey surface peaks										
	C 1s	O 1s	N 1s	Na 1s	Cl 2p	Ca 2p	Si 2p	K 2p	Mg 2p	S 2p	P 2p
Binding energy (Ev)	284	532	399	1072	202	350	100	297	52	165	136

XPS analysis allows the assessment of the elements found on the surface of the chars by the calculation of total peak intensity and the relative sensitivity of each element. **Figures 4.17** and **4.18** show the XPS survey spectra obtained from the BCs and HCs, respectively. As expected for carbonaceous materials, the outermost layer of all BCs and HCs are formed primarily by C, followed by O, and different extents of N and inorganic elements.
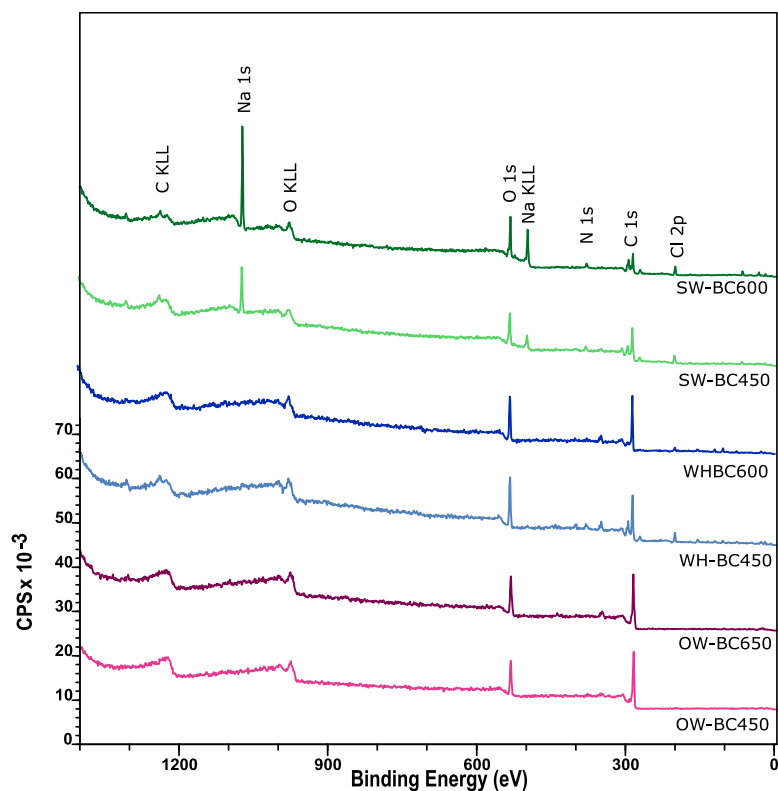
Figure 4.17. XPS survey for biochars analysed at UHV.

The KLL peaks correspond to non-quantifiable Auger electrons.
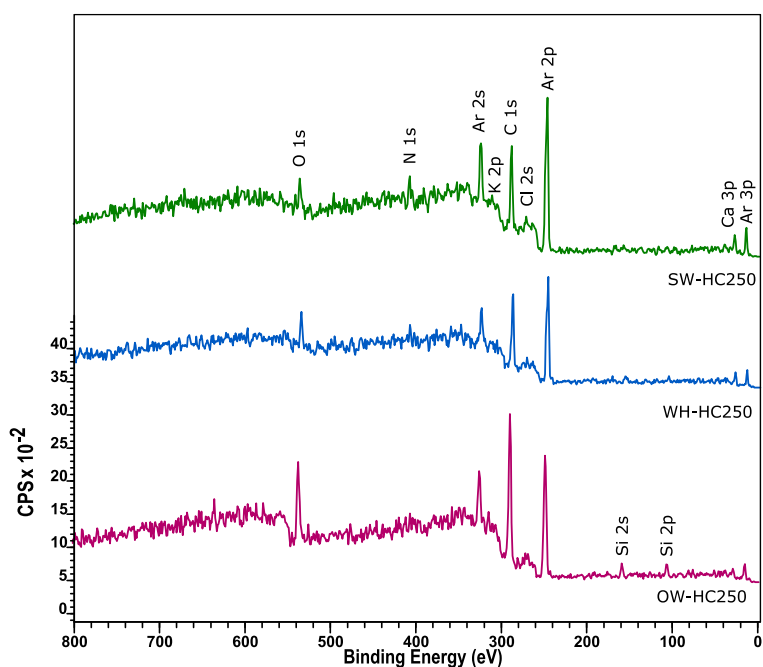
Figure 4.18. XPS survey for hydrochars analysed at NAP.

The peaks Ar 2s (320 eV), Ar 2p (247 eV), Ar 3p (12 eV) observed in the XPS spectra of HCs are due to the flow of argon used during the analysis.

Table 4.6 details the atomic ratios calculated from the XPS surveys. There was no consistent trend for the C and O content towards increasing the pyrolysis temperature, whereas N content appeared to reduce. On the other hand, the HCs exhibited a considerable N content, particularly large for SW-HC250, but lower O values than the BCs, although the HCs were analysed under different conditions (NAP). The chars also exhibited significant amounts of inorganics, including Na, Cl, Ca, Si and K, principally for WH and SW, due to their higher ash content. Nonetheless, it is important to point out the inability to obtain absolute values with XPS analysis since this technique cannot detect H atoms. This affects the ratio of the measured elements C, N, O, and inorganics and thus results in different values than those obtained from elemental analysis.

Table 4.6. Normalised atom ratio of surface elements expressed as (%) for biochars and hydrochars derived from XPS survey.

Char	C	O	N	Na	Cl	Ca	Si	K	Mg	S	Al	P
Oak wood												
OW-HC250	73.49	15.46	3.89	-	-	0.04	7.12	-	-	-	-	-
OW-BC450	81.05	15.97	1.21	-	0.13	0.87	0.37	-	0.21	0.2	-	-
OW-BC650	78.62	17.00	0.86	-	-	2.03	0.59	-	0.23	-	0.28	0.39
Water hyacinth												
WH-HC250	79.12	9.71	2.78	-	0.74	2.60	4.05	0.37	-	0.62	-	-
WH-BC450	57.98	21.20	3.31	0.15	6.03	1.89	1.67	2.93	0.46	-	4.38	-
WH-BC600	67.29	18.94	1.48	0.05	1.42	2.62	4.13	0.64	0.19	-	3.24	-
Saw wrack												
SW-HC250	71.27	10.14	14.37	-	-	-	-	-	-	1.26	-	2.95
SW-BC450	61.57	18.58	1.91	2.64	7.52	1.19	0.76	3.96	0.38	-	0.10	0.79
SW-BC600	43.20	28.48	0.20	7.77	10.77	0	0.92	6.91	0.29	-	0.93	-

- Not detected

To identify the differences in the content of C, O, and N between the surface and matrix of the chars, the results from XPS analysis were compared with those of CHNOS elemental analysis (**Figure 4.19**). For strengthening the comparison, the O:C and N:C ratios were expressed on a daf basis, while H content was excluded for the elemental values due to the inability of XPS to detect the H element. The O:C and N:C ratios calculated from the XPS showed variability in comparison to those obtained by elemental analysis. The absence of a linear correlation is commonly observed for heterogeneous materials, such as chars. This indicates a

difference between the surface composition and the bulk composition of the chars [214].
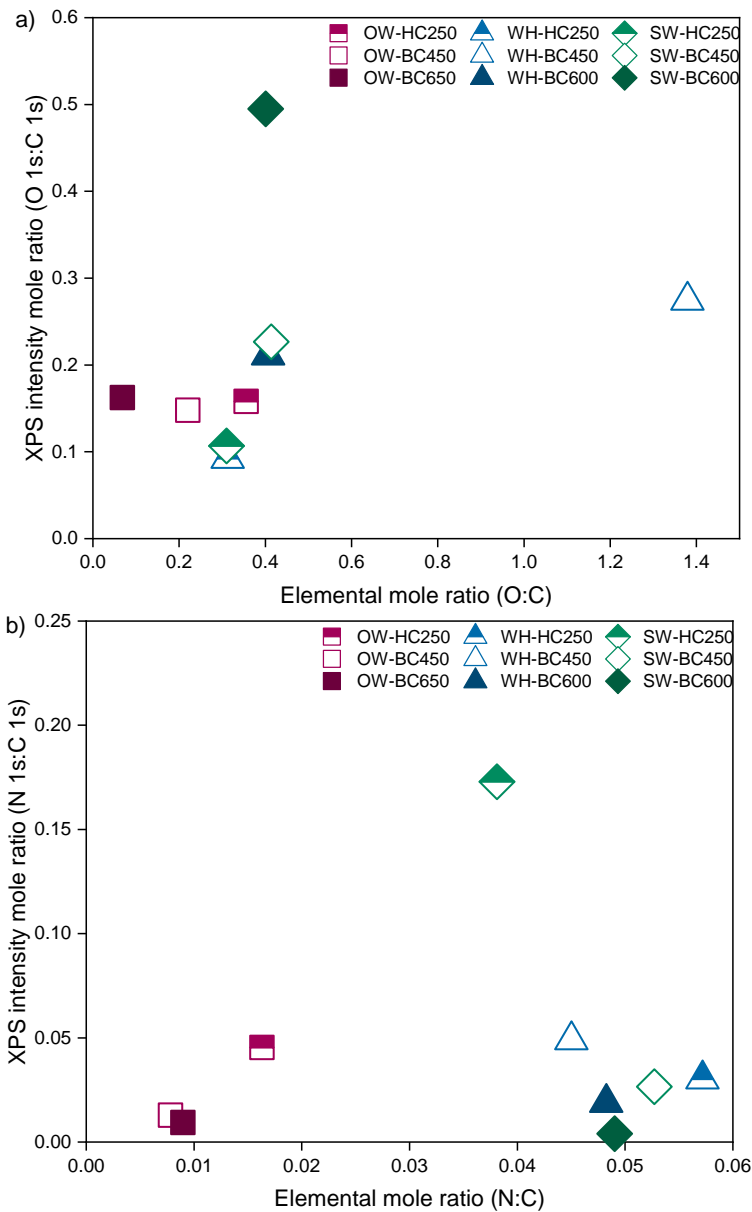
Figure 4.19. Correlation of the surface composition by XPS and the bulk composition by CHNOS analysis for char materials: a) O:C ratio; b) N:C ratio.

The ratios are expressed on a dry ash-free (daf) basis. Elemental values were recalculated without considering H for more accuracy when compared to XPS data according to [214].

The O:C ratio obtained from elemental data was generally higher than the obtained by XPS analysis suggesting a higher O content in the bulk than on the surface. However, it is expected to observe variability between the CHNOS and XPS methods. CHNOS gives the ultimate composition, whereas XPS is considered

a semi-quantitative method. XPS provides the atomic and/or moles ratios of the different chemical bonding states from the outermost layer of the sample [120]. The obtained C-content was generally higher with XPS than CHNOS, influencing thus the O:C and N:C ratios. Such discrepancy in carbon between surface and bulk indicates heterogeneity of the chars and could be attributed to the preferential rearrangement of the C-containing groups located on the surface [214]. It is important to outline that the XPS C:O ratio obtained from the main XPS survey corresponds to the oxygen bound to carbon. Hence for the XPS C:O ratio of biochars, the amount of oxygen bound to carbon is not 100 %, since a certain amount of oxygen would be associated with inorganic moieties (e.g., CaO or SiO$_2$). This is of particular relevance for the lower O:C ratios obtained with XPS for WH and SW chars, given their higher ash content as observed in XRF analysis [121]. Accordingly, WH and SW chars also exhibited a generally lower N:C ratio by XPS than CHNOS, whereas the N:C ratios of OW chars were relatively similar with both methods. This agrees with the higher C content obtained by XPS and the role of greater inorganic content in the case of WH and SW chars.

Figure 4.20 allows the comparison of the XPS semi-quantification of the inorganic elements located on the surface of the chars and the bulk values obtained by XRF. Both techniques reached relatively similar values with the predominance of Ca, Si, Na Al, Cl and K. The XPS inorganic content increased with pyrolysis temperature for OW and SW, although not for WH. Accordingly, SW-BCs showed the highest inorganic content, followed by WH-BCs and finally OW-BCs. On the other hand, HCs showed lower inorganic content than their corresponding BCs, except for OW-HC250 which exhibited a considerably higher content of Si. Regardless of the differences between XPS and XRF, the inorganic content showed consistency between the surface and the bulk of the chars. The latter suggests a relatively uniform distribution of inorganics throughout the char materials.
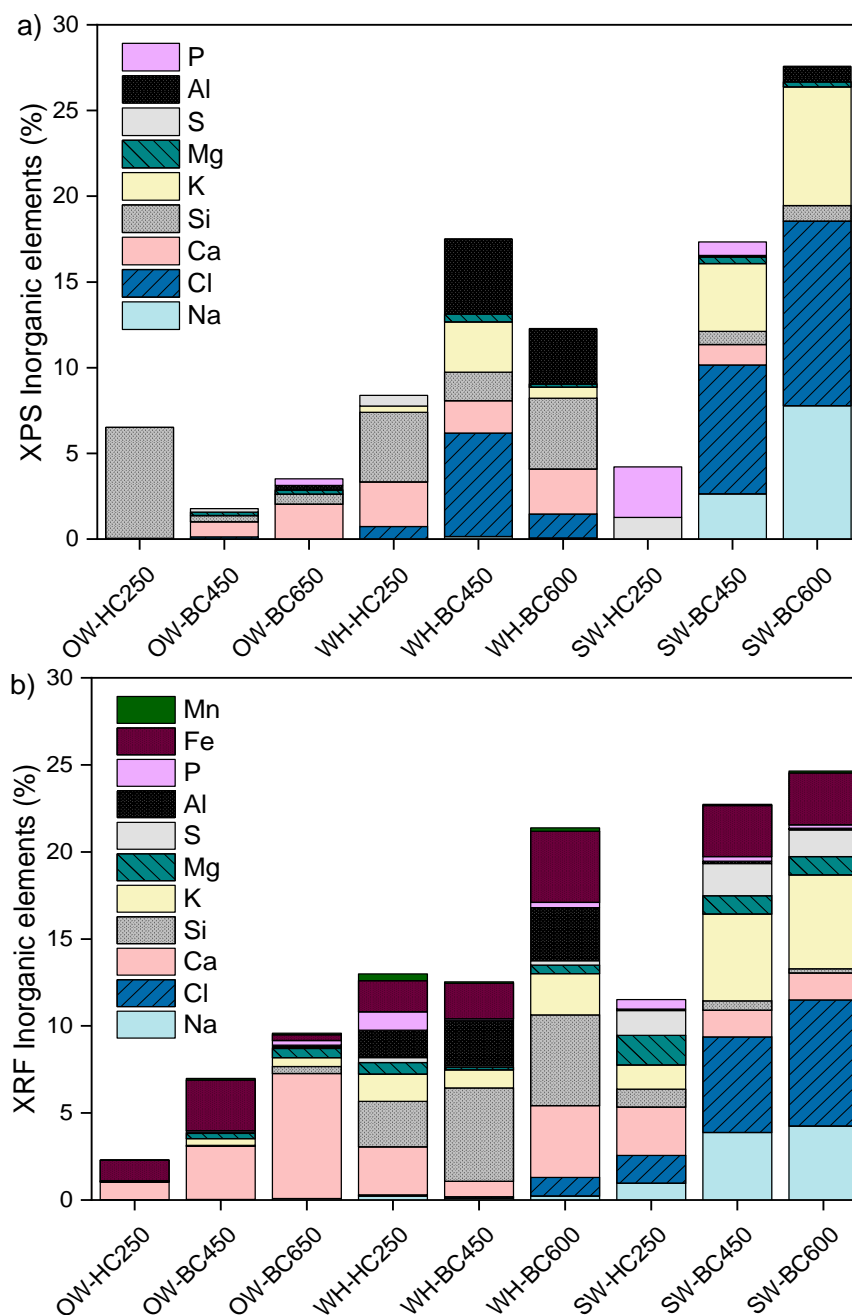
Figure 4.20. Correlation of surface and bulk inorganic content of the chars measured by: a) XPS and b) XRF.

4.5.2.2 Oxygenated functional groups

While the full survey spectrum provided a general breakdown of the surface chemistry of the chars. **Table 4.7** summarised the detailed analysis of the oxygen surface functionality obtained from the high-resolution C 1 s and O 1 s spectra.

Table 4.7. Assignment of high-resolution C 1s, O 1s and N 1s XPS peaks found on the surface of biochar and hydrochar based on [118,120,213].

High-resolution Surface group	Binding energy (E_B)	Assignment
C 1s		
C-C	284.4-285.2	Aromatic C=C, C-C, C-H
C-O	286.1-286.6	Hydroxyl, phenolic, ether
C=O	287.6-288.2	Carbonyl, quinone
COO	288.8-289.3	Carboxyl, ester
π-π^*	291.3	Transition due to conjugation
O 1s		
O=C	531.3-532.3	=O in carbonyl, carboxyl, aromatic structure
O-C	533.3-533.9	C-O-C, C-OH, C-O-P in phenol, ethers, and aromatic structure
N1s		
C-N-C	397.5-398.9	Pyridinic (N-6)
C-N-C	399.0-400.4	Pyrrolic (N-5)
C-N$^+$-C	401.5-401.8	Quaternary-N (N-Q)
C-N$^+$O-C, -NO$_2$	403.9-404.1	N-oxide (N-X)

Figure 4.21 shows the C 1s XPS spectra for the chars with the groups assigned according to E_B values for carbonaceous materials. The broadening of the XPS spectra and the number of peaks used to fit the complex spectra of each char sample varied. The differences in spectra broadening are a result of the optical components of the beamline determined by the excitation energy of each sample. The observed asymmetry of the C 1s peak shape is common for amorphous carbon materials, such as biochar and hydrochar, and it has to be neglected when fitting the C 1s spectra for avoiding a potential misinterpretation of the data [215].
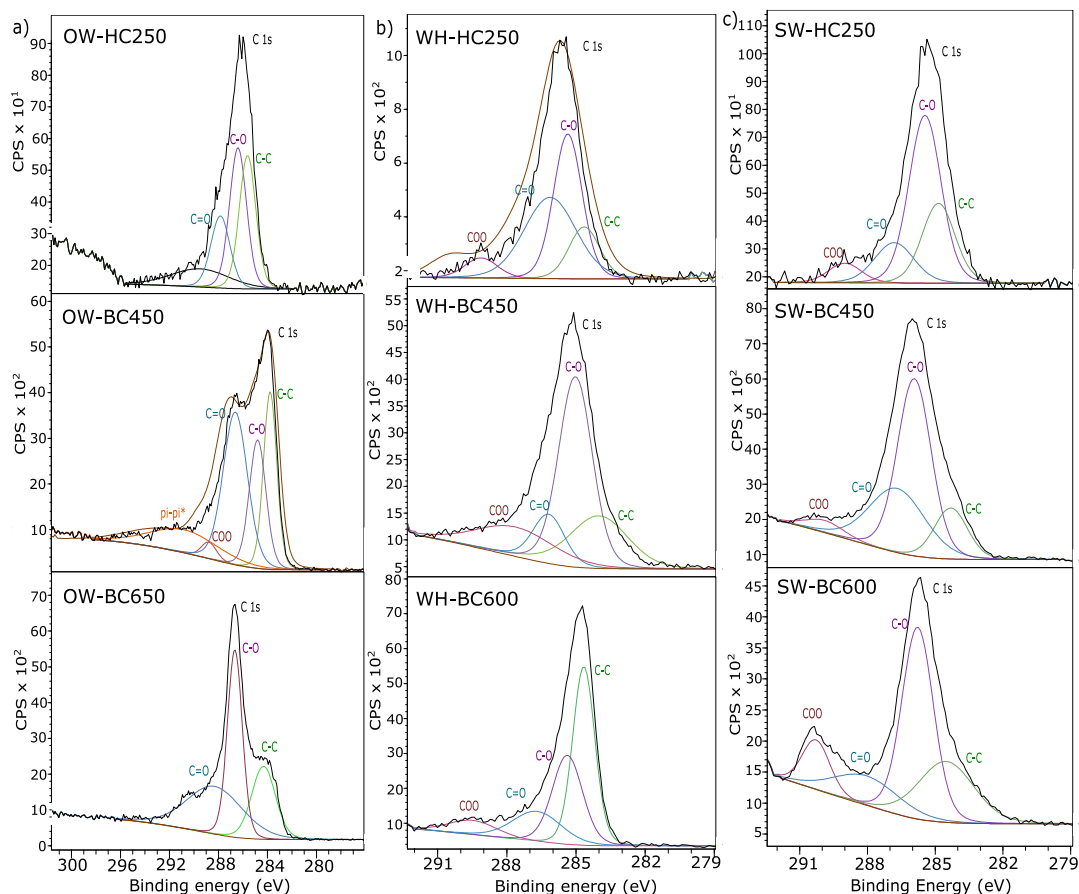
Figure 4.21. C 1s XPS spectra for char materials: a) oak wood; b) water hyacinth; c) saw wrack.

Table 4.8 shows the semi-quantification of the groups assigned to the peaks deconvoluted within the C 1s spectra. Higher-temperature WH and SW BCs generally showed an enhancement of the proportion and peak intensity of C-C groups and a reduction of OFGs. Whereas all OW chars maintained a similar C-C peak intensity. The contribution of C-C of aromatic and aliphatic species on the surface of the chars could be regarded as an indication of the transformation of carbon aromatic structures due to dehydration and aromatisation reactions [209].

Table 4.8. Relative XPS peak area expressed as (%) for the high-resolution C 1s, O 1s and N 1s spectra of biochars and hydrochars.

Char	C1s					O 1s		N 1s			
	C-C	C-O	C=O	COO	π-π*	O=C	O-C	N-6	N-5	N-Q	N-X
Oak wood											
OW-HC250	31.4	34.1	19.5	15.0	-	16.3	83.7	17.8	59.1	9.8	13.4
OW-BC450	30.0	28.9	18.1	18.3	4.7	10.8	89.2	21.0	61.3	9.6	8.1
OW-BC650	29.6	46.6	12.7	11.1	-	34.1	65.9	47.6	30.4	13.1	8.9
Water hyacinth											
WH-HC250	15.1	38.9	39.8	6.2	-	16.7	83.3	32.4	11.1	28.6	27.6
WH-BC450	22.5	49.9	11.1	16.4	-	3.5	96.5	33.9	43.7	10.0	10.0
WH-BC600	45.0	31.5	15.8	7.8	-	67.6	32.4	41.8	33.8	16.5	8.0
Saw wrack											
SW-HC250	25.6	52.6	15.5	6.3	-	23.1	76.9	34.2	28.2	12.6	25.0
SW-BC450	14.4	51.1	30.5	4.0	-	70.2	29.8	16.0	50.8	20.0	15.2
SW-BC600	26.4	47.6	15.3	10.8	-	79.2	20.8	27.4	28.5	21.4	22.7

- Not detected

The feedstock constituents influence the char composition, and hence their OFGs content. Most chars showed a predominance of C-O and C=O groups with smaller contributions of COO and particularly for OW-BC450 the presence of π-π* transition peak due to the conjugation from the aromatic structures or π electrons in aromatic rings [213]. The greater proportion of OFGs for WH and SW BC-450 °C and HCs agrees with their higher O content observed in the CHNOS analysis. Even though the temperature is key for the fate of oxygen groups and the rearrangement of irregular rings to more stable six rings, no obvious trend was observed for the C-O, C=O and COO groups [121]. Therefore, the analysis of O-containing groups is further accompanied by the O 1s spectra (**Figure 4.22**). The deconvoluted O 1s spectrum was used to specify the upper and lower constraints of the three oxygenated peaks identified at the C 1s. The predominant OFGs were O-C from phenolic and aromatic ether moieties and C=O from aromatic carbonyl groups. Accordingly, the O 1s showed a predominance of O-C groups for most low-temperature BCs and HCs, whereas the content of the O=C groups within the BCs was greater for those produced at higher temperatures. The raise in pyrolysis temperature is reported to promote the loss of hydroxyl and ether groups and the formation of double bonds between oxygen and small ring systems [121].
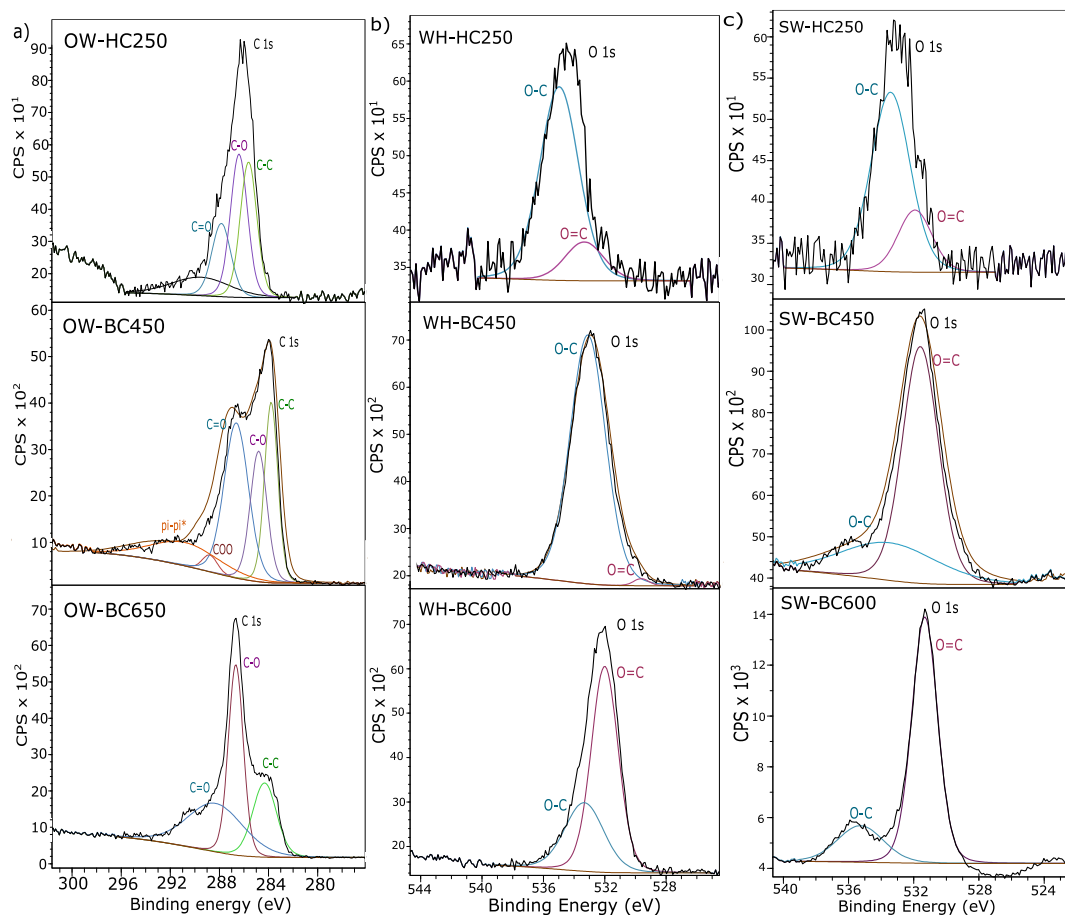
Figure 4.22. O 1s XPS spectra for char materials: a) oak wood; b) water hyacinth; c) saw wrack.

4.5.2.3   Nitrogen functional groups

In addition to the N-content estimated from the XPS survey, the high-resolution N 1s spectra could provide a better understanding of the nitrogen functional groups (NFGs) of the chars. As outlined in **Table 4.7**, the N 1s XPS spectra were deconvoluted into four peaks: pyridinic-N (N-6), pyrrolic-N (N-5), quaternary-N (N-Q), and oxide-N (N-X) (**Figure 4.23**). Pyridinic-N is a 6-membered ring bonded to two C-atoms and it is usually localised in the graphite edge. Pyrrolic-N is a 5-membered ring comprised of one atom of N bonded to two carbons and one hydrogen in a pentagon ring [216]. Quaternary-N is a 6-membered ring, also known as graphitic-N, comprised of N bonded to three nearest adjacent C-atoms [217]. N-oxide is a 6-membered ring, also known as pyridine-N-oxide, comprised of a pyridinic-N bonded to an oxygen atom. The N-oxide is often formed after the reaction of the chars with oxygen upon exposure to ambient air for prolonged periods [218].
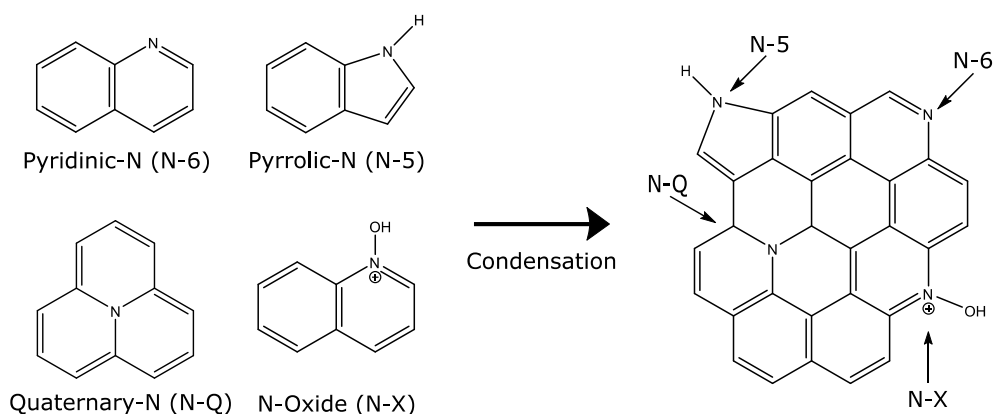
Figure 4.23. Correlation of the surface NFGs of chars and their evolution during thermochemical treatment.

Foremost, the total relative amount of N on the surface of BCs and HCs was estimated at 0.86-3.31 % and 2.78-14.37 %, respectively (**Table 4.6**). Given the smaller relative content of N 1s in comparison to C 1s and O 1s, some peaks within the N 1s XPS spectra were very small and reached similar intensities as the background (**Figure 4.24**). This trend was observed on the spectra for SW-BC600 and all the HCs. Nonetheless, N-5 and N-6 groups were found to be dominant N-components on the surface of the chars in agreement with previous reports [218,219]. The relative amount of N-components differed among the BCs with their pyrolysis temperature and origin feedstock (**Table 4.8**). As pyrolysis progress, the N atoms are integrated into the carbon matrix of the biochar by creating N-Q, N-5 and N-6 species [68]. Low-temperature BCs showed a predominance of N-5, followed by N-6 and different amounts of N-X and N-Q. The above agreed with reports stating that N-6 and N-Q are the only dominant NFGs on chars produced at severe pyrolysis conditions [219]. By increasing the pyrolysis temperature, the biomass is transformed into a more stable and ordered structure where N incorporates into the sp^2 planar graphite of BC increasing the proportion of N-Q and N-6 [216]. Therefore, the evolution of NFGs within the BC structure is a function of the severity of the pyrolysis conditions. Under mild pyrolysis, the non-stable pyridines, protonated N-5, and N-X are converted to N-6. During the condensation of the carbon matrix, N atoms incorporate into the graphene layers by substituting C atoms, whereas the N-5 is converted to N-6. However, under the pyrolysis temperature employed in this study (600-650 °C), the N-5 is not drastically affected since it can only disappear completely if heated above 900 °C. Thus, the higher N-6 when increasing pyrolysis temperature could be attributed to two transformations of 5-membered ring N-containing structures: (i) conversion of pyridine-N to N-6

accompanied by the loss of oxygen; (ii) N-5 suffers a ring expansion resulting in N-6 [218].
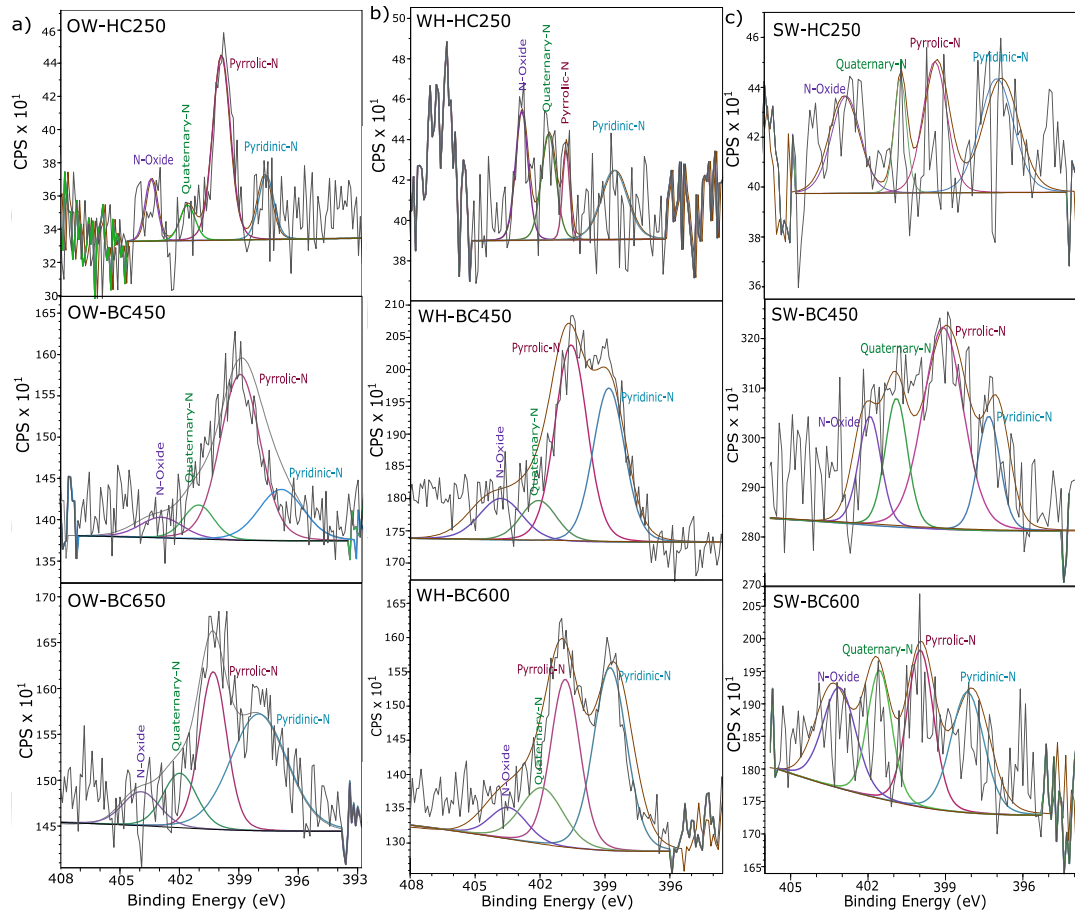
Figure 4.24. N 1s XPS spectra for char materials: a) oak wood; b) water hyacinth; c) saw wrack.

The NFGs on the surface of the BCs with their origin feedstock followed similar trends for most of the BCs. The summary of N-5 and N-6 of the biochars from OW and WH was found in a range of 76 to 82 % with smaller relative amounts of N-Q (9.6-16.6 %) and N-X (8.0-12.5 %). The SW-BCs, on the other hand, exhibited the lowest content of N-6 and in consequence a greater proportion of N-Q (20.0-21.4 %) and N-X (15.2-22.7%). Chars produced under mild pyrolysis do not exhibit considerable proportions of N-Q. Thus, the initially existing N-Q species could be pyridinic forms associated with oxygen functionalities [219]. Hence, the relatively larger proportion of N-Q observed for SW-BCs, particularly for the low-temperature SW-BC450, could be N-6 associated with oxygen. The higher N-X of SW-BCs could be due to their exposition to the ambient, resulting in the transformation of N-6 into N-X. It has been suggested that the origin of the

material has marginal or no importance on the final distribution of the NFGs in the resulting biochars [218]. However, for the BCs here analysed, there was a moderate difference with their origin feedstock, although the pyrolysis temperature remained the most important parameter influencing the evolution of their NFGs.

On the other hand, HCs were comprised principally of N-5 and N-6, which summarised 43.5-79 % of the total NFGs on their surface, whereas the N-X and N-Q ranged at 13.4-27.6 % and 9.8-28.6 %, respectively. The low N-containing OW-HC showed a predominance of N-5, with small values of N-X and N-6. Conversely, the high N-containing WH-HC was primarily comprised of N-6, similar amounts of N-Q and N-X, and a considerably smaller fraction of N-5. Whereas the composition of SW-HC followed the order N-6>N-5>N-X>N-Q. Regardless of the differences observed between the HCs here analysed, HTC temperature was stated as the determinant factor influencing the evolution of nitrogen groups.

During HTC at 200 °C, the condensation reactions involved in the formation of HC spheres result in an initial low conversion of nitrogen species into N-Q. Likewise N-6 and N-Q groups located on the edge of the HC interact with O resulting in oxidation and transformation into N-X groups. By increasing the temperature to 250 °C, the N-5 reduces while N-6 increases, although the mechanisms for this are not clear yet. For instance, it has been suggested that the decrease of N-5 is due to the cleavage of hydroxyl groups from pyridine resulting in N-6, and to the condensation of pyrrole into N-Q at a valley position. While the increase of N-6 has been attributed to the conversion of pyridine and the cleavage of hydrogen bonds in certain N-Q structures during the depolymerisation reactions [220]. Since only one HTC temperature was employed for the HCs here studied, it is difficult to assess the effect of temperature on the NFGs. However, the measured relative content of the N-components on the HCs generally agrees with the described behaviour.

4.6 Conclusions

Determination of the resulting properties of chars and how they vary due to the thermochemical treatment conditions and origin biomass is necessary for assessing their potential applications. In this chapter, the chemical, physical and functional properties of six biochars and three hydrochars were described. A correlation was observed between the composition of the feedstocks, principally their carbohydrate fraction and the severity of the thermochemical treatments

over the final properties of the chars. Proximate, ultimate, FTIR and XPS analysis indicates the increasing loss of volatile matter and O content, while an enhancement of aromatic C content with increasing temperature. The recalcitrant nature of the oak wood is maintained with a lower loss of VM, larger surface area and more developed microporosity. Whereas SW and WH exhibited a greater loss of VM leading to chars with high ash and O:C ratio and lower SA.

CO_2 adsorption at 273 K proved to be a superior method to N_2 at 77 K for the analysis of SA and porosity of the chars. The PV analysis could be complemented with both adsorbates, given that CO_2 provided a detailed description of the microporosity, whereas N_2 facilitated the meso- and microporosity analysis. The chars are heterogeneous materials comprised of micro, meso and microporosity resulting in variable SA and PV values. HCs exhibit a considerably lower SA than BCs due to their microsphere shape. For the BCs, the feedstock played a major role in the final physical structure since lignocellulosic OW-BCs showed the highest SA. In addition, increasing the pyrolysis temperature enhanced the SA of the BCs from all feedstocks.

The surface functionality of the chars proved to be one of the most important properties. XPS proved to be a powerful technique for the semi-quantification of the OFGs and inorganics on the surface of the chars. The XPS analysis indicated that the major functional groups containing C and O include-C-C-, C-O and C=O for all chars. In agreement with the bulk content of inorganics analysed by XRF, the surface of the aquatic chars showed a wide distribution of metals, including Ca, Na, Cl, Si and K. The FTIR spectra for BCs from the same feedstock were similar, whereas HCs showed a higher intensity indicating more surface functionality. HCs are generally considered to have higher functionality because of higher levels of humin formed during the HTC process. Hence, the characterisation of surface functionality by different techniques, such as XPS and FTIR, complemented each other by providing more detailed and consistent results.

In conclusion, the variability observed between the different chars can be attributed to a series of factors. Firstly, the thermochemical treatment employed (pyrolysis or HTC). Secondly, the process conditions, principally reaction temperature. Thirdly, the feedstock diversity and composition, mainly the type of carbohydrates, presence or lack of lignin and metal content comprising each feedstock. The following chapters will rely on the characterisation of the chars here discussed for assessing their potential applications in the biotransformation of substrates for the generation of gaseous biofuels.

Chapter V

Char augmentation on anaerobic digestion of model substrate

5.1 Overview

Chapter 5 aimed at assessing the potential of biochar and hydrochar as amendment additives and immobilisation supports for the anaerobic digestion of the model substrate cellulose in batch digesters. The feedstocks used for char production included the lignocellulosic (oak wood), seaweed (saw wrack) and aquatic plant (water hyacinth). Biochars were obtained by pyrolysis at low temperature (450 °C), including a chemically activated biochar with $MgCl_2$, and high temperature (600-650 °C). Hydrochars from the same feedstocks were produced by hydrothermal carbonisation at 250 °C. Biomethane production improved with the addition of lower-temperature biochars from oak wood and water hyacinth, having doubled the methane production rate. Higher-temperature biochars had no significant effect on anaerobic digestion, while saw wrack-derived BCs and all HCs, regardless of the feedstock, exhibited a detrimental effect. HC addition in AD could be considered a trigger for VFA production, particularly acetic and propionic acid. The versatility of AD relies on the possibility to design a process for producing VFAs, methane and hydrogen either separately or simultaneously. The influence of feedstock and thermochemical treatment over the chemical, physical and physicochemical properties of the chars was established in Chapter 4. The latter facilitated the correlation between such properties and the effect of these chars over AD. From the wide differences of properties exhibited by the chars, surface oxygen functionality appeared to be the most important feature improving digestion performance.

The addition of oak wood biochar chemically activated by magnesium impregnation was also detrimental to digestion. However, different outcomes can be achieved depending on the chosen activation method. The latter suggests that biochars produced by metal activation could be regarded as unsuitable

materials for AD, although other methods, such as physical activation are worth investigating. Additional AD experiments demonstrated the capacity of the chars to serve as immobilisation supports for the anaerobic sludge and subsequent digestions.

The work within this chapter has been published in Bioresource Technology Journal, please see: J Quintana-Najera, AJ Blacker, LA Fletcher and AB Ross "The effect of augmentation of biochar and hydrochar in anaerobic digestion of a model substrate" *Bioresource Technology* 321 (2021): 124494.

5.2 Introduction

The demand for biogas produced by AD continues to grow not only for the countries where this robust technology has been decades established but also for emergent economies. Recent policy changes towards reducing GHG emissions by decarbonising transport are supporting the injection of biomethane into natural gas grids. Nonetheless, the development of biomethane and biogas into a sustainable energy future fluctuates among countries since it depends on technological advances, feedstock availability, prevailing market conditions and policy priorities [13]. Hence, the importance of enhancing the performance and economic viability of the AD process.

AD turns organic matter from a wide variety of locally available residues into two valuable products biogas (biomethane and carbon dioxide) and organic fertilisers (bio-digested slurry) [46]. Biogas, a renewable and energy-rich fuel, can be used to generate heat, electricity, and steam. Additionally, biogas can be further upgraded to biomethane and directly employed as transportation fuel; or be purified to achieve the natural gas quality and be employed for different purposes [47]. The digestate, on the other hand, is unsuitable as a combustible solid fuel due to its high ash content and potential for slagging and fouling. Hence, the digestate is typically used as a fertiliser in agriculture, where it must meet certain criteria to ensure a minimum quality according to the British Standards Institution (BSI) Publicly Available Specification (PAS) [57].

In general, the AD process faces two major problems: operational instability and the quality of the digestate. Easily biodegradable biomass is rapidly hydrolysed, which results in the accumulation of intermediary metabolites, such as organic acids and ammonia. Large amounts of these compounds inhibit the microorganism, being the methanogens the most susceptible, resulting in an unbalanced digester [16]. Some of the reported approaches for preventing

digester failure and improving methane yields are the optimisation of operational conditions, co-digestion, two-phase process, the addition of trace elements, cell immobilisation and the amendment by the addition of adsorbent materials. The addition of carbon materials like biochar, activated carbon, graphite, graphene, carbon nanotubes, and carbon cloth is suggested to improve AD efficiency [48]. The advantages of using chars over other adsorbent carbon materials include their low cost, potential to use a wide range of feedstocks for their production, environmental sustainability, improvement of the digestate, and their advantageous physicochemical properties that can be further tailored to fulfil desired characteristics [31].

The integration of different conversion technologies is proposed to improve the development of biomethane in a more sustainable industry. Righi et al. [221] demonstrated through a Life Cycle Assessment (LCA) that coupling pyrolysis to the AD of corn stover enables a strong reduction of GHGs emissions, without affecting abiotic resource depletion. They also highlighted the economic input of combusting biochar and noted the potential of biochar for improving digestate quality. Other studies have also emphasized the potential of incorporating pyrolysis and HTC with AD for improving digestate quality in terms of nutrient retention and reducing nutrient leaching. For instance, Parmar et al. [185] studied the integration of HTC products in AD, suggesting a beneficial output for enhancing biogas yields and digestate quality. Similarly, Brown et al. [66] stated the importance of integrating HTC of macroalgae with AD for maximising energy efficiency, through HC combustion and digestion of the process waters. In addition to the potential of combusting BC and HC for energy output, other synergistic applications for these materials can be exploited. The addition of chars is reported to provide positive effects on AD, including mitigation of ammonium inhibition, promotion of methanogens proliferation, increasing methane yields, reducing lag time and improving digestate quality [48]. Recently, char materials obtained from the thermochemical treatment of biomass have a growing interest in maintaining operational stability in AD.

The potential of char materials in AD is due to their attractive characteristics, including porosity, surface area (SA), alkalinity and large availability of functional groups [21,25]. A well-developed porous structure is attractive for providing a large surface of interaction for the immobilisation and protection of cells and biofilm formation [99]. While oxygenated functional groups (OFGs) on the surface of chars are reported to serve as anchoring and interaction sites for biomolecules, whether they be whole cells, ions or inhibitory compounds [80]. Conductive materials (CM), mainly carbonaceous CM, have been applied to

improve AD performance by facilitating the syntrophic metabolism, increasing thus acceleration rates, and thermodynamic and kinetic efficiencies [91]. OFGs within the redox-active structures quinone-hydroquinone moieties and/or conjugated π-electron systems within the chars aromatic sub-structures facilitate the direct interspecies electron transfer (DIET) interactions [222]. The latter arises when CM, such as BCs, replace the role of conductive-pili and/or c-type cytochrome appendages found on the outer cells, responsible for DIET interactions [91]. The BCs catalyse the reductive reactions by facilitating the transfer of electrons from bulk chemical electron donors to a receiving organic compound between H_2-producing bacteria and H_2-consuming methanogens, enhancing thus reaction rates and kinetic efficiencies [27,93]. Furthermore, the addition of chars has been reported to provide a buffering effect for the intermediary organic acids of AD [48]. Given the importance of pH for achieving a syntrophic balance, pH adjustment is often necessary for counter-balancing the variations resulting from organic acid generation. The above represents a challenge and cost, especially at a large scale and in rural communities that generate electricity and gas with rudimentary digesters. Hence, it is attractive to assess char augmentation as an option for improving AD performance and maintaining a balanced pH by replacing pH adjustment.

The physicochemical properties of the chars intended for industrial applications might require improvement by an activation agent [60]. The activation can be performed by physical or chemical methods. The objective is to modify the essential properties that govern the catalytic activity of carbon material, such as SA, PV, and surface functionality. The process of activation is reported to increase the PV and SA of BC, which facilitates high mass transfer fluxes and catalyst loading [76]. Moreover, the activation increases the content of OFGs, helping to a better attachment, thus improving the enzyme activity and cell performance, reusability and temperature tolerance [24]. Unlike physical activation, the implementation of chemical agents donates the possibility of employing low temperatures, reducing then the energetic requirements. However, the utilisation of chemical agents creates pollution concerns, which the physical activation does not present. Furthermore, the mechanisms of action of the different activation agents differ. For instance, CO_2 activation involves C-CO_2 reactions that remove carbon atoms, while widening the pores. KOH activation enhances the SA and PV by disrupting the char structure [60]. Magnesium activation is reported to enhance the ion exchange capacity of biochar and surface functionality [223], and to improve the phosphate adsorption capacity of BC [224]. These properties are reported to improve AD performance during BC

augmentation. Thus, the importance of tailoring and optimising these features is related to the selection of the activation method, and its final application [76].

Given the nature of the thermochemical processes and the great differences between biomass sources, the properties of BC and HC differed largely as described in Chapter 4. Regardless of the recent growing interest in AD, their application still requires deep comprehension and extensive assessment. To date, a detailed investigation of the properties of BC and HC and their effect on AD has not been reported. Hence, an understanding of the physicochemical characteristics of the chars is of great importance for their successful development as adsorptive additives during AD. Therefore, the overall aim of this Chapter is to investigate the effect of biochar and hydrochar during the anaerobic digestion of model substrate cellulose. The impact of char augmentation on conventional single-stage mesophilic anaerobic digestion includes a correlation to the characterisation of the chars from Chapter 4. Magnesium-activated BC is evaluated as an adsorbent additive. Furthermore, the capacity to immobilise anaerobic sludge on the chars is also investigated.

5.3 Biochemical methane potential with biochar and hydrochar augmentation

This section aims to evaluate the biochemical methane potential (BMP) of cellulose during AD with the augmentation of biochar and hydrochar. The chars were produced from the feedstocks oak wood (OW), water hyacinth (WH), and saw wrack (SW) and were divided into intermediate-temperature BCs (450 °C), high-temperature BCs (600-650 °C), and HCs (250 °C). Chapter 4 comprised the detailed characterisation of these materials, while **Table 5.1** summarises the most important properties. For the AD experiments, standard process conditions described in Chapter 3 were employed unless stated otherwise. The digesters were fed with cellulose 5 g VS/L at an ISR 1, and char load 3 % (w/v), and incubated at 37 °C for 28 days. The BC experiments were run in triplicate, while the HC and cellulose control were run in duplicate. A blank was run in duplicate and subtracted from the displayed BMP values to confirm accuracy (**Equation 3-6**). It should be noted that the kinetic parameters maximum methane yield (BMP$_{max}$), methane production rate (μ_m), and lag phase (λ) are based on the modified Gompertz model where R^2 states the fitting of the model (**Equation 3-11**). The biodegradability (BD) index is obtained from the experimental BMP and the maximum theoretical BMP$_{Th}$ (**Equation 3-10**). The focus of these results will initially be on the AD performance and effect of chars on the methane yields,

kinetic parameters, VFAs and pH in comparison to the non-char control. Then, the discussion will move towards the correlation between the remarked differences and the properties of the chars.

Table 5.1. Summary of the most relevant properties of the chars used for anaerobic digestion amendment.

Char	Volatile matter (%) db	Ash (%) db	pH	C (%) db	N (%) db	O (%) db	SA (m²/g)
OW-HC250	57.9	3.8	3.9	62	1.2	29.4	44
OW-BC450	21.1	11.7	9.9	65.7	0.6	19.3	221
OW-BC650	11.8	14.3	9.3	76.5	0.8	7	237
WH-HC250	56.8	20.6	5.6	50.8	3.4	20.2	37.1
WH-BC450	30.9	33.9	9.1	26.1	1.7	36.9	38.7
WH-BC600	21.5	42.6	10.6	37.8	2	14.9	89.9
SW-HC250	64	14.3	6.2	54.9	2.4	22.7	40.6
SW-BC450	48.4	33.3	11.1	39.2	2.4	21.6	71.5
SW-BC600	36.1	34.6	12.1	40.4	2.3	21.6	63.5

5.3.1 Biochemical methane potential

Figure 5.1 illustrates the cumulative BMP curves for cellulose digestion for the effect of biochar and hydrochar augmentation in comparison to the cellulose control. There was a lag phase of 2-3 days for most BC systems before they began methane generation, except for SW-BCs whose initial production extended until the 17th day (**Figure 5.1a**). The BMP of most BC systems was found near the mid-exponential phase by the 7th day, although, OW-BC450 and WH-BC450 exhibited a faster production rate by reaching the steady-state earlier than the remaining systems. **Figure 5.1b** shows the curves with HC addition, no initial phase was observed as methane was generated since day 1. This may be due to the presence of VFAs adsorbed onto the surface of the HCs that could be initially used by the methanogens. After this, initial burst, a secondary lag phase occurs followed by a recovery and further production of methane.
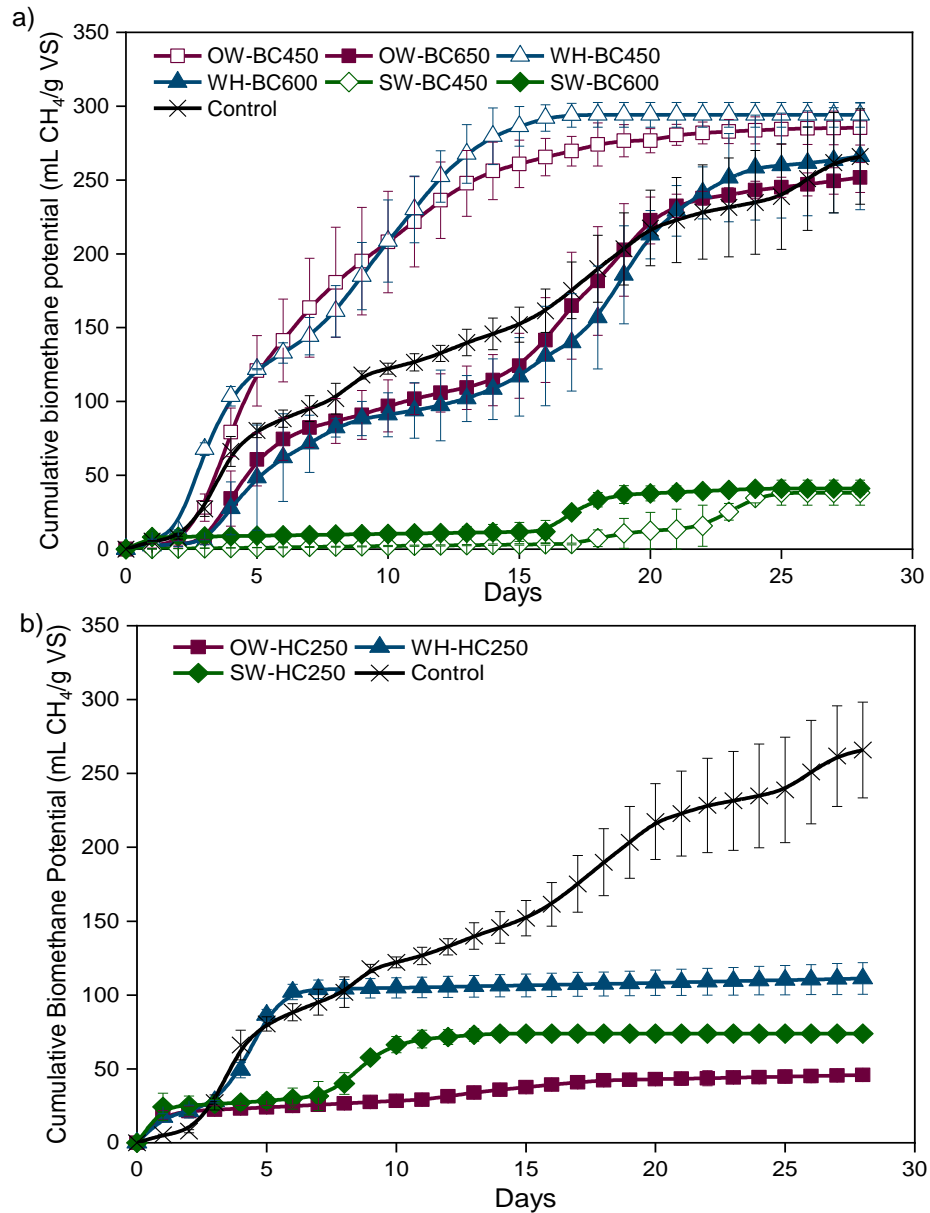
Figure 5.1. Cumulative biomethane production during anaerobic digestion of cellulose (control) and with the addition of a) biochar and b) hydrochar.

Replicates: biochar (n=3), hydrochar (n=2), cellulose control (n=3), blank (n=2).

The final BMP for the experiments augmented with WH-BC450 and OW-BC450 showed a significant difference over the cellulose control (p<0.05) (t-test), corresponding to 10.61 and 7.34 % improvement, respectively (**Table 5.2**). Conversely, the addition of OW-BC650 and WH-BC600 resulted in 5 % less production than the control, though non-significantly different (p> 0.05) (ANOVA) and considerably less than the highest producers. The addition of both SW-BCs drastically affected methane generation, with almost 85 % less final BMP than the control. The biodegradability of biomass into biogas during AD is

usually limited to 60 % [37]. Cellulose itself is relatively easily degradable, under similar AD conditions it is reported to provide a biodegradability of 58 % [225].

Table 5.2. Experimental yields and kinetic parameters obtained with the modified Gompertz model of the AD of cellulose with char addition.

Char	Experimental		Gompertz model			
	BMP_{exp} (mL CH_4/g VS)	BD_{CH4} (%)	BMP_{max} (mL CH_4/g VS)	μ_m (mL CH_4/g VS·day)	λ (days)	R^2
Oak wood						
OW-HC250	45.85	11.05	68.78	1.22	0.0	0.946
OW-BC450	285.46	68.82	285.69	28.08	1.46	0.993
OW-BC650	251.63	60.66	262.45	13.06	2.60	0.972
Water hyacinth						
WH-HC250	111.20	26.81	110.41	24.38	1.51	0.973
WH-BC450	294.15	70.91	298.39	27.31	1.18	0.988
WH-BC600	266.03	64.13	321.28	12.32	3.30	0.979
Saw wrack						
SW-HC250	73.85	17.80	75.79	6.31	0.0	0.930
SW-BC450	38.25	9.22	41.64	4.88	17.33	0.973
SW-BC600	41.05	9.90	56.24	1.90	3.63	0.884
Cellulose control	265.93	64.11	284.85	11.81	0.20	0.985

Maximum BMP_{Th} of cellulose 414 mL CH_4/g VS; maximum methane yield (BMP_{max}), methane production rate (μ_m), lag phase (λ), and coefficient of determination (R^2) to validate the model.

Table 5.2 also shows the biodegradability index for all BC systems within a range of 9 to 71 %. Accordingly, the highest methane producers exhibited the highest BD values. The digestion of cellulose with HC addition resulted in a 57-83 % lower yield than the control and a considerably lower BD index (11- 27 %) than the rest. WH-HC250 was the least inhibitory, followed by SW-HC and finally OW-HC. The greater level of inhibition increased for high lignin-containing HCs such as OW. In summary, seaweed-derived BCs and HCs, regardless of the feedstock, may not be suitable for enhancing AD yields. Whereas systems augmented with low-temperature OW and WH-BCs, showed a positive impact having improved methanogenesis compared to the control.

5.3.2 Kinetic analysis

Table 5.2 outlines the kinetic parameters obtained for the cellulose digestion experiments calculated as described in section 3.3.8. The systems supplemented with BC, particularly the low-temperature BCs, exhibited higher R^2 values, indicating a better fitting than the HCs. The production of methane started early in the digestion, hence most systems exhibited low λ values. The highest BMP_{max} of 321 mL CH_4/g VS was achieved by WH-BC600, whereas WH-BC450 and the OW-BCs obtained similar values to the control. The highest μ_m was observed for OW-BC450 (28 mL CH_4/g VS·day) and WH-BC450 (27 mL CH_4/g VS·day), which represented 2.4 and 2.3 times the obtained with the control, respectively. Conversely, SW-BCs and HCs reached considerably lower BMP_{max} and μ_m. In summary, the kinetic parameter most positively affected by char addition was μ_m as shown for OW-BC450 and WH-BC450, which resulted in the most significant enhancement.

5.3.3 VFAs and pH

Figure 5.2 shows the alcohols and VFAs accumulated at the end of the AD experiments augmented with the different chars. Those systems that produced higher amounts of methane (OW-BCs, WH-BCs, and control) also resulted in a lower accumulation of VFAs and alcohols. Both OW-BCs and WH-BCs reduced the accumulated VFAs to less than half the control. Complete degradation of VFAs by the mentioned systems indicates efficient digestion profiles. Conversely, the addition of all HCs led to a considerably higher accumulation of VFAs. Given that the same processing conditions were employed for all systems, the large differences in the VFAs could be due to the added char. BC addition is reported to accelerate the formation of acetic and butyric acid and further VFAs degradation [36]. Regardless of the positive effect of adding BC to accelerate the VFAs production and consumption, it is argued that it has no significant effect on the average final VFAs accumulation [37]. Other reports state a considerable effect of BC in promoting the growth of microorganisms involved in VFA degradation and methane production. Thus, the lower accumulation of VFAs could be due to the tandem reaction of syntrophic acetate oxidation and hydrogenotrophic methanogens [88,226]. Moreover, Shanmugam et al. [28] suggested the adsorption of VFAs by activated carbon and BCs, especially for materials with high surface area. In the case of hydrochar, Mumme et al. [17] reported a similar behaviour where HC contributed to the cellular stress. They attributed this detrimental effect to the biodegradable fraction of hydrochar that

is converted into inhibitory VFA, suggesting that HCs contribute to the VFA formation.
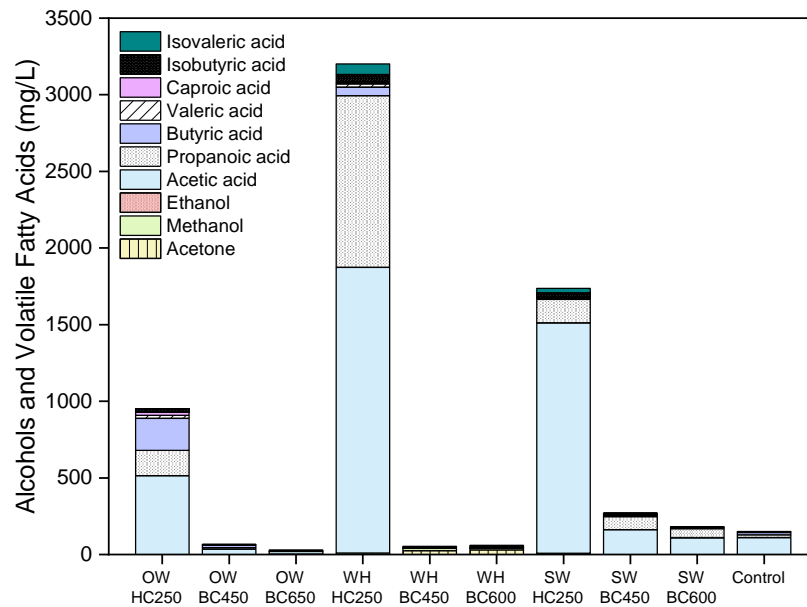
Figure 5.2. Volatile fatty acids accumulated at the end of the anaerobic digestion with the addition of biochar and hydrochar.

The pH of the digesters was measured once the chars were added and before the AD started and at the end of the AD (**Figure 5.3**). No pH adjustment was performed for evaluating the effect of the chars on the pH of the digesters. BCs are known to be more alkaline due to the enhancement of inorganics in the chars after pyrolysis, whereas HCs are well known to be acidic as shown in **Table 5.1**. Accordingly, all systems supplemented with BC showed an initial alkaline pH similar to or higher than the control. The digesters augmented with HCs started closer to neutrality, with WH-HC at proximity to the control. Whereas those supplemented with OW and SW-HCs started slightly below. Nevertheless, most systems started at a suitable pH since the optimal value for single-stage AD is pH 6.8-7.4. Similarly to this work, many reports that evaluated char addition in AD, performed no adjustment on the pH [17,34,231,232,35,39,148,202,227–230]. While others adjusted the initial pH within a range of 6.8-8.0 [28,36,101,171,172,201,233]. This range was generally reached in this work without requiring pH adjustment, except for the SW-BCs systems. The addition of the SW-BCs enhanced the alkalinity of the digesters (pH ~9). This could be due to their increased N-content and increased levels of alkali and alkaline earth metals. The analysis of metals by XRF described in Chapter 4 showed a large

contribution of Cl, Na, K, Fe, Ca, S, and Mg for the SW-BCs. Initial alkaline conditions facilitate the hydrolysis of carbohydrates. However, pH as alkaline as the observed for SW-BCs could detriment further VFA consumption and methanogenic activity. Acetic acids are the main precursor for methane production and were the most accumulated VFA for the HC systems, although WH-HC exhibited a considerable amount of propionic acid. The conversion of propionic acid into methane is not thermodynamically favourable, hence its toxicity [51]. The increasing accumulation of these acids and reduction of pH stress the system resulting in a poor conversion towards methane [49].
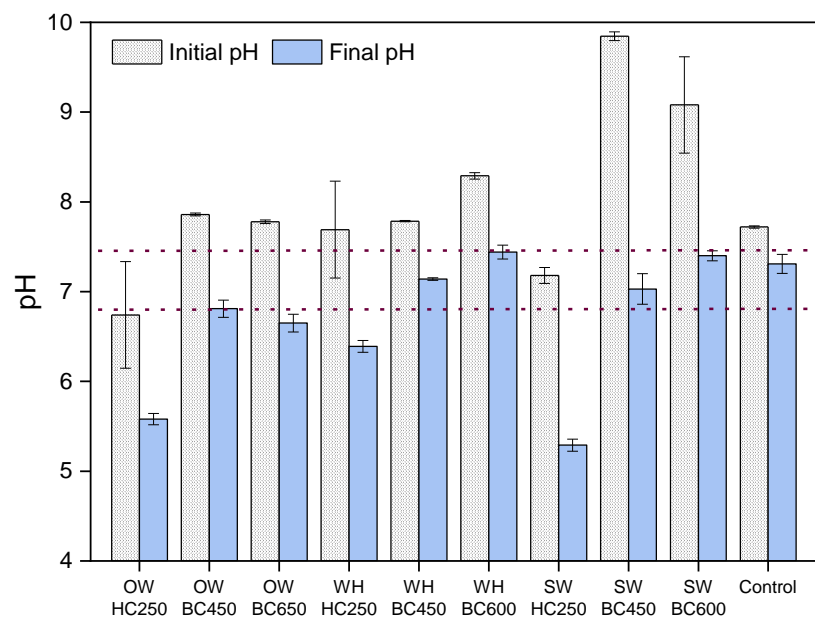
Figure 5.3. Measurement of pH at the beginning and end of the anaerobic digestion of cellulose (control) and with the addition of biochar and hydrochar.

The range within dotted lines corresponds to the optimal zone (pH 6.8-7.4) for AD.

At the end of the AD process, the pH of all reactors had been reduced to different extents. The SW-BCs and HC systems suffered the greatest pH variations, because of VFAs accumulation. The HC systems reached pH levels unfavourable for methanogens (pH 5.3-6.4), while all BCs systems and the control reached final pH values close to the optimal range (pH 6.8-7.4) for single-stage AD. In agreement with the low VFAs accumulation, the systems OW-BCs, WH-BCs, and the control showed minor changes in pH. Given the observed pH variations, it was not possible to attribute a buffering effect from either BC or HC.

5.3.4 Effect of biochar augmentation

The effect of different BCs on the anaerobic digestion of cellulose was evaluated in terms of methane yield and methane production rates. These findings indicated that, while BCs had a range of characteristics that may improve AD, not all the BCs are the same and some BCs may be better suited for AD. Ross et al. [234] reported toxic and/or inhibitory by-products generated during the pyrolysis of seaweed, such as phenols, N-nitrosodimethylamine, and 5-methyl-furfural. The presence of these compounds on the seaweed SW-BCs could have affected microbial metabolism which resulted in poor AD performance. Even though there are several reports of BC addition in AD, there are none regarding BC produced from seaweed or other algae sources which highlights the importance of stating the unsuitability here observed.

In this work, it has been demonstrated that lower temperature BCs enhanced the methane production rate and yield during AD. Even though there was no significant difference in BMP between the systems augmented with OW-BC450 and WH-BC450 ($p<0.05$) (ANOVA), their addition was the most successful having improved methanogenesis and double production rate compared to the control. Conversely, higher temperature OW-BC650 and WH-BC600 offered no significant difference in comparison to the control ($p>0.05$) (t-test). The latter states the importance of pyrolysis temperature and biomass of origin in designing biochars that aim to be used in AD.

Shanmugam et al. [28] studied BCs derived from woody and herbaceous biomass produced within a range of 400-900 °C. The addition of all BCs on the AD of glucose and bio-oil aqueous phase (BOAP), improved the biogas production and COD reduction. For the AD of glucose, they added BC switchgrass and woody BCs. The highest yield 330-332 mL CH_4/g CO (1.7-1.8 times the control) was achieved with the lower temperature BCs of both feedstocks. For the AD of the more complex BOAP substrate, they tested canola meal BC and woody BC. The control exhibited very low BMP (24 mL CH_4/g COD), which once again was improved by the lower-temperature BCs. The woody BC had the highest improvement (12 times the control). The best performance woody BCs showed higher electric donating capacity (EDC) than the other adsorbents (350 and 338 µS/cm). They also possessed a neutral pH (7.0 and 7.3), similar VM (41 and 40 %), FC (4.7 and 6.8 %), ash (4.7 and 6.8 %), and small SA (8.0 and 5.7 m^2/g). However, they stated limitations during the measurement of SA by traditional N_2 adsorption and BET, thus the reported SA is questionable. In addition, the BCs exhibited surface functionality composed of phenazine and quinone moieties. They attributed this

improvement to the presence of redox-active moieties and inorganic moieties in the BCs. It is worth pointing out that they did not consider the high content of oil and crude protein in the canola meal that could have resulted in BCs not being favourable to AD. Notwithstanding, they supported the role of the BCs as a catalyst mediating the electron transfer during the fermentation of glucose and more complex substrates. Like this work, they observed a similar trend regarding pyrolysis temperature and BCs with suitable properties for AD.

Qin et al. [35] studied the addition of BCs produced at 500 °C from different feedstocks into the AD of glucose. The results differed for each BC, the parameters methane yield and production rate improved with woody-BC addition in comparison to their control. Conversely, corn stalk-BC drastically reduced both parameters, also leading to a decrease in the methanogen *Methanosarcina* population. They attributed the enhancement to the properties of the woody-BC, including their high SA and EDC. Accordingly, Shen et al. [148,173] used woody and corn stalk BC produced at 710 °C, observing no significant effect on BMP yields but an improvement in methane production rate. They attributed the positive effect of BC on production rate to buffering capacity, DIET, SA, CO_2 adsorption and lessening NH_3 inhibition.

Given the differences observed in this work and the literature, it is important to outline the necessity of developing an understanding of how the BC properties affect their fitness for AD augmentation. In addition, it could be beneficial to establish a methodology with standardised conditions (e.g. inoculum, ISR, substrate) for reducing the process variables. This knowledge could result useful since these given properties can be tailored by controlling the pyrolysis conditions and feedstock selection [31]. In this section, a discussion about the properties of OW-BC450 and WH-BC450 that could have influenced their positive effect on AD is outlined. Nonetheless, Chapter 7 will cover a detailed compilation of the reports found in the literature regarding biochar addition in AD in correlation to their properties and effect on AD.

Given the large differences between the lower temperature BCs from OW and WH, it is important to understand which inherent physicochemical properties could have influenced their positive impact on AD. These chars were characterised in detail in Chapter 3. Both BCs showed comparable alkaline pH and volatile matter (VM) content. OW-BC450 showed low ash content, high SA (S_{CO2} = 221 m^2/g) and pore volume (PV = 0.08 cm^3/g). Conversely, WH-BC450 exhibited a considerably higher ash content, low SA (S_{CO2} = 39 m^2/g) and PV (0.02 cm^3/g). The high SA and porosity of OW-BC450 could have provided the support

and environment for the interaction and/or adsorption of microorganisms. This benefit could have been reduced for WH-BC450. However, reports of BCs with low and high SA exhibiting the same positive effect on AD have neglected the role of SA. Nanopores contribute largely to the porosity of BCs, although the reduced size of these pores limits their access to microorganisms. Even for BCs with high SA, the predominance of microporosity could reduce the area of interaction between BC and the microorganisms [92].

The inorganics within the BCs could provide a source of alkalinity, conductivity, and trace nutrients, especially for WH-BC450 given its considerably higher ash content. The soluble inorganics (Cl, Ca and K) are reported to enhance BC conductivity and subsequently improve DIET interactions [235]. The concentration of these elements was 934, 10393 and 8633 ppm for WH-BC450 and 0, 30470 and 3896 ppm for OW-BC450, respectively. Notwithstanding, the redox properties of the BCs originated principally from their organic electron-accepting and donating moieties, and to a lesser extent from their inorganic constituents [93].

The XPS analysis of both OW-BC450 and WH-BC450 showed a large contribution of OFGs. The C1s spectra showed C-O, C=O and COO groups for both BCs and a contribution of π-π^* transition peak for OW-BC450 due to the conjugation from the aromatic structures or π electrons in aromatic rings [213]. The O 1s spectra for both BCs exhibited a large content of O-C, followed by O=C. These groups could indicate hydroquinone and quinone moieties, respectively. Klüpfel et al. [93] reported that BCs produced at 400-500 °C showed an extensive redox buffering capacity dominated by quinone/hydroquinone functionalities. Whilst increasing pyrolysis temperature reduced these groups. The above agrees with the behaviour observed for OW-BC650 and WH-BC600. These systems reached BMP yields close to the control, suggesting that no further functionality benefits were provided.

The greater N-content of WH-BC450 is accompanied by a variety of surface nitrogen functional groups (NFGs). The NFGs are reported to provide sites for the adsorption of organic and inorganic compounds. NFGs can also contribute to the electrocatalytic potential for redox reactions. The above is the combined effect of pyridinic-N (N-6) and quaternary-N (N-Q) with an adjacent C-atom to redistribute the charge and subsequently promote the redox reaction [182]. In summary, OW and WH low-temperature BCs could have favoured the intimate proximity between the substrate-oxidisers and the methanogens. The

functionality and redox capacity of these BCs could have triggered syntrophic DIET interactions and enhanced the methanogenic performance.

5.3.5 Effect of hydrochar augmentation

The addition of HCs exhibited a negative impact on methane yields and kinetic parameters. The greater level of inhibition increased for the high lignin-containing OW-HC. This is probably a combination of OW-HC acidic nature (pH 3.9), increased hydrophobicity and aromaticity, and the presence of increased levels of phenolic functionality as observed in the FTIR analysis. Generally, the supplementation with HC from these three different HCs is regarded to inhibit methanogenesis. Compared to BC, there are fewer reports of the addition of HC during AD. Those that have been carried out, however, report the favourable effect of HC on AD, which is contrary to this study. For instance, Codignole-Luz et al. [90] emphasised the influence of HTC temperature on the use of spent coffee HC produced at 180, 220 and 250 °C as a substrate for AD. The HC produced at 180 °C was successfully degraded, whereas HC produced at a higher temperature reduced the BMP yields and extended the lag phase. They attributed this behaviour to the increase of hydrophobicity with raising HTC temperatures. A greater hydrophobicity reduces the contact of the HC surface with the inoculum. Moreover, HC produced at low temperature is more labile and easily degraded for its further uptake as a substrate. Similarly, reports of the addition of HC and HC-slurries to AD increased the methane yields [66,89,90]. Nonetheless, most studies aimed to use HTC as a pre-treatment and HC as a substrate, whereas this study aims to evaluate their potential as supports and not substrate. The HCs used for this work were produced at 250 °C, generally higher than the reports mentioned above. Thus, the addition of low-temperature HC could favour AD, by acting as a substrate rather than a support.

It is suggested that as the temperature of HTC increases, the HC became more inhibitory towards methane generation. This effect could be attributed principally to the humic acids (HA) largely present in the HCs. The HA can act as electron acceptors improving the acetic acid production, while further competing for them with the methanogens, reducing thus VFAs consumption and methane generation [89]. Similar behaviour was observed in these experiments since HC augmentation resulted in a considerable accumulation of VFAs. In a separate set of experiments, the humic acids (HA) were separated from the hydrochar by alkaline extraction. The amount of HA within the OW-HC250 corresponded to 26.6 % of the HC solid. Given the OW-HC250 load of 3 %, the total amount of HA added to the digesters corresponded to 7.98 g/L, which could

have affected methanogens. Khadem et al. [236] reported that up to 1 g/L of HA could inhibit up to 75 % of the methane production rate of all hydrogenotrophic methanogens. Even though the content of HA was not measured for the other HCs, similar inhibitory contributions could be inferred. In addition to the humic substances, HTC often results in undesirable N-containing by-products of Maillard reactions, such as melanoidins and N-heterocycles, which have a considerably inhibitory effect over fermentative bacteria [237]. Moreover, the acidic nature and the high levels of phenolic functionality observed in the FTIR analysis could also have affected the BMP production.

Even though the addition of high-temperature HC in AD does not favour the production of methane, it could be considered a trigger for VFA production, particularly acetic and propionic acid. The versatility of AD relies on the possibility to design a process for producing VFAs, methane and hydrogen either separately or simultaneously. The usefulness of the latter could support the demand for VFAs to be employed as precursors for a series of valuable compounds, such as biopolymers, biofuels, alcohols, aldehydes or ketones [51]. There is a growing interest in the development of sustainable routes of production of acetic acid from renewable sources since the current main route for its production is based on the carbonylation of methanol during the steam reforming of fossil fuels [238]. Hence, the addition of HC could be recognised as a promising option for VFAs production rather than methane.

5.4 Use of activated biochar for anaerobic digestion

The physicochemical properties of the chars that govern their potential as adsorbent material can be further improved by an activation treatment [60]. The activation process could be performed by chemical or physical methods. For the former, the raw material is impregnated with a reagent (e.g., $MgCl_2$, $ZnCl_2$, H_3PO_4, KOH or NaOH), and subsequently pyrolysed under an inert atmosphere. For the latter, the raw material is initially carbonised, followed by the activation with either steam or carbon dioxide [105]. Modifications on essential properties, such as surface area (SA), pore volume (PV), pore size, and surface functionality could offer several advantages. For instance, a greater porosity and SA could facilitate mass transfer fluxes and catalyst loading [76], whereas a greater number of surface functional groups could enhance interaction sites for a better attachment of cells [24]. A previous study performed within the research group by Takaya et al. [224] investigated the improvement of the phosphate adsorption capacity of biochar due to activation. Phosphate recovery is environmentally essential in

agricultural and industrial wastewater, due to its causing eutrophication in water bodies. Phosphate uptake with BCs is a sustainable approach that requires an adsorbent material with a wide surface functionality. They compared chemical activation ($MgCl_2$ and $FeCl_3$) and physical activation (KOH and H_2O_2) of oak wood biochar. BC activated with $MgCl_2$ exhibited the greatest phosphate uptake. BCs activated with $FeCl_3$, and KOH showed a modest phosphate adsorption capacity, whereas BC-H_2O_2 reduced the adsorption capacity and was considered detrimental. Given the better performance observed for BC-$MgCl_2$, this activated BC was selected for AD experiments. Hence, this section evaluates the potential of activated BC as an adsorbent material in AD. As stated in the previous section, low-temperature OW-BC450 positively influenced AD performance. Therefore, the overall aim of the present study was to investigate the effect of activated low-temperature OW-BC during the anaerobic digestion of cellulose. The activated OW-BC450-MgCl was obtained by impregnation in $MgCl_2$ as described in Chapter 3. The digestion conditions consisted of inoculum 10 g VS/L, cellulose 5 g VS/L, ISR 2, and biochar load of 1 and 3 % (w/v).

5.4.1 Biochemical methane potential

Figure 5.4 shows the cumulative BMP generated during the AD of cellulose augmented with 1 % of activated OW-BC. Given the ISR of 2 used for this experiment, the cellulose control showed an improved performance than the observed in the previous section with an ISR of 1. Notwithstanding, for the system amended with the activated BC, methane generation started until day 8 of digestion. The control, on the other hand, started producing methane on day 1 and quickly reached a steady state. The behaviour is different to the observed with traditional non-activated OW-BC450, whose effect improved biomethane production rates and yield. This suggests that activated OW-BC450-MgCl affected the microbial population, whose recovery took up to 28 days to reach BMP values close to the control.

Small amounts of metals, such as Fe, Ni, Ca, and Mg, are reported to stimulate biogas and biomethane generation given their essential role in the metabolic functioning of microorganisms [239]. Given the methodology employed for the activation of OW-BC, the Mg in the BC exceeded the recommended. Further, the addition of activated OW-BC at 3 % resulted in a null biomethane production suggesting greater toxicity by increasing char loads. Similarly, Suanon et al [102] studied the effect of magnetite iron nanoparticles (Fe_3O_4) in the AD of sludge obtaining improved methane production. However, the increasing concentration of the nanoparticles affected the yields since, at loads of 0.5 %, the methane

production was improved whereas at 1 % it was strongly inhibited. They attributed this behaviour to the toxicity of (Fe$_3$O$_4$) nanoparticles and the release of the metal into the liquid bulk.
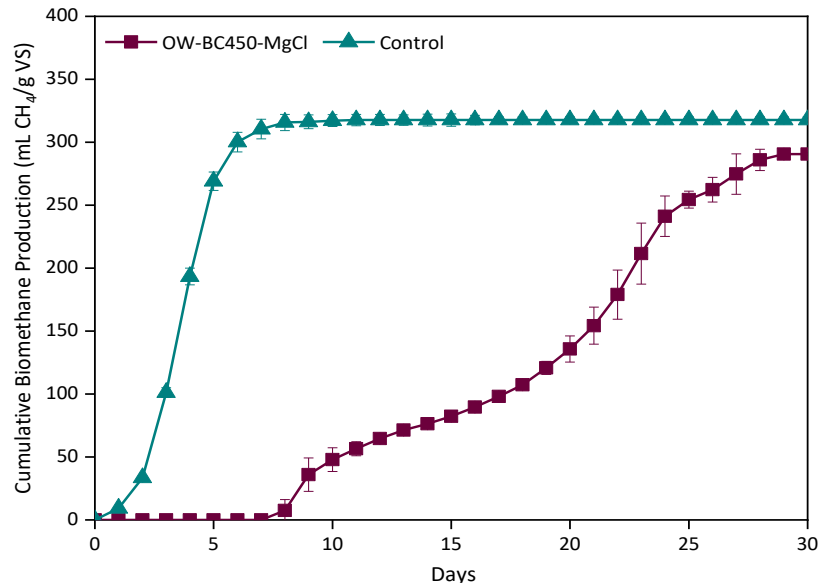
Figure 5.4. Effect of the addition of oak wood biochar activated with magnesium on biomethane production during anaerobic digestion.

Replicates: OW-BC450-MgCl (n=2), cellulose control (n=2), blank (n=2).

Table 5.3 outlines the kinetic parameters obtained for the cellulose digestion experiments. The final BMP yield obtained with OW-BC450-MgCl addition was only 8 % less than the control, although the BD index was relatively good in both cases (70-77 %). The parameters most affected by OW-BC450-MgCl addition were λ and μ_m with values of 4.6 and 5.6 times slower than the control. The delay for the methane generation with the addition of OW-BC450-MgCl at a load of 1 % and the null production with 3 % indicate inhibition or even toxicity. This inhibitory effect could be due to the high amount of MgCl$_2\cdot$6H$_2$O employed during the production of the BC, and the effect of the products resulting after the thermal degradation. According to Huang et al. [240], the thermal decomposition of MgCl$_2\cdot$6H$_2$O above 415 °C leads to the products outlined in **Equation 5-1**. It is worth remarking that both, MgO and HCl are highly inhibitory for cell metabolism. There are even reports on the effective antimicrobial activity of MgO nanoparticles against bacteria, yeast and the formation of biofilms [241].

Table 5.3. Experimental yields and kinetic parameters obtained with the modified Gompertz model.

Char	Experimental		Gompertz model			
	BMP_{exp} (mL CH$_4$/g VS added)	BD_{CH4} (%)	BMP_{max} (mL CH$_4$/g VS added)	μ_m (mL CH$_4$/g VS·day)	λ (days)	R^2
OW-BC450-MgCl	290.65	70.20	386.93	16.57	7.98	0.980
Control	317.60	77.18	354.94	93.02	1.74	0.998

BMP_{exp} experimental final methane yield; BD biodegradability; BMP_{max} maximum methane yield; μ_m methane production rate; λ lag phase; R^2 coefficient of determination to validate the model.

$$MgCl_2 \cdot 6H_2O \rightarrow MgO + 2HCl + 5H_2O$$

Equation 5-1
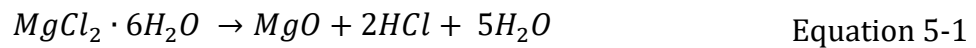
The methodology here used has been reported to provide highly adsorptive MgO-biochar nanocomposites with an excellent capacity for removing phosphate and nitrate from water [107]. Nonetheless, this same methodology might not be the most adequate for obtaining activated biochar that enhances AD and promotes cell adhesion. Therefore, it is worth considering other activation protocols, by either employing lower concentrations of metals or other chemical reagents or even moving towards physical activation. It is possible to control and tailor the physicochemical properties of biochar by controlling the method and activation process. Hence, understanding the properties that biochar must meet for improving AD and selecting an activation method with the best chance of delivering them are of great importance. In this study, it was stated that the chemical activation method here employed resulted in BC with increasing metal content that exhibited a detrimental effect on AD. Other approaches for increasing the surface area and porosity of biochar to desirable levels can be obtained with other methods and activation conditions.

5.5 Cell immobilisation on chars during anaerobic digestion

The immobilisation of whole cells on porous materials, like biochar, is similar to adsorption since it often involves the same physical and chemical interactions. The cells are initially attached to the support (adhesion) and each other (cohesion). Afterwards, the firmly attached cells commence multiplying by remaining attached, thus colonising the support, at the same time that they get entrapped into the macro and micro-porous regions of the matrix [242,243]. The physicochemical parameters of surface area, particle size, pore structure and

functional groups of the support are of great importance for immobilisation [244]. The interactions between the cell and the support depend on the chemical characteristics of the surface of both. It has been reported the importance of OFGs on the surface of the matrix materials for the hydrophilic character, and the promotion of electrostatic interactions that lead to a greater immobilisation performance [27]. Moreover, the surface chemistry of the support has shown a direct effect on the bacterial population and catalytic activity of the immobilised system [97]. The support materials should count with the presence of functional groups for multipoint bindings between the support and the cells [245]. Therefore, the chars used in this work generally fulfil the characteristics mentioned above. The chars exhibited a large availability of OFGs, and particularly for OW-BCs a considerably large surface area as described in Chapter 4.

The potential of the chars to immobilise the anaerobic sludge, followed by the capacity of the attached cells to produce methane during AD was investigated. Only OW chars were selected for this experiment because they are considered reference materials in the research group and given their predominance in the literature. Thus, two consecutive AD runs under standard conditions incorporated with the chars OW-HC250, OW-BC450 and OW-BC650 were performed without replicates. First, digestion with the inoculum 5 g VS/L and 3 % (w/v) of chars at 37 °C for 48 h without substrate addition took place. Since the medium was not supplemented with a carbon source, it was assumed that there was no further bacterial growth. At the end of the fermentation, the supernatant was decanted, and the chars were collected and placed in a sieve. Afterwards, the chars were gently washed with distilled water to remove the excess sludge that was not immobilised onto the biochar materials as described in section **3.3.10**. These chars were employed as the source of both char and inoculum for seeding a second AD batch incorporated with cellulose at 5 g VS/L. Since the amount of inoculum was not fixed for the second run, it is not possible to state the ISR, although it is assumed to be relatively low. Given the short length of the first digestion, methane generation was measured just on the second digestion. The first digestion aimed to promote the immobilisation of the microorganisms on the surface of the chars. While the second digestion aimed to assure that the only inoculum supplemented to the reactors corresponded to the cells previously attached to the chars. Hence, the BMP generated during the second AD was attributed to the anaerobic sludge immobilised onto the chars.

5.5.1 Biochemical methane potential

Figure 5.5 illustrates the cumulative BMP of the second AD fed with the sludge immobilised on the chars. The system incorporated with OW-BC650 started methane generation sooner than the rest. OW-BC450 and OW-HC250 started methane generation on the 10th day of the digestion, although the latter showed poor production. The lag phase was followed by a stepped BMP production and reach of steady-state after 33-39 days of fermentation for the BC systems. Whereas the HC system reached a rapid stabilisation at a lesser BMP yield. It can be assumed a seeding drastically below the initially 5 g VS/L used for the first digestion since the only inoculum provided to the second AD batch was attached to the chars.
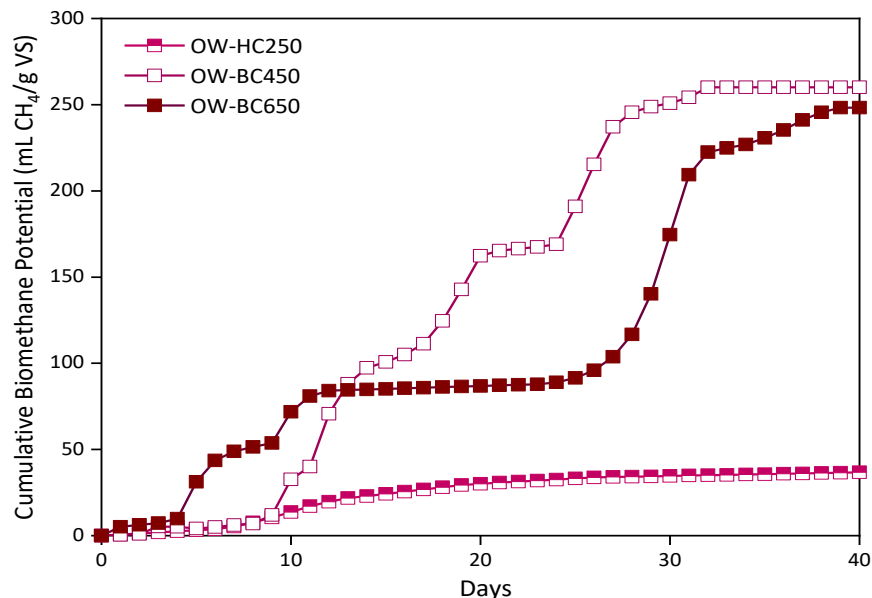
Figure 5.5. Cumulative biomethane production during the anaerobic digestion of sludge immobilised on oak wood chars (n=1).

The initial inoculum concentration influences the rate of biodegradability of the substrate, hence low initial values result in slower anaerobic fermentation [246]. The prolonged lag-phase and stepped curve suggest a deceleration of growth, due to an adaptation of the culture to the digestion conditions. The growth curve of bacteria undergoes various phases accompanied by an adaptation to concentrations of nutrients and inhibitors that causes small time lags. The shape of the growth curve is influenced by a series of factors, including the type of bacteria, physiological state of the initial inoculum, initial concentration of inoculum, process conditions, and type and concentration of substrate [247].

The differences between the char systems generally agree with the observed in section **5.3.1**. The lower temperature OW-BC exhibited better performance than the higher temperature BC and dramatically better than HC. **Table 5.4** shows the kinetic parameters obtained with the modified Gompertz model. Accordingly, the immobilisation on OW-BC450 exhibited the longest λ and the highest μ_m (13.6 mL CH_4/g VS·d) almost doubling the observed for OW-BC650, although similar BMP_{max}. OW-HC250 exhibited the smallest lag phase (4.1 days) but reached considerably lower methane yields. The BMP yields and production rate here achieved were lower than the previously obtained for cellulose and biochar digestion experiments (**5.3.1**). Notwithstanding, the production of methane by itself indicates that anaerobic sludge immobilised on the chars was transferred to new digesters for the continuity of AD. The adaptation time required before methane production could be due to the fewer inoculum available since the provided consisted only of the attached to the chars. Regardless of the necessary long time for adaptation, the generation of methane is an indication of the ability of the biochars, particularly OW-BC450, to successfully attach the anaerobic sludge and allow the digestion performance.

Table 5.4. Experimental and kinetic parameters obtained with the modified Gompertz model for the anaerobic digestion of sludge immobilised on chars.

Immobilised system	Experimental		Gompertz model			
	BMP_{exp} (mL CH_4/g VS added)	BD_{CH4} (%)	BMP_{max} (mL CH_4/g VS added)	μ_m (mL CH_4/g VS·day)	λ (days)	R^2
OW-HC250	37.9	9.1	36.6	2.3	4.1	0.996
OW-BC450	260.1	62.7	272.8	13.6	8.1	0.989
OW-BC650	248.3	59.9	277.8	7.1	4.6	0.928

BMPexp experimental final methane yield; BD biodegradability; BMPmax maximum methane yield; μ_m methane production rate; λ lag phase; R^2 coefficient of determination to validate the model.

5.6 Conclusions

It can be considered that the addition of biochar from lignocellulosic and herbaceous sources produced at low-temperature (450 °C) can improve methane production during AD. The methane yields for the biochars produced at higher temperatures (600-650 °C) from oak wood and water hyacinth were significantly lower. Seaweed biochars and all hydrochars, on the other hand, proved to drastically inhibit methanogenesis. A relationship between the nature of the parent materials along with the thermochemical processing conditions and their influence on AD was established.

Hence, the obtained positive effect could be attributed to a summary of beneficial properties such as high surface area and OFGs for OW-BC450 or even a greater content of OFGs, NFGs and conductive inorganics for WH-BC450. Furthermore, it was established the ability of the biochars, particularly OW-BC450, to successfully attach to the anaerobic sludge and allow the digestion performance. Although the proposed method of low-temperature biochar addition was successful in batch tests, it is worth considering other feedstocks, physical activation methods, immobilisation methods and the potential of hydrochar in the production of VFAs.

Conversely, methane potential and hydrolysis efficiencies of cellulose were noticeably decreased in the presence of seaweed biochars, hydrochars and metal impregnated biochars. These detrimental effects could be attributed to characteristics such as toxic or inhibitory by-products originating from the pyrolysis of seaweed. Humic acids, acidity, and undesirable N-containing by-products of Maillard reactions in the case of hydrochars.

Chapter VI

Biochar augmentation on the anaerobic digestion of complex substrates

6.1 Overview

Given the favourable effect of low-temperature biochars (BC) on anaerobic digestion stated in Chapter 5, the further augmentation of the oak wood biochar produced at 450 °C (OW-BC450) on the digestion of more complex substrates is undertaken in this Chapter. Factorial design of experiments (DoE) was performed to evaluate the effect of crucial processing conditions, such as inoculum-to-substrate ratio (ISR), biochar load and C/N ratio. The content of this chapter is divided into two sections according to the substrate used for AD, (i) microalgae *Chlorella vulgaris*, and (ii) aquatic plant water hyacinth (WH).

Firstly, the anaerobic co-digestion (AcoD) of *C. vulgaris* with a reference substrate with known degradability, in this case, cellulose, allows the effect of BC augmentation on C/N ratios to be investigated and allows optimum C/N ratio to be controlled. To establish the potential of BC for enhancing methane generation during AcoD, exploratory and further DoE experiments were performed. An initial augmentation of BC at ISR 0.5-0.9 and C/N ratio 10-30 offered a pH buffering effect and increased the biomethane yields by 1.8-4.6 times the controls. BC addition amended significantly AcoD, supporting the stability of digestion under less favourable conditions. The effect of the process variables was further studied with a 2^3 factorial design and response optimisation. Under the design conditions, the variables had less influence over methane production. Higher ISRs and C/N ratios favoured AcoD, whereas increasing amounts of BC reduced the biochemical methane potential (BMP) but enhanced the production rate (μ_m). The factorial design highlighted the importance of ISR and BC-load on AcoD, establishing an optimum of 2:1 and 0.58 % (w/v), respectively.

Secondly, a full factorial 2^2 experimental design and further optimisation were performed to identify the best processing conditions for the AD of WH. An ideal

ISR of 1 was established while increasing it dropped the BMP yield and μ_m. The contour plot demonstrated that the maximum BMP_{Exp} and BMP_{max} values can be obtained at BC loads of 0-1.8 and 0-0.5 %, respectively. Whereas μ_m was favoured at all BC loads and more significantly at 3 %. However, BC addition had no significant effect on the digestion of WH. The subsequent AD of WH samples collected from different locations in India and Uganda resulted in highly different BMP yields. BC addition had little effect on BMP performance, and in some cases, it even reduced the BMP.

The performance and trends obtained from the factorial regression models and optimisation differed largely between the co-digestion of *C. vulgaris* and cellulose and the AD of WH samples. The effect and amendment potential of biochar were influenced by the digestion conditions and substrate, particularly when working with complex substrates. Therefore, it is necessary to create an understanding of these relationships to establish the best AD conditions.

The first part of the work within this chapter has been published in Bioresource Technology, please see: J Quintana-Najera, AJ Blacker, LA Fletcher, AB Ross. "Influence of augmentation of biochar during anaerobic co-digestion of *Chlorella vulgaris* and cellulose" *Bioresource Technology* (2022) 343, 126086.

The second part of the work within this chapter has been published in Energies, please see: J Quintana-Najera, AJ Blacker, LA Fletcher, DG Bray, AB Ross. "The Influence of Biochar Augmentation and Digestion Conditions on the Anaerobic Digestion of Water Hyacinth" *Energies* (2022) 15, 2524.

6.2 Introduction

The use of complex substrates in anaerobic digestion is key for developing the biogas industry of a country or a region. For achieving this, several aspects must be taken into consideration, such as feedstock availability, economics, regulatory issues, and national bioenergy production targets. To promote an efficient AD scenario, the substrate selection should be based on the re-use or recycling of existing and long-term available raw materials. Agricultural, industrial, municipal waste and food crops are considered to represent the highest market maturity and economic efficiency in biogas plants. Nonetheless, agricultural residues require pre-treatments for decomposing the lignin fraction and making the fermentable constituents available. Whereas food crops compete with food security and prices [248]. Alternative options that could represent a reliable

supply include the growth of microalgae and the utilisation of non-edible plants with rapid growth, such as water hyacinth (WH) [249,250].

Microalgae is an attractive feedstock for biofuel production due to their highly productive growth, and photosynthetic solar efficiency that doubles that of terrestrial plants. Other advantages include the utilisation of land areas unsuitable for food production, utilising carbon dioxide emissions, resulting in a lower land-use footprint and providing carbon-neutral biofuels [249]. However, microalgae have demanding nutrient requirements, a composition subject to seasonal growth variations, and a recalcitrant cell wall that difficult its hydrolysis and increases the economic and energetic costs [47].

Strategies under investigation to improve the economic and energetic feasibility of microalgae digestion include the integration of microalgae cultivation to remove nutrients from wastewater followed by subsequent co-digestion with different sludges [47,251]. Extraction of oils from microalgae and hydrothermal treatment to produce biocrude and subsequent digestion of the process waters [66,252]. Furthermore, continuous advancements in strain improvement, cultivation and harvesting techniques, strengthen the potential of microalgae as a biofuel substrate [47]. Therefore, coupling microalgae cultivation with AD could overcome some of the inherent limitations, while improving the economic and energetic efficiency. Microalgae as a substrate in AD could allow direct use after cultivation while avoiding the dewatering step [253]. Hence, microalgae are considered a reliable and consistent feedstock supply [47].

There are different types of microalgae, including the 'weed' green species *Chlorella vulgaris* [249]. The uses of *C. vulgaris* are mostly related to the food and pigments industry, although it is considered a promising sustainable source of biomass for bioenergy [254]. *C. vulgaris* is productive biomass with rapid growth, high protein, and low content of toxic compounds, although its composition and recalcitrant cell wall hinder its biodegradability (BD) [253]. BD corresponds to the breaking down of a substrate into smaller compounds by microorganisms. The ability to biodegrade a substrate is limited by the complexity, toxicity and bioavailability of the compounds [47]. One of the main limitations of the breakdown of biomass with a high N-content, such as microalgae, is the generation of ammonia. The unionised ammonia (NH_3-N) is a hydrophobic molecule that passively diffuses into the cells, leading to a proton imbalance and/or potassium deficiency that induces cell distress. The methanogenic bacteria are highly affected by ammonia toxicity since it inhibits enzyme synthesis and in consequence their performance [253]. Increasing the

BD of microalgae can be achieved by physical-chemical pre-treatments, however, this is often uneconomically or energetically unjustified [255]. Hence, another promising approach to improve microalgae degradation is the anaerobic co-digestion (AcoD) in combination with other feedstock [239].

AcoD of substrates offers several technological, ecological, and economic advantages over mono-digestion. Mono-digestion of protein-rich feedstocks can be accompanied by imbalanced C/N ratios, resulting in longer retention time, poor methane production or even digester failure. A properly balanced co-digestion of two or more substrates, on the other hand, can provide synergistic effects, improve the process stability, methane yield, kinetic parameters, and in consequence the economic viability of biogas plants [54]. Reported C/N ratios are found in the range 15-30, although the optimal value depends mainly on the feedstock [256]. For instance, optimal C/N ratio reports include crops 20 [257], corn stover 25 [256], algae 25-30 [258], microalgae (*Chlorella sp* and *Scenedesmus sp*) 20-25 [259]. The latter supports the importance of a balanced C/N ratio for achieving optimal microalgae AcoD.

Furthermore, identifying novel feedstocks highly available in certain regions or countries can be an economical and productive option for AD. Such is the case of water hyacinth (*Eichhornia crassipes*), one of the most invasive aquatic weeds growing throughout the tropical zone around the globe. WH is an aquatic invasive macrophyte with adaptative phenology characteristic of invasive behaviour. The flexible morphology and capacity to hyper-accumulate nutrients available in water bodies donate WH an outstanding adaptation and invasive potential. In natural environments, WH out-competes and negatively affects flora and fauna, hence the importance of its removal from water bodies and further utilisation for economic viability [138]. The zones most affected by WH include Southeast, Central and Western Asia and Central America. WH grows uncontained in water bodies in over 50 countries and is predicted to expand into higher latitudes as temperatures rise due to climate change [260]. Limited efforts and resources have been directed to controlling WH given the costs and labour requirements, and the fact that developing countries are the most affected [261]. Eutrophication on rivers, lakes, water reservoirs and estuaries are an increasing problem due to increasing deforestation and effluent production from WWTP, leaching from farmland, and industrial development. Given its biology, the eradication of WH is practically impossible, and due to its high-water content (95%) its transport, storage or disposal is very costly [262].

Hence, directing the control of WH toward sustainable utilisation could increase the energetic and ecological development of urban and rural areas. Among the several advantages of AD, the ability to process wet biomass makes this technology highly suitable to utilise WH for methane generation [263]. The high ash and water content of WH complicates its use in gasification or pyrolysis, hence it has been suggested the use of WH as a feedstock for compost or biogas production. The methane yields obtained during the AD of WH are generally found in a range from 114 to 240 mL CH_4/g, however, there is limited work for this substrate. The carbohydrate fraction of WH comprised mainly of cellulose and hemicellulose is accompanied by protein, which could offer a substrate with an adequate C/N ratio (~15-30) for AD [142,261]. Nonetheless, WH composition varies with its location and growth conditions, thus, more research is necessary to assess and improve the BMP yields and the viability of digesting WH [263]. It has also been suggested the potential to treat WH by HTC for obtaining valuable products [134,264,265].

To enhance the hydrolysis of complex feedstocks and obtain efficient methane yields, it is necessary to explore and establish suitable AD conditions, including inoculum to substrate ratio (ISR), establish suitable pre-treatment options and investigate the potential for improving digestion using adsorptive additives, such as biochar. The inoculation influences the initial activity and performance of the digester. Hence, ISR is an essential operating condition that needs to be evaluated for optimising digestion [266]. The implementation of optimum ISR helps maintain the digester stability, avoid the accumulation of VFAs, and reduce the necessity of nutrient media supplementation while obtaining better methane yields [267]. As discussed in Chapter 5, BC augmentation in AD enhances the methane production rate and yields, particularly using the low-temperature BCs. Many studies have reported the digestion of *C. vulgaris* [54,251,254,258] and WH [140,268–270], although the addition of BC as an additive for improving AD has not been evaluated for these feedstocks. The effect of BC addition on BMP has varied considerably during this research and among the literature. Hence, it is important to study the BC addition on the AD of variable complex substrates and to evaluate the impact of BC load since an excessive addition could be detrimental to methanogenesis [20].

Therefore, this chapter aims to identify the potential for biochar to enhance methane generation during the AD of complex feedstocks and to establish optimal conditions. In continuity with the results of Chapter 4, OW-BC450 was selected for the augmentation due to its positive performance in AD. The content was divided into two sections, (i) the AcoD of *C. vulgaris* and cellulose, and (ii)

the AD of water hyacinth. The first section aimed to investigate the effect of BC addition during the AcoD of *C. vulgaris* and cellulose. This was followed by the application of factorial design 2^3 for identifying the optimum C/N ratio, BC load and ISR. The second section aimed to evaluate and optimise the ISR and BC load for WH digestion, and further test the obtained optimal conditions on the AD of different WH samples collected from different locations.

6.3 Effect of biochar during the anaerobic co-digestion of cellulose and microalgae at variable C/N ratios

Table 6.1 outlines the experimental conditions employed in this experiment. Standard AD conditions with modifications were used for this experiment, as described in Chapter 3. The composition of *C. vulgaris* was analysed as: i) biochemical (protein 40.5 %, lipids 15.6 %, and carbohydrates 36 %); ii) proximate (volatile matter 77.1 %, fixed carbon 14.3 % and ash 8.6 %); iii) ultimate (C 54.6 %, H 8.1 %, N 9.3 %, O 19.5 %). The digesters contained OW-BC450 at 0 and 3 % (w/v), and fixed concentrations of inoculum and cellulose. Whereas *C. vulgaris* addition was calculated based on its CHNOS composition to achieve the C/N ratios 10, 20 and 30. Hence, lower C/N ratios required more microalgae for increasing the N fraction, which resulted in lower ISR. The selected C/N ratios started at ideal values and moved down to unsuitable ranges to establish the potential of the BC in ameliorating critical processing conditions.

Table 6.1. Experimental conditions for the anaerobic co-digestion of cellulose and *Chlorella vulgaris* with oak wood biochar (OW-BC450) addition.

System	Biochar (%, w/v)	C/N ratio	Cellulose (g/L)	C. vulgaris (g/L)	Total substrate (g/L)	ISR
OWB10	3	10	5	4.5	9.5	0.5
C10	0	10	5	4.5	9.5	0.5
OWB20	3	20	5	1.5	6.5	0.8
C20	0	20	5	1.5	6.5	0.8
OWB30	3	30	5	0.9	5.9	0.9
C30	0	30	5	0.9	5.9	0.9

6.3.1 Biochemical methane potential

Figure 6.1 shows the cumulative BMP curves for the AcoD of cellulose and *C. vulgaris* at the given C/N ratios. All systems started generating methane from day one, exhibiting a negligible lag phase. The non-BC controls at the three C/N ratios rapidly reached maximum production and steady-state, whereas the BC systems showed an initial plateau, followed by a second exponential and stationary phase. For the non-BC controls, reducing the C/N ratio and ISR resulted in lower BMP yields. Increasing the N content (lower C/N ratios) is reported to enhance ammonia accumulation and toxicity that affects the digester balance [258]. Reducing the ISR below 0.8 facilitates the proliferation of acidogens and acetogens while inhibiting methanogens [123]. Nonetheless, the C/N ratio and ISR showed no significant effect over the final BMP_{Exp} yield ($p > 0.05$) (ANOVA).

Figure 6.1a shows the total cumulative volumetric methane generated at the given C/N ratios. The final volumetric methane production at each condition was improved by the BC addition. At the most favourable C/N ratio of 30 and ISR 0.9, the OWB30 produced (569.9 mL CH_4), 1.8 times more methane than the control C30 (321.9 mL CH_4). At the C/N ratio of 20 and ISR 0.8, the addition of BC improved the methane generation even more, with OWBC20 (622.4 mL CH_4) representing 2.6 times the control C20 (237.6 mL CH_4). The highest improvement in AD performance due to BC addition was observed in the most unfavourable conditions. At the lowest C/N ratio of 10 and ISR 0.5, the OWB10 (869.8 mL CH_4) corresponded to 4.5 times the control C10 (193.8 mL CH_4). The increasing volumetric production of biomethane at lower C/N ratios is due to more microalgae substrate added for increasing the N fraction, which also resulted in different ISR at each condition (**Table 6.1**).

Figure 6.1b shows the BMP curves by considering the total amount of substrate added. For the systems augmented with BC, similar final BMP_{Exp} yields ranged at 233-241 mL CH_4/g VS, in agreement with the average 222 mL CH_4/g VS reported for the AcoD of *C. vulgaris* and potato processing waste [254]. These values also corresponded to an enhancement of 4.6, 2.6 and 1.8 times their control, respectively. Evaluating the total volumetric methane expressed as mL of CH_4 rather than BMP highlighted the influence of BC addition in this case that different amounts of substrate were added. The reducing BMP yields obtained at lower C/N ratios and ISR could be attributed to the less favourable conditions for AcoD. The dramatic improvement of BMP yields due to the BC addition suggested that BC could have ameliorated the co-digestion of microalgae and cellulose, particularly under less favourable conditions.
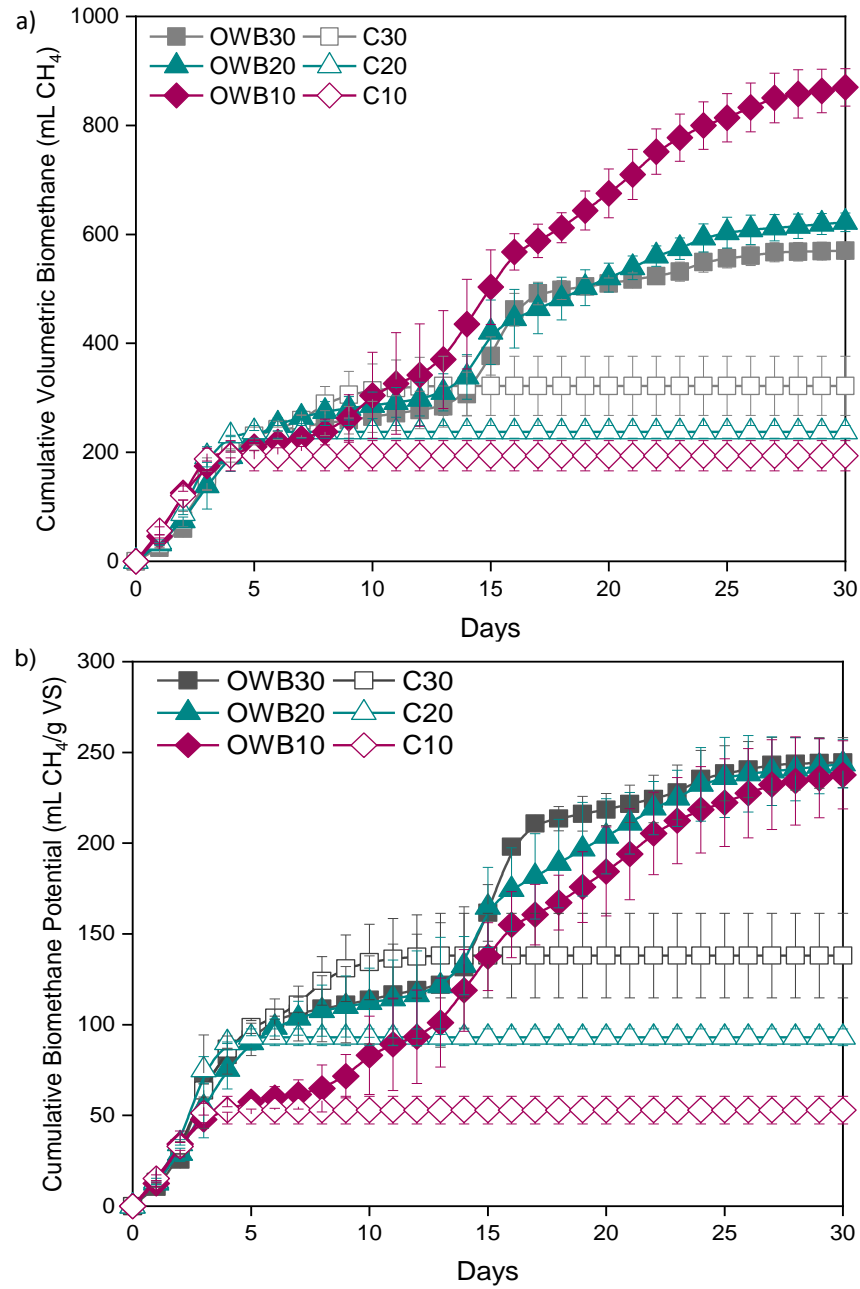
Figure 6.1. Cumulative biomethane production during AcoD of cellulose and *C. vulgaris* with and without biochar (OW-BC450) at different substrate C/N ratios and ISR, expressed as: a) total volumetric methane (mL CH$_4$); b) BMP (mL CH$_4$/g VS).

Replicates: OWB10, OWB20, OWB30 (n=3), C10, C20, C3 (n=2), blank (n=2).

6.3.2 Kinetic modelling

BMP$_{max}$ at the C/N ratios of 10, 20 and 30 was 5.6, 3.0 and 2.0 times higher for the systems augmented with BC in comparison to their control, respectively (**Table 6.2**). The non-BC controls quickly reached the steady-state, which was

reflected in their higher μ_m in comparison to the BC systems. The ANOVA stated that both variables BMP_{max} and μ_m had a statistically significant difference with the BC addition ($p<0.05$). However, neither the C/N ratio nor ISR showed significance over these kinetic parameters ($p>0.05$). Increasing the C/N ratio and ISR reduced the period of the lag phase, although not significantly ($p>0.05$). BC addition was the factor with the highest influence over the AD kinetic parameters, suggesting that BC positively influenced AcoD performance.

Table 6.2. Kinetic parameters of the first-order model and modified Gompertz model for anaerobic co-digestion of cellulose and *C. vulgaris* with the addition of OW-BC450.

System	Biomethane			Modified Gompertz model			
	BMP_{Th} (mL CH_4/g VS)	BMP_{Exp} (mL CH_4/g VS)	BD_{CH4} (%)	BMP_{max} (mL CH_4/g VS)	μ_m (mL CH_4/g VS·day)	λ (days)	R^2
OWB10	506.5	242.6	47.9	296.0	10.4	1.50	0.969
C10	506.5	52.9	10.4	53.0	24.8	0.45	0.993
OWB20	459.6	243.9	53.1	283.5	10.7	0.00	0.969
C20	459.6	93.0	20.2	93.2	54.4	1.21	0.993
OWB30	444.4	244.4	55.0	283.0	10.6	0.00	0.937
C30	444.4	138.0	31.1	138.9	28.9	0.82	0.991

Maximum methane yield (BMP_{max}), methane production rate (μ_m), lag phase (λ), and coefficient of determination (R^2).

6.3.3 Biodegradability

The BMP_{Th} for *C. vulgaris* and cellulose was predicted using Boyle's equation with values of 607 and 414 mL CH_4/g VS, respectively. The considerably higher BMP_{Th} yield for *C. vulgaris* is due to its more energetically dense protein and lipid content [258]. **Table 6.2** shows the variable BMP_{Th} at each C/N ratio resulting from the variable amount of microalgae added for achieving the ratios and used for calculating the BD of the systems.

The BD with the addition of BC and non-BC controls at the three C/N ratios ranged from 48-55 % and 10-31 %, respectively. The achieved BD values were far from the theoretical maximum. This is partially attributed to the limiting biodegradability of microalgae resulting from their thick and recalcitrant cell wall. Even though *C. vulgaris* was physically pre-treated or cracked in a ball mill,

its BD was only improved up to a certain extent since it has been stated that a fraction of undigested microalgae usually remains intact throughout the AD process [253]. Furthermore, the BDs were generally lower in comparison to those obtained in the previous sections for the AD of cellulose as a mono-substrate (BD 64-70 %). Hence, an inhibitory effect originated principally by *C. vulgaris* and low ISR could have hindered the BD and BMP values, less drastically for the systems supplemented with BC than the controls and directly correlated to the reduction of the C/N ratio.

6.3.4 Volatile fatty acids and pH

Figure 6.2 shows the VFAs accumulated at the end of the AcoD experiments. The systems that produced lower amounts of methane also resulted in higher VFAs. The control systems C20 and C30 showed similar final accumulation (980 mg total VFAs/L), while C10 reached 1239 mg total VFAs/L. On the other hand, the BC systems OW10 and OW30 exhibited negligible amounts, whereas OW20 accumulated 363 mL of total VFAs/L.
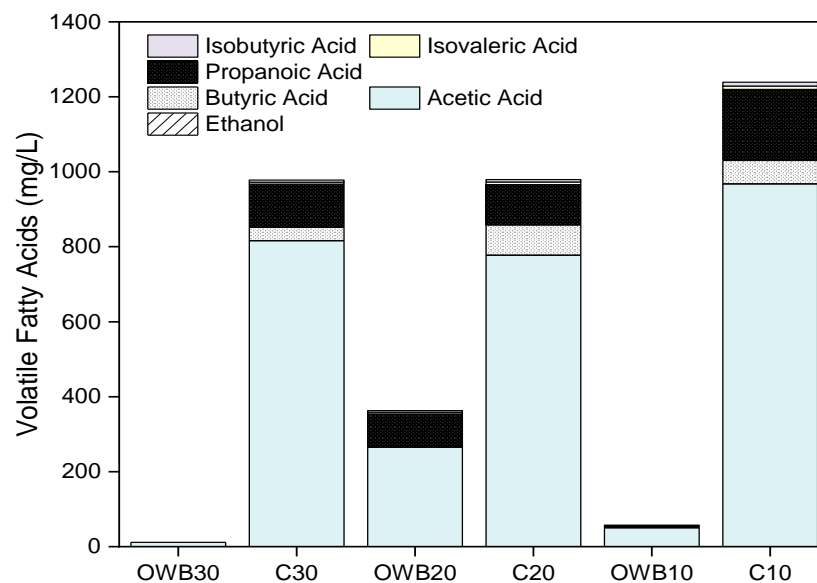
Figure 6.2. Volatile fatty acids produced during the anaerobic co-digestion (AcoD) of cellulose and *C. vulgaris* at different substrate C/N ratios with and without the addition of OW-BC450.

The higher VFA levels exhibited by the controls increased at lower C/N ratios, which could be related to the lower ISR used in each condition. For instance, Raposo et al. [271] studied the impact of ISR on the AD of sunflower oil cake. They observed a significant VFAs accumulation at an ISR of 0.5, which drastically

reduced at ISR 0.8, slightly less at ISR 1 and 1.5, and reached almost none at ISR 2.0 and 3.0. Hence, they suggested ISR 0.8 as a limit value for assuring the stability of the AD process. Notwithstanding, none of the conditions here tested reached toxic levels since acetate inhibition on methanogens is only reported at concentrations above 1619 mg/mL [272].

The pH of the systems was measured at the beginning and the end of the AcoD process (**Figure 6.3**). All systems started with similar pH (7.4-7.7), which by the end of the fermentation suffered negligible variations on the reactors supplemented with BC. The non-BC controls, on the other hand, suffered a drastic pH reduction (pH 5.3-5) that intensified at lower C/N ratios. The drastic changes in pH could be due to the accumulation of VFAs, ammonium and reduced buffering capacity of the systems. The pH, in consequence, affected the methanogens metabolism, which is reported to exhibit great sensitivity to pH variations, especially below their active range (pH 6.7-7.4), and likewise to ammonia and VFAs accumulation [55].
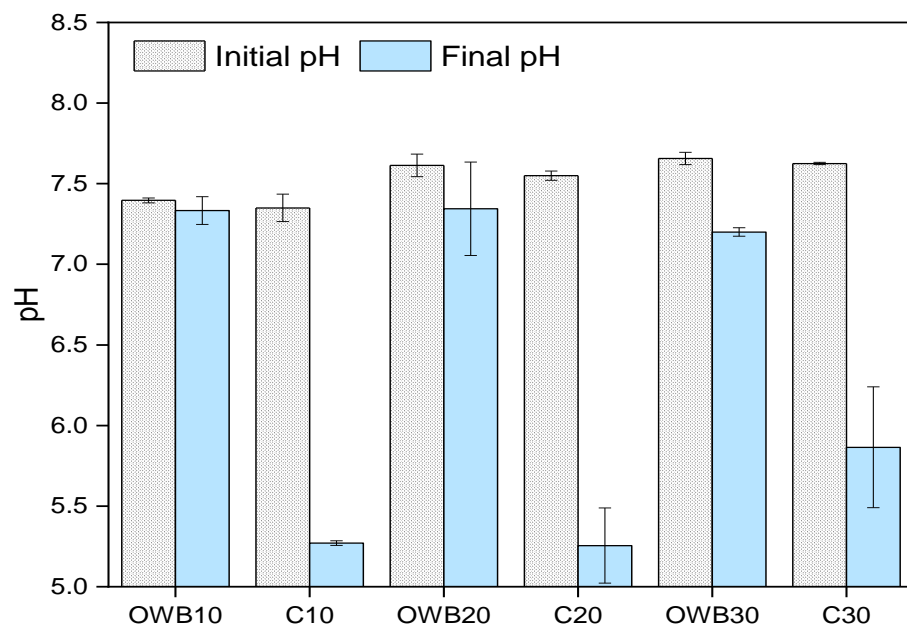
Figure 6.3. Initial and final pH measured during the AcoD of cellulose and *C. vulgaris* at different substrate C/N ratios with and without the addition of OW-BC450.

The changes in pH agree with the BMP_{Exp} values, as those systems whose pH suffers more variation also produced less methane. The latter suggests that OW-BC450 could have provided a buffering effect given its alkaline nature (pH 9.9). Similarly, there are reports of BC having a positive buffering role in AD [39,226].

A digester with adequate alkalinity would stabilise the AD process from variations of VFAs and pH. However, if the alkalinity is insufficient, the digester would undergo acidosis and the methane production would cease [273].

6.3.5 Biochar in anaerobic co-digestion

BMP and BD were hindered by the increasing addition of *C. vulgaris* (C/N reduction) and in consequence the increase of N-content. This behaviour was drastically observed for the controls, whereas it was considerably milder for the BC systems. As discussed in Chapter 5, the better BMP performance in the presence of BC could be attributed to the beneficial properties of BC. Including alkalinity, large surface area, surface functionality and potential role as a facilitator of syntrophic metabolism via DIET interactions [93]. This experiment demonstrated that BC addition could fulfil the necessity of an alkaline source, avoid drastic changes in pH and maintain the stability of the AD process under the conditions here studied. However, it is desirable to establish the best blend ratios for the substrates and inoculum for achieving positive synergisms, nutrient balance, avoiding inhibition, and optimising methane productivity [274]. Hence, the following section evaluates the optimum conditions for the AcoD of microalgae and cellulose to obtain a better BMP performance.

6.4 Optimisation for the anaerobic co-digestion of microalgae and cellulose using a factorial design 2^3

To determine the optimum processing conditions for the AcoD of *C. vulgaris* and cellulose, a full factorial 2^3 experimental design was performed. The study comprised three independent factors C/N ratio, ISR and BC load at two levels, with three replicates and three centre points as shown in **Table 6.3**. The inoculum was fixed at 10 g VS/L, whereas the amount of substrate added ranged from 5 to 10 g VS/L for achieving the corresponding ISR. The amount of *C. vulgaris* and cellulose added for each C/N ratio and ISR were calculated based on their chemical composition. For achieving the C/N ratios of 7, 16 and 25, the ratio of *C. vulgaris* to cellulose were 0.8:0.2, 0.3:0.7 and 0.2:0.8, respectively. The main objective of this experiment was to investigate and optimise the effect of BC load and ISR under variable C/N ratios.

Table 6.3. Design matrix for the full factorial 2^3 design used for the anaerobic co-digestion of *Chlorella vulgaris* and cellulose.

Reactor no.	Orthogonal coding			Actual value		
	C/N	ISR	BC load	C/N ratio	ISR	BC load (%)
R1, R2, R3	-1	-1	-1	7	1	0
R4, R5, R6	-1	-1	1	7	1	3
R7, R8, R9	-1	1	-1	7	2	0
R10, R11, R12	-1	1	1	7	2	3
R13, R14, R15	0	0	0	16	1.5	1.5
R16, R17, R18	1	-1	-1	25	1	0
R19, R20, R21	1	-1	1	25	1	3
R22, R23, R24	1	1	-1	25	2	0
R25, R26, R27	1	1	1	25	2	3

6.4.1 Biochemical methane potential

Figure 6.4 shows the average BMP produced by each condition of the factorial design for the AcoD of *C. vulgaris* and cellulose. All systems started producing methane from day one exhibiting a quick exponential phase while reaching the steady-state by the 10th day of digestion. The final BMP yields differed by up to 17 % among the conditions since they were found in a range of 247-299 mL CH_4/g VS. The highest BMP yield was obtained by the systems with C/N 25, ISR 1.0 and BC load 0 %, while the lowest yield was obtained by C/N 7, ISR 1.0 and BC load 3.0 %. In summary, BMP yields were enhanced by increasing the C/N ratios due to more favourable conditions but reduced by increasing the BC load.

6.4.2 Kinetic modelling

Table 6.4 shows the kinetic parameters obtained with the modified Gompertz model. The values of BMP_{max} were gradually improved as the C/N ratio increased and the BC load reduced. The period of lag phase was almost negligible for all systems, while μ_m showed the greatest variation. The highest μ_m of 70.2 and 66.2 mL CH_4/g VS·d, were obtained at the conditions (C/N 7, ISR 2.0, BC 3.0) and (C/N 25, ISR 2.0, BC 3.0), respectively. The rest of the systems exhibited values of 40-55 mL CH_4/g VS·d, corresponding to 16-39 % lower μ_m than the best performers. The effect of the C/N ratio showed no evident trend over μ_m while increasing both ISR and BC load resulted in the most significant enhancement.
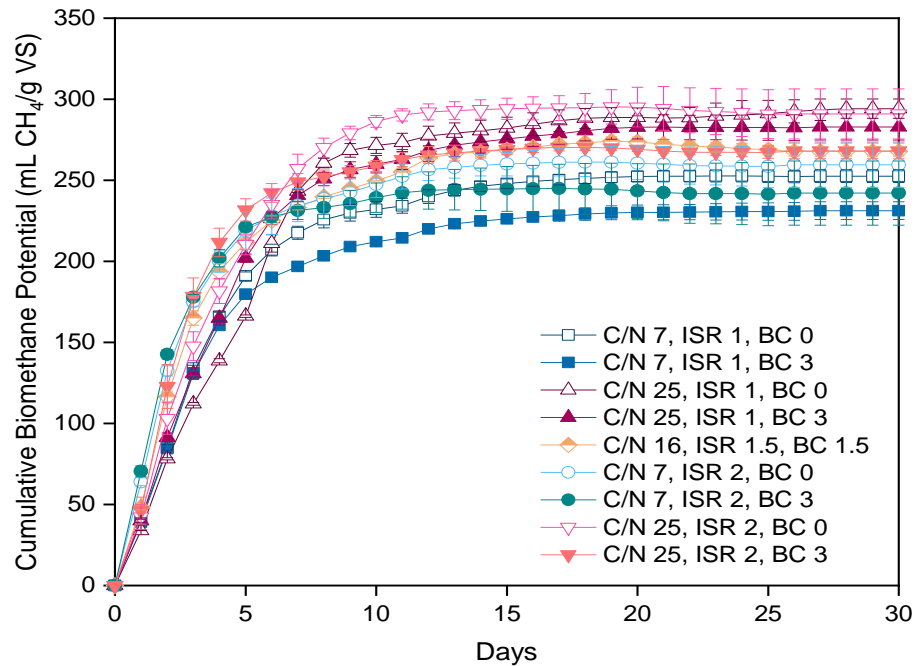
Figure 6.4. Biomethane production for the full factorial 2^3 experimental design used for the anaerobic co-digestion of cellulose and *Chlorella vulgaris.*

Replicates: all runs (n=3), blank (n=2).

Table 6.4. Average methane, fermentation and kinetic parameters for the experimental design conditions used for the anaerobic co-digestion of *Chlorella vulgaris* and cellulose.

Independent variables			Experimental			Modified Gompertz		
C/N	ISR	BC load	BMP_{Exp} (mL CH_4/g VS)	BD (%)	TAN (mg NH_3-N/L)	BMP_{Max} (mL CH_4/g VS)	μ_m (mL CH_4/g VS·d)	λ (d)
7	1	0	270.1	47.3	20.8	265.9	45.3	0.0
7	1	3	247.3	43.3	30.3	242.2	42.8	0.0
7	2	0	277.6	48.6	17.2	274.9	59.0	0.0
7	2	3	259.0	45.3	24.3	258.6	70.2	0.0
16	1.5	1.5	275.0	57.7	19.5	274.0	49.5	0.0
25	1	0	298.9	65.9	17.2	294.2	41.8	0.4
25	1	3	287.5	63.4	22.2	283.7	44.4	0.1
25	2	0	295.7	65.2	15.5	298.5	49.7	0.1
25	2	3	272.5	60.1	17.1	270.2	66.2	0.2

BMP_{Exp} maximum experimental methane yield, BD biodegradability, TAN total ammonia nitrogen measured on the supernatant, BMP_{max} maximum theoretical methane yield, μ_m methane production yield, λ duration of lag phase.

6.4.3 Biodegradability

Table 6.4 shows the BMP_{Th} for the AcoD of *C. vulgaris* and cellulose at each condition. As previously stated, the variable BMP_{Th} is obtained from the mixture of the substrates at the different C/N ratios. The BMP_{Th} at the C/N ratios 7, 16 and 25 corresponded to 571, 477 and 454 mL CH_4/g VS, respectively. The differences in BMP_{Th} in addition to the BMP_{Exp} dramatically affected the BD values, which ranged from 43-to 66 %. Even though the BMP_{Th} increased when lowering the C/N ratio, the actual BMP and BD values were reduced due to the complexity, recalcitrance, and difficult biodegradability of *C. vulgaris* [258]. Hence, an inhibitory effect originated principally by reducing ISR, increasing the content of *C. vulgaris*, and in consequence, reducing the C/N ratio could have hindered the BD values.

6.4.4 Fate of organic nitrogen

To study the fate of organic nitrogen at the end of AcoD of microalgae and cellulose, both solid and liquid phases were separated and analysed (**Table 6.4**). The total ammonia nitrogen (TAN) in the liquid phase was measured by spectrophotometry, while the N-content on the decanted solid was quantified by elemental CHNOS analysis (**Figure 6.5**). TAN values were considerably low for all experimental conditions (17-30 mg/L), slightly higher with BC addition and at a lower C/N ratio. This behaviour contrasts that reported by Lu et al. (2019) for the AcoD of *Chlorella sp.* with septic tank sludge. They obtained a final TAN of approximately 200-2300 mg/L, although even these levels showed no inhibitory effect over methanogenic activity. The N content of the remaining solids was comprised of the digestate, and BC was slightly higher at a lower C/N ratio and without BC addition, although the general values were similar to the N content of the inoculum. This behaviour, in addition to the BMP yields and BD, suggests adequate digestion of the microalgae, without ammonia inhibition even at the lowest C/N ratios.

6.4.5 Volatile fatty acids and pH

Figure 6.6 exhibits the VFAs accumulated at the end of the AcoD experimental design. The less favourable conditions in terms of lower ISR and C/N resulted in a greater VFA accumulation. Nevertheless, such low concentrations could be considered negligible in all cases.
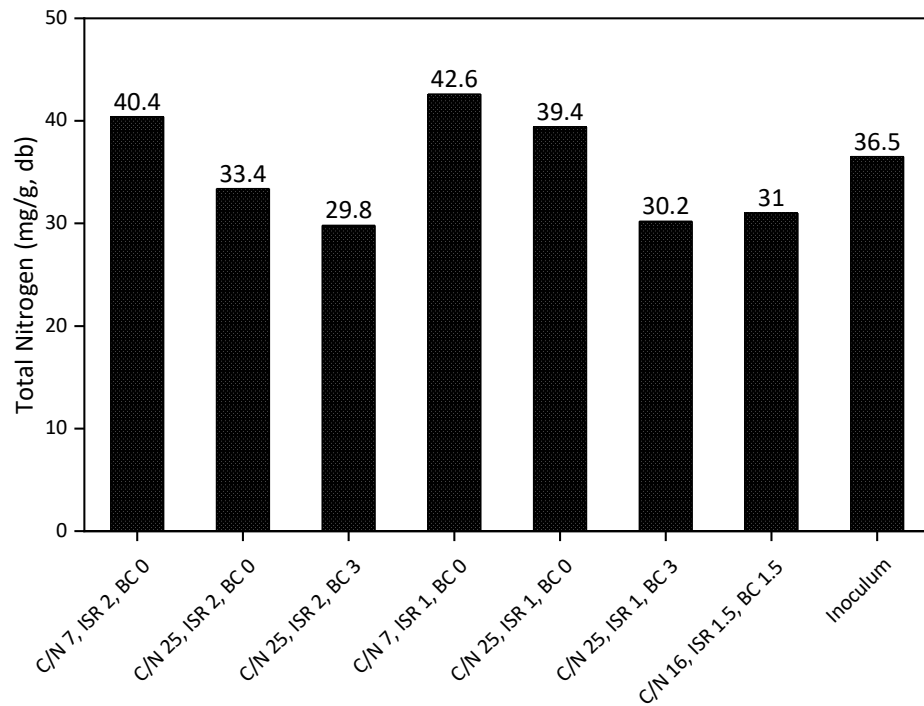
Figure 6.5. Nitrogen content measured by CHNOS for the final solids of the anaerobic co-digestion of cellulose and *Chlorella vulgaris* at different substrate C/N ratios.
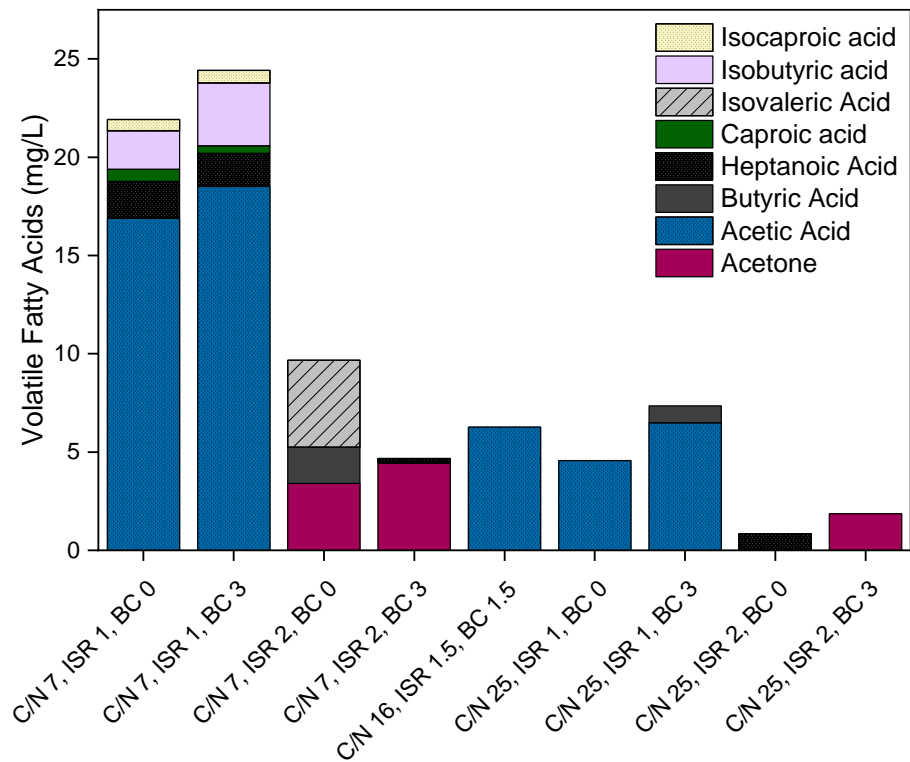
Figure 6.6. Volatile fatty acids accumulated at the end of the AcoD of *Chlorella vulgaris* and cellulose under factorial design conditions.

Figure 6.7 shows the pH at the beginning and end of the AcoD. No pH adjustment was performed to evaluate the effect of the processing conditions C/N ratio, ISR and BC load. The initial pH (7.5-7.9) was similar for all systems, although higher than the optimal levels for the AD process (pH 6.7-7.4). By the end of the digestion, the systems exhibited different pH variations with final pH of 6.8-7.3, within the optimal range. Increasing ISR and C/N ratio reduced the final pH, with a statistically significant effect ($p<0.05$). This effect is contrary to the expected since higher ISR and balanced C/N ratios are associated with pH buffering. Even though BC is an alkaline additive and it previously proved to offer a buffering effect on AcoD, under these conditions its addition had no effect on the pH ($p>0.05$) (ANOVA).
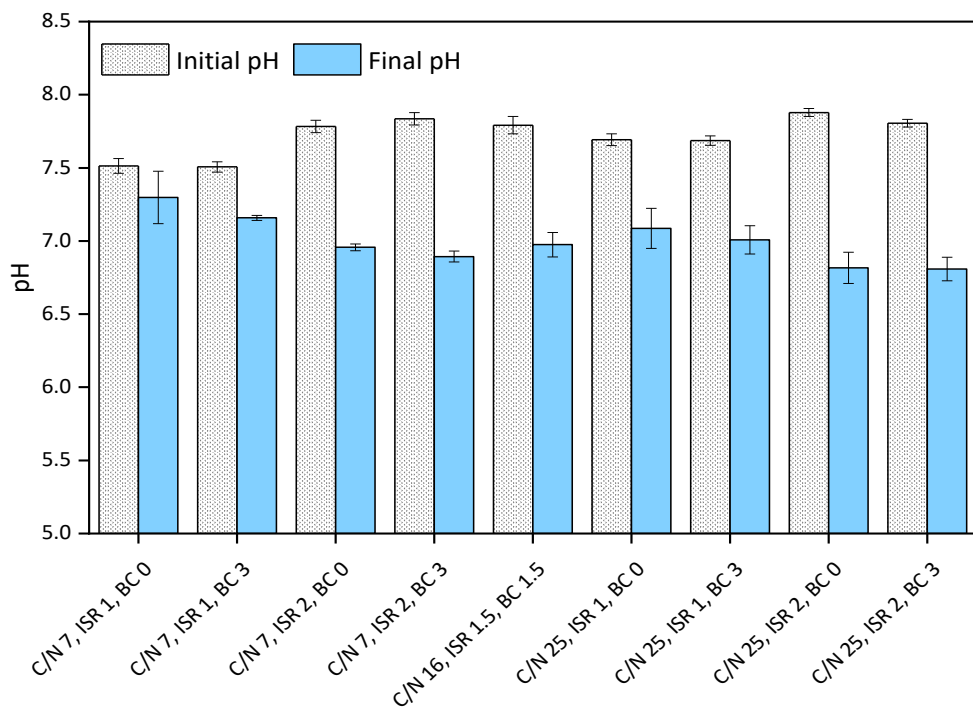
Figure 6.7. Initial and final pH measured during the anaerobic co-digestion of cellulose and *Chlorella vulgaris* at different substrate C/N ratios.

6.4.6 Regression model fitting

The parameters BMP$_{Exp}$, BMP$_{max}$ and μ_m were selected as response variables for the analysis of the factorial design. The regression models obtained were statistically significant with $p<0.05$ and F-value>F-critical at the 0.05 alpha level (**Table 6.5**). The centre points included in the 2^3-design protected against curvature from second-order effects, validating the fitting of the first-order

regression model ($p<0.05$). **Equations 6-1**, **6-2** and **6-3** show the factorial regression models for BMP_{Exp}, BMP_{max} and μ_m, respectively. These regressions exhibited R^2 of 0.73, 0.85 and 0.84, respectively. Hence, only 15-27 % of the variability cannot be explained by the models. The adjusted R^2 0.69-0.80 values were fitted to the actual size of the model and the number of factors, whereas the prediction R^2 0.58-0.67 indicates the variability that the model would explain during the prediction of new data. In brief, the significance and fitting of the quadratic models to the experimental data were satisfactory.

Table 6.5. Evaluation of factorial regression models by analysis of variance.

	Analysis of Variance (ANOVA)		
Variable	BMP_{Exp}	BMP_{max}	μ_m
R^2	0.73	0.85	0.84
Adjusted R^2	0.69	0.80	0.79
Prediction R^2	0.58	0.67	0.66
F	15.24	15.51	14.64
$F_{critical}$	2.51	2.51	2.51
Model p-value	0.00	0.00	0.00
Lack of fit p-value	0.882	0.932	0.367

$$BMP_{Exp}=275.95 + 12.58*CN +0.13*ISR - 9.53*BC – 4.69*CN*ISR \qquad \textbf{Equation 6-1}$$

$$BMP_{max}=273.58 + 13.13*CN + 2.00*ISR - 9.86*BC – 4.32*CN*ISR \qquad \textbf{Equation 6-2}$$

$$\mu_m=52.11 + 8.83*ISR + 3.48*BC + 3.45*ISR*BC \qquad \textbf{Equation 6-3}$$

From the analysis of variance, each factor and interaction of factors offered a specific coefficient and p-value (at 95 % confidence) as listed in **Table 6.6**. The significant specific coefficients ($p<0.05$) for the factors and interactions are part of the regression models. Even though the factor ISR was non-significant for BMP_{Exp} and BMP_{max}, the coefficients were kept based on the hierarchy principle. This principle promotes internal consistency by indicating that if a model contains a high order term (CN*ISR), it must contain all the lower order terms (CN and ISR) [127]. The factors C/N ratio and BC load influenced both BMP_{Exp} and BMP_{max}, with no significant effect from ISR. The C/N ratio did not affect the response variable μ_m, which was influenced exclusively by ISR and BC load and their interaction.

Table 6.6. Statistical evaluation of the factors and interactions comprising the factorial regression models

	Coefficient probability					
	BMP_{Exp}		BMP_{max}		μ_m	
Term	Coefficient	p-value	Coefficient	p-value	Coefficient	p-value
Constant	275.95	0.000	273.58	0.000	52.11	0.000
CN	12.58	0.000	13.13	0.000	-1.91	0.080
ISR	0.13	0.951	2.00	0.246	8.83	0.000
BC	-9.53	0.000	-9.86	0.000	3.48	0.003
CN*ISR	-4.69	0.047	-4.32	0.018	-1.42	0.185
CN*BC	1.69	0.705	0.15	0.927	1.28	0.231
ISR*BC	-0.95	0.671	-1.30	0.447	3.45	0.003
CN*ISR*BC	-1.98	0.380	-3.15	0.075	0.02	0.984

6.4.7 Influence of main factors and interactions

In this experiment, the factor ISR showed no statistically significant differences in BMP_{Exp} and BMP_{max} (**Table 6.6**). Moset et al. [123] reported that regardless of the substrate used, the BMP enhanced as the ISR increased over a range of 1.5-2.5, although not significantly. Similarly, De la Rubia et al. [266] studied the influence of ISR from different inoculum sources on the AD of the process water obtained from the hydrothermal carbonisation of dewatered sewage sludge. When using sewage sludge inoculum, they observed that the ISR had no significant difference over BMP. These reports agree with the negligible impact of ISR on BMP observed in this experiment. Regardless of the nature and complexity of the substrate used, the BMP was not affected by ISR if an appropriate range was selected (ISR 1.0-2.0).

ISR enhanced the response variable μ_m showing a statistically significant effect. The initial inoculum concentration is reported to influence the rate of substrate hydrolysis. Hence, higher ISR often results in faster anaerobic fermentation and as a consequence, an enhanced production rate [246]. Similarly, Raposo et al. [271] studied the impact of ISR 0.8-3.0 on the AD of sunflower oil cake. They observed a maximum production rate at ISR 2.0. However, unlike the linear trend observed in this study, they obtained higher μ_m at ISR 2.0>1.0>3.0>0.8>1.5>0.5.

The impact of microalgae and cellulose addition to changing the C/N ratio showed a significant difference over BMP_{Exp} and BMP_{max} but not over μ_m. The range of C/N ratio selected for this experiment started at an optimal ratio of 25 and moved downward to less favourable conditions. Hence, higher BMP yields

were obtained according to the following C/N ratio order 25>16>7. Similarly, Bohutskyi et al. [258] observed a synergistic effect of co-digesting algae and cellulose. They reported the highest methane yields and production rate at C/N ratios of 21 and 34 than lower ratios or even the mono-digestion of each substrate. Therefore, increasing the C/N ratio enhanced methane yields but did not influence the production rate.

BC load had a statistically significant effect on all variables ($p<0.05$). For BMP yield, the coefficient of BC load had a negative value, which indicates that increasing the BC load would result in lower BMP. This response contrasts with the one observed in the previous section, where BC drastically enhanced BMP yields at ISR 0.5-0.9 and C/N ratio 10-30. On the other hand, increasing BC load led to higher μ_m which partially agrees with previous experiments with the addition of this same oak wood BC in Chapter 5. The addition of BC at a load of 3 % during the AD of cellulose slightly enhanced BMP yields (7 %), whereas it doubled μ_m. Reports of BC addition during the AD of microalgae demonstrated the importance of BC load. Deng et al. [37] studied the AD of *Laminaria digitata* and *Saccharina latissima* at variable BC loads. For *L. digitata*, a BC addition of 0.06 and 0.125 % enhanced BMP yields and μ_m, whereas higher BC loads of 0.5 and 1.0 % reduced both parameters. Conversely, for the AD of *S. latissima* BC loads <0.5 % had no significant influence, whereas BC load of 0.5 and 1.0 enhanced both BMP and μ_m. The latter suggests that BC load influenced BMP yields and production rate, but the effect level was subjected to the substrate employed. Therefore, it is necessary to establish the optimum BC load for achieving the highest BMP yield and productivity for each potential substrate.

6.4.8 Optimisation of biomethane production

Graphical interpretation of the responses facilitates the examination of factors and interactions in regression models. Contour plots with a combination of the three factors C/N, ISR and BC were used for visualising the optimum areas for each response variable (**Figure 6.8**). As expected, the contour plots for BMP_{Exp} and BMP_{max} were similar. The stretching of the axis indicates that maximum BMP values can be obtained at C/N 22-25 and BC 0-1.5 regardless of the ISR. The contour plots for μ_m differed since maximum values were obtained at ISR of 1.7-2.0 and BC load of 1-3, regardless of the C/N ratio. The interaction plots for BMP showed that the C/N ratio played a major role (**Figures 6.8a** and **b**). This factor also interacted strongly with the rest, suggesting a predominant influence. In the case of μ_m, ISR exhibited the major effect, while its interaction with BC load was

significant on the response in agreement with the regression models (**Figure 6.8c**).
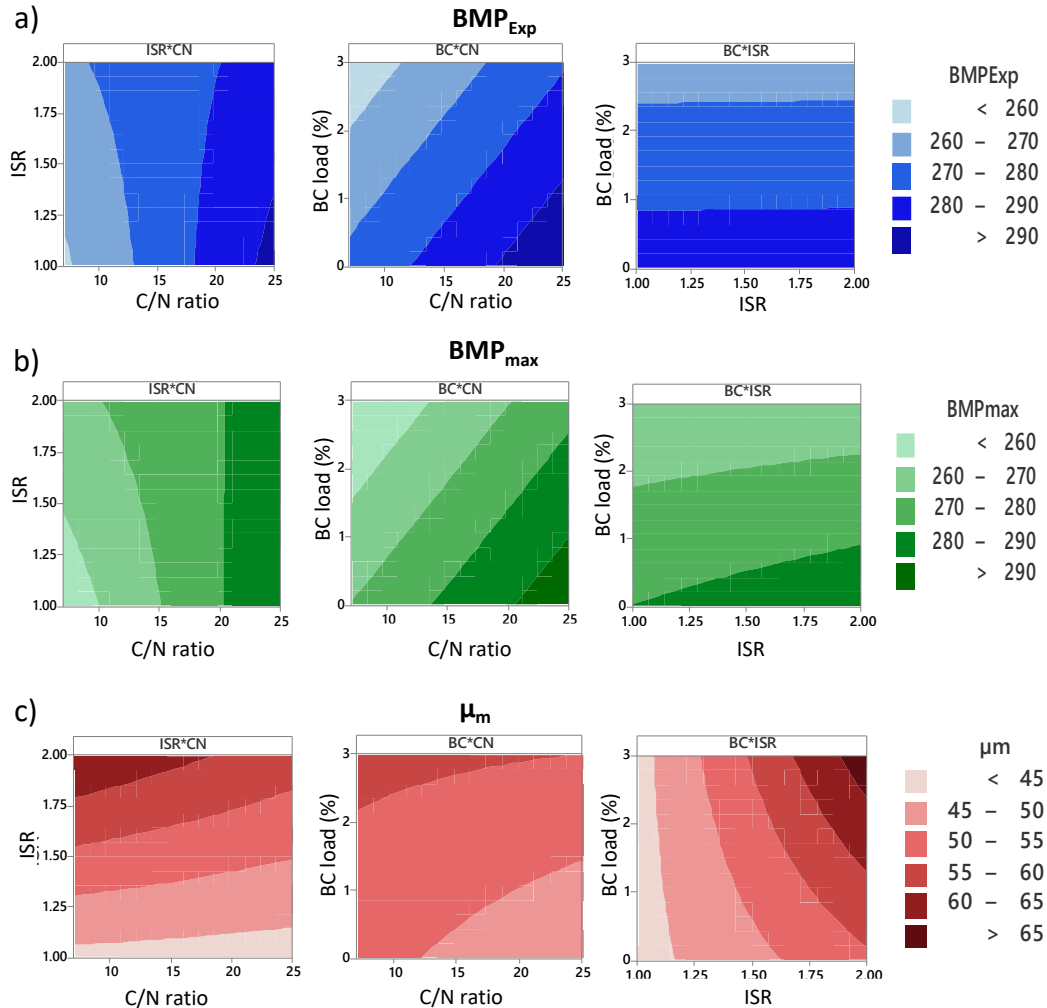
Figure 6.8. Contour plots for interaction effects and optimised area obtained by response surface regression for a) BMP_{Exp}, b) BMP_{max} and c) μ_m.

Factorial regression optimisation for methane production was carried out using the desirability (D) function by considering the response variables BMP_{EXp}, BMP_{max} and μ_m. D function assesses how the combined variables satisfy the response to find the best joint operational conditions for all response variables. D values are found between 0 and 1, where 0 represents an undesirable response, 1 a desirable and ideal response, and intermediate values indicate how adequate, or desirable are the optimised conditions. Thus, the goal of optimisation is to improve these parameters to achieve maximum desirability [128]. **Table 6.7** outlines the optimum conditions for the AcoD, consisting of C/N 25, ISR 2.0 and BC load 0.58. Further, response optimisation for obtaining

maximum biomethane allowed the prediction and evaluation at other C/N ratios. The regression model and response optimisation probed to be useful when working with variable C/N ratios due to variability in substrate composition and availability.

Table 6.7. Factorial regression optimisation by desirability function for the AD parameters BMP_{exp}, BMP_{max} and μ_m.

C/N	ISR	BC load (%)	BMP_{Exp} Fit	BMP_{max} Fit	μ_m Fit	D
25	2	0.58	294.40	293.12	56.67	0.62
16	2	0.34	283.32	284.22	55.58	0.53
7	2	0	272.90	274.93	54.01	0.43

Desirability (D) has a range of zero to one, where one represents the ideal case and zero indicates that at least one response is outside the acceptable limits

To corroborate the AcoD conditions obtained from the regression model and optimisation, a further AD experiment was performed. The D function stated that optimal methane generation could be achieved at a C/N 20, ISR 2 and BC load of 0.58 % (w/v) (**Table 6.7**). Thus, these conditions were further evaluated with the addition of the BC of study (OW-BC450) and another BC (WH-BC450) that in Chapter 5 proved to be equally satisfying. **Figure 6.9** shows the BMP values for the digestion of *C. vulgaris* and cellulose at C/N 20, ISR 2 and BC load 0 (control) and 0.58 % (w/v). The final yield for the non-BC control was 296 mL CH_4/g VS, whereas the addition of OW-BC450 and WH-BC450 resulted in 312 and 286 mL CH_4/g VS, respectively. The augmentation of OW-BC450 reached higher BMP than predicted (**Table 6.7**), although it is important to remark that another inoculum batch was used for these experiments. Nonetheless, the addition of 0.58 % of OW-BC450 improved the BMP by 6.4 % in comparison to the non-BC control, whereas the addition of WH-BC450 resulted in a similar BMP to the control. However, the addition of BC showed no significant difference from the control ($p > 0.05$) (t-test). The properties of OW-BC450 and WH-BC450 were described in Chapter 4, while their positive effect on AD was established in Chapter 5. The addition of 0.58 % of biochar achieved the highest BMP yields, supporting the optimised conditions.
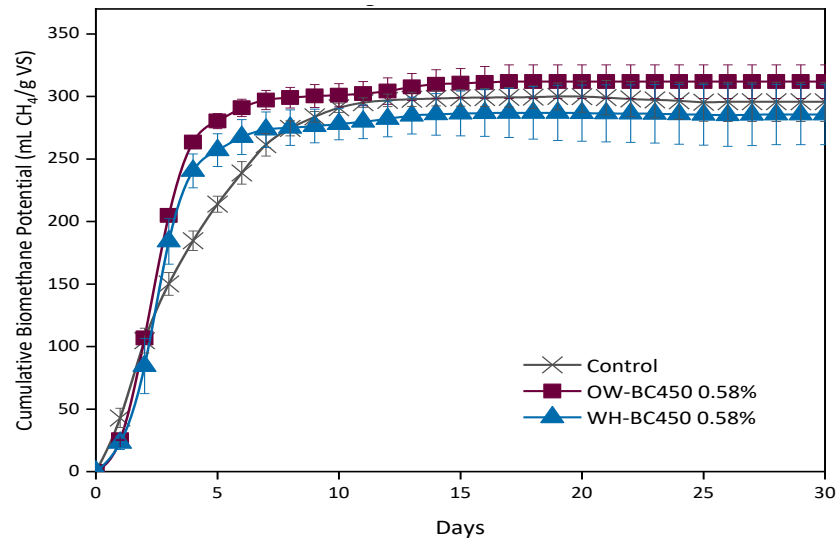
Figure 6.9. Biomethane production for anaerobic co-digestion of cellulose and *C. vulgaris* under optimal conditions C/N 25, ISR 2 and BC load 0.58 % (w/v).

6.5 Evaluation and optimisation for the anaerobic digestion of water hyacinth augmented with biochar

To determine the fermentation conditions and effect of biochar on the AD of raw water hyacinth, a full factorial 2^2 experimental design was performed. OW-BC450 was selected for this experiment given the positive effect stated in Chapter 5. WH sample, named WH-VBU, was collected from the Goyal Para Pond in West Bengal India, oven-dried, and size reduced to 2-5 mm. The two independent factors of the study were ISR (1-2) and BC load (0-3 %) with 3 replicates and 3 centre points as shown in **Table 6.8**. The hypothesis here tested was that the factors ISR and BC load can influence the specific methane potential as well as the degradation kinetics.

Table 6.8. Full factorial 2^2 experimental design used for the anaerobic digestion of water hyacinth.

Reactor no.	Orthogonal design		Actual value	
	ISR	BC load	ISR	BC load (%)
R1, R2, R3	-1	-1	1	0
R4, R5, R6,	-1	1	1	3
R7, R8, R9	0	0	1.5	1.5
R10, R11, R12	1	-1	2	0
R13, R14, R15	1	1	2	3

6.5.1 Biochemical methane potential

The cumulative BMP curves obtained by each condition within the factorial design for the AD of WH are shown in **Figure 6.10**. All systems started producing methane from day one exhibiting a similar behaviour up to the 8th day of digestion. Afterwards, some systems exhibited a quicker exponential phase, although they all reached the steady-state by the 20th day of digestion. The final BMP yields were found in a range of 165.3 to 208.9 mL CH_4/g VS, comprising up to 21 % of the difference among the conditions. Generally, BMP yields appeared to increase at lower ISR and BC load.
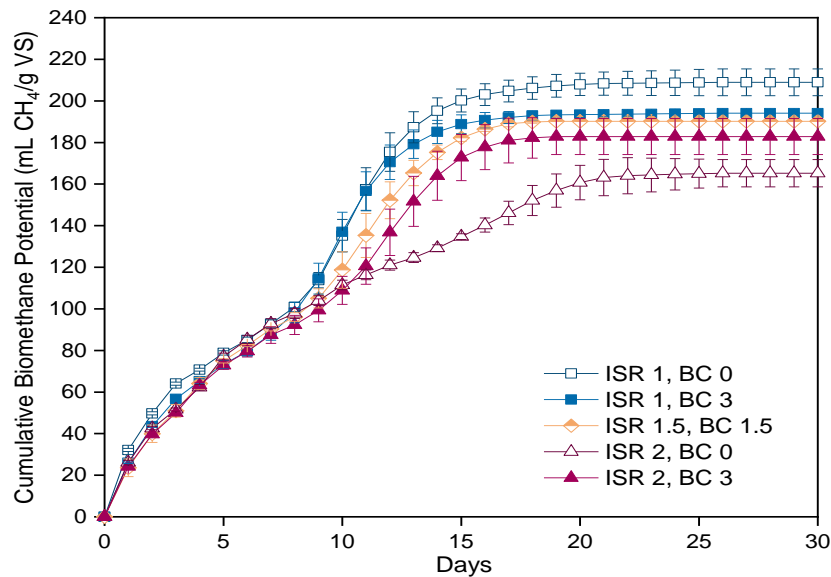
Figure 6.10. Biomethane production for the full factorial 2^2 experimental design used for the anaerobic digestion of VBU water hyacinth.

Replicates: all runs (n=3), blank (n=2).

6.5.2 Kinetic parameters

The values of BMP_{max} obtained from the digestion of VBU-WH gradually improved by reducing the ISR (**Table 6.9**). This trend could have been influenced by the greater energy and substrate demand for cellular maintenance and growth exerted by higher inoculum concentrations and in consequence higher ISR. The trend is less clear for the BC load, since higher values improved BMP_{max} at an ISR of 1, while the opposite was observed at an ISR of 2. On the other hand, μ_m appeared to be improved by reducing ISR and increasing BC load. The period

of lag phase was almost negligible for all systems, showing no apparent trend with the independent variables ISR and BC load.

Table 6.9. Kinetic parameters calculated with the modified Gompertz model for the full factorial 2^2 experimental design used for the anaerobic digestion of VBU water hyacinth.

Variables		Experimental		Modified Gompertz			
ISR	BC load (%)	BMP_{Exp} (mL CH_4/g VS)	BD (%)	BMP_{max} (mL CH_4/g VS)	μ_m (mL CH_4/g VS·day)	λ (days)	R^2
1	0	208.9	65.0	222.8	15.0	0.0	0.9740
1	3	194.1	60.4	204.4	15.3	0.2	0.9777
1.5	1.5	190.2	59.2	203.0	13.7	0.2	0.9807
2	0	165.3	51.4	171.8	10.0	0.0	0.9823
2	3	182.9	56.9	197.4	12.2	0.0	0.9790

6.5.3 Biodegradability

The anaerobic BD can be used to evaluate the performance of WH digestion. Firstly, the BMP_{Th} for VBU-WH was calculated by using Boyle's equation and expressed on a dry ash-free (daf) basis, corresponding to 383.4 mL CH_4/g VS. The BD for the conditions of the study ranged from 51.4 to 65 % (**Table 6.9**). However, the BD values showed no consistent trend concerning the independent variables.

6.5.4 Volatile fatty acids and pH

The amount of VFAs accumulated in the digestate at the end of the AD experiments was negligible for all experiments (**Figure 6.11**). The pH was measured at the beginning and the end of the digestion period. No pH adjustment was performed to evaluate the effect of ISR and BC load. All systems were maintained at a suitable pH initially at 7.6-7.7 and finally at 7.1-7.2 (**Figure 6.12**). In summary, the independent variables ISR and BC load did not affect the accumulation of VFAs and pH of the digester.
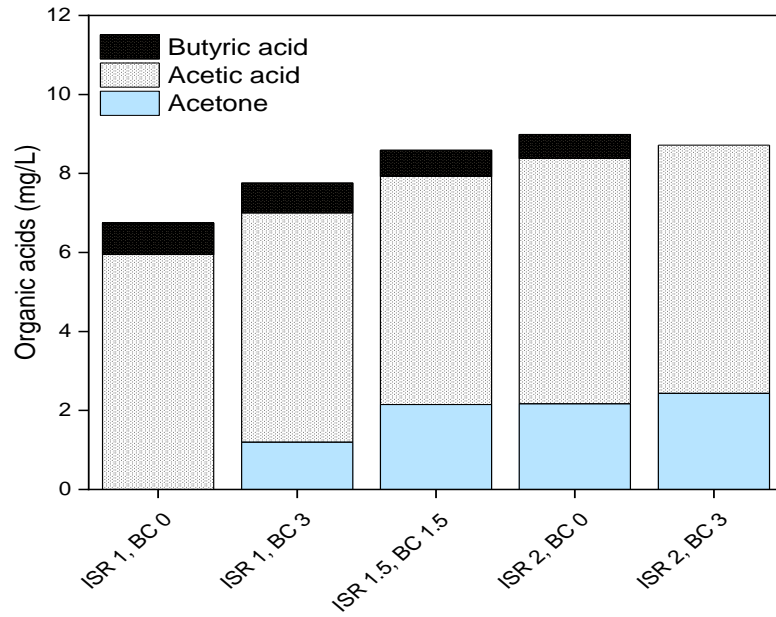
Figure 6.11. Volatile fatty acids accumulated at the end of the anaerobic digestion of VBU water hyacinth.
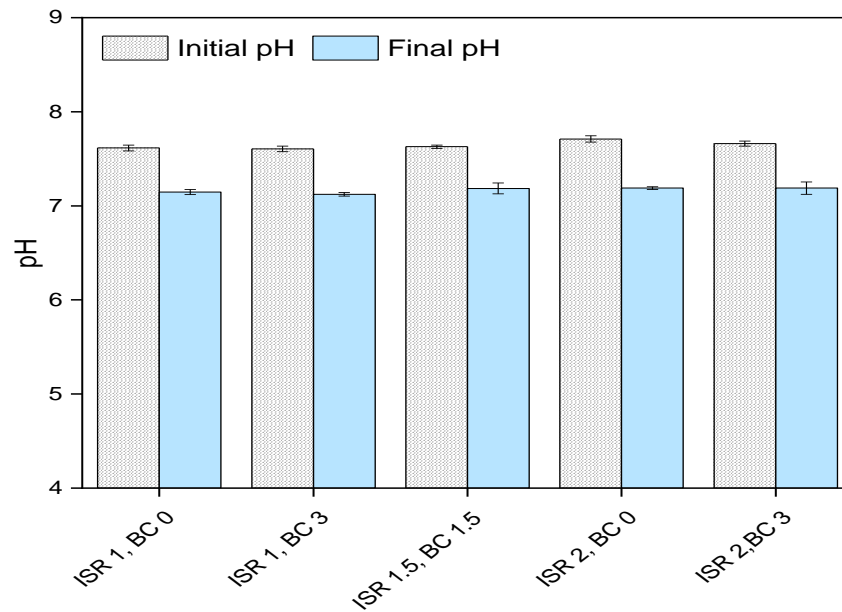
Figure 6.12. Measurement of pH at the beginning and end of the anaerobic digestion of VBU water hyacinth.

6.5.5 Regression model fitting

The parameters BMP_{Exp}, BMP_{max} and μ_m were selected as response variables for the analysis of the factorial design. The regression models obtained were statistically significant with $p < 0.05$ and F-value>F-critical at the 0.05 alpha level (**Table 6.10**). The R^2 exhibited by the factorial regression models for BMP_{Exp},

BMP_{max} and μ_m states that only 9.8-17.6 % of the variability cannot be explained by the models. The adjusted R^2 0.78-0.87 values were fitted to the actual size of the model and the number of factors, whereas the prediction R^2 0.68-0.79 indicates the variability that the model would explain during the prediction of new data. Therefore, the significance and fitting of the quadratic models to the experimental data were satisfactory.

Table 6.10. Analysis of variance for the factorial regression models for VBU water hyacinth anaerobic digestion.

	Analysis of Variance (ANOVA)		
Variable	BMP_{Exp}	BMP_{max}	μ_m
R^2	0.9017	0.8627	0.8243
Adjusted R^2	0.8749	0.8253	0.7763
Prediction R^2	0.7929	0.7166	0.6797
F	33.64	23.04	17.20
Model p-value	0.000	0.000	0.000
Lack of fit p-value	0.521	0.447	0.479

The regression models for BMP_{Exp}, BMP_{max} and μ_m, are outlined in **Equations 6-4**, **6-5** and **6-6**, respectively. The significant specific coefficients (p<0.05) for the factors and interactions were part of the regression models (**Table 6.11**). The independent variable ISR was significant for all responses, although the negative coefficients suggested that increasing ISR could result in lower BMP yields and kinetic parameters. However, the independent variable BC load had no significant effect on the responses. Given the significant influence of the ISR*BC interaction over the variables BMP_{Exp} and BMP_{max}, the coefficient BC load was maintained for these regression equations due to the hierarchy principle [127].

$$BMP_{Exp}= 188.3 -13.7*ISR + 0.7*BC + 8.1\ ISR*BC \qquad \text{Equation 6-4}$$

$$BMP_{max}= 199.9 -14.5*ISR + 1.8*BC + 11.0*ISR*BC \qquad \text{Equation 6-5}$$

$$\mu_m= 13.2 -2.0*ISR \qquad \text{Equation 6-6}$$

Table 6.11. Statistical evaluation of the factors and interactions comprising the factorial regression models for VBU water hyacinth anaerobic digestion.

| Term | Coefficient probability | | | | | |
| | BMP_{Exp} | | BMP_{max} | | μ_m | |
	Coefficient	p-value	Coefficient	p-value	Coefficient	p-value
Constant	188.3	0.000	199.9	0.000	13.2	0.000
ISR	-13.7	0.000	-14.5	0.000	-2.0	0.000
BC	0.7	0.667	1.8	0.429	0.6	0.055
ISR*BC	8.1	0.001	11.0	0.001	0.5	0.145

In this experiment, it was observed that increasing the ISR affected the response variables BMP_{Exp}, BMP_{max} and μ_m. Conversely, most reports state that higher initial ISR results in faster anaerobic fermentation and enhanced BMP yields [267,276]. Others state that increasing the ISR within an adequate range offers no difference [246,277]. Finally, there are reports with variable or ambiguous results. For instance, De la Rubia et al. [266] studied the influence of ISR from different inoculum sources: granular biomass from wastewater reactors treating a brewery; granular biomass from sugar beet industries; and a flocculent inoculum municipal sewage sludge digestate. When increasing the ISR, the brewery inoculum enhanced BMP, whereas the sugar beet reduced. Conversely, the digesters fed with sewage sludge were not significantly affected by ISR variations. Holliger et al. [122] advised the use of inoculum with very low endogenous methane production, and low ISRs for the AD of substrates that result in moderate BMP. This advice could be applied to the conditions used for this experiment since the sewage sludge blank exhibited very low endogenous BMP and the AD of water hyacinth offered moderate BMP and BD.

Even though BC addition improved BMP yield and μ_m, especially at an ISR of 2 (**Table 6.11**), the effect of BC was not statistically significant. Similarly, Qin et al. [35] studied the impact of four woody biomass BCs (pine wood, oak wood, applewood and bamboo) and two agricultural waste BCs (rice straw and corn stalk) produced at 500 °C. They also employed AMPTS systems with a substrate comprised of anaerobic sludge and glucose 9 g/L, ISR 0.18, and biochar 0.5 % (w/v). The addition of all BCs reduced the lag phase, while systems augmented with woody BCs enhanced BMP yields by 2-15 % and μ_m by 40-50 %. However, there was no significant difference in BMP values between the control and the systems with agricultural waste BCs. These BCs exhibited a considerably lower surface area than woody BCs. Hence, they suggested that a small surface area indicated a poor conductivity for the BCs, which failed to promote the

attachment of cells and DIET interactions. However, it has been reported that the electrical conductivity of the BCs is not a rate-limiting factor for its role in the DIET process and other properties could be responsible for enhancing the methanogenic rate [48,91,92].

Furthermore, Deng et al. [37] proposed a cascading circular bioenergy system by incorporating pyrolysis and anaerobic digestion. Waste wood was pyrolysed at 700 °C in a rotatory kiln operated by a pyrolysis plant (Premier Green Energy). The primary use of the BC was for augmentation into AD, while the remaining BC and syngas were combusted for providing heat to the pyrolysis reactor. The resulting BC was sieved to a particle size of 75-500 μ_m and characterised with a SA 161.5 m^2/g, pH 8.95-9.22, TS 87.8 %, and electrical conductivity (EC) 252 $\mu S/cm$. They aimed to assess the effect of BC on the AD of seaweed wet feedstock. They used similar AD conditions to this work, with a substrate concentration of 5 g VS/L, ISR 2 and BC load of 0.031-1 % (w/v). They stated the importance of BC load since BMP was only enhanced with the addition of BC 0.031 and 0.062 %, whereas higher BC loads led to lower BMP than the control. Further addition of BC inhibited methanogenesis, which has been previously attributed to substrate sequestration and changes in the diversity of microorganisms. Small BC loads had a favourable effect on propionic acid by accelerating both its production and degradation, whereas it did not affect butyric acid. They did not observe a buffering effect provided by the BC, although the pH was maintained within an adequate range. It is important to remark that this BC was pyrolysed at 700 °C which would result in a highly aromatic structure. Whereas in the previous chapters, it was pointed out the advantage of lower temperature BCs for AD amendment. In summary, the boost of BMP with the addition of BC varies significantly and for each report, the optimal char loading is dependent on the BC properties and the selected feedstock.

The coefficient for the interaction of ISR*BC load for the variables BMP_{Exp} and BMP_{max} were considerably high, almost of the order of the individual ISR coefficient. This suggests a correlated effect of both ISR and BC load over the BMP yields. Similarly, Cai et al [233] investigated the effect of BC load and ISR on AD of food wastes. They observed that BC addition generally improved AD performance, while at an ISR of 2, BC addition had little effect on BMP. By reducing the ISR to 1 and 0.8, the BMP performance was drastically improved by BC addition. They suggested a correlation between the amount of BC and the concentration of inoculum (ISR) for establishing the effectiveness of BC. In addition, they attributed the positive effect of BC to the immobilisation of cells, the promotion of biofilm growth, and the ability to facilitate the DIET process.

6.5.6 Optimisation

Figure 6.13 shows the contour plots for the graphical interpretation of the variables ISR and BC load over the AD performance. The response variables BMP_{Exp}, BMP_{max} and μ_m were favoured by ISRs closer to 1. The stretching of the Y-axis indicated that maximum BMP_{Exp} and BMP_{max} values can be obtained at BC loads of 0-1.8 and 0-0.5 %, respectively. Whereas μ_m was favoured at all BC loads and more significantly at the highest loads close to 3 %. It can be concluded from these plots that ISR had a major role in the response variables, while its interaction with BC load was significant on the responses BMP_{Exp} and BMP_{max} as stated in the regression models (**Table 6.11**).
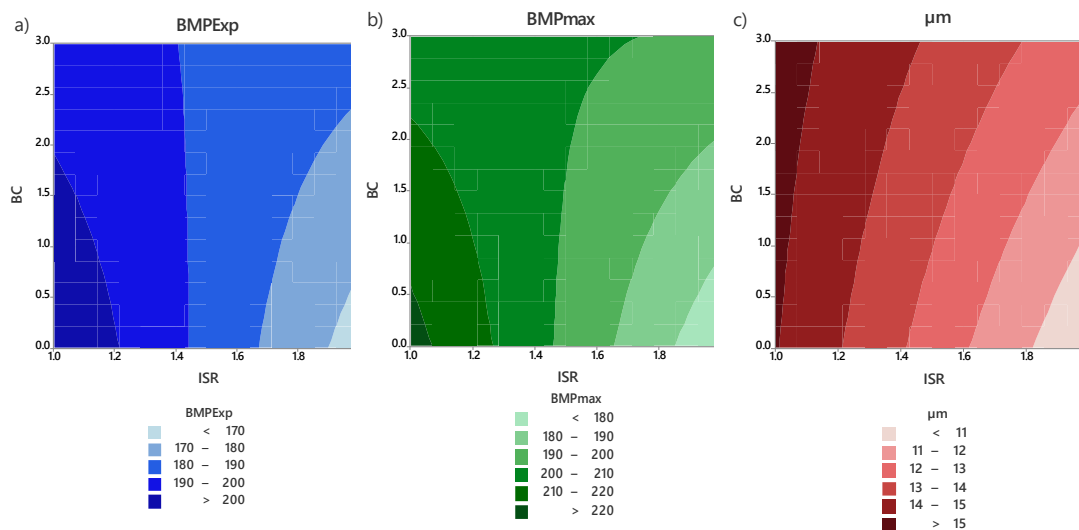
Figure 6.13. Contour plot for the optimised area of the methane parameters.

Factorial regression optimisation for methane production was carried out using the desirability function by considering the response variables BMP_{EXp}, BMP_{max} and μ_m. **Table 6.12** shows the optimum conditions obtained from the regression analysis with a D-value of 0.88, which indicates that all responses were predicted within acceptable limits. Hence, the AD of water hyacinth at an ISR of 1 and BC load of 0 % could provide the highest possible BMP.

Table 6.12. Factorial regression optimisation for the AD of water hyacinth.

Selected parameters: BMP_{exp}, BMP_{max} and μ_m.

ISR	BC	BMPExp Fit	BMPmax Fit	μ_m Fit	D
1	0	209.40	223.56	15.07	0.88

Composite desirability (D) has a range of zero to one, where one represents the ideal case and zero indicates that at least one response is outside the acceptable limits.

The present study showed that the AD of water hyacinth was improved by ISR with values close to 1. Even though BC addition offered no statistically significant effect on AD performance, it was observed that BC loads <1.5 % favoured BMP yields. Whereas μ_m was mainly benefited by BC addition, particularly at higher loads ~3 %. This behaviour contrasts with the results obtained for the experimental design for the AcoD of *C. vulgaris* and cellulose, where ISR was not statistically significant over BMP and low BC loads enhanced digestion. Such variations between complex feedstocks suggest the necessity to establish the best AD conditions for each substrate, including the addition of biochar.

6.5.7 Effect of biochar load

In the previous optimisation section, the best digestion conditions were established at an ISR of 1 and BC load of 0 %. Nonetheless, the contour plots suggested a positive influence of BC loads <1.5 % over the BMP and particularly μ_m. To corroborate, the further digestion of VBU-WH at ISR 1 with the addition of OW-BC450 at 0.25, 0.5, 0.75 and 1.0% (w/v) was performed. In addition, a control for the digestion of 5 g VS/L of VBU-WH as a substrate without BC was run in parallel (**Figure 6.14**).

The BC load of 0.5 % reached slightly higher BMP yields (4 %) and improved μ_m by 1.7 times the control. Conversely, the addition of 0.25, 0.75 and 1% of OW-BC450, exhibited a detrimental effect on BMP yields. Similarly, Shen et al. [173] added 0.8-1.5 % of corn stover BC produced by fast pyrolysis at 710 °C during the AD of sludge. At all BC loads, the final BMP was only ~1 % higher than the control, whereas the production rate was favoured principally at 0.8 % BC load. Linville et al. [232] reported a similar behaviour for the AD of food waste amended with fine walnut shell biochar (FWSB) produced at 900 °C. Small amounts of FWSB biochar (0.4 %) improved AD, while higher doses (0.7%) exhibited an inhibitory effect.
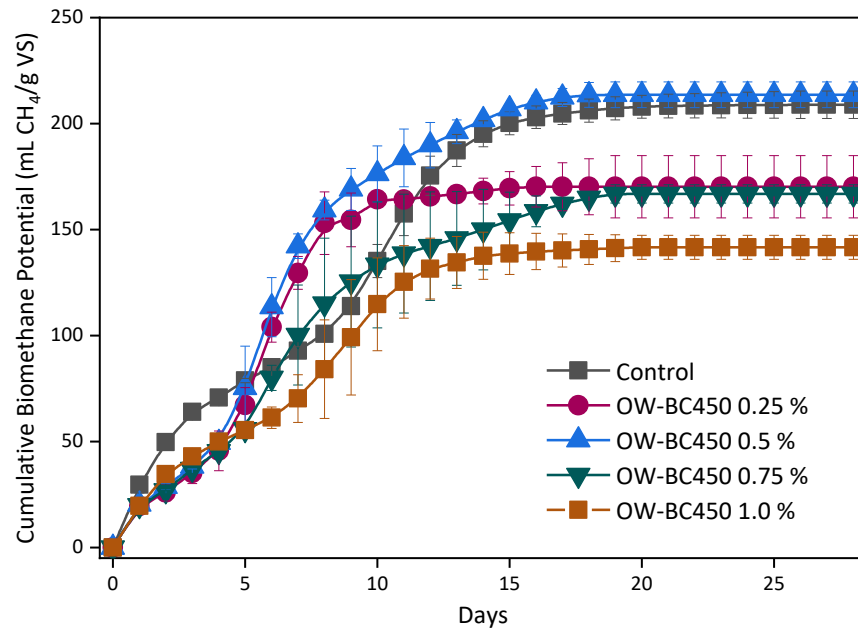
Figure 6.14. Cumulative biomethane production during anaerobic digestion of VBU-WH substrate augmented with OW-BC450 at variable concentrations.

Replicates: all runs (n=2), VBU-WH control (n=2), inoculum blank (n=2).

6.6 Anaerobic digestion of water hyacinth feedstocks from different sources

WH represents a major problem in many locations and is prevalent across Sub-Saharan Africa and India. Due to a current collaborative project (BEFWAM-Bioenergy, fertilisers, and clean water from Invasive Aquatic macrophytes (BB/S011439/1), extensive samples of WH are available from different regions in India and Uganda. Therefore, this section has investigated the AD behaviour of four WH samples from different sources, three from India and one from Uganda.

6.6.1 Anaerobic digestion of water hyacinth substrates

Tables 6.13 and **6.14** describe and summarise the chemical and biochemical composition of the WH substrates, respectively. In agreement with the AD performance for VBU-WH, further WH substrates were digested at an ISR 1 and amended with BC. **Figure 6.15** shows the cumulative BMP obtained from the AD of untreated WH feedstocks augmented with OW-BC450 at BC loads of 0, 0.5 and 1.0 %. All systems exhibited a rapid initial methane generation. The final BMP yields for the controls without BC were significantly different (p<0.05) (ANOVA),

exhibiting the following order VBU-WH > MM-WH > PW-WH > UG-WH. These differences could be attributed to the chemical composition of the WH samples since the highest BMP was achieved by the WH samples with the highest C/N ratio (**Table 6.13**).

Table 6.13. Description and chemical composition of untreated water hyacinth feedstocks. Data produced by BEFWAM group.

Water hyacinth substrate	Sampling site	VM (%) db	FC (%) db	Ash (%) db	C (%)	H (%)	N (%)	O (%)	S (%)	C/N ratio	BMP$_{Th}$ (mL CH$_4$/g VS)
VBU-WH	Goyal Para pond, India	73.43	10.39	16.18	34.24	4.09	1.81	43.68	0	17.8	383.4
MM-WH	Mula Mudtha River, India	76.82	15.35	7.83	36.26	4.64	2.95	48.09	0.23	12.3	331.8
PW-WH	Pawana River, India	73.99	12.30	13.71	32.99	4.63	3.11	45.07	0.49	10.6	351.3
UG-WH	Lake Victoria, Uganda	85.35	0.02	14.63	36.10	3.14	2.49	43.55	0.09	14.5	352.6

VBU Visva Bharati University, MM Mula Mudtha, PW Pawana, UG Uganda, VM volatile matter, FC fixed carbon, BMP$_{Th}$ theoretical methane potential.

Table 6.14. Biochemical composition of untreated water hyacinth feedstocks. Data produced by BEFWAM group.

Water hyacinth substrate	Cellulose (%)	Hemicellulose (%)	Lignin (%)	Oils (%)	Protein* (%)	Free Sugars** (%)
VBU-WH	32.1	25.5	4.7	0.44	8.42	8.69
UG-WH	25.1	22.6	6.8	1	12.39	11.75

*Determined by Kjedahl conversion (factor 4.64); ** Determined by difference.
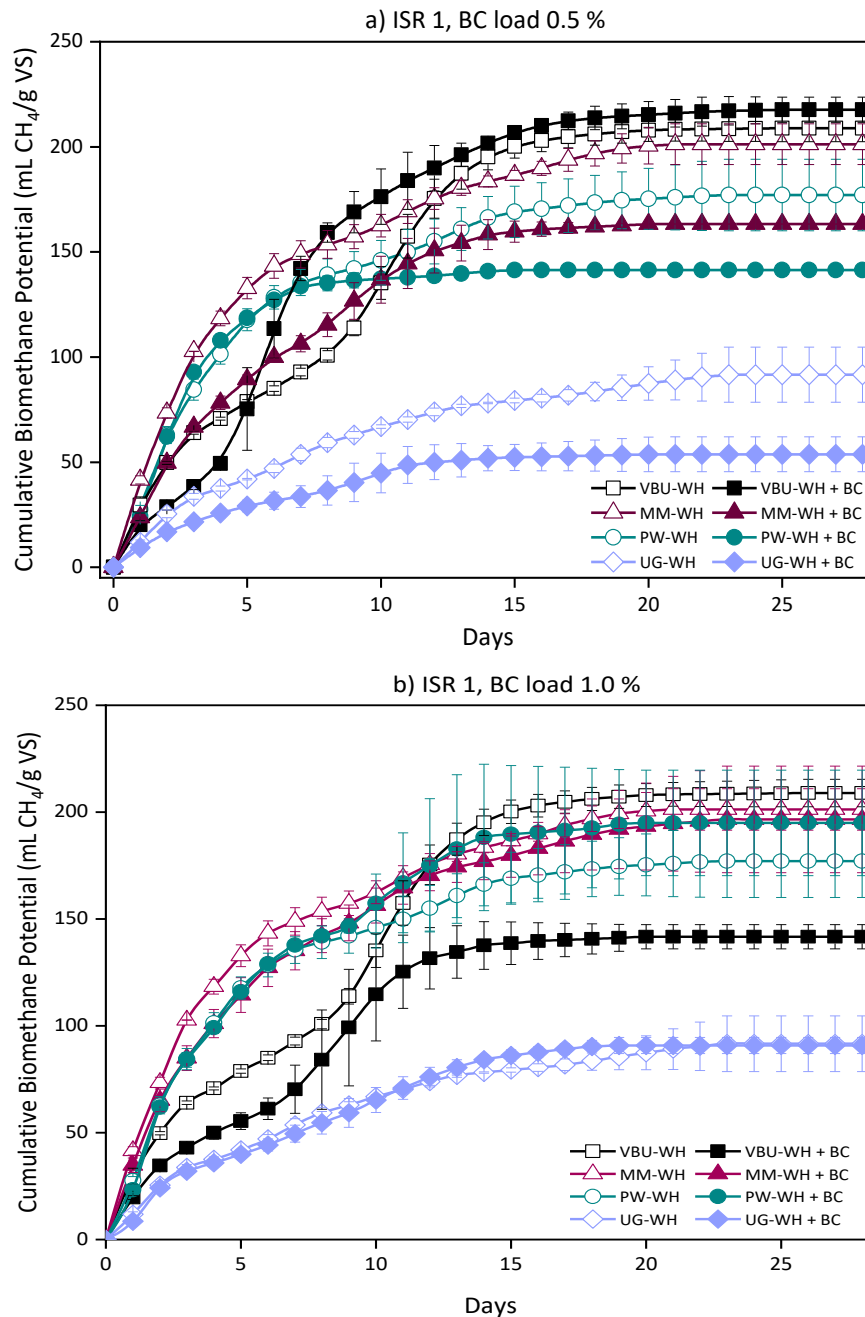
Figure 6.15. Cumulative biomethane potential during the anaerobic digestion of water hyacinth feedstocks with and without the addition of OW-BC450 at biochar load: a) 0.5 % and b) 1 % (w/v), (n=3).

The biochemical composition also seemed to influence AD performance. For instance, VBU-WH showed more cellulose and hemicellulose, but less lignin than the UG-WH. The cellulosic polymers are easily hydrolysed and converted into methane. Whereas increasing the recalcitrant lignin content often restricts the access to the carbohydrates, affecting thus their fermentation [278]. Furthermore, UG-WH exhibited a larger content of protein and oils than the VBU-

WH, which could have been detrimental to AD. A large protein content would result in more inhibitory ammonia released into the digestate, whereas the slower degradation rate of lipids leads to their accumulation, which is reported to block the mass transfer process for the methanogens [256,279]. In summary, the best performance for the digestion of VBU-WH in comparison to UG-WH could be due to a more accessible, degradable, and balanced composition.

Similarly to the previous section, the addition of OW-BC450 at 0.5 % improved the BMP for the digestion of VBU-WH by 4%, whereas it reduced the BMP for the other WH substrates by 19-41 % (**Figure 6.15a**). Increasing the BC load at 1 %, on the other hand, increased the BMP for PW-WH by 10 %, although it reduced the digestion of MM-WH, UG-WH and VBU-WH by 2, 1 and 32 %, respectively (**Figure 6.15b**). Even though all WH substrates were fundamentally alike, the influence of BC load on BMP performance differed among them.

6.6.2 Kinetic parameters

Table 6.15 shows the kinetic parameters obtained by fitting the experimental BMP data to the modified Gompertz model. Methane generation started on day one, hence, the lag phase was negligible for all systems. The addition of OW-BC450 0.5 % improved the μ_m for VBU-WH and PW-WH by 1.7 and 1.6 times the control. Increasing BC load at 1 % still improved μ_m, although to a lesser extent. Conversely, the BC load of 0.5 % reduced the μ_m for MM-WH and UG-WH, whereas increasing the BC to 1 % exhibited no difference with the control. Nevertheless, BC addition had no significant effect on the kinetic variables ($p>0.05$) (ANOVA).

6.6.3 Biodegradability

BMP_{Th} yields were calculated based on the chemical composition of the WH substrates (**Table 6.13**) by using Boyle's equation and expressed on a dry ash-free (daf) basis. The BMP_{Th} values for VBU-WH, MM-WH, PW-WH and UG-WH were estimated at 383.4, 331.8, 351.3 and 352.6 mL CH_4/g VS, respectively. The BMP_{Th} for each WH substrate was used to establish the BD of the AD experiments. The BD values ranged from 25.8 to 60.7 % (**Table 6.15**). The ability to biodegrade a substrate is limited by the complexity, toxicity, and bioavailability of the molecule. For instance, MM-WH showed some of the highest BMP yields and the lowest BMP_{Th}, hence the considerably higher BD (59.2-60.7 %). Once again, BC addition had no statistically significant effect on the BD of WH substrates ($p>0.05$) (ANOVA).

Table 6.15. Kinetic parameters calculated with the modified Gompertz model for the anaerobic digestion of water hyacinth feedstocks.

	Experimental		Gompertz model			
	BMP_{exp} (mL CH_4/ g VS)	BD (%)	BMP_{max} (mL CH_4/ g VS)	μ_m (mL CH_4/ g VS·day)	λ (days)	R^2
VBU-WH	208.9	54.5	222.8	15.0	0.0	0.974
VBU-WH + BC 0.25%	170.4	44.4	172.3	26.9	1.9	0.983
VBU-WH + BC 0.5%	217.7	56.8	217.4	24.9	1.5	0.991
VBU-WH + BC 0.75%	173.3	45.2	179.3	17.4	1.0	0.990
VBU-WH + BC 0.1%	141.7	37.0	145.1	13.0	0.4	0.978
MM-WH	201.3	60.7	196.6	20.2	0.0	0.967
MM-WH + BC 0.5%	163.3	49.2	164.6	15.8	0	0.989
MM-WH + BC 0.1%	196.6	59.2	194.5	17.5	0.0	0.981
PW-WH	177.1	50.4	172.9	19.8	0.0	0.977
PW-WH + BC 0.5%	141.4	40.2	140.5	32.6	0.2	0.995
PW-WH + BC 1%	194.9	55.5	194.6	19.9	0.0	0.978
UG-WH	91.6	26.0	93.4	6.8	0.0	0.987
UG-WH + BC 0.5%	53.7	15.2	54.4	5.0	0	0.983
UG-WH + BC 1%	90.8	25.8	94.2	7.0	0.0	0.986

6.6.4 Volatile fatty acids and pH

Figure 6.16 shows the intermediary alcohols and VFAs accumulated at the end of the digestion. The intermediaries mostly found were methanol, acetone, ethanol, and acetic acid, although their total amount was below 40 mg/L for all experiments, which could be considered negligible. In agreement with the behaviour observed on the previous DoE, increasing the BC load affected the digestion of VBU-WH and MM-WH, resulting in a greater VFA accumulation. These two WH substrates exhibited the highest C/N ratios, 17.8 and 12.3, respectively. This is of relevance since the production and accumulation of VFAs during AD is highly related to the nature of the employed feedstock, particularly the C/N ratio [20]. In the case of PW-WH, the addition of BC 0.5 % exhibited a greater acetone and ethanol accumulation, in agreement with the lower BMP yields in comparison to the control. By comparing the effect of BC in such different and complex substrates, it was not possible to outline an evident trend, although the concentrations of alcohols and VFAs were too low to have a significant effect on the systems.
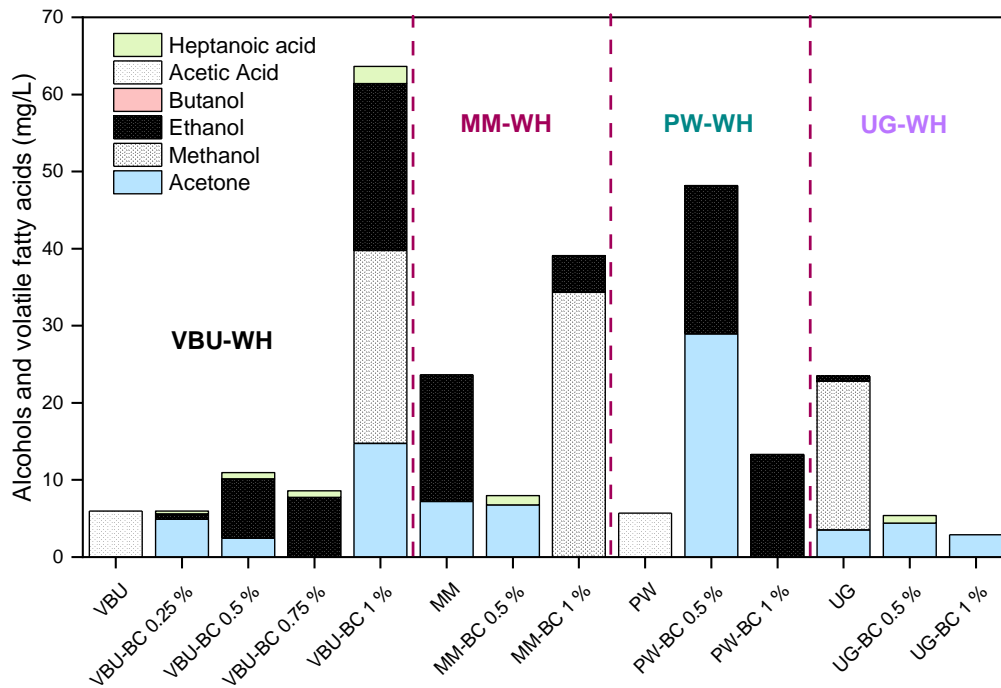
Figure 6.16. Volatile fatty acids and alcohols accumulated at the end of the anaerobic digestion of water hyacinth substrates as analysed by GC.

Furthermore, the pH was measured at the beginning and the end of the digestion period, without pH adjustment. All systems started at a suitable pH of 7.5-7.8 and suffered little variation by the end of the digestion with values ranging from 6.8-7.4 (**Figure 6.17**). In summary, the digestion of the different WHs resulted in minimal accumulation of VFAs and pH variation without exhibiting a significant difference due to BC addition.
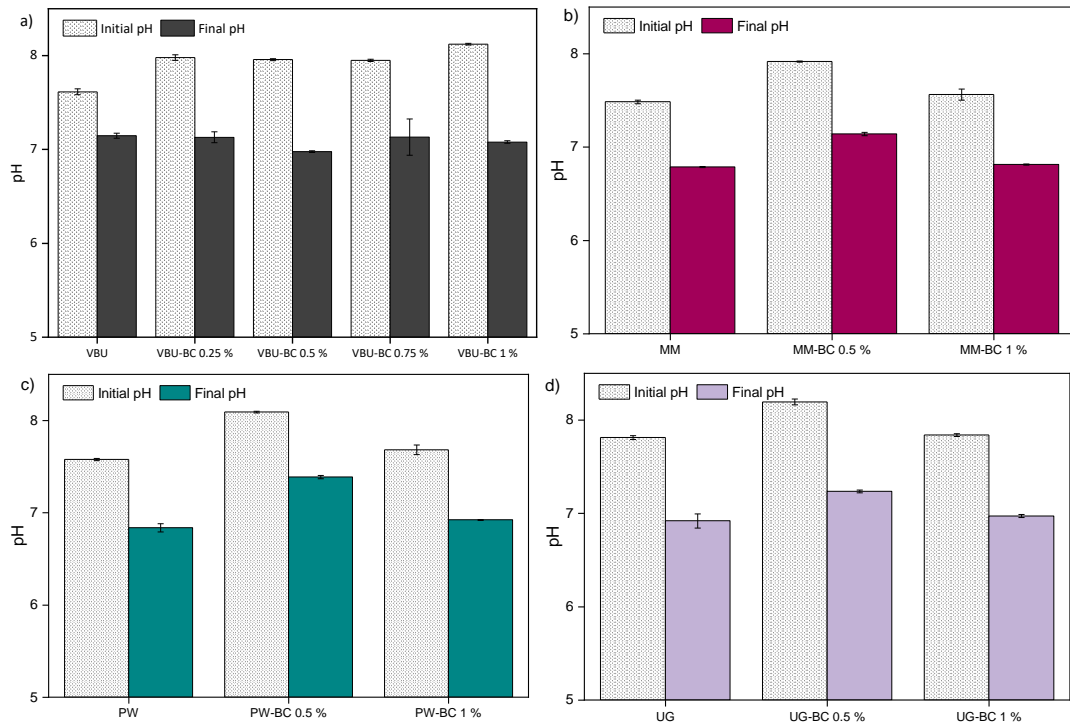
Figure 6.17. Measurement of pH at the beginning and end of the anaerobic digestion of the water hyacinth substrates augmented with biochar. A) VBU-WH; b) MM-WH; c) PW-WH; d) UG-WH.

6.7 Conclusions

This study demonstrated the importance of the C/N ratio, ISR and BC load during the AcoD of *C. vulgaris* and cellulose. BC addition drastically improved the low biomethane yields achieved under unfavourable digestion conditions (ISR 0.5-0.9). Under these conditions, the BC provided a pH buffering effect and promoted the consumption of VFAs for methane generation. The latter supports that BC addition could fulfil the requirement of an alkaline source, avoid drastic changes in pH and maintain the stability of the AD process under the conditions here studied.

The further factorial design and regression models highlighted the beneficial role of BC at higher C/N ratios, suggesting that the BC effect is highly dependent on the digestion conditions. Lower BC loads favoured the BMP yields while increasing the BC load favoured μ_m, hence the subsequent optimisation analysis facilitated defining the ideal conditions. Regardless of the complexity of the substrate here used, the final BMP was not affected by ISR if an appropriate range was selected (ISR 1.0-2.0). As the C/N ratio is reduced, the BC load should also be reduced to achieve better performance.

The regression model for the AD of WH established the importance of the ISR in the process, although it suggested that increasing ISR could result in lower BMP yields and μ_m. The BC load had no significant effect on the production of methane, although it showed a positive interaction with the ISR. The further optimisation stated that an ISR closer to 1 was ideal for the AD of WH. Whereas a BC load <0.5 % could favour the BMP yields and BC loads ≤3 % could improve μ_m. Nonetheless, the factorial regression optimisation with the desirability function stated that the AD of WH at an ISR of 1 and BC load of 0 % could provide the highest possible BMP. The AD of WH samples collected from different locations in India and Uganda provided variable BMP yields. For these substrates, BC addition had little effect on BMP performance, and in some instances, it even reduced methane generation.

The effect of ISR and BC load was contradictory between the co-digestion *of C. vulgaris* and cellulose and the AD of WH samples. Such variations between complex feedstocks suggest that the BC effect is influenced by the digestion conditions and employed substrate. Hence, it is necessary to create an understanding of these relationships to establish the best AD conditions for each system of study.

Chapter VII

Principal component analysis of biochar augmentation on anaerobic digestion

7.1 Overview

Chapter 7 established the main factors behind the amendment effect of biochar in methane generation, by evaluating both publications and the results from this research. These were selected based on the data they provide: production of biochar, the digestion conditions, and the effect they had on AD. The BMP and μ_m values evaluated in this chapter indicated how much the addition of a given BC affected them, in comparison to their corresponding control. A positive effect of BC addition was observed, being more considerable for μ_m and to a lesser extent to BMP yield. These changes were evaluated individually against different factors, including operating conditions (substrate, ISR and BC load), pyrolysis temperature, and biochar properties (ash content and O:C ratio). The relevance of these parameters was identified and corroborated by principal component analysis (PCA).

Woody derived BCs, produced at 450-550 °C, containing an ash content of 3.1-6.3%, and O:C ratio of 0.20, was responsible for having the greatest positive impact on AD. The amount of BC added to the digesters influenced AD performance. Increasing BC loads favoured μ_m, although this could be detrimental to the BMP yields. Therefore, BC loads of approximately 0.4-0.6 % (w/v) were optimal for improving AD performance.

The substrate used for methane production and the operational conditions influenced the effect of the BC on AD. For easily hydrolysed substrates, the benefits of BC addition were more significant at low ISR. Moreover, the BC provided certain protection from inhibitory concentrations of ammonia during the digestion of biomass rich in protein. On the other hand, BC had a negligible impact on the digestion of aquatic biomass such as water hyacinth and seaweed, whereas it highly improved the mono and co-digestion of complex or inhibitory substrates, such as microalgae bio-oil aqueous phase, and citrus peel waste.

Furthermore, it could be argued that the BC amendment in AD was more substantial under stressful conditions.

7.2 Introduction

The role of BC in amending the stressful factors affecting the performance of AD has been a topic of considerable discussion. This area of research has focussed largely on the role of BC in providing a series of benefits to AD. It is generally accepted that BC can act as a support for the immobilisation of cells from anaerobic sludge; provide a buffering effect; adsorb metabolites; and intermediate during the direct interspecies electron transfer (DIET) process, as described in Chapter 2. Also, properties, such as surface functionality and surface area (SA) may influence the effectiveness of BC in AD, as discussed in Chapter 5.

Some publications have tried to improve the understanding between BC and its effect on AD. Pan et al. [20] suggested that BC can couple the biological and chemical transformations occurring during AD, resulting in better performance and stability. They concluded that the main impacts of BC addition on AD included the reduction of lag phase (λ), the promotion of hydrolysis and acidogenesis-acetogenesis, buffering acid stress, stabilisation of methanogenesis, and enhancing of BMP yields and production rate (μ_m) and promoting syntrophic interactions. They suggested that BC with a smaller particle size appeared more favourable for AD and the excessive addition of BC could be detrimental to methanogenesis. Deng et al. [280] stated that AD improvement differs significantly depending on BC properties, although this correlation is not understood yet. They suggested that BC with a moderate level of aromaticity and abundance of oxygen and nitrogen functional groups would likely stimulate DIET interactions and improve methane generation, consistent with the results from Chapter 5.

Wang et al. [281] supported the role of BC as an adsorbent material during AD. The ability to improve methanogenesis under high concentrations of ammonium has been initially attributed to the cation exchange capacity (CEC), and the H-bonds between the ammonium ions and the functional groups of the BC. However, the role of ammonia in AD could be influenced by other factors, such as the competition and precipitation with some common ions found in water (i.e. Ca^{2+}, CO_3^{2-}, Na^+ and SO_4^{2-}) [281]. Other works have stated that the capacity of the BC to amend ammonia inhibition could be limited to the total ammonia nitrogen (TAN) concentration. Lü et al. [172] observed that the capacity of BC to adsorb ammonia is exceeded at concentrations above 7 g TAN/L, after this value the

input of BC becomes insignificant. It is under this higher concentration of TAN that the microbial community has the primary responsibility of regulating TAN since some microorganisms, such as *Methanosarcina*, can acclimate to the higher TAN values. Even though BC can adsorb ammonia and amend AD conditions, the latter suggests that this capacity is finite [172].

It has also been suggested that the potential of BC in AD is subjected to the digestion temperature. For instance, Shen et al. [148] compared the addition of pine and oak wood BCs for the mesophilic (37 °) and thermophilic (53 °C) AD of sludge. The BMP was considerably higher for the thermophilic systems, due to the accelerated reaction rate coefficient (k) at a higher temperature. For the thermophilic systems, the methane production with and without BC addition offered no variation, whereas, under mesophilic conditions, only the oak wood BC improved methane yields. Similarly, Li et al. [229] studied the thermophilic (55 °C) AD of cardboard amended with BC. They observed that the BMP with BC loads of 0.3-1 % were equal to the control, whereas higher loads of 1.5-5.0 % decreased the yield. Hence, it can be argued that BC has a better impact on mesophilic than thermophilic AD. Because of the latter and the fact that all experiments from this research were performed at 37 °C, the evaluation of this Chapter will focus exclusively on mesophilic fermentation.

Some buffering agents commonly used in AD are $CaCO_3$, $NaHCO_3$, and lime mud. However, they add cost and are reported to affect the microbial communities. On the other hand, the potential of BC as a buffering agent has been reported repeatedly. This has been attributed to the rise in the pH and increased methanogenesis at high concentrations of organic acids [281]. The buffering capacity is derived from the functional groups, ash-inorganic alkalis, and organic alkalis within the BC. Hence, the BC provides a buffering effect, while mediating redox reaction via DIET that result in greater oxidation of organic acids into methane [226]. Furthermore, the BC promotes the growth of archaea (*Methanosaeta* and *Methanosarcina*) and bacteria (*Bacterioidetes* and *Geobacter*) involved in VFA degradation and methane production [38,88,92,202].

The application of BC in AD has been investigated mainly in batch systems such as BMP tests and fewer long-term continuous systems. It is therefore still necessary to upgrade the use of BC at the pilot plant scale and prove the feasibility of BC augmentation at an industrial level. Nonetheless, in batch systems, the effect of BC on methane production is often ambiguous. This could be due to a series of factors, such as the AD conditions and the properties of the BC resulting from their production. This includes the pyrolysis treatment (e.g.,

slow, fast or flash pyrolysis) and the pyrolysis temperature [281]. Previous studies have investigated a wide variety of BC and most authors have attempted to attribute their effect on AD to the physicochemical properties of the BC. Nonetheless, a correlation between the inherent properties of the BCs and their effective influence on AD performance based on a larger data set has not been reported. Therefore, this chapter aims to understand and correlate the most important factors influencing AD performance using the multivariate statistical method PCA, along with quantitative and qualitative descriptive analysis, to evaluate the variations of AD performance with the addition of BCs.

7.3 Compilation of publications for biochar addition on anaerobic digestion

A review of literature reports using BC as an additive in AD was compiled and assessed in this Chapter. A total of 23 publications comprised of 88 experimental conditions, using 44 different BCs were evaluated. As well, the results from this work, reported in Chapters 5 and 6 for BC addition in AD were included. The data extracted from the publications have been divided based on the substrate converted into methane: model carbohydrates (**Table 7.1**), food waste (FW) (**Table 7.2**), anaerobic sludge (AS) and animal manure (**Table 7.3**), aquatic plants and algae (**Table 7.4**), other complex substrates (**Table 7.5**) and co-digestion (**Table 7.6**). The information within these tables has been sub-divided into three-parameter categories. Firstly, the feedstock and pyrolysis conditions (temperature and retention time) are used for producing the BCs. Secondly, the processing conditions used during AD, including reactor type, incubation temperature, substrate, BC load and ISR. Thirdly, the kinetic parameters BMP yield and production rate (μ_m), were obtained for the systems augmented with BC and their corresponding control. The consequence of each of these parameters is discussed in the following sections.

Table 7.1. Summary of the reports for the biochar addition on anaerobic digestion of model carbohydrate substrates.

Feedstock	Pyrolysis Conditions	Conditions	BC load (% w/v)	BMP	μ_m	Ref.
Oak wood	450 °C	AMPTS, cellulose 5 g VS/L, ISR 1, 37 °C	0	265.9	11.8	This work
			3	285.5	28.1	
	650 °C		3	251.6	13.1	
Saw wrack	450 °C, 1h		3	38.3	4.9	
	600 °C, 1h		3	41.1	1.9	
Water hyacinth	450 °C, 1 h		3	294.2	27.3	
	600 °C, 1 h		3	266.0	12.3	
Fruitwoods	800 °C	SB 500 mL, glucose 2 g/L, ISR 0.5, 35 °C	0	15.7	2.8	[87]
			1	15.3	2.3	
		HRT 30 d, Glucose 4 g/L, ISR 0.25	0	16.6	1.1	
			1	13.7	2.1	
		Glucose 6 g/L, ISR 0.17 BMP (mmol CH$_4$/g)	0	14.2	1.3	
			1	13.7	1.5	
		Glucose 8 g/L, ISR 0.125	0	15.1	1.0	
			1	13.3	1.0	
Rice straw	500 °C 2 h	AMPTS, glucose 9 g/L, ISR 0.18, 35 °C	0	142.0	6.5	[35]
			0.5	143.6	8.2	
Corn stover			0.5	138.0	6.3	
Bamboo			0.5	145.0	9.8	
Pine wood			0.5	156.4	9.7	
Oak wood			0.5	158.9	9.0	
Apple wood			0.5	163.8	9.2	
Switchgrass	500 °C, 72 s	SB 160 mL, WV 55 mL, glucose 1 g COD/L, ISR 0.24, 37 °C, HRT 10 d	0	193	NR	[28]
			1	332.0		
Ashe juniper	400 °C, 30m		1.0	330	NR	
Fruitwoods	800 °C	ISR 1:6, glucose 6 g/L, TAN 0.3 g/L, BC-PS 0.5-1 mm, 35°C	0	13.2[a]	1.3[b]	[172]
			1	12.9[a]	1.5[b]	
		TAN 3.5 g-N/L, BC-PS 0.5-1 mm	0	13.5	0.59	
			1	13.3	0.65	
		TAN 7 g-N/L, BC-PS 0.5-1	0	13.6	0.34	
			1	13.8	0.42	
		BC-PS 2-5 mm	1	15.2	0.50	
		BC-PS 75-150 µm	1	14.0	0.49	
Rice straw	500 °C	UASB 5.5 L, 35 °C, sucrose HRT 24 and 12-6 h	0	NR	8.0[c]	[88]
			0.4		7.1[c]	

BMP expressed in mL CH$_4$/g and μ_m expressed in mL CH$_4$/g·d, unless stated otherwise; a BMP (mmol CH$_4$/g); b μ_m (mmol CH$_4$/g·d); c μ_m (L/m^3·d); NR not reported; SB serum bottle; WV working volume; COD chemical oxygen demand; HRT hydraulic retention time; TAN total ammonia nitrogen; BC-PS biochar particle size.

Table 7.2. Summary of the reports for the biochar addition on anaerobic digestion of food waste and OFMSW.

Feedstock	Pyrolysis Conditions	Conditions	BC load (% w/v)	BMP	μm	Ref.
Fruitwoods	900 °C	SB 1.1 L, FW 4 g/L, ISR 2, 35 °C	0	490.0	0.05	[233]
			0.2	480.1	0.08	
			0.5	493.1	0.07	
			1	507.5	0.15	
		FW 8 g/L, ISR 1,	0	440.0	0.03	
			0.2	460.3	0.07	
			0.5	530.5	0.06	
			1	476.6	0.07	
		FW 10 g/L, ISR 0.8	0	340.0	0.03	
			0.2	490.2	0.04	
			0.5	478.1	0.06	
			1	471.9	0.05	
Pine sawdust	650 °C 20m	SB 100 mL, 60 mL WV, 35 °C, FW 13.7 g/L	0	1070[a]	113[b]	[204]
			0.83	1137[a]	156[b]	
			1.66	1057[a]	160[b]	
			2.51	956[a]	145[b]	
			3.33	931[a]	138[b]	
Pine sawdust	650 °C, 20 m	SB 100 mL, WV 60 mL, FW 496 g VS/L, 37 °C	0	1487[a]	272[b]	[36]
			1.5	2092[a]	362[b]	
	900 °C, 20 m		1.5	2187[a]	389[b]	
Wallnut shell	900 °C*	SB 650 mL, WV 550 mL, FW 4 g VS/L, ISR 1.36, 37 °C	0	484		[232]
			0.35	492	NR	
			0.70	131		
Wheat bran pellet	800 °C, 3 h	SB 120 mL, FW ferment 1.5 g /L, ISR 0.13, 20 °C				[92]
Coppiced woodlands	500 °C		2.5	NR	NR	
Orchard pruning	500 °C					
Vineyard pruning	550 15 min	Erlenmeyer flask 250 mL, citrus peel waste, ISR 1, 37 °C	0	103	10.9	[282]
			1	209	14.3	
			3	298	14.2	
Coconut shell Wood Rice husk	450 °C	SB 500 mL, WV 300 mL, citrus peel waste, ISR 0.3, 35 °C	0	165.9	21.8	[171]
			0.96	186.8	26.0	
			096	171.3	18.4	
			0.96	172.1	26.6	
Rice straw	500 °C 2 h	AMPTS, 35 °C, ISR 1, OFMSW 8.6 g /L	0	174.2[c]	72.5[d]	[202]
			0.5	92.4[c]	40.1[d]	

BMP expressed in mL CH$_4$/g and μm expressed in mL CH$_4$/g·d, unless stated otherwise; a BMP (mL CH$_4$/L); b μm (mL CH$_4$/L·d); c BMP (mL CH$_4$); d μm (mL CH$_4$/d); NR not reported; SB serum bottle; WV working volume; VS volatile solids; COD chemical oxygen demand; FW food waste; OFMSW organic fraction of the municipal solid waste.

Table 7.3. Summary of the reports for the biochar addition on anaerobic digestion of sewage sludge and animal manure.

Feedstock	Pyrolysis Conditions	Conditions	BC load (% w/v)	BMP	μ_m	Ref.
Cornstalk	710 °C 7 s	Digester 600 mL, WV 550 mL, sludge 4.3 g TS/L, ISR 2, 55 °C, μ_m (mL/d)	0	488.9	125.5[a]	[173]
			0.8	494.3	160.1 [a]	
			1.1	494.9	144.5 [a]	
			1.3	495.2	143.6 [a]	
			1.6	494.5	131.5 [a]	
Vineyard pruning	550 °C 15 min	Erlenmeyer flask 250 mL, sludge ISR 1, 37 °C	0	273	18.7	[282]
			1	364	23.1	
			3	425	33.4	
Pine wood Oak wood	710 °C 7 s	2-step 600 mL digester, WV 550 mL, sludge, 37 °C/HRT 1.2 d, 53 °C/HRT 12 d	0	0.31[b]	72.5[a]	[148]
			3.1	0.31 [b]	82.9 [a]	
			6.3	0.31 [b]	71.4 [a]	
Oak wood	710 °C 7 s		2.8	0.33 [b]	83.2 [a]	
			5.6	0.32 [b]	79.4 [a]	
Almond shell residue	550 °C	SB, WV 250 mL, swine manure 6 g VS/L, ISR 1, 35 °C	0	298.7	21.2	[230]
			1.2	395.4	24.5	
		Pre-treated swine manure	0	416.7	27.5	
			1.2	433.2	28.8	
Dairy manure	350 °C 3 h	SB 280 mL, 35 °C, dairy manure, HRT 35 d	0	374.7	28.2	[201]
			0.1	394.9	29.9	
			1.0	466.5	37.4	

BMP expressed in mL CH_4/g and μ_m expressed in mL CH_4/g·d, unless stated otherwise; a (mL CH_4/d); b BMP (mL CH_4/g COD degraded); ISR inoculum to substrate ratio; SB serum bottle; NR not reported; WV working volume; VS volatile solids; TS total solids.

Table 7.4. Summary of the reports for the biochar addition on anaerobic digestion of aquatic plants and algae.

Feedstock	Pyrolysis Conditions	Conditions	BC load (% w/v)	BMP	μ_m	Ref.
Oak wood	450 °C	VBU-WH 5 g VS/L, ISR 1	0	208.9	15.0	This work
			0.5	217.7	24.9	
			1	141.7	13.0	
		MM-WH	0	201.3	20.2	
			0.5	163.3	15.8	
			1	196.6	17.5	
		PG-WH	0	177.1	19.8	
			0.5	141.4	32.6	
			1	194.9	19.9	
		UG-WH	0	91.6	6.8	
			0.5	53.7	5.0	
			1	90.8	7.0	
Waste wood	700 °C, 1h	AMPTS, *L. digitata* 5 g VS/L, ISR 2, 37 °C	0	200.1	22.1	[37]
			0.03	211.5	25.8	
			0.06	212.9	24.2	
			0.12	234.0	24.7	
			0.5	180.0	19.5	
			1	179.7	20.3	

BMP expressed in mL CH_4/g and μ_m expressed in mL CH_4/g·d, unless stated otherwise; ISR inoculum to substrate ratio; SB serum bottle; WV working volume; VS volatile solids.

Table 7.5. Summary of the reports for the biochar addition on anaerobic digestion of other substrates.

Feedstock	Pyrolysis Conditions	Conditions	BC load (% w/v)	BMP	μ_m	Ref.
Ashe juniper	400 °C, 30 m	SB 160 mL, WV 55 mL, BOAP 4 g COD/L, ISR 0.24, 37 °C, HRT 10 d	0	24	NR	[28]
			1	296		
	600 °C, 30 m		1	88		
Canola meal	700 °C, 2 h		1	43	NR	
	900 °C, 2 h		1	37		
Paper sludge and wheat husks 1:2	500 °C 20 m	Syringe 100 mL, 42 °C, $(NH_4)_2CO_3$ TAN 0.5-5 g/kg, HRT 63 d	0	4.4[a]	0.03[b]	[17]
			2	4.5[a]	0.03[b]	
Cornstalk pellet	400 °C 10 m	Syringe 100 mL, APL 35 g COD/L, ISR 0.6, 40 °C	0	12[c]	0.1[d]	[283]
			8	20[c]	0.2[d]	

BMP expressed in mL CH_4/g and μ_m expressed in mL CH_4/g·d, unless stated otherwise; ISR inoculum to substrate ratio; SB serum bottle; NR not reported; WV working volume; VS volatile solids; HRT hydraulic retention time; BOAP bio-oil aqueous phase; APL aqueous pyrolysis liquid; a BMP (mL/g); b μ_m (d[-1]); c BMP (g COD_{CH4}/L); d μ_m (g COD_{CH4}/L·d).

Table 7.6. Summary of the reports for the biochar addition on anaerobic co-digestion.

Feedstock	Pyrolysis Conditions	Conditions	BC load (% w/v)	BMP (%)	μm (%)	Ref.
Oak wood	450 °C*	*C. vulgaris*-cellulose, C/N 10, ISR 0.5	0	50.8	23.6	This work
			3	232.7	9.5	
		C/N 20, ISR 0.8	0	91.2	39.5	
			3	239.1	10.0	
		C/N 30, ISR 0.9	0	136.2	22.7	
			3	241.2	12.4	
		C/N 25, ISR 2	0	296	49.6	
			0.58	312	99.0	
Water hyacinth	450, 1 h	C/N 25, ISR 2	0.58	286	92.3	
Sawdust	500 °C 1.5 h	SB, WV 90 mL, 150 rpm, 35 °C, HRT 55 d, FW-sludge 2 g VS/L, ISR 0.67, BMP (mL), μm (mL/d)	0	111.7	6.7	[226]
			0.2	114.6	8.7	
			0.6	116.2	9.4	
			1.0	112.1	8.2	
			1.5	109.5	7.8	
Vineyard pruning	550 15 min	Erlenmeyer flask 250 mL, citrus peel waste and sludge, ISR 1, 37 °C	0	298	14.4	[282]
			1	500	66.3	
			3	704	75.5	

BMP expressed in mL CH_4/g and μ_m expressed in mL CH_4/g·d, unless stated otherwise; ISR inoculum to substrate ratio; SB serum bottle; NR not reported; WV working volume; VS volatile solids; HRT hydraulic retention time; BOAP bio-oil aqueous phase.

7.4 Effect of biochar addition on anaerobic digestion performance

The effect of BC on AD performance was based on the results obtained with BC addition compared to their corresponding control without biochar from the previous tables. These reports were compiled in a general frequency analysis over four levels of effect: improved, reduced, unchanged and not reported (**Figure 7.1**). Firstly, for the variable methane yield, 57 % of the cases benefited from BC addition, whilst 25 % were negatively affected and 18 % showed no change (**Figure 7.1a**). Secondly, for the effect of BC on μ_m, it is necessary to outline that 22 of the conditions failed to report these values. Thus, from the ones that included it, 83 % of the cases improved μ_m (**Figure 7.1b**). Thirdly, 57 % of the cases showed a positive effect of BC addition in AD by shortening the lag phase. Whereas 32 % extended this period and 11% showed no variation. The BCs that reduced λ were mostly produced at 450-500 °C [150,171,202], including

this work, and some BCs produced at 650-700 °C [37,204]. In summary, BC addition largely favoured digestion performance, principally μ_m.
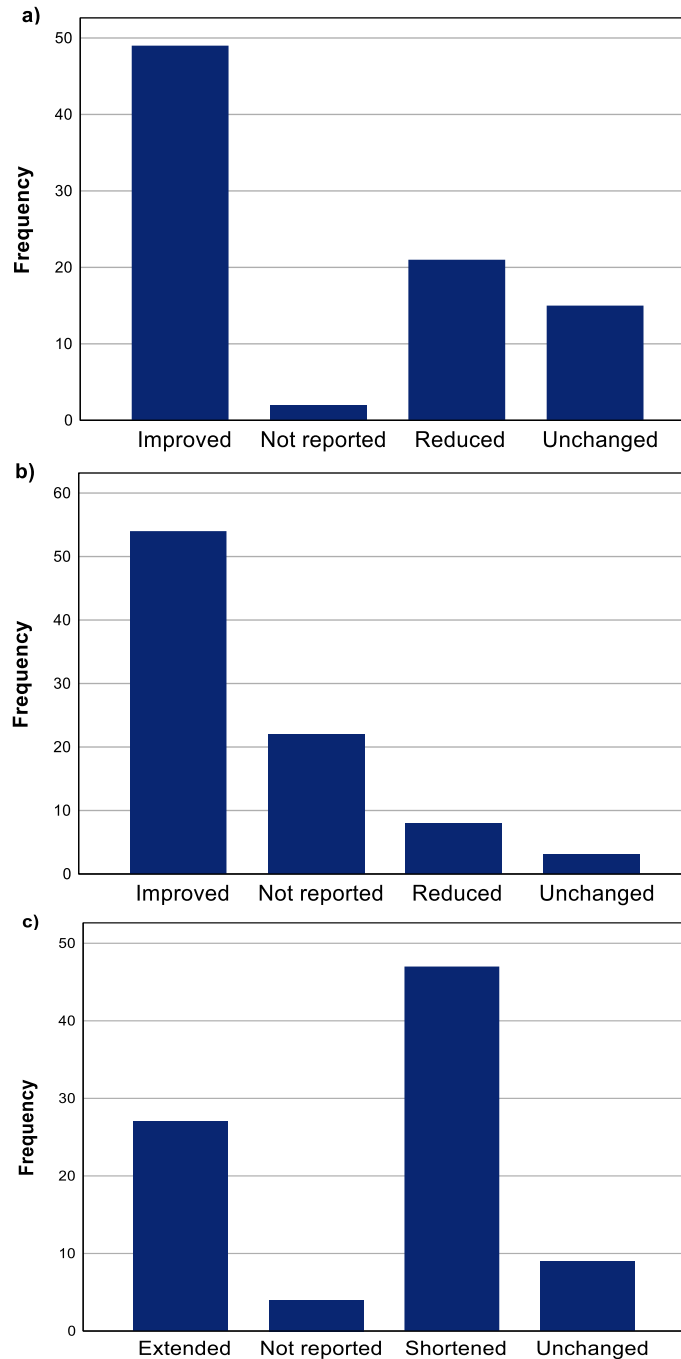
Figure 7.1. Frequency (repeats) of the effect of biochar addition on anaerobic digestion performance. a) BMP yield; b) biomethane production rate (μ_m); c) lag phase (λ).

Biochars can catalyse reductive reactions by facilitating the transfer of electrons from bulk chemical electron donors to a receiving organic compound [93]. Thus,

it is understandable that promoting these interactions resulted in a faster μ_m. Moreover, additional factors can also contribute to methane production, including reactor type, choice of substrate and composition, ISR, and BC load. The interaction and response to changes taking place in complex systems, such as AD, are difficult to understand and can even lead to ambiguous observations. Hence, it is important to evaluate the factors both individually and collectively to understand and correlate the behaviours observed.

For estimating how much BC addition influenced methane generation, the changes in BMP yield and μ_m for each condition of **Tables 7.1-7.6** were compared to their corresponding control. The calculated values are listed in the Appendix **Table B.1**. The effects were expressed as % of variation where 0 % represents the value obtained being the same as the control, whereas 100 % represents the addition BC doubling the value obtained compared to the control. Moreover, a positive value represents an improvement of a particular effect, while a negative value represents the BC addition causing a detrimental effect. The effect of BC addition in AD is discussed in the following sections and finally integrated into the PCA.

7.5 Biochar properties and effect of the biochar on AD

7.5.1 Pyrolysed feedstocks for biochar production

A wide variety of feedstocks were employed for BC production (**Figure 7.2**). The majority is derived from woody or another lignocellulosic source (oak, pine, rice straw, ashe juniper, fruitwood, vineyard pruning, almond shell residual, coconut shell, corn stalk, sawdust, walnut shell, husks, and coppice woodland pellet). Other feedstocks included high-cellulose (water hyacinth, switchgrass, and bamboo), algae (*F. serratus*), and other high-protein feedstock (dairy manure and canola meal). It is worth remarking on the limited work done on algae BC in AD since those listed in this compilation corresponded only to the SW-BCs studied in Chapter 5. Generally, woody derived BCs exhibited the greatest benefits during the AD amendment.
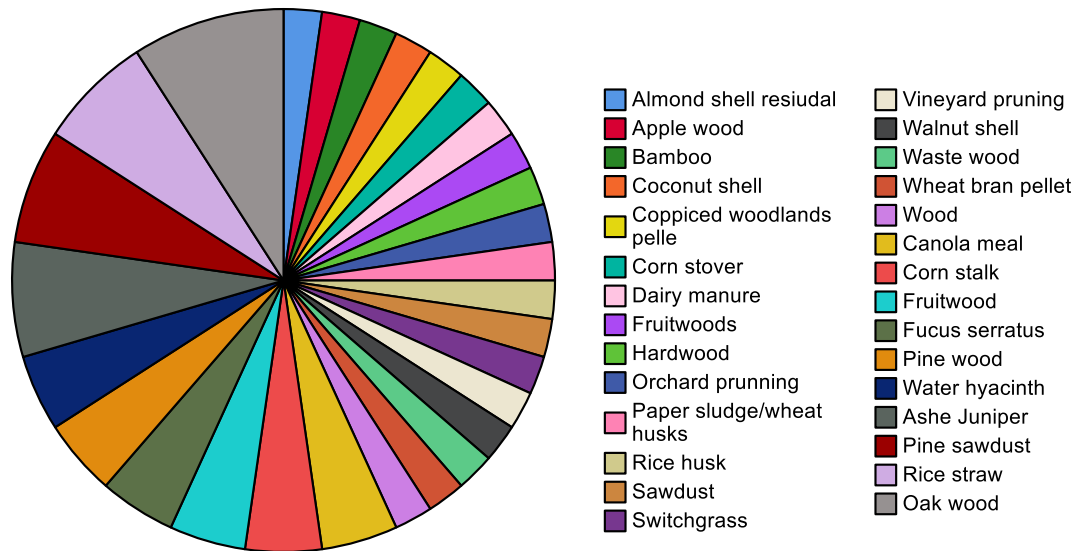
Figure 7.2. Frequency (repeats) of feedstocks used for producing the biochar added to AD in the selected publications.

7.5.2 Pyrolysis temperature

Figure 7.3 shows the pyrolysis temperature used for producing the BCs added to AD. The temperatures used were wide and ranged between 350 to 900 °C. Only three BCs were produced at low temperatures (350-400 °C), whereas the majority were produced at an intermediate temperature (450-550 °C). There were a few reports of BCs at 600-650 °C, comprised mostly of those studied in this work, whereas 12 BCs were produced at higher temperatures of 700-900 °C.
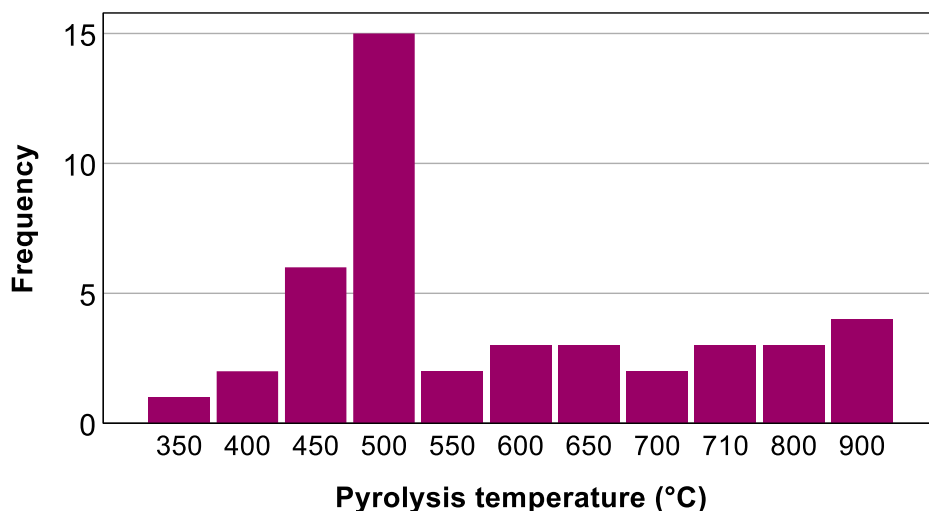
Figure 7.3. Frequency (repeats) of pyrolysis temperature used for producing the biochar added in anaerobic digestion.

Pyrolysis temperature is the main factor affecting the properties of BC, hence, its relevance to the effect of BC in AD. The distribution for the effect of pyrolysis temperature on the BMP and μ_m was standardised into box plots (**Figure 7.4**). Most pyrolysis temperatures showed a tendency to improve the kinetic parameters. The effect of pyrolysis temperature had a significant effect on μ_m ($p<0.05$) (ANOVA), but not on BMP yield. Accordingly, μ_m was improved in most cases, with a few exceptions in the literature [37,87,171,202]. Also from this work, the addition of SW-BC450, SW-BC600 on the AD of cellulose, and OW-BC450 for the AD of water hyacinth reduced μ_m.
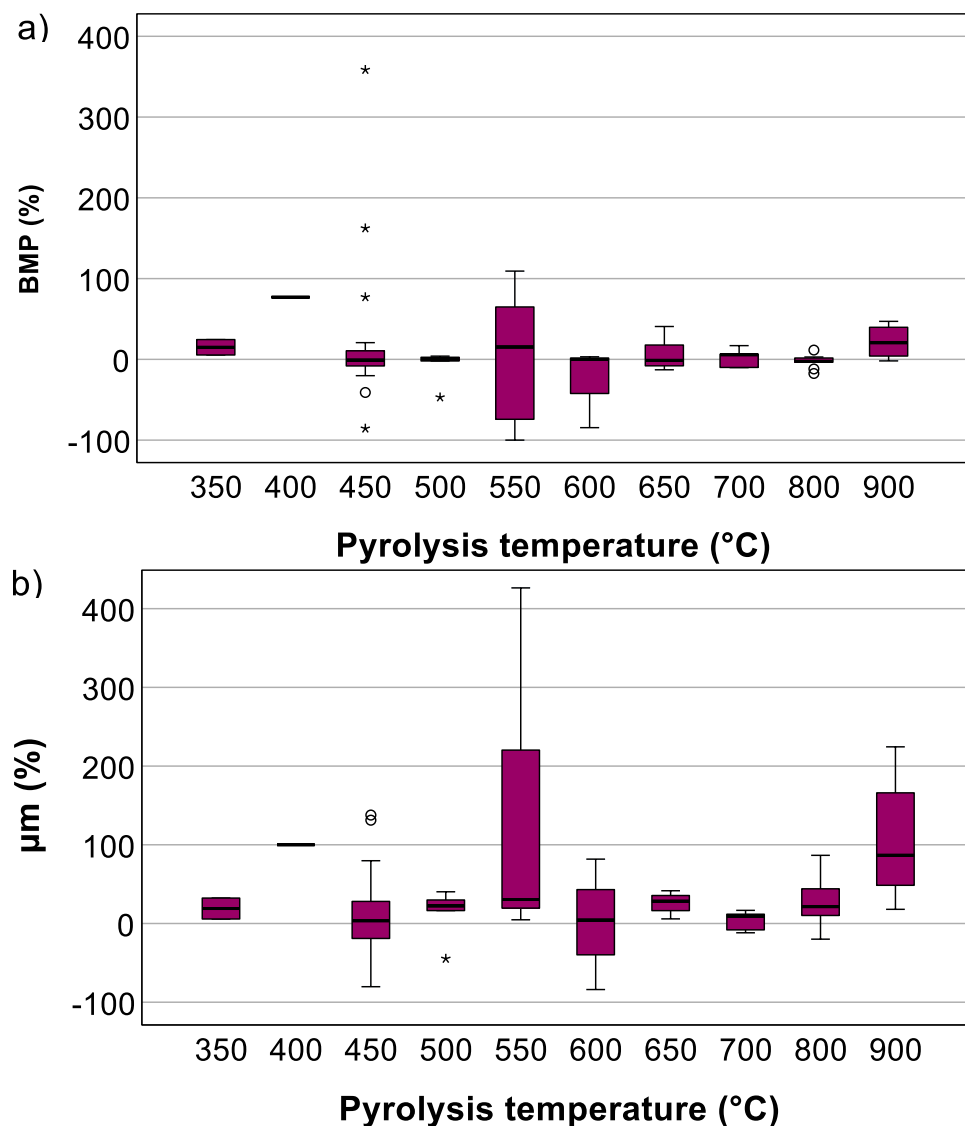
Figure 7.4. Box plot for the distribution of the relation between pyrolysis temperature and BC effect on a) BMP; b) μ_m.

The greatest improvements in BMP yield in comparison to their control due to BC addition corresponded to the slow pyrolysis BCs. These include the following: ashe juniper BC 400 and 600 °C, switchgrass BC 500 °C and canola meal BC 700 °C [28], corn stalk BC 400 °C [283], vineyard pruning BC 550 °C [282], and the addition of OW-BC450 during the AcoD of *C. vulgaris* and cellulose at ISRs 0.5-0.9 from Chapter 6. Particularly for μ_m, the BCs whose effect was more favourable were the following: vineyard pruning BC 550 °C [282], fruitwoods BC 800 and 900 °C [87,233], corn stalk BC 400 °C [283], bamboo and pine woods 500 °C [35], OW-BC450 and WH-BC450 for the AD of cellulose as stated in Chapter 5.

The effect of BCs produced at 550 °C largely improved methane production, corresponding to two publications. The addition of almond shell residues BC 550 °C and vineyard pruning BC 550 °C significantly improved both BMP, and μ_m, but extended λ [230,282]. Similar behaviour was observed for fruitwoods BC 900 °C, and corn stalk BC 400 °C [233,283]. Whereas the addition of pine sawdust BC produced at either 650 or 900 °C exhibited similar BMP yield and μ_m improvement [36]. Conversely, waste wood BC 700 °C, wood BC 450°C, and rice straw 500 °C reduced BMP and μ_m but shortened the λ [37,171,202]. Generally, BCs produced at intermediate temperature (450-500 °C) had the most positive effect on AD performance, although BCs 700-900 °C also contributed favourably. Nonetheless, most reports used BC produced only at one temperature, avoiding the evaluation of this factor in the potential of BC in AD.

In Chapter 5, it was stated that BCs produced at 450 °C were more adequate for AD than higher temperature BCs. It has been suggested that BCs produced at 400-500 °C exhibit an extensive redox buffering capacity dominated by quinone/hydroquinone functionalities. Other favourable features of these BCs are electron exchange capacity, and a well-developed surface area and porosity [93]. Similarly, Shanmugam et al. [28] identified that BCs produced at 400-500 °C could reduce the λ and enhance μ_m. They attributed these benefits to the conductive properties and redox-active organic and inorganic moieties of the BC. Conversely, higher temperature BCs exhibit less oxygen content, more aromaticity and ring condensation, which subsequently results in less quinone and hydroquinone moieties [28]. As pyrolysis temperature increases, so do the pH, ash content, and hydrophobicity since more polar functional groups are removed and aromaticity is enhanced [67]. The changes in these properties due to temperature could support the superiority of intermediate temperature BC for AD purposes.

7.5.3 Biochar composition

Two of the most important characteristics of BC, ash content and O:C atomic ratio, were correlated with their effect on AD. The distribution for the effect of these properties on the BMP and μ_m was standardised into box plots. It is worth remarking that not all reports described the BC composition and only those that provided it was evaluated in this section [17,36,172,226,230,233,282]. The effect of BC ash content as demonstrated by ANOVA had a significant effect on both BMP and μ_m (p<0.05). BCs with an ash content of 3.1-6.3%, mainly woody BCs, generally improved BMP and μ_m (**Figure 7.5**).
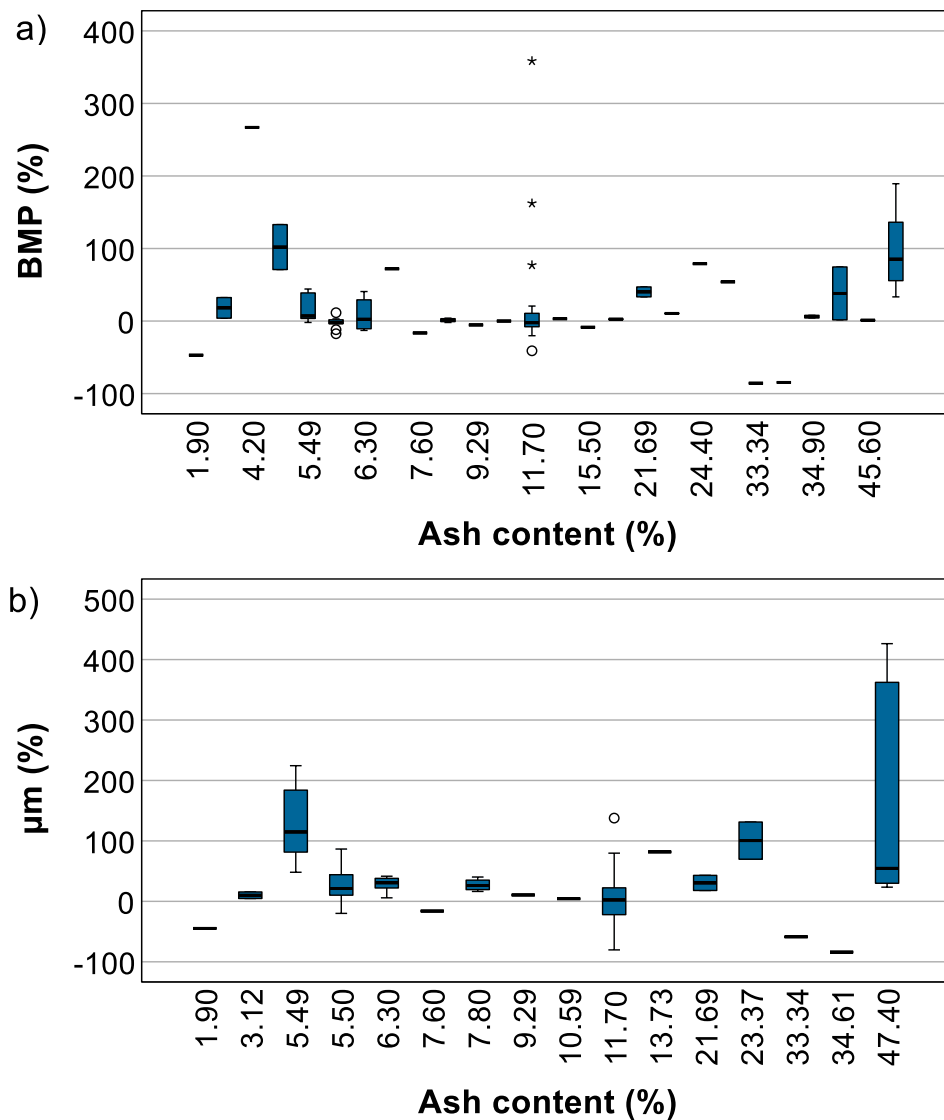
Figure 7.5. Box plot for the distribution of the relation between BC ash content and their effect on a) BMP and b) μ_m.

However, the larger distribution linked to BC with higher ash contents (>6.3%) was restricted to one publication [282] and the work produced in this research. Martínez et al. [282] pyrolysed vineyard pruning at 550 °C resulted in BC with a high ash content (47.4 %). This BC was added to the mono and co-digestion of sludge and citrus peel waste, and it considerably increased both BMP and μ_m. The other high-ash BC improving kinetic parameters corresponded to WH-BC450 with 23.4 % of ash. As discussed in Chapter 5, the inorganics within the BCs could provide a source of alkalinity, conductivity, and trace nutrients. The soluble inorganics Cl, Ca and K are even reported to increase BC conductivity and subsequently improve DIET interactions [235].

Figure 7.6 shows the box plot distribution for the effect of the BC O:C ratio on AD performance. The importance of the OFGs as intermediaries for the DIET process has been previously stated to serve as the anchoring sites for intermolecular and interspecies interactions [48,91,92]. The BCs used in the reports and this work showed an O:C ratio within a range of 0.06-0.41. BCs with an O:C ratio of 0.20 was responsible for most of the improvement for BMP and μ_m, corresponding to BCs produced at low temperature 450-500 °C, mainly OW-BC450 and the vineyard pruning BC 550 °C [282]. Also, fruitwoods BC produced at 800-900 °C (O:C ratios 0.06-0.07), had a favourable impact in AD [172,233]. Hence, the O:C ratio of the BCs had a significant effect on μ_m ($p<0.05$) (ANOVA), although not on BMP yield.

The correlation between the parameters used for AD and those related to the BCs used provided insight for establishing what properties and conditions are more appropriate for AD amendment. However, the complexity of this type of system suggested that these parameters did not act individually, and they all contributed to the effect of BC in AD. Therefore, it is necessary to establish which are the most relevant and which are correlated.
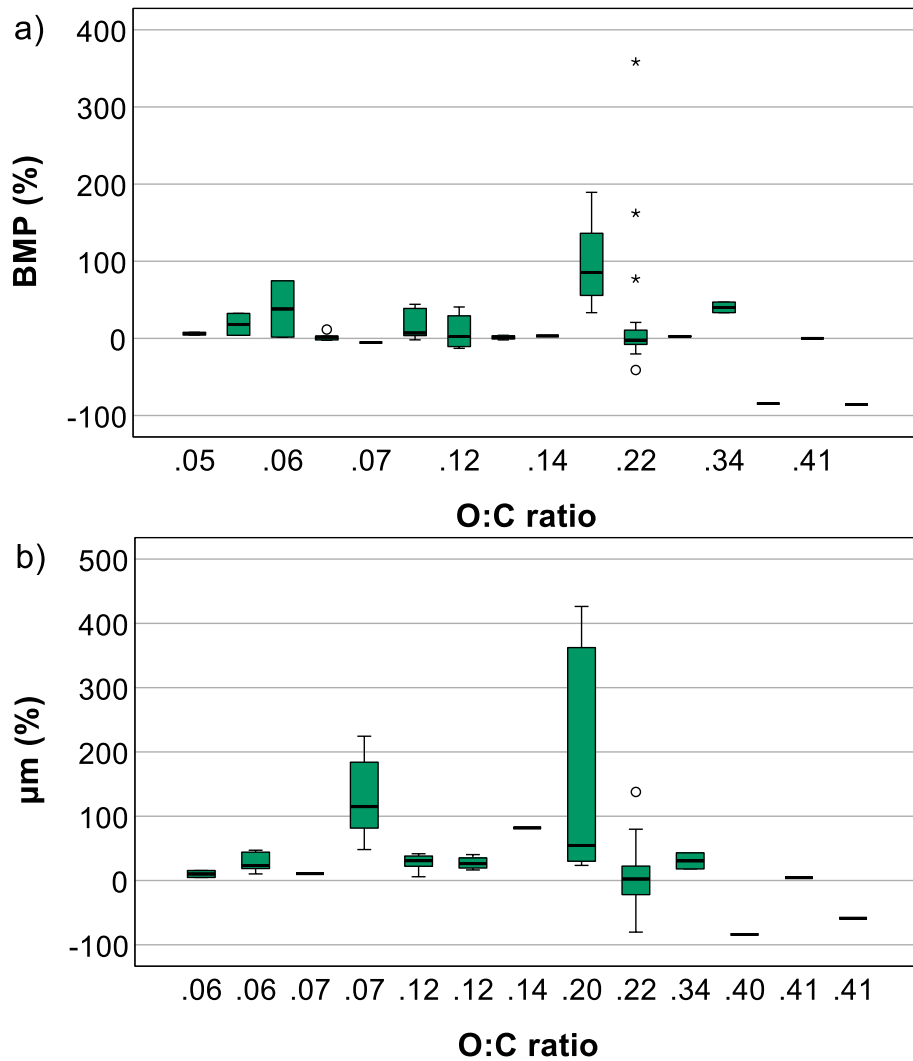
Figure 7.6. Box plot for the distribution of the relation between BC O:C ratio and their effect on a) BMP and b) μ_m.

7.6 Operating conditions

7.6.1 Reactor design

The performance of a bioreactor is influenced by several factors. Such as metabolism, inoculum, enzymatic activities, substrate concentration, substrate and/or product inhibition, mixing efficiency, shear stress, mass and heat transfer, among others [284]. The operation conditions used in the reports are listed in **Tables 7.1-7.6**. Most systems consisted of batch experiments using either an AMPTS or serum bottles of variable sizes (100-1100 mL), with one continuous and long-term operation report [88].

The effect of the BCs on the batch experiments mainly benefited AD, although some conditions had a detrimental effect, creating ambiguity. The report from the continuous systems showed a favourable effect for BC addition in AD. Wang et al. [88] tested two continuous 5.5 L UASB reactors for the AD of sucrose, R1 with BC 4 g/L and R2 without BC. The synthetic media fulfilled all nutrient requirements, including small amounts of nitrogen and trace elements, while the pH of the reactors was maintained with a phosphate buffer. The operation was divided into stage I (1-63 days) at an HRT of 24 h and an increasing substrate influent of 4-15 g COD/L; stage II (64-100 days) with a decreasing HRT of 12-6 h, and a fixed inlet of 5 g COD/L. The R1 generally exhibited a shorter λ, higher BMP yields, and less accumulation of VFAs than R2. The HRT was reduced for stage II, resulting in better performance and BMP for R1 than R2. They stated that the BC acted as inert support by promoting the granulation, improving the conductivity and hydrophobicity of the sludge. Also, it facilitated the enrichment of the microorganisms involved in the DIET process. In a continuous system, a shorter HRT is desirable for increasing the process efficiency, however, this could dilute the sludge and lead to digestate failure. One of the proposed advantages of BC as immobilisation support is to provide stability and protection to the cells for improving their performance, particularly at higher fluxes and lower HRT [94]. Hence, it is important to outline the potential of BC for stabilising continuous long-term operations, and the necessity to study this area.

7.6.2 pH

The pH is a key factor for achieving a successful AD process given that methanogens are very sensitive to drastic pH variations. The methanogens are very active at pH 6.7-7.4, although their optimal activity takes place at pH 7.0-7.2. The methane production rate is highly affected if the pH varies below 6.3 or above 8.0. Therefore, it is common to adjust the pH of the reactor with additional chemicals, although this is often challenging and costly. Thus, it has been suggested that BC has the potential to provide an alkaline buffering that counterparts the pH changes resulting from VFAs production [55]. Several studies have adjusted the initial pH within the range of 6.8-8.0 when evaluating BC augmentation [28,36,87,171,172,201,226,233]. In addition to this work, several reports worked without pH adjustment, while maintaining a neutral or slightly alkaline pH with the addition of BC and in most cases even for the non-BC controls [17,35,37,39,148,173,202,230,232].

The potential of BC to act as a buffering agent has been reported repeatedly [34,39,173,226,283], while others have observed no significant effect [37,87].

Even so, Wang et al. [226] highlighted an outstanding buffering capacity from sawdust BC 500 °C during the co-digestion of food waste and dewatered activated sludge. Similarly, in Chapter 6, the addition of OW-BC450 offered a buffering effect on the AcoD of *C. vulgaris* and cellulose at ISRs 0.5-0.9. This was not the case for the rest of the experiments where higher ISRs were employed, although the pH was generally maintained at an adequate range. The buffering effect of BC is reported to stabilise AD reactors given that BC could raise the pH and promote methanogenesis even at high concentrations of VFAs [281].

The sources of alkalinity within BC can be been divided into four categories: surface organic functional groups (conjugate bases), soluble organic compounds (conjugate bases of weak acids), carbonates and inorganic alkalis (e.g. oxides, hydroxides, sulphates, sulphides, phosphates) [285]. Nonetheless, buffering capacity is derived principally from the organic functional groups within the BC [281]. Fundamentally, the role of biochar in stabilising the pH of the digester is attributed to an enhanced electron transfer capacity for directing VFAs conversion in DIET-involved methanogens. The latter is achieved via the redox-active structures, quinone-hydroquinone moieties and/or conjugated π-electron systems within the condensed aromatic sub-structures of the BCs. Hence, the redox properties of the BCs are due principally to their organic electron-accepting and donating moieties [93]. It has also been proposed that the concentration of ash, particularly alkali and alkaline earth metals (e.g. K, Na, Mg and Ca) influence the alkalinity and conductivity of the BCs, and contribute to the catalytic and buffering capacity [48,67]. It has also been stated the role of metals contained in the BC, such as Fe, is to act as a reducing agent and stimulate the degradation of VFAs [36]. Besides the ash, the total base cations and carbonates within the BC are reported to increase the alkalinity [197]. Furthermore, Giwa et al. [228] stated that the buffering capacity and amendment of BC during the AD of food waste was a combination of the organic functional groups, inorganic alkaline compounds, basic cations and metals like Fe.

7.6.3 Substrate

A wide variety of substrates were tested for methane generation during the compilation of AD experiments augmented with BC. As stated in the earlier sections, the data extracted from the publications have been divided based on the employed substrate: model carbohydrates (**Table 7.1**), food waste (FW) (**Table 7.2**), anaerobic sludge (AS) and animal manure (**Table 7.3**), aquatic plants and seaweed (**Table 7.4**), other substrates (**Table 7.5**) and co-digestion (**Table 7.6**). Most of the experiments consisted of the mono-digestion of one

substrate, with a few reports of co-digestion. The frequency of their use is summarised in **Figure 7.7**. The substrates more commonly used were food waste and glucose, followed by the AcoD of *C. vulgaris* and cellulose from Chapter 6.
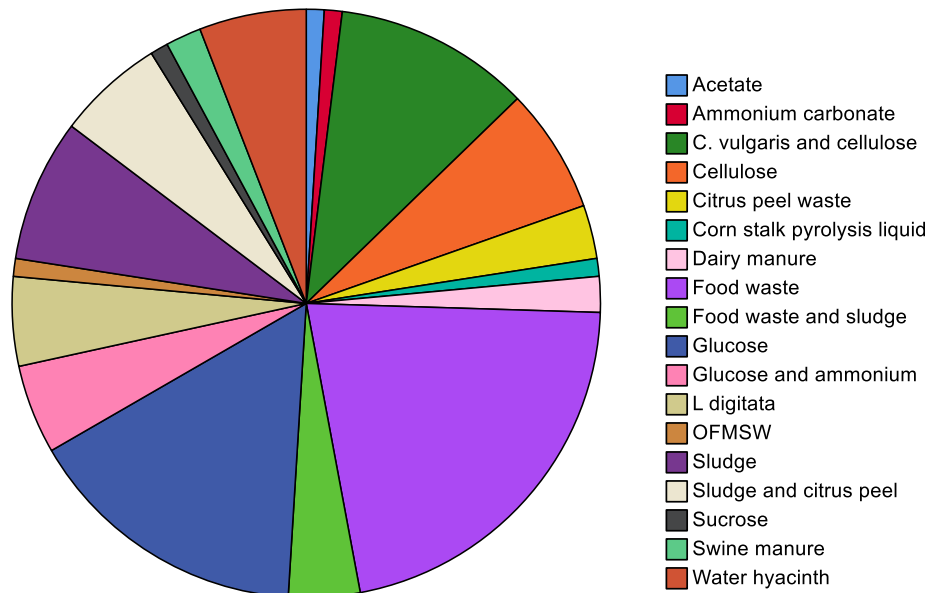
Figure 7.7. Substrates converted into methane on the anaerobic digestion reports

7.6.3.1 Model carbohydrate substrates

Model carbohydrate substrates, such as cellulose, glucose and sucrose, are easily degraded by the hydrolytic bacteria in the AD digesters. The addition of the different BCs generally improved the BMP and more significantly the μ_m (**Table 7.1**). In Chapter 5, the digestion of cellulose was dependent on the used BC since the OW-BC450 and WH-BC450 slightly improved BMP but doubled μ_m. Higher-temperature BCs offered no variation, while algae BCs highly affected the digestion performance. Similarly, Qin et al. [35] compared the addition of different BCs produced at 500 °C for the digestion of glucose. Woody BCs offered the highest benefits accompanied by a mild improvement of the BMP and a superior μ_m. Shanmugam et al. [28] digested glucose at a particularly low ISR of 0.24. The BMP progressed from 193 mL CH$_4$/g COD for the control up to 330 mL CH$_4$/g COD for the BC systems. Luo et al. [87] also evaluated the role of ISR on the AD of glucose amended with fruitwood BC 800 °C. The BC addition generally reduced the lag phase, and improved the BMP only at the lowest ISR, whereas the μ_m was generally favoured. Lü et al. [172] studied the importance of BC-

particle size (BC-PS) at variable TAN concentrations. The μ_m was highly favoured by all BCs, particularly at higher TAN, although only the larger BC-PS significantly improved the BMP yields. These authors generally attributed the improved μ_m to the BC influence on enhancing the production and degradation of intermediary organic acids and the proliferation of methanogenic archaea. The above suggests that BC addition for the AD of easily fermentable substrates could be more beneficial when the digestion system is under stressful or sub-optimal conditions.

7.6.3.2   Food waste

Food waste is composed principally of cereals, fruits and vegetables, and smaller amounts of meat, dairy, roots, and oil. The easy digestion of FW and rapid formation of VFAs reduce the pH and often compromise AD stability. Also, the high protein could lead to inhibitory TAN levels, while the lipids could cause digester foaming [286]. It has been discussed throughout this research that BC could ameliorate these drawbacks. **Table 7.2** summarises the reports of the BC amendment during the AD of FW and OFMSW. BC addition generally improved methane generation. The μ_m was significantly improved in most cases, while the BMP yield was favoured by low BC loads. The most successful report corresponded to the addition of fruitwoods BC produced at 900 °C. In agreement with the previous section, the BC effect was more favourable at lower ISRs [233]. On the other hand, Qin et al. [202] stated that rice straw BC 500°C offered no positive impact on the AD of OFMSW. It is worth remarking that rice straw BC has proven repeatedly not to offer a great difference in comparison to the control [35,88]. Therefore, these results support the fact that easily degradable substrate quickly generates VFAs, whose further consumption of VFAs towards methane generation is favoured by BC. Therefore, the positive impact of BC could promote DIET synergy, avoiding VFA accumulation and digestate failure.

7.6.3.3   Sewage sludge and animal manure

Large amounts of sewage sludge and animal manure are produced from municipal wastewater treatment (MWWT) plants and animal farming, respectively. The further utilisation of these substrates for methane generation is commonly adopted, and some reports were aiming to improve AD performance by adding BC as summarised in **Table 7.3**. In this compilation, BC addition generally improved methane generation. The addition of cornstalk, and woody fast pyrolysis BCs 710 °C for the AD of sewage sludge slightly improved the BMP yield, but considerably enhanced μ_m. The authors attributed the positive

effect of BC in AD to buffering capacity, facilitating the DIET process, increasing the EC of the sludge, reducing TAN inhibition, and even adsorption of CO_2 [148,173]. On the other hand, Martínez et al. [282] observed a better improvement in methane generation with the increasing addition of vineyard pruning BC 550 °C. Similar behaviour was reported by Jang et al. [201] for the AD of dairy manure. Gómez et al. [230] added almond shell residue BC 550 °C to the digestion of swine manure, resulting in BMP yield and μ_m increased by 32 and 16 %, respectively. The swine manure exhibited a large content of ash 28 % and 2.8 g TAN/L. The swine manure was further pre-treated by microwave, which facilitated the degradation of the lipid and protein complex fractions. Hence, considerably higher BMP yields were obtained, even though the TAN was maintained after the pre-treatment. In this case, the BC addition offered a minimal improvement on BMP. Even though the BC influence was non-significant on the TAN or VFAs evolution, it offered some extent of protection and stability that allowed higher yields, particularly for the untreated substrate.

7.6.3.4   Aquatic plants and seaweed

Table 7.4 summarises the results from the addition of OW-BC450 during the AD of water hyacinth (WH) described in Chapter 6. The BC load had no significant effect on the production of methane, although the contour plots suggested that a BC load ~0.5 % could favour the BMP. WH samples collected from different locations resulted in variable BMP yields. For these substrates, BC addition had little effect on BMP performance, and in some instances, it even reduced methane generation. Deng et al. [37] evaluated the use of waste wood BC 700 °C at variable BC loads of 0.03-1 % on the digestion of the seaweed *Laminaria digitata*. The control fed with *L. digitata* produced 200 mL CH_4/g VS. BMP was modestly enhanced with BC addition ≤ 0.125 %, whereas higher doses led to lower BMP than the control, which has been previously attributed to substrate sequestration and changes in the diversity of microorganisms.

7.6.3.5   Anaerobic co-digestion

Publications of BC addition during AcoD and the addition of OW-BC450 for the AcoD of *C. vulgaris* and cellulose, discussed in Chapter 6, are listed in **Table 7.6**. From this work, BC addition had a significant impact on variable C/N ratios and unfavourable ISR 0.5-0.9. The BMP yields were drastically enhanced, the BC provided a pH buffering effect and promoted the consumption of VFAs for methane generation. Although the impact of BC was moderate during AcoD experiments at higher ISRs 1-2, where low BC loads were more appropriate.

Wang et al. [226] co-digested food waste and dewatered activated sludge amended with sawdust BC 500°C. The BC addition reduced the λ reduction, and enhanced the μ_m by 16-40 %, but had no significant effect on the BMP yield. Vineyard pruning BC 550°C added during the co-digested citrus peel waste and sewage sludge reducing the λ and improving the BMP yield and μ_m by 1.7-2.4 and 4.6-5.2 times the non-BC control, respectively [282]. They associated this positive effect with the adsorption of limonene and polyphenols and the promotion of DIET interactions by the BC. From these reports, it can be outlined that BC addition was more favourable during stressful AcoD, such as low ISR and the presence of inhibitory compounds. Hence, the variability of the effect of the BC suggested that other factors were influencing its role.

7.6.4 Inoculum to substrate ratio

The inoculation influences the initial activity of the digester, and the adaptation of the microorganisms to the digestion conditions and the substrate used [266]. Moset et al. [123] studied the impact of ISR on the AD of wheat straw and fresh whole crop maize. Regardless of the substrate used, they observed that an ISR range of 1.5-2.0 showed no statistically significant difference over BMP. Whereas ISR of 0.25 affected the microbial population with a proliferation of acidogens and acetogens. Generally, the BMP was enhanced by increasing ISR, thereby highlighting the importance of a balanced initial ISR.

From the reports in **Table 7.1**, the distribution of the ISR and the effect of BC on AD performance were evaluated (**Figure 7.8**). BC addition had a negligible effect on BMP at ISR ≤0.18, 0.30 and 0.67, whereas it was largely favoured at ISR 0.24, 0.5, 0.6, and 0.8-1.36. There were reports of both improving and reducing the BMP at ISR of 1 and 2, which increased the distribution. On the other hand, μ_m was favoured at ISRs 0.1-0.3, 0.6-0.7, 1 and 2, although μ_m was reduced at ISR 0.5 0.8-0.9. Nonetheless, the ANOVA stated that ISR had a significant effect on BMP yield ($p < 0.05$), but not on μ_m.
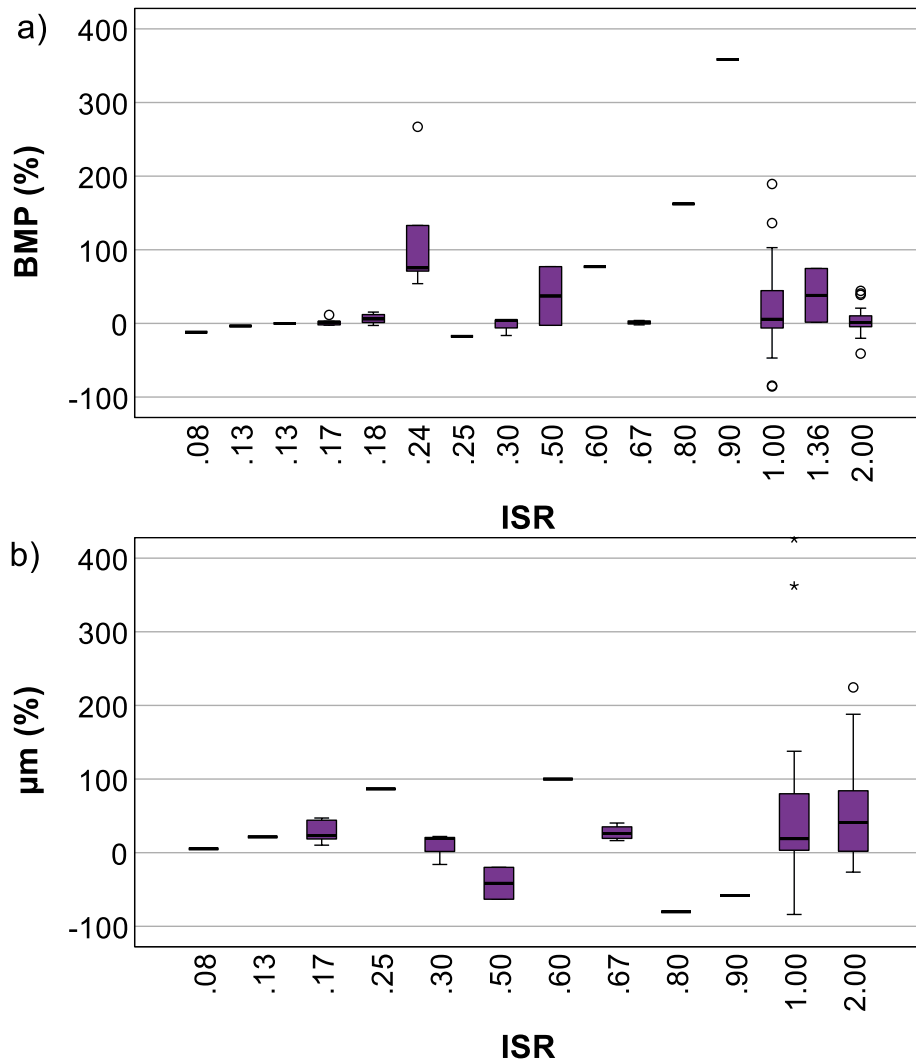
Figure 7.8. Box plot for the distribution of the relation between ISR and BC effect: a) BMP; b) μ_m.

Chapter 6 stated the great improvement of BMP yield with the addition of OW-BC450 at ISRs 0.5-0.9 during the AcoD of *C. vulgaris* and cellulose. By increasing the ISR to 1-2, the effect was reduced, although an optimum ISR of 2 was established. Similarly, Cai et al. [233] studied BC addition on the AD of food wastes. At an ISR of 2, BC addition had little effect on BMP. By reducing the ISR to 1 and 0.8, the BMP performance was drastically improved with BC addition. It has been suggested that BC addition improves AD performance, principally under stressful conditions [38].

7.6.5 BC load

The amount of these BCs added to the AD reactor ranged between 0.03 to 8.0 % (w/v), with a predominance of 1 % (**Figure 7.9**). Such a diverse range of

temperature and BC load found in these reports were used for examining the correlation between pyrolysis temperature and the role of BC in AD in the following sections. The BC load was evaluated to establish its contribution to AD performance (**Figure 7.10**). In Chapter 6, it was stated that increasing concentrations of BC could hinder AD performance, thereby the necessity to establish an optimal BC load.
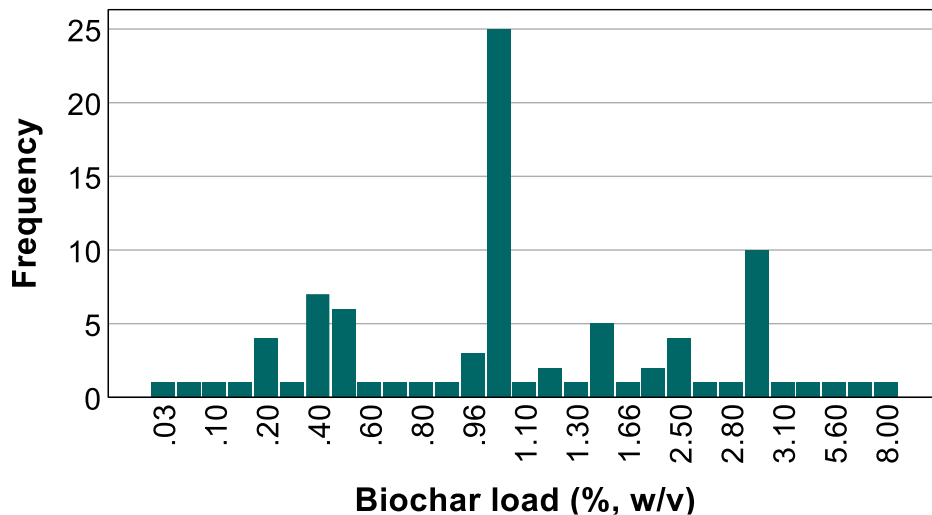
Figure 7.9. Frequency of biochar load used in anaerobic digestion reports.

From the reports in **Table 7.1**, most BC loads improved or had little effect on the BMP, while increasing BC loads favoured μ_m, although non statistically significant ($p > 0.05$) (ANOVA). Nonetheless, the largest variability was obtained for BC loads of 0.5, 1.0 and 3 %, corresponding mainly to the varying results from the previous Chapters. The AD of cellulose and its co-digestion with *C. vulgaris* at ISRs 0.5-0.9 were promoted at a BC load of 3 %, whereas the further DoE suggested that lower BC loads were more favourable. Conversely, Martínez et al. [282] employed vineyard pruning BC 550 °C, at BC loads of 1 and 3 %, and observed that increasing the BC addition improved AD performance. Wang et al. [226] evaluated sawdust BC 500 °C loads of 0.2-1.5 % (w/v), observing little variation in the BMP, whereas μ_m increased by 16-40 %, and an optimal BC load of 0.6 % was stated.
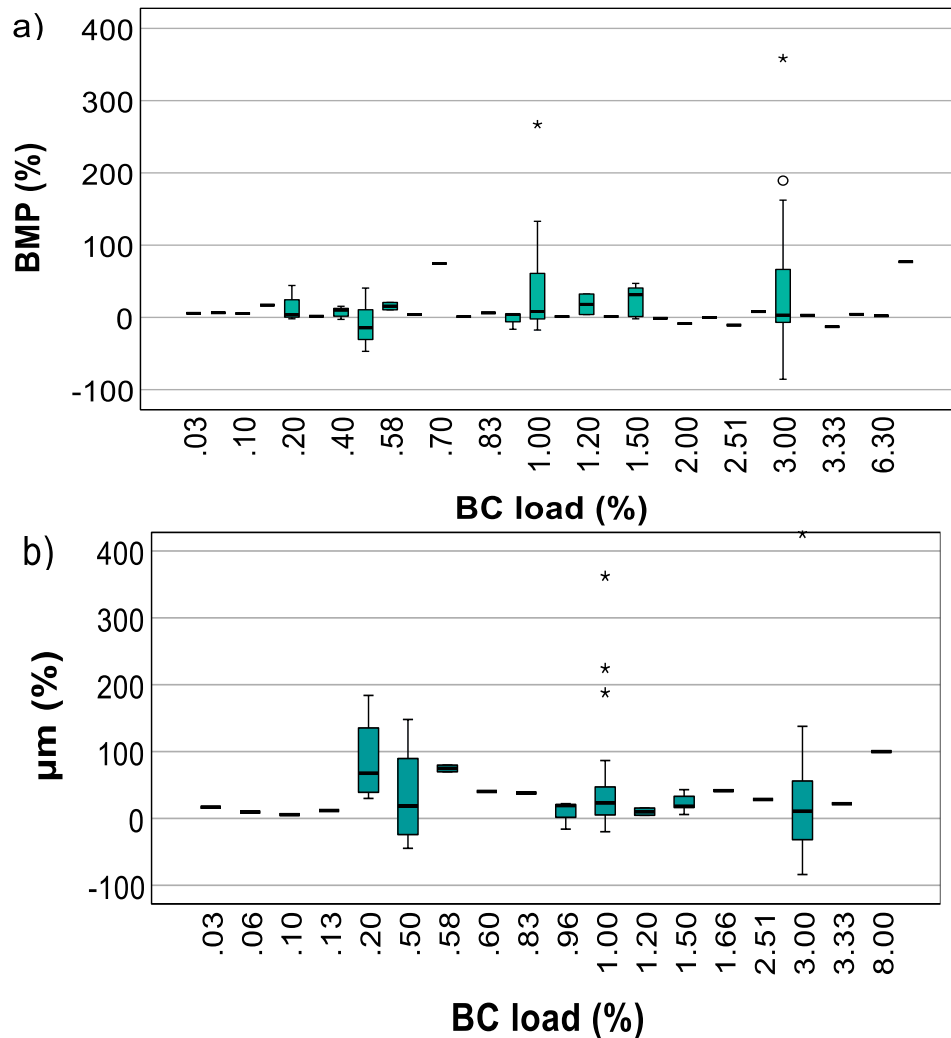
Figure 7.10. Box plot for the distribution of the relation between BC load and BC effect: a) BMP; b) μ_m.

Other reports that also remarked on the importance of BC load in AD, used high-temperature BCs. Linville et al. [232] reported that 0.4 % of FWSB-BC 900 °C improved AD, while higher doses (>0.7%) exhibited an inhibitory effect. Sunyoto et al. [204] added 0.08-0.33 % of pine sawdust BC 650 °C during the AD of food waste. A BC load of 0.08 % slightly improved the BMP, although it was reduced by increasing the BC load, conversely, the μ_m was enhanced at all BC loads, with the highest values at BC 0.17 %. Furthermore, Cai et al. [233] studied the addition of fruitwood BC 900 °C with loads of 0.2-1 % (w/v) during the AD of food wastes, observing that all BC loads increased BMP and μ_m, although an optimal load of 0.5 % was established. Shen et al [173] added 0.8-1.5 % of fast pyrolysis corn stover BC 710 °C during the AD of sludge. The final BMP was only ~1 % higher than the control at all BC loads, whereas μ_m was favoured principally at a BC load

of 0.8 %. In summary, low BC loads (~0.4-0.6 %) are optimal for improving AD performance, particularly μ_m.

7.7 Principal component analysis

PCA is also known as a projection method, whose principal objective is the explanation of large data into smaller and more informative components. The results obtained from this work in addition to those gathered from the literature (**Tables 7.1-7.6**) comprised the dataset used for the PCA analysis. The parameters of the study included pyrolysis temperature, ash content of the BC, O:C atomic ratio of the BC, biochar load, ISR, methane yield (BMP), methane production rate (μ_m) and lag phase (λ). The variables pyrolysis temperature, ash content, and O:C ratio are related to the properties of the BCs, whereas the variables ISR, and BC load are related to the anaerobic conditions and finally BMP, μ_m and λ to the performance. The parameters BMP, μ_m and λ were calculated based on the comparison to their corresponding control (**Equation 3.14-3.16**). It is recommended to re-scaled and homogenised the data when different scales and units are being used. In this case, the initial data used units of pH, temperature, and percentage, hence, the values for the variables were mean centred and divided by their standard deviations and then used for the PCA [130].

Initially, it is important to assess if the data is appropriate for PCA. Thus, the Kaiser-Meyer-Olkin (KMO) method, Bartlett's test of sphericity and communalities were used. KMO examines the suitability of the data and is found between 0 and 1, where average values >0.5 are good and >0.9 are perfect. Bartlett´s test of sphericity indicates if there is a significant difference among the correlations between the variables (p<0.05). Further, the communalities indicate the relationship or amount of common variance of each variable with the entire set of data. It is not desirable for the correlations to be extremely low or non-existent or to be extremely high because these might indicate a lack of variation in the data [129]. Therefore, the analysis of this data resulted in average sample adequacy with a KMO value of 0.6 and a significant correlation between the variables with Bartlett´s test of sphericity (p<0.05). The communalities were adequate within a range of 0.555 to 0.700 (**Table 7.7**). Meaning for instance, that the communality of 0.652 for biochar load indicates that 65.2 % of the variance is explained by the variable and suchlike for the rest of the factors.

Table 7.7. Communalities from extraction PCA

	Initial	Extraction
Pyrolysis temperature	1.000	0.682
Biochar load	1.000	0.652
ISR	1.000	0.636
Ash content of biochar	1.000	0.700
O:C atomic ratio of biochar	1.000	0.688
Methane yield	1.000	0.614
Methane production rate	1.000	0.555
Lag phase	1.000	0.697

The PCs are defined as the linear depiction of the original dataset and represent the most important sources of variability explaining a certain amount of information within the original data. The Eigenvalue illustrated in the scree plot helps to determine the total number of PCs (**Figure 7.11**). This value represents the total amount of variance that can be explained by a given PC [130].
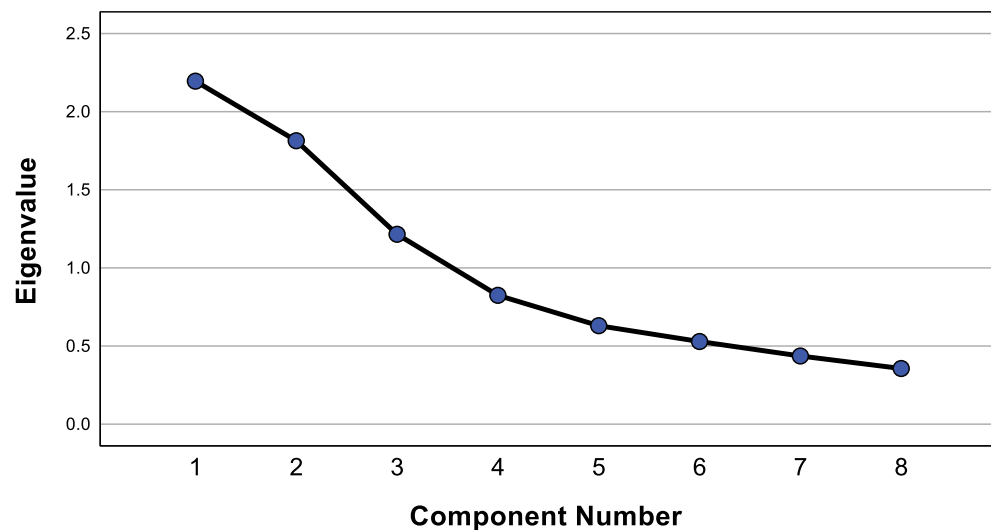
Figure 7.11. Scree plot of output variables from PCA analysis.

The PCA initially produced eight PCs, corresponding to each variable of the study, however, not all the PCs are used because most of the variance and the patterns followed by the data are represented by the first few PCs established with the Eigenvalues. Therefore, the variance of this dataset can be explained in three dimensions instead of eight because the analysis produced three PCs with eigenvalues greater than 1 (**Table 7.8**). The first PC contains the greatest source

of information explaining the data set, whereas each subsequent PC contains less information than the previous one.

Table 7.8. Eigenvalues and explained variances for the data set.

Component	Eigenvalue (λ)	Explained variance (%)	Cumulative variance (%)
1	2.20	27.44	27.44
2	1.81	22.67	50.11
3	1.22	15.19	65.30
4	0.83	10.31	75.61
5	0.63	7.88	83.49
6	0.53	6.61	90.10
7	0.44	5.45	95.55
8	0.36	4.45	100.00

Information about the correlation of variables of study can be obtained from the PCA plots. It is important to outline that the oblique rotation used for the PCA analysis assumed that all factors were correlated. **Figure 7.12** shows the analysis of the exploratory variables by PCA for the three PC exhibiting Eigenvalues greater than 1. The three PCs account for 65.3 % of the total variation in the data set. The blue circles correspond to the loading for each variable, which represents the association strength between each variable and factor [130]. However, illustrating the loadings in a three-dimensional plot difficult their interpretation, hence it is useful to evaluate two PCs at the time.

The biplot is one of the most informative visual representations of a multivariate dataset. The biplot can plot the sample information within two representations of the data, the scores, and the loadings. Firstly, a score is the orthogonal projection of each sample distributed in the PC space that describes the variability of the dataset. The distance of the samples distributed along the axis is an indication of how much of their information is contained within the PC. PCA scores clustering represent samples with similar variability pattern. Scores close to the origin indicate that those samples have average characteristics, show the least variability, and could be considered less important or not well described by the PCA model. Whereas the scores located at the extremes of the PC axis represent the samples with most of the variability. The proximity of the score to one PC states how much of its variability is explained for that particular PC, whereas the scores found in the space between the PC1 and PC2 axis are influenced by variables relevant for both axes [130].
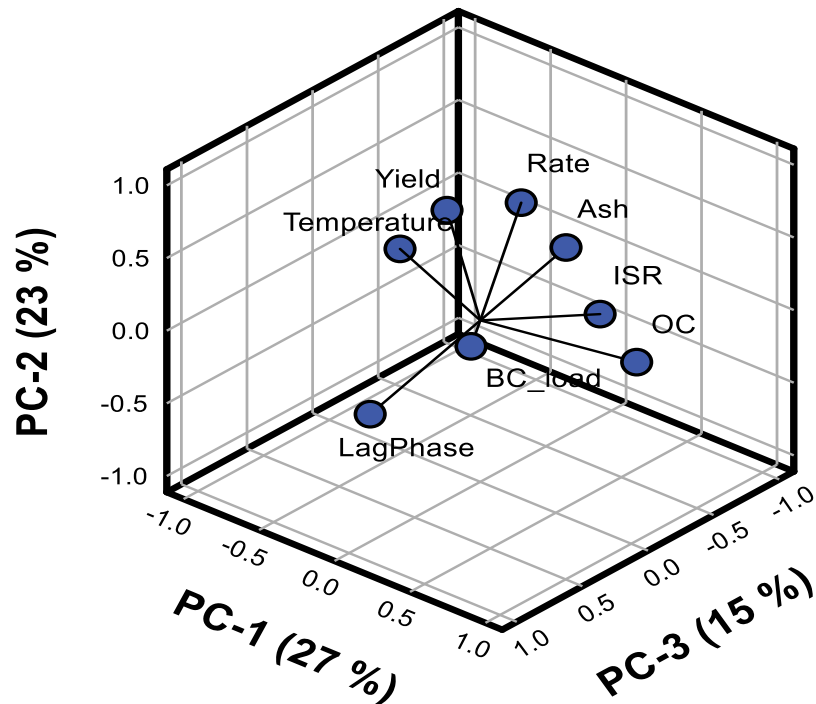
Figure 7.12. Correlation loadings plot for the three principal component analysis.

Pyrolysis temperature; methane yield (BMP biochemical methane potential); μ_m methane production rate; λ lag phase; ISR inoculum-to-substrate ratio; biochar ash content; biochar O:C ratio dry ash-free basis; biochar load. Dataset from this work and reports from the literature.

Furthermore, information about the correlation between the samples can also be deduced from the biplot. Such correlation is described by the cosine of the angle between the scores. Samples positively correlated are in a similar direction, while opposite directions indicate a negative correlation [132]. Thus, smaller angles lead to a higher correlation between samples. Secondly, PCA loadings arrange the dataset by plotting it as the individual contribution of the input of variables and their information in the PC space. The loadings indicate the contribution placed on each variable to describe the PCs and can be found on a scale of -1 to 1. Like the scores, loadings with the highest values and farther from the origin indicate the most important variables, whereas those closer to the origin or values of zero contribute little to describing the samples in the PCs [130]. The table of loadings facilitates the analysis of the biplot by stating which variable have high loadings, either positive or negative, indicating their contribution to each PC (**Table 7.9**).

Table 7.9. PCA loading for the contribution of the variables of study over the PCs.

Variable	Loading PC1	Loading PC2	Loading PC3
Pyrolysis temperature	-0.48345	-0.14571	0.32867
Biochar load	0.53153	0.08503	0.12434
Methane (BMP) yield	0.10731	0.32931	0.56779
Methane production rate (μ_m)	-0.307	0.39531	0.23161
Lag phase (λ) reduction	0.35406	-0.47786	0.07807
Ash content of BC	0.22736	0.55817	0.1286
O:C ratio of biochar	0.24295	0.35783	-0.51872
Inoculum to substrate ratio (ISR)	-0.3767	0.19715	-0.45693

To facilitate the visualisation, two-dimensional biplots containing only two PCs at the time are outlined in **Figure 7.13.** The biplot for PC1-PC2 describes most of the variation (50.11 %), followed by the graphical representation of PC1-PC3 corresponding to a variation of 42.6 %. Most scores are projected as scattered data lying along the PC1 indicating a higher influence by variables highly represented by that PC. The scores located in the space between the PC1-PC2 and PC1-PC3 axes are influenced by variables that are important on both PCs. **Figure 7.13a** shows the biplot PC1-PC2, and the values for the loadings are listed in **Table 7.9**. The loadings pyrolysis temperature, ISR and BC load are largely described by the PC1, whereas the rest contribute to describing both PCs. The magnitude of the loadings indicates a greater contribution of the variable pyrolysis temperature and BC load to describe the PC1, while the loadings ash content and lag phase largely describe the PC1 and PC2. The rest of the variables described both PCs, although the loadings for BMP and C:O were closer to the origin, suggesting the least variability and contribution.
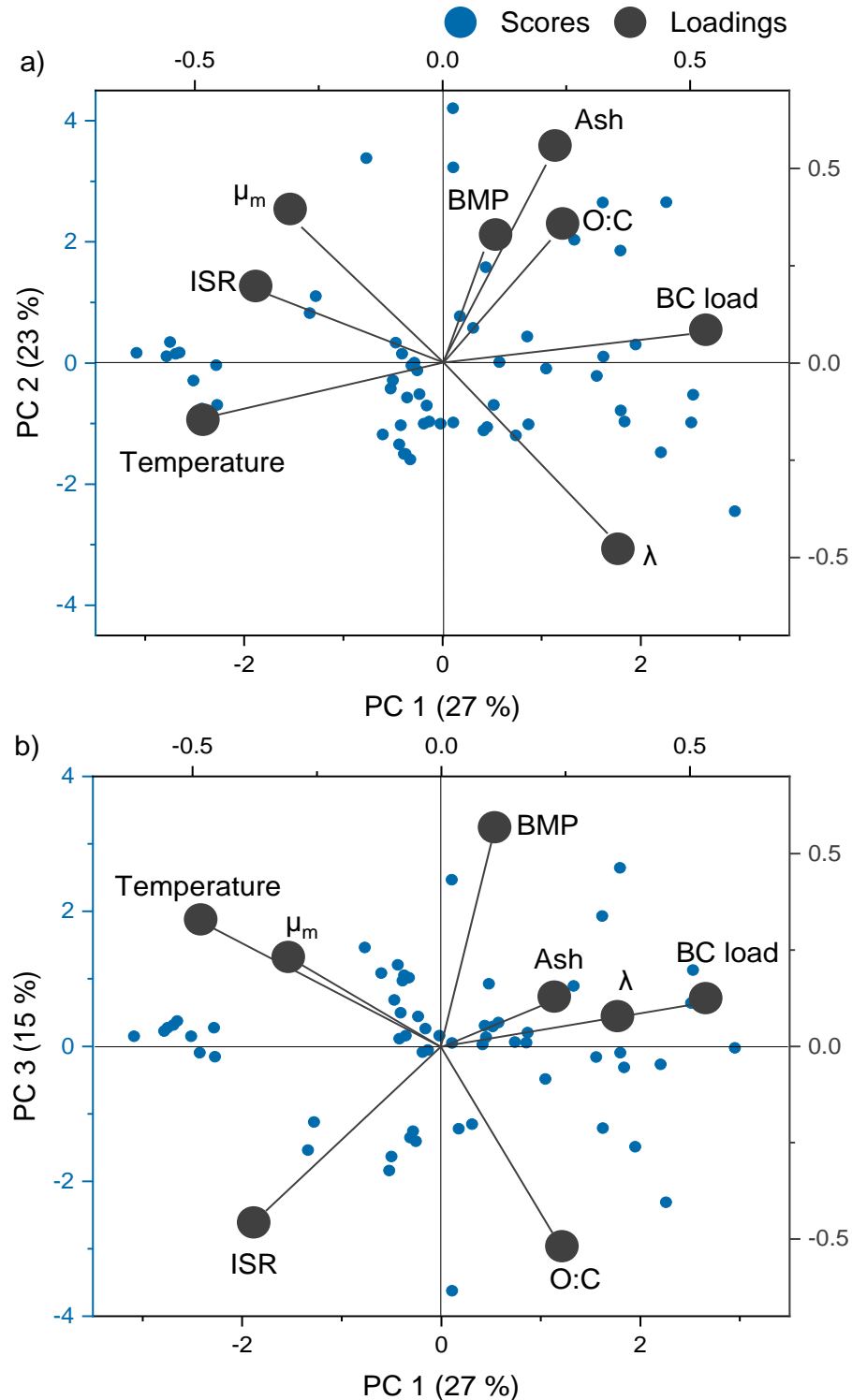
Figure 7.13. Principal component analysis biplot for the parameters influencing biochar augmentation in anaerobic digestion for: a) PC1 vs PC2; b) PC1 vs PC3.

PCA for the results of this work and those compiled from the literature. Pyrolysis temperature; methane yield (BMP biochemical methane potential); μ_m methane production rate; λ lag phase; ISR inoculum-to-substrate ratio; biochar ash content; biochar O:C ratio dry ash-free basis; biochar load. Dataset from this work and literature reports.

The pyrolysis temperature used for generating the BCs further used in AD was highly correlated to ISR and μ_m (**Figure 7.13a**). It has been previously argued that BCs produced at intermediate temperature (400-550 °C) were more favourable to AD. In Chapter 5 it was observed that the addition of OW and WH high-temperature BCs (600-650°C) slightly increased μ_m, whereas the intermediate-temperature BCs (450 °C) doubled μ_m. These BCs could facilitate DIET interactions due to their OFGs, functionalities reduced by increasing the temperature [93]. Thus, the temperature is the utmost important parameter in pyrolysis, since it determines most of the properties of the produced BCs and thus their effect on AD. The variables ash, O:C and BMP yield were highly correlated, meaning that as the ash and O:C ratio of the BC increases, so does the BMP yield. The correlation between the ash content and the O:C ratio was expected because these variables are related to the BC composition. Whereas their correlation with BMP yields supports the observations from Chapter 5 where the lower-temperature OW-BC450 and WH-BC450 contain a large presence of OFGs, and the latter a considerable ash content improved the AD of cellulose. This highlights that certain compositional features donate the BC the ability to improve the BMP yields.

The angles separating the BMP yield and μ_m were below 90 °, suggesting a positive correlation, thereby as the BMP increases so does the μ_m (**Figure 7.13a**). The same correlation principle is applied for μ_m and ISR, thereby higher μ_m could be achieved by employing larger ISRs. It is known that inoculation influences the initial activity and performance of the digester [266]. Conversely, loadings orthogonal (perpendicular) to each other are negatively correlated as observed for ISR with BC load and λ [131]. Extremely low ISRs are responsible for inclining the microbial population towards the proliferation of acidogens and acetogens, affecting thus methane production [123]. Hence, an appropriate ISR is essential for the methanogens and in consequence BMP yield and μ_m. On the other hand, large ISRs provide the inoculum with adequate conditions that reduce the λ and the necessity of additives, thereby the negative correlation between ISR and BC load.

Furthermore, the correlation between μ_m and λ is expected because these two variables are time-dependent. An orthogonal projection was also observed for the pyrolysis temperature and BC load, meaning that as the carbonisation degree of the BC increases, its addition to the digester must be reduced. Moreover, BC load was independently correlated to the O:C ratio and λ. The BC load could be quantitatively correlated to the amount of BC containing OFGs present in the digestate to facilitate the DIET process. In this work, it has been stated the

negative impact that higher doses of BC could exhibit over AD, including λ. Whereas more sensible BC loads ($\sim$0.4-0.6 %) could substantially improve AD performance as stated in section 7.6.5. All these observations agree with the results from Chapter 5 where higher temperature BCs offered no additional improvement on the digester performance. Also, the AcoD of cellulose and *C. vulgaris* from section 6.4 where the methane production was favoured by a higher ISR and lower BC loads.

Figure 7.13b shows the biplot PC1-PC3, describing how each variable contributes to the PC1 and PC3 corresponding to 42.6 % of the data variation. The variables pyrolysis temperature, BC load, and lag phase (λ) are once more highly described by the PC1. The magnitude and distribution of the loadings on the PC area indicate that the variable BMP, O:C ratio and ISR yield are highly described by the PC3 (**Table 7.9**). Like the biplot PC1-PC2, **Figure 7.13b** suggests a correlation between the variable pyrolysis temperature and μ_m. The loading for λ is now near the variable ash and BC load, which could be attributed to the role of the BC in facilitating DIET interactions that promote the methanogenesis and reduce the λ. The variables BMP and ISR largely describe the PC3 with loading values of 0.57 and -0.56, respectively. These two variables are positioned orthogonally, suggesting that by increasing one the other is reduced. This pattern was observed for the AD digestion of water hyacinth in section 6.5. The reports gathered for section 7.6.4 showed that the BMP could be either improved or reduced at variable ISRs. Whereas the results from the AcoD of cellulose and *C. vulgaris* from section 6.4 support the obtainment of greater BMP yields at higher ISR. There are also reports stating that the addition of BC in AD improves methane production, especially under stressful conditions, like low ISRs [38]. Therefore, the effect of ISR during BC augmentation in AD could be simultaneously influenced by other variables.

On the other hand, the loading for the O:C ratio is perpendicular or negatively correlated to pyrolysis temperature, and μ_m. This supports the role of lower pyrolysis temperature for obtaining BCs with a greater O:C ratio. However, the orthogonal projection between the O:C ratio and μ_m could suggest that BCs with higher O:C ratios could reduce μ_m. It is important to outline that the variable O:C ratio contributes principally to the PC3 with a loading value of -0.519, and to a lesser extent to PC1 and PC2 (**Table 7.9**). Nonetheless, the PC1-PC2 biplot and the observations from Chapter 5, support that BCs with a larger presence of OFGs facilitate the syntrophic metabolism and DIET interactions improving BMP yield and μ_m. In addition, the analysis from section 7.5.3 evaluated BCs with O:C ratios ranging from 0.06 to 0.41 and demonstrated that BCs with an O:C ratio of 0.20

were responsible for most of the improvement for BMP and μ_m. Furthermore, any relationship identified between variables must be evident in all the retained PCs.

Generally, there was a positive correlation between the variables related to the BC properties (ash content and O:C ratio) and an orthogonal projection for pyrolysis temperature, particularly for the PC1-PC2. The variables related to the anaerobic condition ISR, and BC load were also orthogonally projected. Finally, those related to the AD performance BMP yield and μ_m were positively correlated and orthogonal to λ reduction. These patterns were mostly maintained in both biplots. In summary, the PCA simplified the analysis of complex data with several variables while retaining trends and patterns on a limited number of PCs. The standardisation of data for the PCA allowed the evaluation of data with different scales as used for this work. This PCA outlined the importance of the variables involved during BC addition in AD, as valuable information was deduced from the plots. Hence, PCA proved to be a useful statistical method for evaluating the effect of BC addition on AD.

7.8 Conclusions

The BCs largely used in AD were produced from a wide variety of feedstocks and pyrolysis conditions. Their addition in AD reactors exhibited a significant effect on the process performance and kinetic parameters. The general behaviour was a considerable faster production rate and a moderate improvement in BMP yield and a reduction in the lag phase.

The operating conditions used in the AD experiments influenced the effect of the BCs on the digestion performance. Most experiments consisted of batch configurations on AMPTS or serum bottles of variable sizes. Hence, it is important to highlight the necessity to study BC implementation on continuous long-term operations for creating a more thorough and tangible assessment of the BC amendment. The ISR was not the most significant factor in these experiments, although BC addition favoured the BMP yield and μ_m at most ISRs, with exceptional cases at low ISRs <1. Therefore, it could be argued that BC addition could relieve AD performance, principally under stressful conditions.

A myriad of substrates was used for generating methane, while BC addition was favourable for most. For easily hydrolysed substrates BC addition generally reduced λ and increased the μ_m, whereas the improvement of the BMP was only significant at the lowest ISR. This type of substrate usually leads to good yields,

which are negatively affected under stressful or sub-optimal conditions, thereby it is under these conditions that BC proved to be more successful. The digestion of biomass with considerable protein content, such as algae, animal or even food waste, often results in inhibitory concentrations of total ammonia nitrogen. Generally, the BC offered certain amending of TAN, although it was limited to moderate concentrations suggesting its adsorption capacity is not limitless. On the other hand, BC addition offered minimal benefits for the digestion of aquatic biomass, such as water hyacinth and seaweed. Nonetheless, it could be argued that BC addition was even more favourable for complex substrates, although more research in this matter would be necessary for a proper correlation.

The feedstock, pyrolysis conditions and the final properties of the BCs influenced their further impact on AD. Of all the BCs evaluated, woody derived with an ash content of 3.1-6.3%, O:C ratio of 0.20, and produced at an intermediate pyrolysis temperature BCs 450-550 °C were responsible for having the greatest positive impact on AD. Besides the composition and the conditions for producing the BC, the amount of BC added to the digesters influenced AD performance. Increasing BC loads favoured μ_m, although this could hinder BMP yields. Therefore, low BC loads (~0.4-0.6 %) were optimal for improving AD performance, particularly μ_m without affecting the BMP yields.

The potential of BC to act as a buffering agent was constantly reported, although it was more tangible under sub-optimal conditions, such as low ISRs and the co-digestion of complex substrates. Hence, the BC can stabilise AD reactors and provide a buffering effect by increasing the pH and promoting methanogenesis. Fundamentally, the role of biochar in stabilising the pH of the digester is attributed to an enhanced electron transfer capacity for directing VFAs conversion in DIET-involved methanogens. The benefits of BC also include the ability to facilitate the colonisation/immobilisation of microbial cells, while promoting the proliferation of those involved in DIET interactions, particularly methanogenic archaea. It is important to outline that most works reported the increase in the concentration of these microbial populations, although the mechanisms behind it are not fully understood.

PCA allowed the explanation of the large data gathered from this work and literature reports for the addition of BC in AD into smaller and more informative components. Certain features exhibited a high correlation, including (i) ash, O:C and BMP yield, (ii) μ_m, ISR and pyrolysis temperature, and (iii) BC load and λ. The correlation between the ash content and the O:C ratio was expected because these features are connected to the BC composition. The correlation of ash and

O:C ratio with BMP yields supported the principle that not all BCs are suitable for AD, and certain compositional features donate the BC the ability to improve the BMP yields. The latter was also strengthened by the importance of pyrolysis temperature in the effect of BC addition in AD. The correlation of pyrolysis temperature with μ_m supports the statement that BCs produced at intermediate temperature (400-550 °C) are more favourable to AD. Besides the BC properties, it was established that the effect of BC in AD was influenced by some fermentation conditions. It was stated the importance of an appropriate ISR for the methanogens and in consequence BMP yield and μ_m. The BC load also proved to be an important parameter in the BC amendment in AD, suggesting that all the mentioned benefits were subjected to limiting the amount of BC added to the digester.

Chapter VIII

Conclusions

8.1 Summary

The introduction of this thesis outlined the necessity for acting on mitigating climate change to decelerate global warming. The energy sector must transition towards more sustainable technologies to reduce fossil fuel dependency and meet the established targets for sustainable energy. Gaseous biofuels are identified as a suitable alternative to natural gas in the transport, electrical and heating sectors and are likely to gain relevance. This has gained even more importance recently due to increased demand for natural gas resulting in a huge spike in wholesale gas prices increasing domestic energy costs and bankrupting energy suppliers. Even though anaerobic digestion is a well established industry, its development and industrialisation are still limited to certain countries. Furthermore, AD is a complex fermentation process and still faces challenges in implementing a wider range of substrates whilst maintaining digestate stability. In some regions, small-scale AD is used extensively to produce cooking gas, however, the digesters are often operated under suboptimal conditions by non-experienced users and tend to undergo stability issues, resulting in poor performance. The addition of biochar to anaerobic digestion to improve digester performance has received increasing attention in the literature with multiple benefits being highlighted, however, the exact interactions are still widely debated and poorly understood. There is therefore a need to expand the current understanding of this research field and this research has contributed to this goal. Analysis of the literature suggests there is a positive effect, and this research develops a further understanding based on the fundamental objectives stated in Chapter 1.

Objective 1. *Perform an extensive literature review of the behaviour of biochar and hydrochar during anaerobic digestion.*

There were few reports of biochar augmentation on AD by the time this project was conceptualised. During this PhD research, the interest in this topic has increased considerably with numerous publications released, supporting the

pertinence and potential of its application. The reports in the literature included biochars from numerous feedstocks produced under different conditions. The addition of these biochars to the AD of several substrates and conditions has largely reported an enhancement in the production rate and reduced the lag phase, although a minority reported no effect or even a detrimental one. Biochar addition was highly favourable for the digestion of complex substrates, whilst for easily hydrolysed substrates, biochar amendment was more significant at low ISR. There is a consensus in the literature supporting the potential of biochar to facilitate the reactions involved in AD, buffering acid stress, enhancing methanogenesis, promoting syntrophic interactions and enhancing methane yield and production rate. These benefits are also attributed to the capacity of the biochar to immobilise microorganisms, exhibiting a proliferation of methanogens, and stabilising the digester. The publications for hydrochar addition in AD are limited. The addition of hydrochar has an inhibitory effect on methanogenesis, especially if produced at high temperatures. This behaviour suggests that the hydrochar is not a suitable additive for AD, although the potential of mild HTC as a pre-treatment of biomass could be a better approach.

Objective 2. *Develop a quantitative understanding of the impact of processing conditions and feedstock choice on the final properties of biochar and hydrochar.*

Contributes to our understanding of the property function relationships by assessing the impact of processing conditions and feedstock properties. The feedstocks oak wood, water hyacinth and saw wrack were treated by pyrolysis at two temperature sets (450 and 600-650 °C) and one HTC temperature set (250 °C). The biochars and hydrochars obtained were analysed to establish their chemical, physical and functional properties. The carbonisation treatments resulted in the loss of volatile matter and oxygen content whilst enhancing their aromaticity and carbon content. The differences between the selected feedstocks were reflected in the loss of volatile matter, the surface areas achieved, and the presence of oxygenated functional groups (OFGs). X-ray photoelectron spectroscopy (XPS) proved to be a powerful technique for the semi-quantification of the functional groups in the chars, one of the most important properties of these materials. There were many differences between biochars and hydrochars. These are inherent in the choice of feedstock, and the processing conditions employed, in particular reaction temperature. The biochemical content (e.g., carbohydrate, protein, and lignin content) and the metal and ash content of each feedstock have a large influence on the final properties and

composition of the chars. The insight obtained from this analysis allowed the further correlation of their impact when implemented in anaerobic digestion.

Objective 3. *Assess the potential of biochar and hydrochar to be used as amendment additives and immobilisation supports during the anaerobic digestion of the model substrate cellulose. Correlate the properties of the chars with their impact on methane generation and digestion performance.*

Assessing the potential of biochar and hydrochar as amendment additives during the anaerobic digestion of a model substrate became a fundamental task for achieving Objective 3. The best performance was obtained with the addition of the lower-temperature oak wood and water hyacinth biochars. The methane yield was moderately improved, whereas the methane production rate almost doubled compared to the control. These benefits were attributed principally to the OFGs located on the surface of the biochars, responsible for facilitating the exchange of electrons between the microorganisms involved in hydrolysing the substrate into organic acids and H^+, and those that use these compounds to produce methane. The relevance of the OFGs was more evident when compared to the higher OW and WH biochars. Similar levels of methane were produced with the addition of these BCs and the control, suggesting that no further functionality benefits were provided. It could be argued that additional reactions of decarboxylation and aromaticity occurring at higher pyrolysis temperature resulted in biochars with fewer OFGs and reduced potential for AD amendment. Furthermore, the addition of different hydrochars produced at 250 °C had a detrimental effect on methane generation, although it promoted the formation of organic acids, particularly acetic acid. Some unfavourable properties of the HC on AD include acidic pH and the large presence of humic acids, and given the high HTC temperature, it is possible that undesirable N-containing by-products of Maillard reactions. Nonetheless, it is desirable to develop routes for producing acetic acid from renewable sources, thereby it could be worth considering and exploring the potential of the HC in this research area.

Objective 4. *Use of factorial design of experiments to evaluate and optimise the effect of biochar on anaerobic mono and co-digestion of complex substrates and identify optimum digestion conditions.*

Once it was established which biochar was more favourable for AD, in this case, OW-BC450 was employed in the digestion of more complex substrates to reach Objective 4. Two sets of experiments were undertaken and consisted of the anaerobic co-digestion of the microalgae *Chlorella vulgaris* and cellulose and the

AD of the aquatic plant water hyacinth. By performing factorial experimental designs and optimisation, it was possible to establish the best digestion conditions and biochar load for achieving the highest possible methane production in each case. During the AcoD of *C. vulgaris*, a correlation was observed between the inoculum to substrate ratio (ISR) and the effect of the biochar on AD. The methane yield increased by 1.8-4.6 times at unfavourably low ISRs 0.5-0.9 and variable C/N ratios, whereas, at ISRs 1.0-2.0, the improvement due to BC addition was more moderate. This behaviour suggests that the positive effect of BC could be more tangible under stressful or unfavourable conditions. The effect of BC addition on the AcoD of *C. vulgaris* and cellulose differed from the observed for water hyacinth. The addition of BC on the AD of WH samples from different origins provided no significant effect on the methane yield or production rate. In summary, it was established that high biochar loads could have a detrimental effect on AD, while small amounts could achieve the best performance for complex substrates.

Objective 5. *Identify the most relevant biochar properties and fermentation conditions influencing the anaerobic digestion performance of both the experimental data produced in this work, in combination with data published in the literature via descriptive statistics and principal component analysis.*

By gathering the results from this work and those reported in the literature regarding the effect of biochar in AD, a certain ambiguity was observed with many questions arising. Hence, a series of descriptive statistical and principal component analyses were performed to establish the main factors behind the amendment effect of biochar in methane production, according to Objective 5. Biochars produced from several feedstocks and pyrolysis conditions were implemented for the AD of numerous substrates and processing conditions. The general behaviour was a considerably faster production rate, a moderate improvement in BMP yield and a reduction in the lag phase. From the analysis, a correlation between the digestion conditions, and the effect of the BC, existed. It could be argued that BC addition could amend AD performance, principally under stressful conditions, such as low ISRs and complex substrates. Also observed during these conditions, was the potential of the BC to act as an intensified buffering agent. Hence, the BC can stabilise AD reactors, provide a buffering effect by increasing the pH and promote methanogenesis. In summary, woody biochars with an ash content of 3.1-6.3%, O:C ratio of 0.20, produced at an intermediate pyrolysis temperature of 450-550 °C, and added at BC loads of 0.4-0.6 % can offer the best benefits for AD. Furthermore, PCA allowed the

identification of the most important variables and correlations affecting BC addition in AD. The relevance of pyrolysis temperature and the correlation for ash and O:C ratio with methane yields supported the principle that not all BCs are suitable for AD, and certain compositional features donate the BC the ability to improve the BMP yields. The BC load proved that all the mentioned benefits were subjected to limiting the amount of BC added to the digester. The major contribution of this work was to donate a guide to the scientific community about which biochars are best for AD and how to use them for achieving the best methane performance.

8.2 Future work

If more time was available for this research, additional anaerobic digestion experiments would have been run and other aspects of the research could have been explored. There are numerous areas to study, to systematically understand what makes the biochar active for a specific response. It would be interesting to take advantage of statistical tools, such as the design of experiments, for extending this project. Further studies of factors involving pyrolysis conditions, feedstock composition and the effect of BC on AD could be useful for increasing the understanding of this relationship.

During the evaluation of the BC composition and their effect in AD, it was outlined that the water hyacinth BC produced at 450 °C contained a considerably high ash content and yet exhibited a favourable effect on methane generation. The trend obtained from the PCA suggested that low-ash BCs are more suitable for AD, however, most of the biochars compiled for the analysis originated from low-ash feedstocks, particularly from wood or other plant species, whereas there were few high-ash biochars including almost exclusively those from this work. Hence it would be useful to pursue the effect of ash by evaluating different BCs within a wide range of ash content, and simultaneously analysing the metals comprising the BCs to understand their effect on alkalinity and their possible role in conductivity and trace nutrients. Testing biochars from different feedstocks and thereby different compositions but produced at equal pyrolysis conditions could contribute greatly to the understanding of biochar augmentation in AD.

Furthermore, evaluating biochar addition during the AD of a wide range of feedstocks highly available in different parts of the world where guaranteeing cooking gas is still neglected or if there is a large production of organic waste and a need for exploitation. For instance, the waste from different industrial sectors

involving biomass such as breweries, distilleries, sugarcane, tequila, and agave waste, all stages from domestic to industrial producing food waste, among others. This research indicated that the benefits from biochar augmentation increased under sub-optimal AD conditions. Hence, it would be valuable to select unsuitable conditions that could occur in either small rudimentary digesters or large-scale reactors. Such variables could be ISR, AcoD of different complex feedstocks, substrate load and composition, or even selecting other sources of nitrogen, such as urea or ammonia to explore the effect of biochar at variable C/N ratios. Moreover, the large-scale AD industry is developed only in a few countries, hence the sources and availability of inoculum would differ. Therefore, it would be interesting to explore inoculums from different sources, such as animal dung, activated sludge, and inoculum from any technology employed at local WWT plants, either municipal or within another industrial area. All these conditions could be evaluated by DOE to facilitate and validate the experiments. It has been suggested that biochar influences the microbial community by promoting the proliferation of methanogens. Therefore, if different inoculum sources could be studied simultaneously, it would be extremely beneficial to extract DNA samples and perform DNA sequencing to evaluate the changes in the microbial community due to biochar augmentation.

If this project could have had a couple of months extra, it would have been beneficial to perform a few other experiments. For instance, another DOE study on the variable C/N ratio, obtained from mixing cellulose and ammonia, or cellulose and urea, and the variable substrate load. Also, exploring the effect of the biochar on the biogas quality. The AMPTS equipment used for AD is connected to a NaOH trap that catches and solubilises the by-product CO_2. Hence, the quantified product was exclusively methane for all runs. It would be useful to remove this trap to allow the volumetric measurement of all the biogas, and to analyse its composition. This would assist in observing if, and how much, the biochar could improve the methane fraction and quality of the biogas. Simultaneously, this would allow the evaluation of the capacity of the biochar to adsorb CO_2 and its potential for biogas upgrading.

A short hydraulic retention time is desirable for a continuous system since it increases process efficiency. However, high fluxes could dilute the suspended inoculum and lead to digestate failure. One of the proposed advantages of BC as immobilisation support is to provide stability and protection to the cells for improving their performance, particularly at higher fluxes and lower HRT. Hence, it is important to outline the potential of BC for stabilising semi-continuous or continuous long-term operations, and the necessity to study this.

This implementation could at the same time raise more research questions. For instance, is the adsorption capacity of biochar limited to the groups located on their surface or is it dynamic? Is it worth periodically adding small amounts of biochar into the digester to maintain stability or is it enough to incorporate only one initial load?

The research performed in this work on the anaerobic digestion of water hyacinth accompanied by biochar amendment covered only the surface. There are still many variables to consider and opportunities to contribute. It is imperative to consider the differences in materials and resources based on the location. Firstly, it was easy to access inoculum from a WWT plant in the UK, however, this industrial sector is underdeveloped in other countries, especially those most affected by water hyacinth. In India and Uganda, it is easier to have access to other sources of inoculum, such as cow dung. Secondly, the water hyacinth used in this research was collected and dried for shipment to the UK where it was digested. Whereas it could be removed from the water bodies it invades and be directly used in AD without the necessity to dry it. Thirdly, the reactors used in this research consisted of 500 mL bottles within an AMPTS system. It would be beneficial to test the potential of AD in larger digesters as a continuous or semi-continuous process. With the potential for profitability, this larger-scale approach could provide a better way to solve regional problems.

The addition of high-temperature HC in AD promoted the production of VFAs, particularly acetic and propionic acid. The production of acetic acid is currently dominated by the carbonylation of methanol during the steam-reforming of fossil fuels. Therefore, there is a growing interest in developing sustainable routes for producing acetic acid from renewable sources. This is where hydrochar addition in AD, or even could be considered an option. It would be interesting to develop some experiments to try out this hypothesis and establish another application for the hydrochar products.

Bibliography

[1]   United States Environmental Protection Agency, Global Greenhouse Gas Emissions Data, (n.d.). https://www.epa.gov/.

[2]   IPCC Intergovernmental Panel on Climate Change, AR6 Climate Change 2021: The Physical Science Basis, 2021. https://www.ipcc.ch/report/sixth-assessment-report-working-group-3/ (accessed March 8, 2022).

[3]   IPCC Intergovernmental Panel on Climate Change, AR5 Climate Change 2014: Mitigation of Climate Change, 2014. www.ipcc.ch/.

[4]   United Nations, The Sustainable Development Goals Report, 2021. https://unstats.un.org/sdgs/report/2021/ (accessed March 8, 2022).

[5]   R. Stavins, J. Zou, T. Brewer, M. Conte Grand, M. den Elzen, M. Finus, J. Gupta, N. Höhne, M.-K. Lee, A. Michaelowa, M. Paterson, K. Ramakrishna, G. Wen, J. Wiener, H. Winkler, International Cooperation: Agreements and Instruments. In: Climate Change 2014: Mitigation of Climate Change, in: Cambridge University Press (Ed.), Contrib. Work. Gr. III to Fifth Assess. Rep. Intergov. Panel Clim. Chang., 2014: pp. 1001–1082.

[6]   IPCC Intergovernmental Panel on Climate Change, Renewable Energy Sources and Climate Change Mitigation, Cambridge, 2011. https://www.ipcc.ch/ (accessed September 1, 2021).

[7]   IEA, OECD share of total energy supply by source, (2019). https://www.iea.org/ (accessed September 1, 2020).

[8]   IEA, Renewable power generation by technology in the Sustainable Development Scenario 2000-2030 – Charts – Data & Statistics - IEA, (2021). https://www.iea.org/ (accessed September 1, 2021).

[9]   IEA, Renewables 2020 – Analysis and forecast to 2025, 2021. https://www.iea.org/ (accessed September 1, 2021).

[10]   IEA, Renewable electricity – Renewables 2020, (2020). https://www.iea.org/reports/renewables-2020/renewable-electricity-2 (accessed May 11, 2022).

[11]   L.M. Agudelo-Escobar, U. Salazar-Álvarez, M. Peñuela, Yeast immobilization in lignocellulosic wastes for ethanol production in packed bed bioreactor, Rev. Fac. Ing. Univ. Antioquia. (2012) 66–76.

[12]   W.-C. Huang, I.-C. Tang, Bacterial and Yeast Cultures – Process Characteristics, Products, and Applications, in: Bioprocess. Value-Added Prod. from Renew. Resour., Elsevier, 2007: pp. 185–223.

[13]   IEA, Outlook for biogas and biomethane. International Energy Agency, 2020. https://www.iea.org/ (accessed May 8, 2020).

[14]   J. Song, Y. Wang, S. Zhang, Y. Song, S. Xue, L. Liu, X. Lvy, X. Wang, G. Yang,

Coupling biochar with anaerobic digestion in a circular economy perspective: A promising way to promote sustainable energy, environment and agriculture development in China, Renew. Sustain. Energy Rev. 144 (2021) 110973.

[15] Q. Yang, H. Zhou, P. Bartocci, F. Fantozzi, O. Mašek, F.A. Agblevor, Z. Wei, H. Yang, H. Chen, X. Lu, G. Chen, C. Zheng, C.P. Nielsen, M.B. McElroy, Prospective contributions of biomass pyrolysis to China's 2050 carbon reduction and renewable energy goals, Nat. Commun. 12 (2021) 1–12.

[16] M.O. Fagbohungbe, B.M.J. Herbert, L. Hurst, C.N. Ibeto, H. Li, S.Q. Usmani, K.T. Semple, The challenges of anaerobic digestion and the role of biochar in optimizing anaerobic digestion, Waste Manag. 61 (2017) 236–249.

[17] J. Mumme, F. Srocke, K. Heeg, M. Werner, Use of biochars in anaerobic digestion, Bioresour. Technol. 164 (2014) 189–197.

[18] M. Aziz, A. Darmawan, F.B. Juangsa, Hydrogen production from biomasses and wastes: A technological review, Int. J. Hydrogen Energy. (2021).

[19] A. Funke, F. Ziegler, Hydrothermal carbonization of biomass: A summary and discussion of chemical mechanisms for process engineering, Biofuels, Bioprod. Biorefining. 4 (2010) 160–177.

[20] J. Pan, J. Ma, L. Zhai, T. Luo, Z. Mei, H. Liu, Achievements of biochar application for enhanced anaerobic digestion: A review, Bioresour. Technol. 292 (2019) 122058.

[21] M.E. González, M. Cea, N. Sangaletti, A. González, C. Toro, M.C. Diez, N. Moreno, X. Querol, R. Navia, Biochar Derived from Agricultural and Forestry Residual Biomass : Characterization and Potential Application for Enzymes Immobilization, J. Biobased Mater. Bioenergy. 7 (2013) 724–732.

[22] M. Pecchi, M. Baratieri, Coupling anaerobic digestion with gasification, pyrolysis or hydrothermal carbonization: A review, Renew. Sustain. Energy Rev. 105 (2019) 462–475.

[23] D. Woolf, J.E. Amonette, F.A. Street-Perrott, J. Lehmann, S. Joseph, Sustainable biochar to mitigate global climate change, Nat. Commun. 1 (2010) 1–9.

[24] K. Khosla, R. Rathour, R. Maurya, N. Maheshwari, E. Gnansounou, C. Larroche, I. Shekhar, Biodiesel production from lipid of carbon dioxide sequestrating bacterium and lipase of psychrotolerant Pseudomonas sp . ISTPL3 immobilized on biochar, Bioresour. Technol. 245 (2017) 743–750.

[25] A. Downie, A. Crosky, P. Munroe, Physical Properties of Biochar, in: J. Lehman, S. Joseph (Eds.), Biochar Environ. Manag. Sci. Technol., First, Earthscan, 2009: pp. 13–32.

[26] F.G. de Mendonça, I.T. da Cunha, R.R. Soares, J.C. Tristão, R.M. Lago, Tuning the surface properties of biochar by thermal treatment, Bioresour. Technol. 246 (2017) 28–33.

[27] J. Zhang, F. Zhang, H. Yang, X. Huang, H. Liu, J. Zhang, S. Guo, Graphene Oxide as a Matrix for Enzyme Immobilization, Langmuir. 26 (2010) 6083–6085.

[28] S.R. Shanmugam, S. Adhikari, H. Nam, S. Kar Sajib, Effect of bio-char on methane generation from glucose and aqueous phase of algae liquefaction using mixed anaerobic cultures, Biomass and Bioenergy. 108 (2018) 479–486.

[29] T. Kan, V. Strezov, T.J. Evans, Lignocellulosic biomass pyrolysis: A review of product properties and effects of pyrolysis parameters, Renew. Sustain. Energy Rev. 57 (2016) 1126–1140.

[30] W. Suliman, J.B. Harsh, N.I. Abu-Lail, A.M. Fortuna, I. Dallmeyer, M. Garcia-Perez, Influence of feedstock source and pyrolysis temperature on biochar bulk and surface properties, Biomass and Bioenergy. 84 (2016) 37–48.

[31] J. Lee, K.H. Kim, E.E. Kwon, Biochar as a Catalyst, Renew. Sustain. Energy Rev. 77 (2017) 70–79.

[32] L. Zhao, X. Cao, O. Mašek, A. Zimmerman, Heterogeneity of biochar properties as a function of feedstock sources and production temperatures, J. Hazard. Mater. 257 (2013) 1–9.

[33] C.B. Arenas, W. Meredith, C.E. Snape, X. Gómez, J.F. González, E.J. Martinez, Effect of char addition on anaerobic digestion of animal by-products: evaluating biogas production and process performance, Environ. Sci. Pollut. Res. 27 (2020) 24387–24399.

[34] C.G. Achi, A. Hassanein, S. Lansing, Enhanced Biogas Production of Cassava Wastewater Using Zeolite and Biochar Additives and Manure Co-Digestion, Energies. 13 (2020) 1–13.

[35] Y. Qin, X. Yin, X. Xu, X. Yan, F. Bi, W. Wu, Specific surface area and electron donating capacity determine biochar's role in methane production during anaerobic digestion, Bioresour. Technol. 303 (2020) 122919.

[36] Y. Sugiarto, N.M.S. Sunyoto, M. Zhu, I. Jones, D. Zhang, Effect of biochar addition on microbial community and methane production during anaerobic digestion of food wastes: The role of minerals in biochar, Bioresour. Technol. 323 (2021) 124585.

[37] C. Deng, R. Lin, X. Kang, B. Wu, R. O'Shea, J.D. Murphy, Improving gaseous biofuel yield from seaweed through a cascading circular bioenergy system integrating anaerobic digestion and pyrolysis, Renew. Sustain. Energy Rev. 128 (2020) 109895.

[38] L. Shao, S. Li, J. Cai, P. He, F. Lü, Ability of biochar to facilitate anaerobic digestion is restricted to stressed surroundings, J. Clean. Prod. 238 (2019) 117959.

[39] K. Paritosh, V. Vivekanand, Biochar enabled syntrophic action: Solid state anaerobic digestion of agricultural stubble for enhanced methane production, Bioresour. Technol. 289 (2019) 121712.

[40] D.M. Alonso, J.Q. Bond, J.A. Dumesic, Catalytic conversion of biomass to biofuels, Green Chem. 12 (2010) 1493–1513.

[41] M. Fatih Demirbas, M. Balat, H. Balat, Biowastes-to-biofuels, Energy Convers. Manag. 52 (2011) 1815–1828.

[42] M.F. Ibrahim, S.W. Kim, S. Abd-aziz, Advanced bioprocessing strategies for biobutanol production from biomass, Renew. Sustain. Energy Rev. 91 (2018) 1192–1204.

[43] O.M. Adeniyi, U. Azimov, A. Burluka, Algae biofuel: Current status and future applications, Renew. Sustain. Energy Rev. 90 (2018) 316–335.

[44] R. Khandeparker, R.K. Sani, Biobutanol Production Using Recombinant Microorganisms, in: R.K. Sani, N.K. Rathinam (Eds.), Extrem. Microb. Process. Lignocellul. Feed. to Biofuels, Value-Added Prod. Usable Power, Springer International Publishing, Cham, 2018: pp. 47–62.

[45] S.M. Scully, J. Orlygsson, Amino Acid Metabolism of Thermoanaerobacter Strain AK90 : The Role of Electron-Scavenging Systems in End Product Formation, J. Amino Acids. 2015 (2015) 1–10.

[46] J.C. Akunna, Anaerobic Waste-Wastewater Treatment and Biogas Plants, 1st ed., CRC Press/Taylor & Francis Group, Boca Raton, FL, 2018.

[47] B. Bharathiraja, T. Sudharsana, J. Jayamuthunagai, R. Praveenkumar, S. Chozhavendhan, J. Iyyappan, Biogas production-A review on composition, fuel properties, feed stock and principles of anaerobic digestion Article in Renewable and Sustainable Energy Reviews · Optimization of Anaerobic Conditions for the Treatment of Textile Dye Wastewater using Mixed, Renew. Sustain. Energy Rev. 90 (2018) 570–582.

[48] J. Zhang, W. Zhao, H. Zhang, Z. Wang, C. Fan, L. Zang, Recent achievements in enhancing anaerobic digestion with carbon- based functional materials, Bioresour. Technol. 266 (2018) 555–567.

[49] N. Duan, X. Dai, B. Dong, L. Dai, Anaerobic digestion of sludge differing in inorganic solids content: Performance comparison and the effect of inorganic suspended solids content on degradation, Water Sci. Technol. 74 (2016) 2152–2161.

[50] M. Zhou, B. Yan, J.W.C. Wong, Y. Zhang, Enhanced volatile fatty acids production from anaerobic fermentation of food waste: A mini-review focusing on acidogenic metabolic pathways, Bioresour. Technol. 248 (2018) 68–78.

[51] M.A. Khan, H.H. Ngo, W.S. Guo, Y. Liu, L.D. Nghiem, F.I. Hai, L.J. Deng, J. Wang, Y. Wu, Optimization of process parameters for production of volatile fatty acid, biohydrogen and methane from anaerobic digestion, Bioresour. Technol. 219 (2016) 738–748.

[52] M. Wang, J.F. Tomb, J.G. Ferry, Electron transport in acetate-grown Methanosarcina acetivorans, BMC Microbiol. 11 (2011) 1–10.

[53] S. Arif, R. Liaquat, M. Adil, Applications of materials as additives in anaerobic digestion technology, Renew. Sustain. Energy Rev. 97 (2018) 354–366.

[54] R. Li, N. Duan, Y. Zhang, Z. Liu, B. Li, D. Zhang, T. Dong, Anaerobic co-digestion of chicken manure and microalgae Chlorella sp.: Methane potential, microbial diversity and synergistic impact evaluation, Waste Manag. 68 (2017) 120–127.

[55] X. Meng, D. Yu, Y. Wei, Y. Zhang, Q. Zhang, Z. Wang, J. Liu, Y. Wang, Endogenous ternary pH buffer system with ammonia-carbonates-VFAs in high solid anaerobic digestion of swine manure: An alternative for alleviating ammonia inhibition?, Process Biochem. 69 (2018) 144–152.

[56] D. Georgacakis, D.M. Sievers, E.L. Iannotti, Buffer stability in manure digesters, Agric. Wastes. 4 (1982) 427–441.

[57] WRAP, BSI PAS 110: Specification for whole digestate, separated liquor and separated fibre derived from the anaerobic digestion of source-segregated biodegradable materials, 2014.

[58] M. Logan, C. Visvanathan, Management strategies for anaerobic digestate of organic fraction of municipal solid waste: Current status and future prospects:, Waste Manag. Res. 37 (2019) 27–39.

[59] O. Nartey, B. Zhao, Biochar preparation, characterization, and adsorptive capacity and its effect on bioavailability of contaminants: an overview, Hindawi Publ. Corp. Adv. Mater. Sci. Eng. 2014 (2014) 1–12.

[60] H.S. Kambo, A. Dutta, A comparative review of biochar and hydrochar in terms of production, physico-chemical properties and applications, Renew. Sustain. Energy Rev. 45 (2015) 359–378.

[61] J.E. Amonette, S. Joseph, Characteristics of Biochar: Microchemical Properties, in: Biochar Environ. Manag. Sci. Technol., Routledge, 2009: pp. 65–84.

[62] V. Dhyani, T. Bhaskar, A comprehensive review on the pyrolysis of lignocellulosic biomass, Renew. Energy. 129 (2018) 695–716.

[63] W.-J. Liu, H. Jiang, H.-Q. Yu, Development of Biochar-Based Functional Materials: Toward a Sustainable Platform Carbon Material, Chem. Rev. 115 (2015) 12251–12285.

[64] R. Becker, U. Dorgerloh, E. Paulke, J. Mumme, I. Nehls, Hydrothermal carbonization of biomass: Major organic components of the aqueous phase, Chem. Eng. Technol. 37 (2014) 511–518.

[65] H.S. Kambo, J. Minaret, A. Dutta, Process Water from the Hydrothermal Carbonization of Biomass: A Waste or a Valuable Product?, Waste and Biomass Valorization. 9 (2018) 1181–1189.

[66] A.E. Brown, G.L. Finnerty, M.A. Camargo-Valero, A.B. Ross, Valorisation of macroalgae via the integration of hydrothermal carbonisation and anaerobic digestion, Bioresour. Technol. 312 (2020) 123539.

[67] K. Weber, P. Quicker, Properties of biochar, Fuel. 217 (2018) 240–261.

[68] D.C. Li, H. Jiang, The thermochemical conversion of non-lignocellulosic biomass to form biochar: A review on characterizations and mechanism elucidation, Bioresour. Technol. 246 (2017) 57–68.

[69] L.D. Mafu, H.W.J.P. Neomagus, R.C. Everson, C.A. Strydom, M. Carrier, G.N. Okolo, J.R. Bunt, Chemical and structural characterization of char development during lignocellulosic biomass pyrolysis, Bioresour. Technol. 243 (2017) 941–948.

[70] International Biochar Initiative, Standardized Product Definition and Product Testing Guidelines for Biochar That Is Used in Soil, 2015.

[71] L.B. Santos, M. V. Striebeck, M.S. Crespi, C.A. Ribeiro, M. De Julio, Characterization of biochar of pine pellet, J. Therm. Anal. Calorim. 122 (2015) 21–32.

[72] E.S. Krull, J.A. Baldock, J.O. Skjemstad, R.J. Smernik, J.A. Baldock, J.O. Skjemstad, R.J. Smernik, Characteristics of Biochar: Organo-chemical Properties, in: Biochar Environ. Manag. Sci. Technol., Routledge, 2009: pp. 85–98.

[73] K.Y. Chan, Z. Xu, Biochar: Nutrient Properties and Their Enhancement, in: Biochar Environ. Manag. Sci. Technol., Routledge, 2009: pp. 99–116.

[74] D. Knežević, W.P.M. van Swaaij, S.R.A. Kersten, Hydrothermal Conversion of Biomass: I, Glucose Conversion in Hot Compressed Water, Ind. Eng. Chem. Res. 48 (2009) 4731–4743.

[75] M. Sevilla, A.B. Fuertes, The production of carbon materials by hydrothermal carbonization of cellulose, Carbon N. Y. 47 (2009) 2281–2289.

[76] A. Jain, R. Balasubramanian, M.P. Srinivasan, Hydrothermal conversion of biomass waste to activated carbon with high porosity: A review, Chem. Eng. J. 283 (2016) 789–805.

[77] V.K. La Mer, Nucleation in Phase Transitions, Ind. Eng. Chem. 44 (1952) 1270–1277.

[78] C. Rodriguez Correa, M. Bernardo, R.P.P.L. Ribeiro, I.A.A.C. Esteves, A. Kruse, Evaluation of hydrothermal carbonization as a preliminary step for the production of functional materials from biogas digestate, J. Anal. Appl. Pyrolysis. 124 (2017) 461–474.

[79] W.-J. Liu, F.-X. Zeng, H. Jiang, X.-S. Zhang, Preparation of high adsorption capacity bio-chars from waste biomass, Bioresour. Technol. 102 (2011) 8247–8252.

[80] M.O. Castro, M.Q. De Santiago, K.S. Nascimento, M. Oliveira-Castro, M. Queiroz de Santiago, K. Santiago Nascimento, B. Sousa Cavada, M.E. de Castro, A. Jardim de Paula, O. Pastor Ferreira, M. Queiroz de Santiago, K. Santiago Nascimento, Hydrochar as protein support: preservation of biomolecule properties with non-covalent immobilization, J. Mater. Sci. 52 (2017) 13378–13389.

[81] Q. Wu, S. Yu, N. Hao, T. Wells, X. Meng, M. Li, Y. Pu, S. Liu, A.J. Ragauskas, Characterization of products from hydrothermal carbonization of pine, Bioresour. Technol. 244 (2017) 78–83.

[82] A.D. Hughes, K.D. Black, I. Campbell, J.J. Heymans, K.K. Orr, M.S. Stanley, M.S. Kelly, H.A. Ruiz, R.M. Rodríguez-Jasso, B.D. Fernandes, A.A. Vicente, J.A. Teixeira, A.D. Hughes, K.D. Black, I. Campbell, J.J. Heymans, K.K. Orr, M.S. Stanley, M.S. Kelly, E. Allen, J. Browne, S. Hynes, J.D. Murphy, M. Alvarado-Morales, A. Boldrin, D.B. Karakashev, S.L. Holdt, I. Angelidaki, T. Astrup, A.D. Hughes, K.D. Black, I. Campbell, J.J. Heymans, K.K. Orr, M.S. Stanley,

M.S. Kelly, J. Yanik, R. Stahl, N. Troeger, A. Sinag, M. Hitzl, A. Corma, F. Pomares, M. Renz, E. Allen, D.M. Wall, C. Herrmann, A. Xia, J.D. Murphy, H. Chen, D. Zhou, G. Luo, S. Zhang, J. Chen, N.V.S.N.M. Konda, S. Singh, B.A. Simmons, D. Klein-Marcuschamer, M. Sharifzadeh, L. Wang, N. Shah, M.J. Black, J. Sadhukhan, K. Day, G. Drage, R.J. Murphy, K. Özdenkçi, C. De Blasio, H.R. Muddassar, K. Melin, P. Oinas, J. Koskinen, G. Sarwar, M. Järvinen, S. Raikova, C.D. Le, T.A. Beacham, R.W. Jenkins, M.J. Allen, C.J. Chuck, M.J. Cocero, Á. Cabeza, N. Abad, T. Adamovic, L. Vaquerizo, C.M. Martínez, M.V. Pazo-Cepeda, J. Sadhukhan, E. Martinez-Hernandez, R.J. Murphy, D.K.S. Ng, M.H. Hassim, K. Siew Ng, W. Yoke Kin, I.F.M. Jaye, M.Y. Leung Pah Hang, V. Andiappan, K. Sudhakar, R. Mamat, M. Samykano, W.H. Azmi, W.F.W. Ishak, T. Yusaf, Comments on "Prospects for the use of macroalgae for fuel in Ireland and UK: An overview of marine management issues," Mar. Policy. 38 (2013) 554–556.

[83] J.S. Cha, S.H. Park, S.C. Jung, C. Ryu, J.K. Jeon, M.C. Shin, Y.K. Park, Production and utilization of biochar: A review, J. Ind. Eng. Chem. 40 (2016) 1–15.

[84] A. Jain, R. Balasubramanian, M.P. Srinivasan, Tuning hydrochar properties for enhanced mesopore development in activated carbon by hydrothermal carbonization, Microporous Mesoporous Mater. 203 (2015) 178–185.

[85] M. Li, Y. Zheng, Y. Chen, X. Zhu, Biodiesel production from waste cooking oil using a heterogeneous catalyst from pyrolyzed rice husk, Bioresour. Technol. 154 (2014) 345–348.

[86] J.R. Kastner, S. Mani, A. Juneja, Catalytic decomposition of tar using iron supported biochar, Fuel Process. Technol. 130 (2015) 31–37.

[87] C. Luo, F. Lü, L. Shao, P. He, Application of eco-compatible biochar in anaerobic digestion to relieve acid stress and promote the selective colonization of functional microbes, 68 (2015) 710–718.

[88] C. Wang, Y. Liu, X. Gao, H. Chen, X. Xu, L. Zhu, Role of biochar in the granulation of anaerobic sludge and improvement of electron transfer characteristics, Bioresour. Technol. 268 (2018) 28–35.

[89] X. Wang, J. Zhao, Q. Yang, J. Sun, C. Peng, F. Chen, Q. Xu, S. Wang, D. Wang, X. Li, G. Zeng, Evaluating the potential impact of hydrochar on the production of short-chain fatty acid from sludge anaerobic digestion, Bioresour. Technol. 246 (2017) 234–241.

[90] F. Codignole Luz, M. Volpe, L. Fiori, A. Manni, S. Cordiner, V. Mulone, V. Rocco, Spent coffee enhanced biomethane potential via an integrated hydrothermal carbonization-anaerobic digestion process, Bioresour. Technol. 256 (2018) 102–109.

[91] Y. Wu, S. Wang, D. Liang, N. Li, Conductive materials in anaerobic digestion: From mechanism to application, Bioresour. Technol. 298 (2020) 122403.

[92] C. Cruz Viggi, S. Simonetti, E. Palma, P. Pagliaccia, C. Braguglia, S. Fazi, S. Baronti, M.A. Navarra, I. Pettiti, C. Koch, F. Harnisch, F. Aulenta, Enhancing methane production from food waste fermentate using biochar: The added value of electrochemical testing in pre-selecting the most effective type of biochar, Biotechnol. Biofuels. 10 (2017) 303.

[93]   L. Klüpfel, M. Keiluweit, M. Kleber, M. Sander, Redox properties of plant biomass-derived black carbon (biochar), Environ. Sci. Technol. 48 (2014) 5601–5611.

[94]   R.A. Sheldon, Enzyme immobilization: The quest for optimum performance, Adv. Synth. Catal. 349 (2007) 1289–1307.

[95]   C. Garcia-Galan, Á. Berenguer-Murcia, R. Fernandez-Lafuente, R.C. Rodrigues, Potential of different enzyme immobilization strategies to improve enzyme performance, Adv. Synth. Catal. 353 (2011) 2885–2904.

[96]   G. Kumar, A. Mudhoo, P. Sivagurunathan, D. Nagarajan, A. Ghimire, C.-H. Lay, C.-Y. Lin, D.-J. Lee, J.-S. Chang, Recent insights into the cell immobilization technology applied for dark fermentative hydrogen production, Bioresour. Technol. 219 (2016) 725–737.

[97]   M. Quirós, A.B. García, M.A. Montes-Morán, Influence of the support surface properties on the protein loading and activity of lipase/mesoporous carbon biocatalysts, Carbon N. Y. 49 (2011) 406–415.

[98]   J. Huang, H. Dai, R. Yan, P. Wang, Enhanced production of butyric acid through immobilization of Clostridium tyrobutyricum in a novel inner disc-shaped matrix bioreactor, Ann. Microbiol. 66 (2016) 121–129.

[99]   L.A. Ramírez-Montoya, V. Hernández-Montoya, M.A. Montes-Morán, F.J. Cervantes, Correlation between mesopore volume of carbon supports and the immobilization of laccase from Trametes versicolor for the decolorization of Acid Orange 7, J. Environ. Manage. 162 (2015) 206–214.

[100] W. Yan, N. Shen, Y. Xiao, Y. Chen, F. Sun, V. Kumar Tyagi, Y. Zhou, The role of conductive materials in the start-up period of thermophilic anaerobic system, Bioresour. Technol. 239 (2017) 336–344.

[101] R. Lin, J. Cheng, L. Ding, J.D. Murphy, Improved efficiency of anaerobic digestion through direct interspecies electron transfer at mesophilic and thermophilic temperature ranges, Chem. Eng. J. 350 (2018) 681–691.

[102] F. Suanon, Q. Sun, D. Mama, J. Li, B. Dimon, C.P. Yu, Effect of nanoscale zero-valent iron and magnetite (Fe3O4) on the fate of metals during anaerobic digestion of sludge, Water Res. 88 (2016) 897–903.

[103] S. Krigstin, S. Wetzel, A review of mechanisms responsible for changes to stored woody biomass fuels, Fuel. 175 (2016) 75–86.

[104] T. Koottatep, K. Fakkaew, N. Tajai, S. V. Pradeep, C. Polprasert, Sludge stabilization and energy recovery by hydrothermal carbonization process, Renew. Energy. 99 (2016) 978–985.

[105] D. Angın, E. Altintig, T. Ennil, Influence of process parameters on the surface and chemical properties of activated carbon obtained from biochar by chemical activation, Bioresour. Technol. 148 (2013) 542–549.

[106] V. Sricharoenchaikul, C. Pechyen, D. Aht-Ong, D. Atong, Preparation and characterization of activated carbon from the pyrolysis of physic nut (Jatropha curcas L.) waste, Energy and Fuels. 22 (2008) 31–37.

[107] M. Zhang, B. Gao, Y. Yao, Y. Xue, M. Inyang, Synthesis of porous MgO-

biochar nanocomposites for removal of phosphate and nitrate from aqueous solutions, Chem. Eng. J. 210 (2012) 26–32.

[108] L. Wang, D. O'Connor, J. Rinklebe, Y.S. Ok, D.C.W. Tsang, Z. Shen, D. Hou, Biochar Aging: Mechanisms, Physicochemical Changes, Assessment, and Implications for Field Applications, Environ. Sci. Technol. 54 (2020) 14797–14814.

[109] T.A. Saleh, V.K. Gupta, Structural Characterization of Nanomaterial-Polymer Membranes, in: Nanomater. Polym. Membr. - Synth. Charact. Appl., Elsevier, 2016: pp. 187–203.

[110] B. Singh, M.M. Dolk, Q. Shen, M. Camps-Arbestein, Biochar pH, electrical conductivity and liming potential, in: B. Singh, M. Camps-Arbestain, J. Lehmann (Eds.), Biochar A Guid. to Anal. Methods, CRC Press, 2017: pp. 23–38.

[111] K.S.W. Sing, D.H. Everet, R.A.W. Haul, L. Mocou, R.A. Pierotti, J. Rouquérol, T. Siemieniewska, Provisional reporting physisorption data for gas/solid systems with special reference to the determination of surface area and porosity, Pure Appl. Chem. 57 (1985) 603–619.

[112] P.I. Ravikovitch, A. Vishnyakov, R. Russo, A. V Neimark, Unified Approach to Pore Size Characterization of Microporous Carbonaceous Materials from N2, Ar, and CO2 Adsorption Isotherms, Langmuir. 5 (2000) 2311–2320.

[113] K. Sing, The use of nitrogen adsorption for the characterisation of porous materials, Colloids Surfaces A Physicochem. Eng. Asp. 188 (2001) 3–9.

[114] S. Lowell, J.E. Shields, M.A. Thomas, M. Thommes, Adsorption Mechanism, in: Charact. Porous Solids Powders Surf. Area, Pore Size Density, Springer, Dordrecht, 2004: pp. 15–57.

[115] P. Tarazona, Free-energy density functional for hard spheres, Phys. Rev. A. 31 (1985) 2672–2679.

[116] P. Tarazona, U.M.B. Marconi, R. Evans, Phase equilibria of fluid interfaces and conflned fluids non-local versus local density functionals, Mol. Phys. 60 (1987) 573–595.

[117] J. Schmitt, H.C. Flemming, FTIR-spectroscopy in microbial and material analysis, Int. Biodeterior. Biodegrad. 41 (1998) 1–11.

[118] J.F. Watts, J. Wolstenholme, An introduction to surface analysis by XPS and AES, J. Wiley, 2003.

[119] G.C. Smith, X-ray photoelectron spectroscopy analysis of biochar, in: B. Singh, M. Camps-Arbestain, J. Lehmann (Eds.), Biochar a Guid. to Anal. Methods, 2017: pp. 229–244.

[120] H. Konno, X-ray Photoelectron Spectroscopy, in: F. Kang, H. Konno (Eds.), Mater. Sci. Eng. Carbon, Butterworth-Heinemann, 2016: pp. 153–171.

[121] M. Smith, L. Scudiero, J. Espinal, J.S. McEwen, M. Garcia-Perez, Improving the deconvolution and interpretation of XPS spectra from chars by ab initio calculations, Carbon N. Y. 110 (2016) 155–171.

[122] C. Holliger, M. Alves, D. Andrade, I. Angelidaki, S. Astals, U. Baier, C. Bougrier, P. Buffière, M. Carballa, V. de Wilde, F. Ebertseder, B. Fernández, E. Ficara, I. Fotidis, J.-C. Frigon, H.F. de Laclos, D.S.M. Ghasimi, G. Hack, M. Hartel, J. Heerenklage, I.S. Horvath, P. Jenicek, K. Koch, J. Krautwald, J. Lizasoain, J. Liu, L. Mosberger, M. Nistor, H. Oechsner, J.V. Oliveira, M. Paterson, A. Pauss, S. Pommier, I. Porqueddu, F. Raposo, T. Ribeiro, F. Rüsch Pfund, S. Strömberg, M. Torrijos, M. van Eekert, J. van Lier, H. Wedwitschka, I. Wierinck, Towards a standardization of biomethane potential tests, Water Sci. Technol. 74 (2016) 2515–2522.

[123] V. Moset, N. Al-zohairi, H.B. Møller, The impact of inoculum source, inoculum to substrate ratio and sample preservation on methane potential from different substrates, Biomass and Bioenergy. 83 (2015) 474–482.

[124] A.M. Buswell, H.F. Mueller, Mechanism of Methane Fermentation, Ind. Eng. Chem. 44 (1952) 550–552.

[125] C. Aragon-Briceno, O. Grasham, A.B. Ross, V. Dupont, M.A. Camargo-Valero, Hydrothermal carbonization of sewage digestate at wastewater treatment works: Influence of solid loading on characteristics of hydrochar, process water and plant energetics, Renew. Energy. 157 (2020) 959–973.

[126] M.H. Zwietering, I. Jongenburger, F.M. Rombouts, K. Van't Riet, Modeling of the bacterial growth curve, Appl. Environ. Microbiol. 56 (1990) 1875–1881.

[127] D.C. Montgomery, Design and analysis of experiments, Eight Edit, John Wiley & Sons, Inc., 2013.

[128] L. Vera Candioti, M.M. De Zan, M.S. Cámara, H.C. Goicoechea, Experimental design and multiple response optimization. Using the desirability function in analytical methods development, Talanta. 124 (2014) 123–138.

[129] L. Plonsky, S. Loewen, T. Gonulal, Exploratory Factor Analysis and Principal Components Analysis, in: Adv. Quant. Methods Second Lang. Res., Routledge, 2015: pp. 182–212.

[130] B. Swarbrick, F. Westad, An overview of chemometrics for the engineering and measurement sciences, in: Handb. Meas. Sci. Eng., John Wiley & Sons, Inc., Hoboken, NJ, USA, 2016: pp. 2307–2407.

[131] O. Matthias, Pattern Recognition and classification, in: Chemom. Stat. Comput. Appl. Anal. Chem., 3rd ed., Springer Nature, 2017: pp. 135–211.

[132] V. Dandikas, H. Heuwinkel, F. Lichti, J.E. Drewes, K. Koch, Correlation between Biogas Yield and Chemical Composition of Grassland Plant Species, Energy and Fuels. 29 (2015) 7221–7229.

[133] A.D. Flores, G.L. Kurgan, X. Wang, Engineering Bacterial Sugar Catabolism and Tolerance Toward Lignocellulose Conversion, in: Eng. Microorg. Prod. Chem. Biofuels from Renew. Resour., Springer International Publishing, Cham, 2017: pp. 147–180.

[134] Y. Gao, X. Wang, J. Wang, X. Li, J. Cheng, H. Yang, H. Chen, Effect of residence time on chemical and structural properties of hydrochar obtained by hydrothermal carbonization of water hyacinth, Energy. 58 (2013) 376–

383.

[135] J. Lehmann, S. Joseph, S. Joseph, Biochar for Environmental Management: An Introduction, in: Biochar Environ. Manag. Sci. Technol., Routledge, 2009: pp. 33–44.

[136] M. Andérez Fernández, J. Rissanen, A. Pérez Nebreda, C. Xu, S. Willför, J. García Serna, T. Salmi, H. Grénman, Hemicelluloses from stone pine, holm oak, and Norway spruce with subcritical water extraction – comparative study with characterization and kinetics, J. Supercrit. Fluids. 133 (2018) 647–657.

[137] I. López-Cano, M. Cayuela, C. Mondini, C.A. Takaya, A.B. Ross, M. Sánchez-Monedero, Suitability of Different Agricultural and Urban Organic Wastes as Feedstocks for the Production of Biochar—Part 1: Physicochemical ChLópez-Cano, I., Cayuela, M., Mondini, C., Takaya, C., Ross, A.B., Sánchez-Monedero, M., 2018. Suitability of Different Agr, Sustainability. 10 (2018) 2265.

[138] Z.H. Zhang, J.Y. Guo, J.Y. Guo, Biology of Water Hyacinth, in: Water Hyacinth Environ. Challenges, Manag. Util., CRC Press, 2017: pp. 15–43.

[139] V.B. Barua, A.S. Kalamdhad, Effect of various types of thermal pretreatment techniques on the hydrolysis, compositional analysis and characterization of water hyacinth, Bioresour. Technol. 227 (2017) 147–154.

[140] V. Patel, M. Desai, D. Madamwar, Thermochemical pretreatment of water hyacinth for improved biomethanation, Appl. Biochem. Biotechnol. 42 (1993) 67–74.

[141] S. Bolenz, H. Omran, K. Gierschner, Treatments of water hyacinth tissue to obtain useful products, Biol. Wastes. 33 (1990) 263–274.

[142] X.M. Ye, Utilization of Biomass for Energy and Fertilizer, in: Water Hyacinth Environ. Challenges, Manag. Util., CRC Press, 2017: pp. 253–276.

[143] A.B. Ross, J.M. Jones, M.L.M. Kubacki, T. Bridgeman, Classification of macroalgae as fuel and its thermochemical behaviour, Bioresour. Technol. 99 (2008) 6494–6504.

[144] J. Hammerton, L.R. Joshi, A.B. Ross, B. Pariyar, J.C. Lovett, K.K. Shrestha, B. Rijal, H. Li, P.E. Gasson, Characterisation of biomass resources in Nepal and assessment of potential for increased charcoal production, J. Environ. Manage. 223 (2018) 358–370.

[145] İ.C. Kantarli, M. Pala, Y. Yildirim, J. Yanik, M.H. Abreu, Fuel characteristics and combustion behavior of seaweed-derived hydrochars, Turkish J. Chem. 43 (2019) 475–491.

[146] Z. Liu, F.S. Zhang, J. Wu, Characterization and application of chars produced from pinewood pyrolysis and hydrothermal treatment, Fuel. 89 (2010) 510–514.

[147] A. Mukherjee, A.R. Zimmerman, W. Harris, Surface chemistry variations among a series of laboratory-produced biochars, Geoderma. 163 (2011) 247–255.

[148] Y. Shen, J.L. Linville, P.A.A. Ignacio-de Leon, R.P. Schoene, M. Urgun-Demirtas, Towards a sustainable paradigm of waste-to-energy process: Enhanced anaerobic digestion of sludge with woody biochar, J. Clean. Prod. 135 (2016) 1054–1064.

[149] A.T. Tag, G. Duman, S. Ucar, J. Yanik, Effects of feedstock type and pyrolysis temperature on potential applications of biochar, J. Anal. Appl. Pyrolysis. 120 (2016) 200–206.

[150] G. Wang, Q. Li, M. Dzakpasu, X. Gao, C. Yuwen, X.C. Wang, Impacts of different biochar types on hydrogen production promotion during fermentative co-digestion of food wastes and dewatered sewage sludge, Waste Manag. 80 (2018) 73–80.

[151] X. Domene, A. Enders, K. Hanley, J. Lehmann, Ecotoxicological characterization of biochars: Role of feedstock and pyrolysis temperature, Sci. Total Environ. 512–513 (2015) 552–561.

[152] E. Sjostrom, Wood chemistry: fundamentals and applications, Gulf proffesional publishing, 1993.

[153] E.M. Eid, Determination of carbohydrate allocation patterns in water hyacinth to discover the potential physiological weak points in its life cycle, J. Freshw. Ecol. 33 (2018) 381–394.

[154] P.T. Williams, J. Onwudili, Subcritical and Supercritical Water Gasification of Cellulose, Starch, Glucose, and Biomass Waste, Energy & Fuels. 20 (2006) 1259–1265.

[155] X.J. Lee, H.C. Ong, Y.Y. Gan, W.H. Chen, T.M.I. Mahlia, State of art review on conventional and advanced pyrolysis of macroalgae and microalgae for biochar, bio-oil and bio-syngas production, Energy Convers. Manag. 210 (2020) 112707.

[156] K.A. Jung, S.-R. Lim, Y. Kim, J.M. Park, Potentials of macroalgae as feedstocks for biorefinery, Bioresour. Technol. 135 (2013) 182–190.

[157] N. Wei, J. Quarterman, Y.-S. Jin, Marine macroalgae: an untapped resource for producing fuels and chemicals, Trends Biotechnol. 31 (2013) 70–77.

[158] K. Anastasakis, A.B. Ross, J.M. Jones, Pyrolysis behaviour of the main carbohydrates of brown macro-algae, Fuel. 90 (2011) 598–607.

[159] A. Enders, K. Hanley, T. Whitman, S. Joseph, J. Lehmann, Characterization of biochars to evaluate recalcitrance and agronomic performance, Bioresour. Technol. 114 (2012) 644–653.

[160] Y. Zhu, Y. Si, X. Wang, W. Zhang, J. Shao, H. Yang, H. Chen, Characterization of Hydrochar Pellets from Hydrothermal Carbonization of Agricultural Residues, Energy and Fuels. 32 (2018) 11538–11546.

[161] S. Kang, X. Li, J. Fan, J. Chang, Characterization of hydrochars produced by hydrothermal carbonization of lignin, cellulose, d-xylose, and wood meal, Ind. Eng. Chem. Res. 51 (2012) 9023–9031.

[162] X. Lu, N.D. Berge, Influence of feedstock chemical composition on product formation and characteristics derived from the hydrothermal

carbonization of mixed feedstocks, Bioresour. Technol. 166 (2014) 120–131.

[163] J.L. Liang, Y.H. Liu, J. Zhang, Effect of solution pH on the carbon microsphere synthesized by hydrothermal carbonization, in: Procedia Environ. Sci., Elsevier B.V., 2011: pp. 1322–1327.

[164] S.N. Pawar, K.J. Edgar, Alginate derivatization: A review of chemistry, properties and applications, Biomaterials. 33 (2012) 3279–3305.

[165] A. Broch, U. Jena, S.K. Hoekman, J. Langford, Analysis of solid and aqueous phase products from hydrothermal carbonization of whole and lipid-extracted algae, Energies. 7 (2014) 62–79.

[166] S. Kim, R.W. Kramer, P.G. Hatcher, Graphical Method for Analysis of Ultrahigh-Resolution Broadband Mass Spectra of Natural Organic Matter, the Van Krevelen Diagram, Anal. Chem. 75 (2003) 5336–5344.

[167] S. Schimmelpfennig, B. Glaser, One Step Forward toward Characterization: Some Important Material Properties to Distinguish Biochars, J. Environ. Qual. 41 (2012) 1001.

[168] S.K. Hoekman, A. Broch, C. Robbins, Hydrothermal carbonization (HTC) of lignocellulosic biomass, Energy and Fuels. 25 (2011) 1802–1810.

[169] L. Bottezini, D.P. Dick, A. Wisniewski, H. Knicker, I.S. Carvalho Carregosa, Phosphorus species and chemical composition of water hyacinth biochars produced at different pyrolysis temperature, Bioresour. Technol. Reports. 14 (2021) 100684.

[170] Z. Yao, X. Ma, Z. Xiao, The effect of two pretreatment levels on the pyrolysis characteristics of water hyacinth, Renew. Energy. 151 (2020) 514–527.

[171] M.O. Fagbohungbe, B.M.J. Herbert, L. Hurst, H. Li, S.Q. Usmani, K.T. Semple, Impact of biochar on the anaerobic digestion of citrus peel waste, Bioresour. Technol. 216 (2016) 142–149.

[172] F. Lü, C. Luo, L. Shao, P. He, Biochar alleviates combined stress of ammonium and acids by firstly enriching Methanosaeta and then Methanosarcina, Water Res. 90 (2016) 34–43.

[173] Y. Shen, J.L. Linville, M. Urgun-Demirtas, R.P. Schoene, S.W. Snyder, Producing pipeline-quality biomethane via anaerobic digestion of sludge amended with corn stover biochar with in-situ CO2 removal, Appl. Energy. 158 (2015) 300–309.

[174] T. Wang, Y. Zhai, Y. Zhu, C. Peng, B. Xu, T. Wang, C. Li, G. Zeng, Influence of temperature on nitrogen fate during hydrothermal carbonization of food waste, Bioresour. Technol. 247 (2018) 182–189.

[175] M.I. Bird, C.M. Wurster, P.H. de Paula Silva, A.M. Bass, R. de Nys, Algal biochar - production and properties, Bioresour. Technol. 102 (2011) 1886–1891.

[176] J.H. Choi, S.S. Kim, D.J. Suh, E.J. Jang, K. Il Min, H.C. Woo, Characterization of the bio-oil and bio-char produced by fixed bed pyrolysis of the brown alga Saccharina japonica, Korean J. Chem. Eng. 33 (2016) 2691–2698.

[177] K.W. Jung, T.U. Jeong, H.J. Kang, K.H. Ahn, Characteristics of biochar derived from marine macroalgae and fabrication of granular biochar by entrapment in calcium-alginate beads for phosphate removal from aqueous solution, Bioresour. Technol. 211 (2016) 108–116.

[178] S. Kloss, F. Zehetner, A. Dellantonio, R. Hamid, F. Ottner, V. Liedtke, M. Schwanninger, M.H. Gerzabek, G. Soja, Characterization of Slow Pyrolysis Biochars: Effects of Feedstocks and Pyrolysis Temperature on Biochar Properties, J. Environ. Qual. 41 (2012) 990.

[179] M. Li, Y. Tang, N. Ren, Z. Zhang, Y. Cao, Effect of mineral constituents on temperature-dependent structural characterization of carbon fractions in sewage sludge-derived biochar, J. Clean. Prod. 172 (2016) 3342–3350.

[180] S.H. Park, H.J. Cho, C. Ryu, Y.K. Park, Removal of copper(II) in aqueous solution using pyrolytic biochars derived from red macroalga Porphyra tenera, J. Ind. Eng. Chem. 36 (2016) 314–319.

[181] S.C. Peterson, M. Appell, M.A. Jackson, A.A. Boateng, Comparing Corn Stover and Switchgrass Biochar: Characterization and Sorption Properties, J. Agric. Sci. 5 (2013) 1–8.

[182] L. Leng, S. Xu, R. Liu, T. Yu, X. Zhuo, S. Leng, Q. Xiong, H. Huang, Nitrogen containing functional groups of biochar: An overview, Bioresour. Technol. 298 (2019) 122286.

[183] A.M. Smith, S. Singh, A.B. Ross, Fate of inorganic material during hydrothermal carbonisation of biomass: Influence of feedstock on combustion behaviour of hydrochar, Fuel. 169 (2016) 135–145.

[184] A.M. Smith, U. Ekpo, A.B. Ross, The influence of pH on the combustion properties of bio-coal following hydrothermal treatment of swine manure, Energies. 13 (2020) 1–20.

[185] K.R. Parmar, A.B. Ross, Integration of hydrothermal carbonisation with anaerobic digestion; Opportunities for valorisation of digestate, Energies. 12 (2019) 1586.

[186] J. Petrović, N. Perišić, J.D. Maksimović, V. Maksimović, M. Kragović, M. Stojanović, M. Laušević, M. Mihajlović, Hydrothermal conversion of grape pomace: Detailed characterization of obtained hydrochar and liquid phase, J. Anal. Appl. Pyrolysis. 118 (2016) 267–277.

[187] M. Volpe, J.L. Goldfarb, L. Fiori, Hydrothermal carbonization of Opuntia ficus-indica cladodes: Role of process parameters on hydrochar properties, Bioresour. Technol. 247 (2018) 310–318.

[188] A.M. Smith, A.B. Ross, The influence of residence time during hydrothermal carbonisation of miscanthus on bio-coal combustion chemistry, Energies. 12 (2019) 13–22.

[189] Y. Gao, X. Wang, J. Wang, X. Li, J. Cheng, H. Yang, H. Chen, Effect of residence time on chemical and structural properties of hydrochar obtained by hydrothermal carbonization of water hyacinth, Energy. 58 (2013) 376–383.

[190] P. Gao, Y. Zhou, F. Meng, Y. Zhang, Z. Liu, W. Zhang, G. Xue, Preparation and

characterization of hydrochar from waste eucalyptus bark by hydrothermal carbonization, Energy. 97 (2016) 238–245.

[191] A. Kruse, F. Koch, K. Stelzl, D. Wüst, M. Zeller, Fate of Nitrogen during Hydrothermal Carbonization, Energy and Fuels. 30 (2016) 8037–8042.

[192] C.I. Aragón-Briceño, A.K. Pozarlik, E.A. Bramer, L. Niedzwiecki, H. Pawlak-Kruczek, G. Brem, Hydrothermal carbonization of wet biomass from nitrogen and phosphorus approach: A review, Renew. Energy. 171 (2021) 401–415.

[193] E. Erdogan, B. Atila, J. Mumme, M.T. Reza, A. Toptas, M. Elibol, J. Yanik, Characterization of products from hydrothermal carbonization of orange pomace including anaerobic digestibility of process liquor, Bioresour. Technol. 196 (2015) 35–42.

[194] J.L. Jones, R.O. Jenkins, P.I. Haris, Extending the geographic reach of the water hyacinth plant in removal of heavy metals from a temperate Northern Hemisphere river, Sci. Rep. 8 (2018) 1–15.

[195] P.E. Amaral Debiagi, M. Trinchera, A. Frassoldati, T. Faravelli, R. Vinu, E. Ranzi, Algae characterization and multistep pyrolysis mechanism, J. Anal. Appl. Pyrolysis. 128 (2017) 423–436.

[196] E.J. Leijenhorst, W. Wolters, L. Van De Beld, W. Prins, Inorganic element transfer from biomass to fast pyrolysis oil: Review and experiments, Fuel Process. Technol. 149 (2016) 96–111.

[197] H. Li, X. Dong, B. Evandro, L.M. De Oliveira, Y. Chen, L.Q. Ma, Mechanisms of metal sorption by biochars : Biochar characteristics and modifications, Chemosphere. 178 (2017) 466–478.

[198] D. Lozano-Castelló, D. Cazorla-Amorós, A. Linares-Solano, Usefulness of CO2 adsorption at 273 K for the characterization of porous carbons, Carbon N. Y. 42 (2004) 1233–1242.

[199] M. Thommes, K. Katsumi, A. V Neimark, J.P. Olivier, F. Rodriguez-Reinoso, J. Rouquerol, K.S. Sing, Physisorption of gases, with special reference to the evaluation of surface area and pore size distribution (IUPAC Technical Report), Pure Appl. Chem. 87 (2015) 1051.

[200] K.S. Sing, Reporting physisorption data for gas/solid systems with special reference to the determination of surface area and porosity (Recommendations 1984), Pure Appl. Chem. 57 (1985) 603–619.

[201] H.M. Jang, Y.-K.K. Choi, E. Kan, Effects of dairy manure-derived biochar on psychrophilic, mesophilic and thermophilic anaerobic digestions of dairy manure, Bioresour. Technol. 250 (2018) 927–931.

[202] Y. Qin, H. Wang, X. Li, J.J. Cheng, W. Wu, Improving methane yield from organic fraction of municipal solid waste (OFMSW) with magnetic rice-straw biochar, Bioresour. Technol. 245 (2017) 1058–1066.

[203] M. Kyriakou, V.K. Chatziiona, C.N. Costa, M. Kallis, L. Koutsokeras, G. Constantinides, M. Koutinas, Biowaste-based biochar: A new strategy for fermentative bioethanol overproduction via whole-cell immobilization, Appl. Energy. 242 (2019) 480–491.

[204] N.M.S. Sunyoto, M. Zhu, Z. Zhang, D. Zhang, Effect of biochar addition on hydrogen and methane production in two-phase anaerobic digestion of aqueous carbohydrates food waste, Bioresour. Technol. 219 (2016) 29–36.

[205] L. Leng, Q. Xiong, L. Yang, H. Li, Y. Zhou, W. Zhang, S. Jiang, H. Li, H. Huang, An overview on engineering the surface area and porosity of biochar, Sci. Total Environ. 763 (2021) 144204.

[206] H.S. Heo, H.J. Park, J.H. Yim, J.M. Sohn, J. Park, S.S. Kim, C. Ryu, J.K. Jeon, Y.K. Park, Influence of operation variables on fast pyrolysis of Miscanthus sinensis var. purpurascens, Bioresour. Technol. 101 (2010) 3672–3677.

[207] N.M. Mkhize, B. Danon, P. van der Gryp, J.F. Görgens, Condensation of the hot volatiles from waste tyre pyrolysis by quenching, J. Anal. Appl. Pyrolysis. 124 (2017) 180–185.

[208] C.T. Johnston, Biochar analysis by Fourier-transform infra-red spectroscopy, in: B. Singh, M. Camps-Arbestain, J. Lehmann (Eds.), Biochar A Guid. to Anal. Methods, CSIRO Publishing, 2017: pp. 199–213.

[209] X. Qian, L. Song, Y. Hu, R.K.K. Yuen, Preparation and thermal properties of novel organic/inorganic network hybrid materials containing silicon and phosphate, J. Polym. Res. 19 (2012) 1–10.

[210] Y. Jiang, F. Xin, J. Lu, W. Dong, W. Zhang, M. Zhang, H. Wu, J. Ma, M. Jiang, State of the art review of biofuels production from lignocellulose by thermophilic bacteria, Bioresour. Technol. 245 (2017) 1498–1506.

[211] I. Fleming, D.H. Williams, Spectroscopic methods in organic chemistry, 5th Editio, McGraw Hill Book Company Europe, 1966.

[212] T. Sun, B.D.A. Levin, M.P. Schmidt, J.J.L. Guzman, A. Enders, C.E. Martínez, D.A. Muller, L.T. Angenent, J. Lehmann, Simultaneous Quantification of Electron Transfer by Carbon Matrices and Functional Groups in Pyrogenic Carbon, Environ. Sci. Technol. 52 (2018) 8538–8547.

[213] A.P. Terzyk, The influence of activated carbon surface chemical composition on the adsorption of acetaminophen (paracetamol) in vitro. Part II. TG, FTIR, and XPS analysis of carbons and the temperature dependence of adsorption kinetics at the neutral pH, Colloids Surfaces A Physicochem. Eng. Asp. 177 (2001) 23–45.

[214] J. Song, P. Peng, Surface Characterization of Aerosol Particles in Guangzhou, China: A Study by XPS, Aerosol Sci. Technol. 43 (2009) 1230–1242.

[215] R. Blume, D. Rosenthal, J.P. Tessonnier, H. Li, A. Knop-Gericke, R. Schlögl, Characterizing Graphitic Carbon with X-ray Photoelectron Spectroscopy: A Step-by-Step Approach, ChemCatChem. 7 (2015) 2871–2881.

[216] H. Kiuchi, T. Kondo, M. Sakurai, D. Guo, J. Nakamura, H. Niwa, J. Miyawaki, M. Kawai, M. Oshima, Y. Harada, Characterization of nitrogen species incorporated into graphite using low energy nitrogen ion sputtering, Phys. Chem. Chem. Phys. 18 (2016) 458–465.

[217] T. Kondo, S. Casolo, T. Suzuki, T. Shikano, M. Sakurai, Y. Harada, M. Saito,

M. Oshima, M.I. Trioni, G.F. Tantardini, J. Nakamura, Atomic-scale characterization of nitrogen-doped graphite: Effects of dopant nitrogen on the local electronic structure of the surrounding carbon atoms, Phys. Rev. B - Condens. Matter Mater. Phys. 86 (2012) 035436.

[218] J.R. Pels, F. Kapteijn, J.A. Moulijn, Q. Zhu, K.M. Thomas, Evolution of nitrogen functionalities in carbonaceous materials during pyrolysis, Carbon N. Y. 33 (1995) 1641–1653.

[219] Y. Zhang, J. Zhang, C. Sheng, J. Chen, Y. Liu, L. Zhao, F. Xie, X-ray photoelectron spectroscopy (XPS) investigation of nitrogen functionalities during coal char combustion in O2/CO2 and O2/Ar atmospheres, Energy and Fuels. 25 (2011) 240–245.

[220] Z. Wang, Q. Li, Z. Lin, R. Whiddon, K. Qiu, M. Kuang, K. Cen, Transformation of nitrogen and sulphur impurities during hydrothermal upgrading of low quality coals, Fuel. 164 (2016) 254–261.

[221] S. Righi, V. Bandini, D. Marazza, F. Baioli, C. Torri, A. Contin, Life Cycle Assessment of high ligno-cellulosic biomass pyrolysis coupled with anaerobic digestion, Bioresour. Technol. 212 (2016) 245–253.

[222] Z. Zhao, Y. Zhang, T.L. Woodard, K.P. Nevin, D.R. Lovley, Enhancing syntrophic metabolism in up-flow anaerobic sludge blanket reactors with conductive carbon materials, Bioresour. Technol. 191 (2015) 140–145.

[223] D. Zhang, K. Zhang, X. Hu, Q. He, J. Yan, Y. Xue, Cadmium removal by MgCl2 modified biochar derived from crayfish shell waste: Batch adsorption, response surface analysis and fixed bed filtration, J. Hazard. Mater. 408 (2021) 124860.

[224] C.A. Takaya, L.A. Fletcher, S. Singh, K.U. Anyikude, A.B. Ross, Phosphate and ammonium sorption capacity of biochar and hydrochar from different wastes, Chemosphere. 145 (2016) 518–527.

[225] W. Li, H. Khalid, Z. Zhu, R. Zhang, G. Liu, C. Chen, E. Thorin, Methane production through anaerobic digestion: Participation and digestion characteristics of cellulose, hemicellulose and lignin, Appl. Energy. 226 (2018) 1219–1228.

[226] G. Wang, Q. Li, X. Gao, X.C. Wang, Synergetic promotion of syntrophic methane production from anaerobic digestion of complex organic wastes by biochar: Performance and associated mechanisms, Bioresour. Technol. 250 (2018) 812–820.

[227] S. Xu, C. He, L. Luo, F. Lü, P. He, L. Cui, Comparing activated carbon of different particle sizes on enhancing methane generation in upflow anaerobic digester, Bioresour. Technol. 196 (2015) 606–612.

[228] A.S. Giwa, H. Xu, F. Chang, J. Wu, Y. Li, N. Ali, S. Ding, K. Wang, Effect of biochar on reactor performance and methane generation during the anaerobic digestion of food waste treatment at long-run operations, J. Environ. Chem. Eng. 7 (2019) 103067.

[229] D. Li, L. Song, H. Fang, P. Li, Y. Teng, Y.-Y. Li, R. Liu, Q. Niu, Accelerated bio-methane production rate in thermophilic digestion of cardboard with

appropriate biochar: Dose-response kinetic assays, hybrid synergistic mechanism, and microbial networks analysis, Bioresour. Technol. 290 (2019) 121782.

[230] X. Gómez, W. Meredith, C. Fernández, M. Sánchez-García, R. Díez-Antolínez, J. Garzón-Santos, C.E. Snape, Evaluating the effect of biochar addition on the anaerobic digestion of swine manure: application of Py-GC/MS, Environ. Sci. Pollut. Res. 25 (2018) 25600–25611.

[231] J. Xu, A.M. Mustafa, H. Lin, U.Y. Choe, K. Sheng, Effect of hydrochar on anaerobic digestion of dead pig carcass after hydrothermal pretreatment, Waste Manag. 78 (2018) 849–856.

[232] J.L. Linville, Y. Shen, P.A. Ignacio-de Leon, R.P. Schoene, M. Urgun-Demirtas, In-situ biogas upgrading during anaerobic digestion of food waste amended with walnut shell biochar at bench scale, Waste Manag. Res. 35 (2017) 669–679.

[233] J. Cai, P. He, Y. Wang, L. Shao, F. Lü, Effects and optimization of the use of biochar in anaerobic digestion of food wastes, Waste Manag. Res. 34 (2016) 409–416.

[234] A.B. Ross, K. Anastasakis, M. Kubacki, J.M. Jones, Investigation of the pyrolysis behaviour of brown algae before and after pre-treatment using PY-GC/MS and TGA, J. Anal. Appl. Pyrolysis. 85 (2009) 3–10.

[235] R. Chintala, T.E. Schumacher, S. Kumar, D.D. Malo, J.A. Rice, B. Bleakley, G. Chilom, D.E. Clay, J.L. Julson, S.K. Papiernik, Z. Rong, Molecular characterization of biochars and their influence on microbiological properties of soil, J. Hazard. Mater. 279 (2014) 244–256.

[236] A.F. Khadem, S. Azman, C.M. Plugge, G. Zeeman, J.B. van Lier, A.J.M. Stams, Effect of humic acids on the activity of pure and mixed methanogenic cultures, Biomass and Bioenergy. 99 (2017) 21–30.

[237] R. Lin, J. Cheng, J.D. Murphy, Inhibition of thermochemical treatment on biological hydrogen and methane co-production from algae-derived glucose/glycine, Energy Convers. Manag. 158 (2018) 201–209.

[238] B. Jorgensen, S. Egholm Christiansen, M. Dahl Thomsen, C. Christensen, Aerobic oxidation of aqueous ethanol using heterogeneous gold catalysts: Efficient routes to acetic acid and ethyl acetate, J. Catal. 251 (2007) 332–337.

[239] C. Mao, Y. Feng, X. Wang, G. Ren, Review on research achievements of biogas from anaerobic digestion, Renew. Sustain. Energy Rev. 45 (2015) 540–555.

[240] Q. Huang, G. Lu, J. Wang, J. Yu, Thermal decomposition mechanisms of $MgCl_2 \cdot 6H_2O$ and $MgCl_2 \cdot H_2O$, J. Anal. Appl. Pyrolysis. 91 (2011) 159–164.

[241] N.-Y.T. Nguyen, N. Grelling, C.L. Wetteland, R. Rosario, H. Liu, Antimicrobial Activities and Mechanisms of Magnesium Oxide Nanoparticles (nMgO) against Pathogenic Bacteria, Yeasts, and Biofilms, Sci. Rep. 8 (2018) 16260.

[242] T.R. Garrett, M. Bhakoo, Z. Zhang, T. Roger, M. Bhakoo, Z. Zhang, Bacterial adhesion and biofilms on surfaces, Prog. Nat. Sci. 18 (2008) 1049–1056.

[243] M.C. van Loosdrecht, J. Lyklema, W. Norde, A.J. Zehnder, Influence of interfaces on microbial activity., Microbiol. Rev. 54 (1990) 75–87.

[244] T. Jesionowski, J. Zdarta, B. Krajewska, Enzyme immobilization by adsorption: A review, Adsorption. 20 (2014) 801–821.

[245] G.A. Kovalenko, L. V. Perminova, Immobilization of glucoamylase by adsorption on carbon supports and its application for heterogeneous hydrolysis of dextrin, Carbohydr. Res. 343 (2008) 1202–1211.

[246] F. Raposo, V. Fernández-Cegrí, M.A. de la Rubia, R. Borja, F. Béline, C. Cavinato, G. Demirer, B. Fernández, M. Fernández-Polanco, J.C. Frigon, R. Ganesh, P. Kaparaju, J. Koubova, R. Méndez, G. Menin, A. Peene, P. Scherer, M. Torrijos, H. Uellendahl, I. Wierinck, V. de Wilde, Biochemical methane potential (BMP) of solid organic substrates: Evaluation of anaerobic biodegradability using data from an international interlaboratory study, J. Chem. Technol. Biotechnol. 86 (2011) 1088–1098.

[247] N. Kythreotou, G. Florides, S.A. Tassou, A review of simple to scientific models for anaerobic digestion, Renew. Energy. 71 (2014) 701–714.

[248] J. Chodkowska-Miszczuk, S. Martinát, D. van der Horst, Changes in feedstocks of rural anaerobic digestion plants: External drivers towards a circular bioeconomy, Renew. Sustain. Energy Rev. 148 (2021) 111344.

[249] I.S. Chronakis, M. Madsen, Algal proteins, in: Handb. Food Proteins, Woodhead P, Woodhead Publishing, 2011: pp. 353–394.

[250] R. Kothari, A. Vashishtha, H.M. Singh, V. V. Pathak, V. V. Tyagi, B.C. Yadav, V. Ashokkumar, D.P. Singh, Assessment of Indian bioenergy policy for sustainable environment and its impact for rural India: Strategic implementation and challenges, Environ. Technol. Innov. 20 (2020).

[251] M. Wang, A.K. Sahu, B. Rusten, C. Park, Anaerobic co-digestion of microalgae Chlorella sp. and waste activated sludge, Bioresour. Technol. 142 (2013) 585–590.

[252] H.A. Ruiz, R.M. Rodríguez-Jasso, B.D. Fernandes, A.A. Vicente, J.A. Teixeira, Hydrothermal processing, as an alternative for upgrading agriculture residues and marine biomass according to the biorefinery concept: A review, Renew. Sustain. Energy Rev. 21 (2013) 35–51.

[253] A.J.J. Ward, D.M.M. Lewis, F.B.B. Green, Anaerobic digestion of algae biomass: A review, Algal Res. 5 (2014) 204–214.

[254] Y. Zhang, G.S. Caldwell, A.M. Zealand, P.J. Sallis, Anaerobic co-digestion of microalgae Chlorella vulgaris and potato processing waste: Effect of mixing ratio, waste type and substrate to inoculum ratio, Biochem. Eng. J. 143 (2019) 91–100.

[255] J. Jimenez, E. Latrille, F. Daniel, G. Christian, W. Francis, O. Bernard, V.A. Hugo, D. Zitomer, D. Totzke, H. Spanjers, F. Jacobi, A. Guwy, R. Dinsdale, G. Premier, S. Mazhegrane, G.R. Aurora, S. Thierry, P.J. Steyer, Instrumentation and control of anaerobic digestion processes : a review and some research challenges, (2015) 615–648.

[256] Y. Yao, R. Zhang, B. Wang, S. Zhang, Modeling and optimization of

anaerobic digestion of corn stover on biogas production: Initial pH and carbon to nitrogen ratio, Energy Sources, Part A Recover. Util. Environ. Eff. 39 (2017) 1497–1503.

[257] M. Piątek, A. Lisowski, A. Kasprzycka, B. Lisowska, The dynamics of an anaerobic digestion of crop substrates with an unfavourable carbon to nitrogen ratio, Bioresour. Technol. 216 (2016) 607–612.

[258] P. Bohutskyi, D. Phan, A.M. Kopachevsky, S. Chow, E.J. Bouwer, M.J. Betenbaugh, Synergistic co-digestion of wastewater grown algae-bacteria polyculture biomass and cellulose to optimize carbon-to-nitrogen ratio and application of kinetic models to predict anaerobic digestion energy balance, Bioresour. Technol. 269 (2018) 210–220.

[259] H.W. Yen, D.E. Brune, Anaerobic co-digestion of algal sludge and waste paper to produce methane, Bioresour. Technol. 98 (2007) 130–134.

[260] A.M. Villamagna, B.R. Murphy, Ecological and socio-economic impacts of invasive water hyacinth (Eichhornia crassipes): a review, Freshw. Biol. 55 (2010) 282–298.

[261] C.C. Gunnarsson, C.M. Petersen, Water hyacinths as a resource in agriculture and energy production: A literature review, Waste Manag. 27 (2007) 117–129.

[262] S.H. Yan, J.Y. Guo, J.Y. Guo, Introduction, in: Water Hyacinth Environ. Challenges, Manag. Util., CRC Press, 2017: pp. 1–11.

[263] D. Güereña, H. Neufeldt, J. Berazneva, S. Duby, Water hyacinth control in Lake Victoria: Transforming an ecological catastrophe into economic, social, and environmental benefits, Sustain. Prod. Consum. 3 (2015) 59–69.

[264] C. Zhang, X. Ma, T. Huang, Y. Zhou, Y. Tian, Co-hydrothermal carbonization of water hyacinth and polyvinyl chloride: Optimization of process parameters and characterization of hydrochar, Bioresour. Technol. 314 (2020) 123676.

[265] S. Román, B. Ledesma, A. Álvarez, C. Coronella, S. V. Qaramaleki, Suitability of hydrothermal carbonization to convert water hyacinth to added-value products, Renew. Energy. 146 (2020) 1649–1658.

[266] M.A. De la Rubia, J.A. Villamil, J.J. Rodriguez, A.F. Mohedano, Effect of inoculum source and initial concentration on the anaerobic digestion of the liquid fraction from hydrothermal carbonisation of sewage sludge, Renew. Energy. 127 (2018) 697–704.

[267] C.K. Okoro-Shekwaga, M.V. Turnell Suruagy, A.B. Ross, M.A. Camargo-Valero, Particle size, inoculum-to-substrate ratio and nutrient media effects on biomethane yield from food waste, Renew. Energy. 151 (2020) 311–321.

[268] C.H. Lay, B. Sen, C.C. Chen, J.H. Wu, S.C. Lee, C.Y. Lin, Co-fermentation of water hyacinth and beverage wastewater in powder and pellet form for hydrogen production, Bioresour. Technol. 135 (2013) 610–615.

[269] K.K. Moorhead, R.A. Nordstedt, Batch anaerobic digestion of water

hyacinth: effects of particle size, plant nitrogen content and inoculum volume, Bioresour. Technol. 44 (1993) 71–76.

[270] J.H. Patil, M.A. Raj, P.L. Muralidhara, S.M. Desai, G.K.M. Raju, D. Güereña, H. Neufeldt, J. Berazneva, S. Duby, C. O'Sullivan, B. Rounsefell, A. Grinham, W. Clarke, J. Udy, K.K. Moorhead, R.A. Nordstedt, D. Güereña, H. Neufeldt, J. Berazneva, S. Duby, C. O'Sullivan, B. Rounsefell, A. Grinham, W. Clarke, J. Udy, J.H. Patil, M.A. Raj, P.L. Muralidhara, S.M. Desai, G.K.M. Raju, Kinetics of Anaerobic Digestion of Water Hyacinth Using Poultry Litter as Inoculum, Int. J. Environ. Sci. Dev. 36 (2012) 94–98.

[271] F. Raposo, R. Borja, M.A. Martín, A. Martín, M.A. de la Rubia, B. Rincón, Influence of inoculum-substrate ratio on the anaerobic digestion of sunflower oil cake in batch mode: Process stability and kinetic evaluation, Chem. Eng. J. 149 (2009) 70–77.

[272] K.K. Xiao, C.H. Guo, Y. Zhou, Y. Maspolim, J.Y. Wang, W.J. Ng, Acetic acid inhibition on methanogens in a two-phase anaerobic process, Biochem. Eng. J. 75 (2013) 1–7.

[273] M.C. Sterling, R.E. Lacey, C.R. Engler, S.C. Ricke, Effects of ammonia nitrogen on H2 and CH4 production during anaerobic digestion of dairy cattle manure, Bioresour. Technol. 77 (2001) 9–18.

[274] J. Mata-Alvarez, J. Dosta, S. Macé, S. Astals, Codigestion of solid wastes: A review of its uses and perspectives including modeling, Crit. Rev. Biotechnol. 31 (2011) 99–111.

[275] D. Lu, X. Liu, O.G. Apul, L. Zhang, D.K. Ryan, X. Zhang, Optimization of biomethane production from anaerobic Co-digestion of microalgae and septic tank sludge, Biomass and Bioenergy. 127 (2019) 105266.

[276] C.K. Okoro-Shekwaga, A.B. Ross, M.A. Camargo-Valero, Improving the biomethane yield from food waste by boosting hydrogenotrophic methanogenesis, Appl. Energy. 254 (2019) 113629.

[277] B. Wang, S. Strömberg, C. Li, I.A. Nges, M. Nistor, L. Deng, J. Liu, Effects of substrate concentration on methane potential and degradation kinetics in batch anaerobic digestion, Bioresour. Technol. 194 (2015) 240–246.

[278] S.M. Scully, J. Orlygsson, Conversion of Lignocellulosic Feedstocks into Bioethanol Using Extremophiles, in: R.K. Sani, N.K. Rathinam (Eds.), Extrem. Microb. Process. Lignocellul. Feed. to Biofuels, Value-Added Prod. Usable Power, Springer International Publishing, Cham, 2018: pp. 25–46.

[279] Y. Sun, D. Wang, J. Yan, W. Qiao, W. Wang, T. Zhu, Effects of lipid concentration on anaerobic co-digestion of municipal biomass wastes, Waste Manag. 34 (2014) 1025–1034.

[280] C. Deng, R. Lin, X. Kang, B. Wu, D.M. Wall, J.D. Murphy, What physicochemical properties of biochar facilitate interspecies electron transfer in anaerobic digestion: A case study of digestion of whiskey by-products, Fuel. 306 (2021) 121736.

[281] G. Wang, Y. Li, L. Sheng, Y. Xing, G. Liu, G. Yao, H.H. Ngo, Q. Li, X.C. Wang, Y.Y. Li, R. Chen, A review on facilitating bio-wastes degradation and energy

recovery efficiencies in anaerobic digestion systems with biochar amendment, Bioresour. Technol. 314 (2020).

[282] E.J. Martínez, J.G. Rosas, A. Sotres, A. Moran, J. Cara, M.E. Sánchez, X. Gómez, Codigestion of sludge and citrus peel wastes: Evaluating the effect of biochar addition on microbial communities, Biochem. Eng. J. 137 (2018) 314–325.

[283] C. Torri, D. Fabbri, Biochar enables anaerobic digestion of aqueous phase from intermediate pyrolysis of biomass, Bioresour. Technol. 172 (2014) 335–341.

[284] P. Fernandes, J.M.S. Cabral, Bioreactors, in: Multiph. Catal. React., John Wiley & Sons, Inc., Hoboken, NJ, USA, 2016: pp. 156–170.

[285] R.B. Fidel, D.A. Laird, M.L. Thompson, M. Lawrinenko, Characterization and quantification of biochar alkalinity, Chemosphere. 167 (2017) 367–373.

[286] F. Xu, Y. Li, X. Ge, L. Yang, Y. Li, Anaerobic digestion of food waste – Challenges and opportunities, Bioresour. Technol. 247 (2018) 1047–1058.

[287] J. Quintana-Najera, A.J. Blacker, L.A. Fletcher, A.B. Ross, The effect of augmentation of biochar and hydrochar in anaerobic digestion of a model substrate, Bioresour. Technol. 321 (2021) 124494.

[288] J. Quintana-Najera, A.J. Blacker, L.A. Fletcher, A.B. Ross, Influence of augmentation of biochar during anaerobic co-digestion of Chlorella vulgaris and cellulose, Bioresour. Technol. 343 (2022) 126086.

A. Appendix A

Composition of the chars

Table A.1. Proximate and ultimate composition of biomass feedstocks and chars expressed in dry ash-free basis.

Material	C (%) daf	H (%) daf	N (%) daf	O (%) daf	S (%) daf	O:C	H:C	N:C
Oak wood								
Untreated	52.3	7.6	1.5	38.5	0.0	0.55	1.74	0.03
OW-HC250	64.5	5.2	1.2	30.5	0.0	0.36	0.96	0.02
OW-BC450	74.4	3.1	0.7	21.9	0.0	0.22	0.49	0.01
OW-BC650	89.3	1.6	0.9	8.2	0.0	0.07	0.22	0.01
Water hyacinth								
Untreated	45.2	3.9	3.1	47.7	0.2	0.79	1.04	0.06
WH-HC250	63.9	5.4	4.2	25.4	0.1	0.30	1.01	0.06
WH-BC450	39.4	2.2	2.6	55.8	0.3	1.06	0.65	0.05
WH-BC600	67.9	1.8	3.6	26.7	0.0	0.30	0.31	0.05
Saw wrack								
Untreated	51.5	1.6	1.6	43.4	1.9	0.55	0.38	0.03
SW-HC250	64.1	5.3	2.8	26.5	1.3	0.31	0.99	0.04
SW-BC450	58.3	2.7	3.6	32.1	2.6	0.41	0.56	0.05
SW-BC600	61.8	1.4	3.5	33.0	0.5	0.40	0.27	0.05

Table A2. Inorganic element analysis of untreated feedstocks and chars obtained by XRF.

ppm (db)	OW-U	OW-HC250	OW-BC450	OW-BC650	WH-U	WH-HC250	WH-BC450	WH-BC600	FS-U	FS-HC250	FS-BC450	FS-BC600
Na	16	27	358	809	852	2209	1083	2216	37700	9700	38786	42455
Mg	226	104	2912	5168	895	6626	1276	4924	7700	17100	10635	10659
Al	68	77	265	1274	14017	15863	25996	30563	600	900	1543	1149
Si	124	153	637	4016	28344	26095	53803	52234	1700	10400	5466	2507
P	97	100	936	2757	664	10558	1035	3102	1500	5400	2540	1907
S	88	140	361	598	715	2797	978	2426	15600	14100	18339	15178
Cl	70	104	0	83	854	823	934	10698	62700	15900	55007	72611
K	23	25	3896	5141	7513	15738	10393	23633	49400	13800	49789	53843
Ca	10471	10271	30470	71823	7672	27486	8633	41267	12200	27800	15183	15277
Mn	156	252	890	898	624	3778	755	1893	200	700	839	948
Fe	6473	11824	29105	3305	17348	17927	20403	40826	400	700	29279	29887
Co	7	15	66	0	0	0	0	41	0	0	45	0
Ni	271	367	2429	268	376	22	232	968	0	0	1295	1709
Cu	15	24	117	38	26	13	32	77	0	0	97	83
Sr	36	33	108	329	48	463	64	278	700	1700	997	598
Mo	14	23	94	19	0	0	0	64	0	0	68	85
Ba	89	0	0	0	0	470	659	0	0	0	0	0
Ti	0	0	0	129	829	1087	1556	0	0	100	944	161
Zn	0	0	11	22	18	109	30	89	800	800	345	276

B. Appendix B

Anaerobic digestion
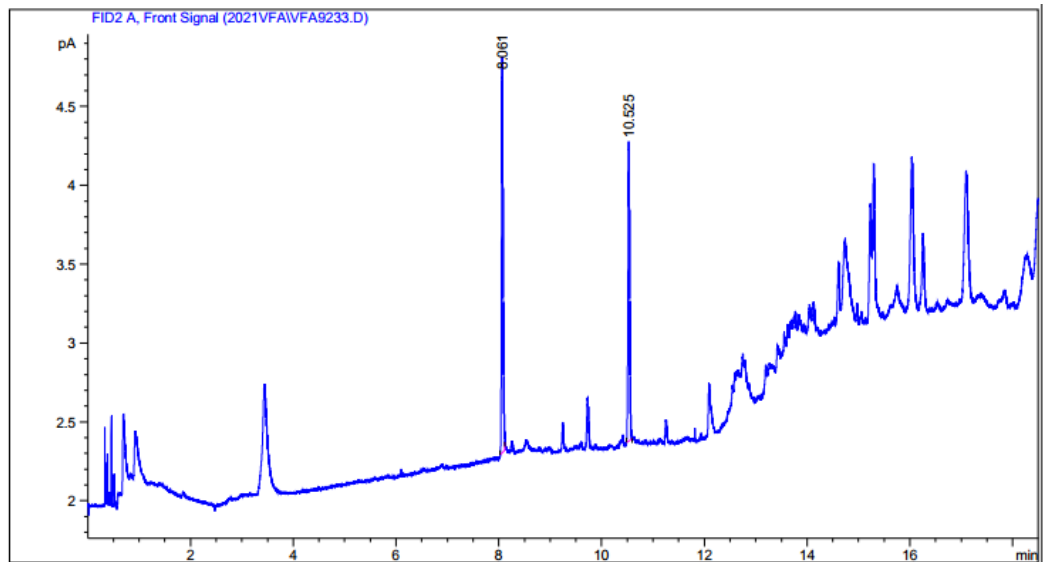

```
FID2 A, Front Signal (2021VFA\VFA9233.D)

Sorted By               :       Retention Time
Calib. Data Modified    :       13/01/2020 16:19:05
Multiplier              :       1.0000
Dilution                :       1.0000
Use Multiplier & Dilution Factor with ISTDs


Signal 1: FID2 A, Front Signal

RetTime Sig Type     Area      Amt/Area    Amount    Grp    Name
 [min]             [pA*s]                 [ng/ul]
-------|--|------|----------|----------|----------|--|----------------
  0.710  1            -          -          -            Acetone
  0.846  1            -          -          -            Methanol
  0.934  1            -          -          -            Ethanol
  2.625  1            -          -          -            Butanol
  8.061  1 BB    5.11895    1.39813    7.15696          Acetic Acid
  9.340  1            -          -          -            Propanoic Acid
  9.702  1            -          -          -            Isobutyric Acid
 10.525  1 BB    4.21007 6.07073e-1    2.55582          Butyric Acid
 10.952  1            -          -          -            Isovaleric Acid
 11.754  1            -          -          -            Valeric Acid

 12.396  1            -          -          -            Isocaproic Acid
 12.690  1            -          -          -            Caproic Acid
 13.236  1            -          -          -            Heptanoic Acid
```

Figure B1. Chromatogram and standard report for the quantification of volatile fatty acids via gas chromatography - flame ionisation detector (GC-FID).

Table B. 1 Data used for the principal component analysis for the effect of biochar addition in anaerobic digestion.

Feedstock	Effect of biochar addition — Values calculated in comparison to the corresponding control.							Effect of biochar addition. — Standardised data by $\frac{Mean\ centred\ value}{Standard\ deviation}$							Ref
	Pyrolysis temperature	Ash (%)	O:C daf	BC load (%) w/v	Yield (%)	μ_m (%)	λ reduction (%)	Pyrolysis temperature	Ash	O:C daf	BC load	Yield	μ_m	λ reduction	Ref
Fruitwoods	900	5.49	0.07	1	8.3	188.0	-54.3	1.69	-0.74	-0.58	-0.40	-0.14	1.97	-1.05	[233]
				0.5	40.6	114.8	-54.0	1.69	-0.74	-0.58	-0.77	0.12	1.01	-1.05	
				1	38.8	81.5	-45.0	1.69	-0.74	-0.58	-0.40	0.11	0.57	-0.90	
				0.5	20.6	148.0	-43.8	1.69	-0.74	-0.58	-0.77	-0.04	1.44	-0.88	
				0.2	4.61	184.0	-43.3	1.69	-0.74	-0.58	-1.00	-0.17	1.92	-0.87	
				0.2	44.2	48.2	-36.2	1.69	-0.74	-0.58	-1.00	0.15	0.13	-0.75	
				1	3.57	224.4	-11.6	1.69	-0.74	-0.58	-0.40	-0.17	2.45	-0.34	
				0.5	0.6	48.9	-6.9	1.69	-0.74	-0.58	-0.77	-0.20	0.14	-0.26	
				0.2	-1.9	86.7	18.8	1.69	-0.74	-0.58	-1.00	-0.22	0.64	0.16	
Wheat bran pellet	800			2.5	0	3.9		1.09			0.72	-0.20			[92]
Coppiced woodlands pellet	500			2.5	0	4.6		-0.70			0.72	-0.20			
Orchard pruning	500			2.5	0	5		-0.70			0.72	-0.20			

Table continues.

Feedstock	Pyrolysis temperature	Ash (%)	O:C daf	BC load (%) w/v	Yield (%)	μm (%)	λ reduction (%)	Pyrolysis temperature	Ash	O:C daf	BC load	Yield	μm	λ reduction	Ref
Waste wood	700			1	-10.2	-8.1	6.7	0.49			-0.40	-0.28	-0.61	-0.04	[37]
				0.5	-10	-11.8	13.3	0.49			-0.77	-0.28	-0.65	0.07	
				0.06	6.4	9.5	46.7	0.49			-1.10	-0.15	-0.37	0.63	
				0.03	5.7	16.7	46.7	0.49			-1.12	-0.16	-0.28	0.63	
				0.13	17	11.8	53.3	0.49			-1.05	-0.07	-0.34	0.74	
Rice husk	450			0.96	5	22.02	4.5	-1.00			-0.43	-0.16	-0.21	-0.07	[171]
Coconut shell	450			0.96	4.2	19.3	45.5	-1.00			-0.43	-0.17	-0.25	0.61	
Wood	450			0.96	-16.4	-16	49.3	-1.00	-0.60		-0.43	-0.33	-0.71	0.67	
Almond shell residual	550	3.12	0.06	1.2	32.4	15.6	-33.9	-0.40	-0.90	-0.62	-0.25	0.06	-0.30	-0.71	[230]
				1.2	4.0	4.7	-0.9	-0.40	-0.90	-0.62	-0.25	-0.17	-0.44	-0.16	
Dairy manure	350			0.1	5.4	5.7	10.1	-1.60			-1.07	-0.16	-0.42	0.02	[201]
				1	24.5	32.3	26.9	-1.60			-0.40	-0.01	-0.08	0.30	
Walnut shell	900	43.2	0.06	0.347	1.65			1.69	1.87	-0.62	-0.89				[232]
				0.696	74.59			1.69	1.87	-0.62	-0.63			-0.04	

The two major header spans read: "Effect of biochar addition — Values calculated in comparison to the corresponding control." and "Effect of biochar addition. Standardised data by $\frac{\text{Mean centred value}}{\text{Standard deviation}}$".

Table continues.

Feedstock	Pyrolysis temperature	Ash (%)	O:C daf	BC load (%) w/v	Yield (%)	μ$_m$ (%)	λ reduction (%)	Pyrolysis temperature	Ash	O:C daf	BC load	Yield	μ$_m$	λ reduction	Ref
								Effect of biochar addition. Standardised data by $\frac{Mean\ centred\ value}{Standard\ deviation}$							
Fruitwood	800	5.5	0.06	1	2.9	44.1	-5.9	1.09	-0.74	-0.60	-0.40	-0.18	0.08	-0.25	[172]
				1	-2	10.2	13	1.09	-0.74	-0.60	-0.40	-0.22	-0.37	0.07	
				1	1.7	23.5	23.8	1.09	-0.74	-0.60	-0.40	-0.19	-0.19	0.25	
				1	11.5	47.1	23.9	1.09	-0.74	-0.60	-0.40	-0.11	0.12	0.25	
				1	-2.4	18.6	30.4	1.09	-0.74	-0.60	-0.40	-0.22	-0.26	0.36	
Fruitwood	800	5.5			-17.5	86.6	11.4	1.09	-0.74		-0.40	-0.34	0.64	0.04	[87]
					-2.6	-19.9	16.5	1.09	-0.74		-0.40	-0.22	-0.76	0.13	
					-11.9	5.2	21.6	1.09	-0.74		-0.40	-0.30	-0.43	0.21	
					-3.5	21.4	30.3	1.09	-0.74		-0.40	-0.23	-0.22	0.35	
Vineyard pruning	550	47.4	0.2	3	-100.0	426.3	-55.4	-0.40	2.16	-0.02	1.09	-1.00	5.10	-1.07	[282]
				1	-100.0	362.3	-51.3	-0.40	2.16	-0.02	-0.40	-1.00	4.26	-1.00	
				3	97.4	29.9	-44.5	-0.40	2.16	-0.02	1.09	0.58	-0.11	-0.89	
				1	26.6	31.0	-41.9	-0.40	2.16	-0.02	-0.40	0.01	-0.09	-0.85	
				1	-48.4	23.5	-33.9	-0.40	2.16	-0.02	-0.40	-0.59	-0.19	-0.71	
				3	109.3	78.3	-25.5	-0.40	2.16	-0.02	1.09	0.67	0.53	-0.57	

Table continues.

Feedstock	Effect of biochar addition Values calculated in comparison to the corresponding control.							Effect of biochar addition. Standardised data by $\frac{Mean\ centred\ value}{Standard\ deviation}$							Ref
	Pyrolysis temperature	Ash (%)	O:C daf	BC load (%) w/v	Yield (%)	μ_m (%)	λ reduction (%)	Pyrolysis temperature	Ash	O:C daf	BC load	Yield	μ_m	λ reduction	
Paper sludge/wheat husks	500	15.5	0.44	2	-8.5	0		-0.70	-0.05	1.01	0.34	-0.27	-0.50	-0.15	[17]
Rice straw	500	1.9		0.5	-47	-44.7	69.4	-0.70	-0.99		-0.77	-0.58	-1.09	1.00	[202]
Corn stover	500			0.4	-2.8	-2		-0.70			-0.85	-0.22	-0.53		[35]
Rice straw	500			0.4	1.2	27		-0.70			-0.85	-0.19	-0.14		
Oak wood	500			0.4	12	39.2		-0.70			-0.85	-0.11	0.02		
Apple wood	500			0.4	15.4	41.3		-0.70			-0.85	-0.08	0.04		
Pine wood	500			0.4	10.2	49.1		-0.70			-0.85	-0.12	0.15		
Bamboo	500			0.4	2.1	51.7		-0.70			-0.85	-0.19	0.18		
Rice straw	500			0.4	13.0		28.6	-0.70			-0.85	-0.10	-0.50	0.33	[88]

Table continues.

Feedstock	Pyrolysis temperature	Ash (%)	O:C daf	BC load (%) w/v	Yield (%)	μm (%)	λ reduction (%)	Pyrolysis temperature	Ash	O:C daf	BC load	Yield	μm	λ reduction	Ref
							Effect of biochar addition. Values calculated in comparison to the corresponding control.				Effect of biochar addition. Standardised data by $\frac{Mean\ centred\ value}{Standard\ deviation}$				
Canola meal	900	24.9		1	54			1.69	0.60		-0.40	0.23			[28]
Ashe Juniper	400	4.7		1	71			-1.30	-0.80		-0.40	0.37			
Switchgrass	500	6.8		1	72			-0.70	-0.65		-0.40	0.37			
Canola meal	700	24.4		1	79			0.49	0.57		-0.40	0.43			
Ashe Juniper	600	4.2		1	267			-0.10	-0.83		-0.40	1.93			
Ashe Juniper	400	4.7		1	1133			-1.30	-0.80		-0.40	8.86			
Pine wood	900	9		1				1.69	-0.50		-0.40	-0.20			[38]
Corn stalk	710	45.6		1.5	1.2	4.8		0.55	2.03		-0.03	-0.19	-0.44		[173]
		45.6		1.3	1.3	14.4		0.55	2.03		-0.18	-0.19	-0.31		
		45.6		1.1	1.2	15.1		0.55	2.03		-0.33	-0.19	-0.30		
		45.6		0.8	1.1	27.6		0.55	2.03		-0.55	-0.19	-0.14		
Pine wood	710	18.7	0.25	6.3	2.2			0.55	0.17	0.19	3.55	-0.18			[148]
		18.7	0.25	3.1	3			0.55	0.17	0.19	1.17	-0.18			
Oak wood	710	34.9	0.05	5.6	4.3			0.55	1.29	-0.66	3.03	-0.17			
		34.9		2.8	7.9			0.55	1.29	-0.66	0.94	-0.14			

Table continues

Feedstock	Effect of biochar addition. Values calculated in comparison to the corresponding control.							Effect of biochar addition. Standardised data by $\frac{Mean\ centred\ value}{Standard\ deviation}$							Ref
Feedstock	Pyrolysis temperature	Ash (%)	O:C daf	BC load (%) w/v	Yield (%)	μ_m (%)	λ reduction (%)	Pyrolysis temperature	Ash	O:C daf	BC load	Yield	μ_m	λ reduction	Ref
Pine sawdust	650	6.3	0.12	1.5	29.3	5.845588	0	0.19	-0.68	-0.35	-0.03	0.03	-0.42	-0.15	[36]
					40.7	33.08824	0	1.69	0.38	0.59	-0.03	0.06	-0.26	-0.15	
Pine sawdust	900	21.7	0.34	1.5	33.3	18.0	0	0.19	-0.68	-0.35	-0.03	0.12	-0.06	-0.15	
					47.1	43.0	0	1.69	0.38	0.59	-0.03	0.17	0.07	-0.15	
Pine sawdust	650	6.3	0.12	0.83	6.2	38.1	41	0.19	-0.68	-0.35	-0.53	-0.15	0.00	0.53	[204]
				3.33	-12.9	22.1	43	0.19	-0.68	-0.35	1.34	-0.31	-0.21	0.57	
				1.66	-1.2	41.6	43	0.19	-0.68	-0.35	0.09	-0.21	0.05	0.57	
				2.51				0.19	-0.68	-0.35	0.73	-0.29	-0.13	0.60	
Cornstalk	400			8	13		28.6	-1.30			4.82	0.41	0.81	-1.11	[283]
Sawdust	500	7.8	0.12	0.2	2.6	29.9	28.6	-0.70	-0.58	-0.35	-1.00	-0.18	-0.11	0.33	[150]
				0.6	4.0	40.3	42.9	-0.70	-0.58	-0.35	-0.70	-0.17	0.03	0.56	
				1	0.4	22.4	51.9	-0.70	-0.58	-0.35	-0.40	-0.20	-0.21	0.71	
				1.5	-2.0	16.4	63.2	-0.70	-0.58	-0.35	-0.03	-0.22	-0.28	0.90	

Table continues.

Feedstock	Effect of biochar addition Values calculated in comparison to the corresponding control.							Effect of biochar addition. Standardised data by $\frac{Mean\ centred\ value}{Standard\ deviation}$							Ref
	Pyrolysis temperature	Ash (%)	O:C daf	BC load (%) w/v	Yield (%)	μ_m (%)	λ reduction (%)	Pyrolysis temperature	Ash	O:C daf	BC load	Yield	μ_m	λ reduction	
Saw wrack	600	34.6	0.40	3	-84.6	-83.9	0.0	-0.10	1.27	0.84	1.09	-0.88	-1.60	-0.15	[287]
Saw wrack	450	33.3	0.41	3	-85.6	-58.7	0.0	-1.00	1.18	0.90	1.09	-0.89	-1.27	-0.15	
Water hyacinth	600	10.6	0.41	3	0.0	4.3	0.0	-0.10	-0.39	0.87	1.09	-0.20	-0.44	-0.15	
Oak wood	650	9.3	0.07	3	-5.4	10.6	0.0	0.19	-0.48	-0.58	1.09	-0.25	-0.36	-0.15	
Shea nut	600	13.7	0.14	3	3.2	81.8	0.0	-0.10	-0.17	-0.27	1.09	-0.18	0.58	-0.15	
Water hyacinth	450	23.4	1.38	3	10.6	131.2	0.0	-1.00	0.50	5.05	1.09	-0.12	1.22	-0.15	
Oak wood	450	11.7	0.22	3	7.4	137.8	0.0	-1.00	-0.31	0.07	1.09	-0.14	1.31	-0.15	

Table continues.

Feedstock	Pyrolysis temperature	Ash (%)	O:C daf	Effect of biochar addition. Values calculated in comparison to the corresponding control.				Effect of biochar addition. Standardised data by $\frac{Mean\ centred\ value}{Standard\ deviation}$							Ref
				BC load (%) w/v	Yield (%)	μ_m (%)	λ reduction (%)	Pyrolysis temperature	Ash	O:C daf	BC load	Yield	μ_m	λ reduction	
Oak wood	450	11.7	0.22	0.5	-20.2	64.4	-100.0	-1.00	-0.31	0.07	-0.77	-0.36	0.35	-1.81	This work
				0.5	-41.0	-26.4	0.0	-1.00	-0.31	0.07	-0.77	-0.53	-0.85	-0.15	
				0.5	-18.9	-22.0	0.0	-1.00	-0.31	0.07	-0.77	-0.35	-0.79	-0.15	
				1	-2.3	-13.0	0.0	-1.00	-0.31	0.07	-0.40	-0.22	-0.67	-0.15	
				1	10.1	0.4	0.0	-1.00	-0.31	0.07	-0.40	-0.12	-0.49	-0.15	
				1	-0.9	3.5	0.0	-1.00	-0.31	0.07	-0.40	-0.21	-0.45	-0.15	
Water hyacinth	450	23.4	1.38	0.58	10.5	69.7	-99.3	-1.00	0.50	5.05	-0.71	-0.12	0.42	-1.80	

Table continues.

Feedstock	Pyrolysis temperature	Ash (%)	O:C daf	Effect of biochar addition. Values calculated in comparison to the corresponding control.				Effect of biochar addition. Standardised data by $\frac{Mean\ centred\ value}{Standard\ deviation}$							Ref
				BC load (%) w/v	Yield (%)	μ_m (%)	λ reduction (%)	Pyrolysis temperature	Ash	O:C daf	BC load	Yield	μ_m	λ reduction	
Oak wood	450	11.7	0.22	3	162.3	-80.3	100.0	-1.00	-0.31	0.07	1.09	1.10	-1.55	1.51	[288]
				3	77.1	-63.2	100.0	-1.00	-0.31	0.07	1.09	0.41	-1.33	1.51	
				3	358.5	-58.2	-70.4	-1.00	-0.31	0.07	1.09	2.67	-1.26	-1.32	
				3	-8.4	-5.4	163.3	-1.00	-0.31	0.07	1.09	-0.27	-0.57	2.57	
				3	-7.1	2.3	100.0	-1.00	-0.31	0.07	1.09	-0.26	-0.47	1.51	
				3	-3.8	6.1	307.6	-1.00	-0.31	0.07	1.09	-0.23	-0.42	4.96	
				3	-6.7	18.7	-83.9	-1.00	-0.31	0.07	1.09	-0.26	-0.25	-1.54	
				3	10.7	22.4	100.0	-1.00	-0.31	0.07	1.09	-0.12	-0.21	1.51	
				3	-7.9	33.7	-49.7	-1.00	-0.31	0.07	1.09	-0.26	-0.06	-0.97	
				0.58	20.7	79.8	-99.3	-1.00	-0.31	0.07	-0.71	-0.04	0.55	-1.80	

Table B. 2 Summarised values for the standardisation of the data used for the principal component analysis.

	Pyrolysis temperature	Ash (%)	O:C daf	BC load (%) w/v	Yield (%)	μ_m (%)	λ reduction (%)
sj standard deviation	167.56	14.46	0.23	1.34	125.02	76.12	60.18
Average	617.45	16.21	0.20	1.54	25.25	38.02	8.95